DIPG: rodant cap a l'esperança

Validació d'un mètode de diagnòstic prematur i objectiu del DIPG a partir de la creació d'un model animal inoculat amb cèl lules mare tumorals causants de la malaltia.

Curs 2013-2014

Agraïments

M'agradaria agrair al Dr. Ángel Montero Carcaboso tota la dedicació, paciència i confiança que ha tingut amb mi durant la realització d'aquest projecte. També la oportunitat que m'ha donat de gaudir de treballar durant un estiu dins del seu grup de recerca del laboratori d'oncologia de l'Hospital Sant Joan de Déu de Barcelona.

D'altra banda agrair a Nagore Gené els infinits coneixements que m'ha donat sobre biomedicina en general i sobre treball de laboratori, també per l'ajuda oferta en tot moment. Donar-li les gràcies també per permetre que inclogués el meu treball en la seva investigació personal i confiar en mi.

Gràcies també a la resta del grup de recerca, Carles Monterrubio i Guillem Pascual, per fer-me sentir part de l'equip des de primer moment.

Donar les gràcies al Dr. Andreu Parareda (pediatre del Servei d'Oncologia de l'HSJD) per obrir-me les portes i facilitar-me el contacte amb el Dr. Montero i l'hospital.

Donar gràcies també al Dr. Jaume Mora i Graupera, cap del Servei d'Oncologia de l'HSJD, per permetre'm realitzar les pràctiques del meu treball al seu departament.

Gràcies a la meva mare, Dra. Eulàlia Farrés, per facilitar-me el contacte amb el Dr. Andreu Parareda i fer aportacions/correccions científiques al treball realment necessàries.

Gràcies al meu pare per la paciència i ajut en el grafisme del treball, com també per les crítiques fetes.

Gràcies a la meva tutora Patrícia Campdelacreu i Rocabruna per la seva implicació i exigència en el treball.

*"La science est composée par des erreurs, qui
sont eux-mêmes des étapes vers la vérité"*

(La ciència es composa d'errors, que alhora
són els passos vers la veritat)

Jules Verne

Índex

0. Introducció

El tumor difús de tronc cerebral (a partir d'ara, DIPG[1]) és un tumor cerebral infantil, incurable i relativament poc comú. A aquestes variables se li suma el poc coneixement tant per part de la comunitat científica com també per part de la població. Un diagnòstic difícil i normalment en un estadi bastant avançat, un patiment extrem per part del pacient, la seva localització i biologia, i la franja d'edat en el qual la malaltia apareix el fan un dels pitjors tipus de tumors cerebrals de desenvolupament que existeixen.

La recerca, doncs, té encara molt camí per recórrer en aquest camp. Per tal de trobar una cura efectiva per a aquesta lesió fa falta un coneixement previ molt ampli tant de la seva morfologia, fisiologia i biologia *in vivo*, com també *in vitro*. Aprendre com el tumor creix i com reacciona a diferents estímuls externs és la clau per l'avenç en la investigació tant en el camp d'aquest tipus de lesió, com també en el de l'oncologia en general.

Les particularitats d'aquesta malaltia i la possibilitat de poder desenvolupar part pràctica de l'estudi al laboratori d'oncologia de l'Hospital Sant Joan de Déu de Barcelona durant una gran part de l'estiu 2013, gràcies a la fundació privada de la qual aquest gaudeix i rep finançament, van ser claus a l'hora d'escollir el treball.

En aquest treball s'ha pogut provar en models animals un aparell no utilitzat anteriorment en el DIPG, amb la finalitat de diagnosticar la malaltia en un estadi mínim i poder començar el tractament amb anterioritat a com es duu a actualment.

L'aparell emprat és l'anomenat *Rotarod*, que consisteix en un rodet que gira a una velocitat o acceleració desitjades. Aquest dispositiu s'ha utilitzat anteriorment en el diagnòstic d'altres malalties del sistema nerviós (punt aprofundit a l'apartat *2.2.*).

---

[1] Diffuse Intinsic Pontine Glioma

1. Objectius i hipòtesi

El DIPG és un tumor infantil incurable. Per fer possible l'estudi de la biologia d'aquesta malaltia i la recerca de tractaments contra ella, recentment s'han desenvolupat els primers models animals de DIPG mitjançant la injecció intracerebral de cèl·lules mare obtingudes dels tumors dels pacients. Quan els animals desenvolupen la malaltia mostren evidents símptomes d'atàxia. No obstant això, no existeix un mètode validat per quantificar de manera objectiva el grau d'atàxia i correlacionar-lo amb el grau anatomopatològic de malaltia o amb l'efecte terapèutic (o tòxic) dels possibles tractaments.

Segons la hipòtesi inicial, aquest sistema permetria valorar de manera objectiva i precoç el grau d'atàxia (símptoma propi d'aquest tumor, i indicador d'un estadi molt avançat) relacionat amb l'aparició anatomo-patològica de la malaltia en els animals inoculats (ratolins immunodeprimits de la soca *Nod-Scid*) amb cèl·lules de DIPG humà infantil. És a dir, que ens permetrà predir l'aparició de la malaltia abans que la simptomatologia es faci evident ja que els animals no s'aguantaran sobre el rodet en moviment.

Altres hipòtesis plantejades són que només els ratolins inoculats moririen o bé presentarien símptomes propis de la malaltia.

Alhora, els objectius es centraran en aprendre sobre el procés d'inoculació, valorar els canvis de psicomotricitat a simple vista en els models animals inoculats amb DIPG humà, i relacionar-los amb els resultats del Rotarod.

Per dur a terme la investigació es van realitzar dos tipus d'experiments:

1. *In vitro:* Fer créixer diferents línies cel·lulars del DIPG a partir de cinc biòpsies i una necròpsia realitzades a pacients de l'hospital, per tal d'inocular i fer créixer el tumor d'una manera difusa als animals (a imatge del tumor humà real).

2. *In vivo:* Utilitzar el mètode *Rotarod* per tal d'intentar avançar el moment de diagnòstic de la malaltia. Es van tenir en compte les variables següents:

- Compliment del *Rotarod*.
- OS (Overage Survival): Mortalitat, deguda al tumor inoculat.
- EFS (Event Free Survival): Aparició dels primers símptomes apreciables.

2. Antecedents

2.1. El DIPG

2.1.1. La malaltia

Els tumors difusos de tronc cerebral (DIPG), són un tipus de tumor de desenvolupament (estrictament infantil) molt agressius i tot i que només representen un 10-20% dels tumors cerebrals pediàtrics, constitueixen la principal causa de mort dins d'aquest grup. Aquest percentatge es tradueix en uns 20 casos detectats anualment a Espanya i uns 200 als Estats Units (dades del 2010). Cal recordar que els tumors cerebrals són els tumors sòlids més freqüents a pediatria i el segon tipus de càncer infantil després de les leucèmies. Alhora, els DIPG's representen entre un 75% i un 80% dels tumors de tronc cerebral infantils. Només un 10% dels pacients sobreviuen a aquesta malaltia més de dos anys després del diagnòstic; en la resta de casos, l'esperança de vida no sobrepassa els 16 mesos.

Actualment, i després del diagnòstic de la malaltia, s'apliquen dos tractaments principals: la radioteràpia i la quimioteràpia (detallats més endavant: punts *2.1.4.1.* i *2.1.4.2.*), tot i que cap dels dos és realment efectiu. Una vegada finalitzats aquests dos processos, l'infant entra en un *estat bombolla* (un estadi en què s'obra un parèntesi en l'avanç de la malaltia) en el què els símptomes desapareixen i sembla estar curat; no obstant, després d'uns sis mesos de mitjana aquests tornen a evidenciar-se i evolucionen ràpidament causant la mort del pacient.

Tal com indica el seu nom, aquest tipus de tumors es localitzen al tronc cerebral[2]. El tronc cerebral es una part crucial del nostre cos, ja que al seu interior s'hi allotgen diversos nuclis reguladors i és també l'origen de molts nervis (parells cranials) que regulen des de la respiració i el ritme cardíac, fins al control de la majoria de músculs facials, les extremitats i la coordinació de

---

[2] Estructura del sistema nerviós que connecta entre si la medul·la espinal, el cervell i el cerebel.

l'equilibri. Aquest tumor també és denominat glioma de tronc[3], pel tipus de cèl·lules que el formen (cèl·lules glials, i en major part astròcits: punt *2.1.1.1.*), sense tenir en compte les neurones.

El DIPG és un glioma que creix des de la part central del tronc, el pons, com s'observa a la *Fig: 2*; la porció del tronc de l'encèfal que s'ubica entre el bulb raquidi i el mesencèfal. La seva funció és connectar la medul·la espinal i en bulb raquidi amb estructures superiors, com l'encèfal o el cerebel. Des del pons infiltra els teixits normals de la protuberància, fent impossible la seva delimitació. En la seva progressió inexorable segueix unes vies de disseminació característiques en les que hi destaca el fet que no pot difondre's cap avall, on hi ha el bulb raquidi, per la barrera anatòmica que suposa l'encreuament de les fibres que descendeixen cap a la medul·la. El tumor també es dissemina, contiguament, cap al mesencèfal[4], la medul·la i productes cerebel·losos.

---
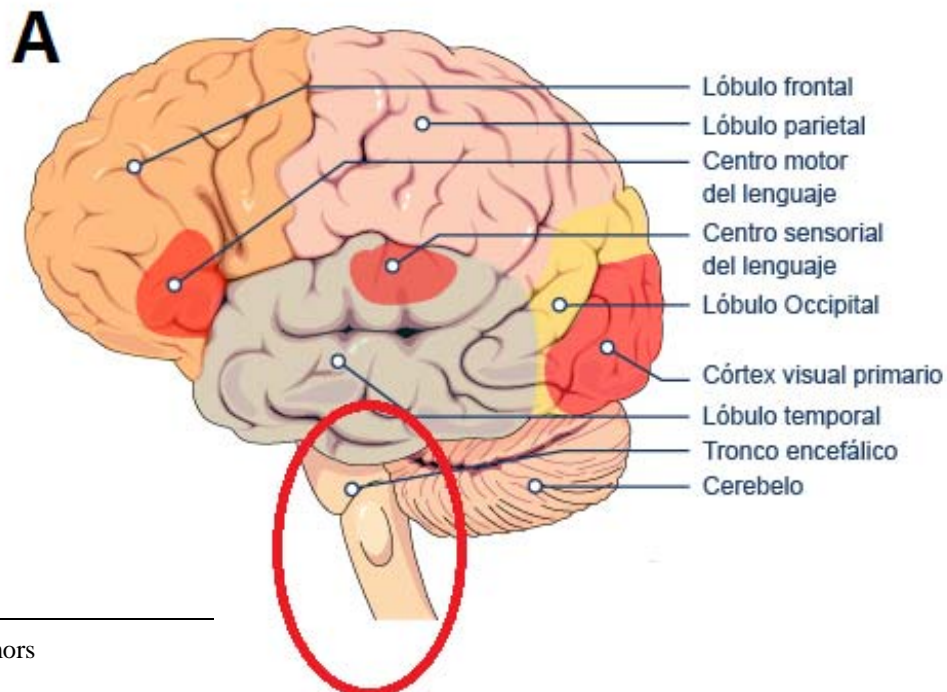
[3] Brainstem tumors

[4] Part superior del tronc de l'encèfal, que comprèn els peduncles cerebrals (anteriorment), la cinta de Reil, els nuclis vermells i els tubercles quadrigeminats (posteriorment). Connecta entre si la protuberància anular, el cerebel i el diencèfal.
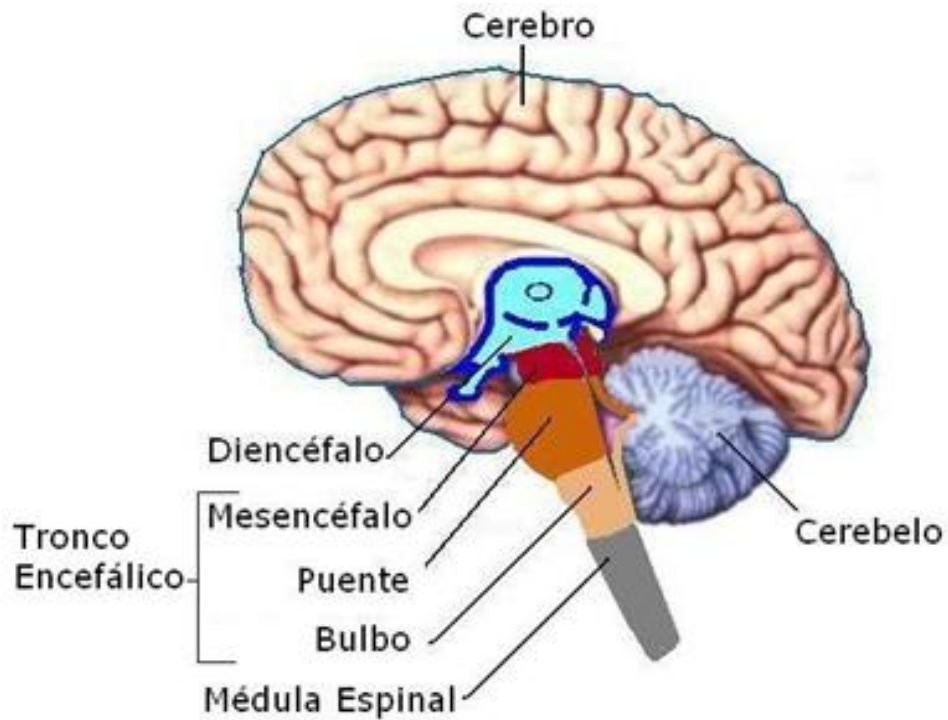
Fig. 1: (A) Anatomia d'un cervell humà sa. Encerclat en vermell, el tronc cerebral. (B) Ampliació del tronc cerebral.

Font: (A) PORTAL DE SALUD Y MEDICINA ONMEDA. Enciclopedia, Anatomía, Anatomía del cerebro, Edtructura del cerebro. *http://www.onmeda.es/enciclopedia/anatomia/anatomia_cerebro-estructura-del-cerebro-1478-2.html.* [Consulta: 10.11.2013].

(B) FACULTAD DE MEDICINA UNIVERSIDAD LA FRONTERA. Apuntes neuroanatomía-UFRO. *http://www.med.ufro.cl/Recursos/neuroanatomia/archivos/1_introduccion.htm.* [Consulta: 10.11.2013]

Les característiques infiltratives i la seva ubicació fan que el DIPG sigui impossible d'eliminar mitjançant cirurgia i alhora dificulta la seva biòpsia. Així doncs, el DIPG es diagnostica habitualment mitjançant una ressonància magnètica (punt aprofundits més endavant).
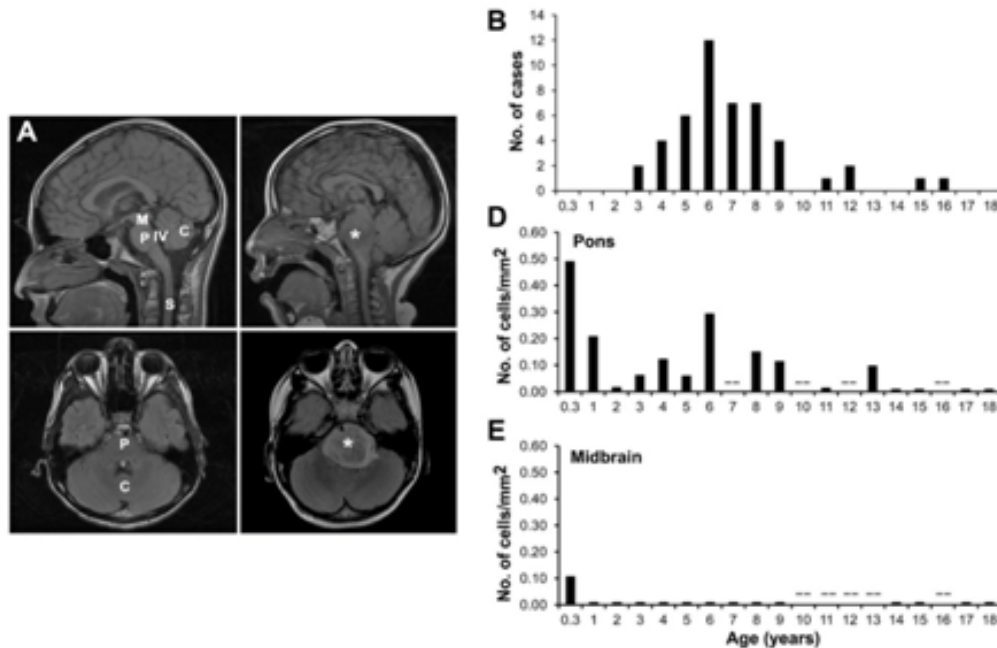
Fig. 2: Distribució espaciotemporal del pons ventral i la incidència del DIPG. (A) MRI sagital i axial mostrant l'anatomia normal d'un cervell (esquerra) i un d'infiltrat amb DIPG. (B) Incidència del DIPG expressat amb l'edat de diagnòstic.

Font: Hedgehog-responsive candidate cell of origin for diffuse intrinsic pontine glioma *(Monje, M., et al. 2011).* [Consulta: 15.05.2013]

2.1.1.1.   Els astròcits

Els astròcits deriven de les cèl·lules encarregades de dirigir la migració de precursors durant el desenvolupament i s'originen en les primeres etapes del desenvolupament del sistema nerviós central (a partir d'ara, SNC).

Estan directament associats tant a les neurones com a la resta de l'organisme. S'encarreguen d'aspectes bàsics pel manteniment de la funció neuronal, enllaçant-se al voltant de la neurona per formar una xarxa, actuant així, com una barrera filtradora entre la sang i la neurona, la barrera

hematoencefàlica[5], que conté regions especialitzades d'alta conductància que controlen el pas de nutrients, oxigen, vitamines i hormones cap al teixit nerviós.
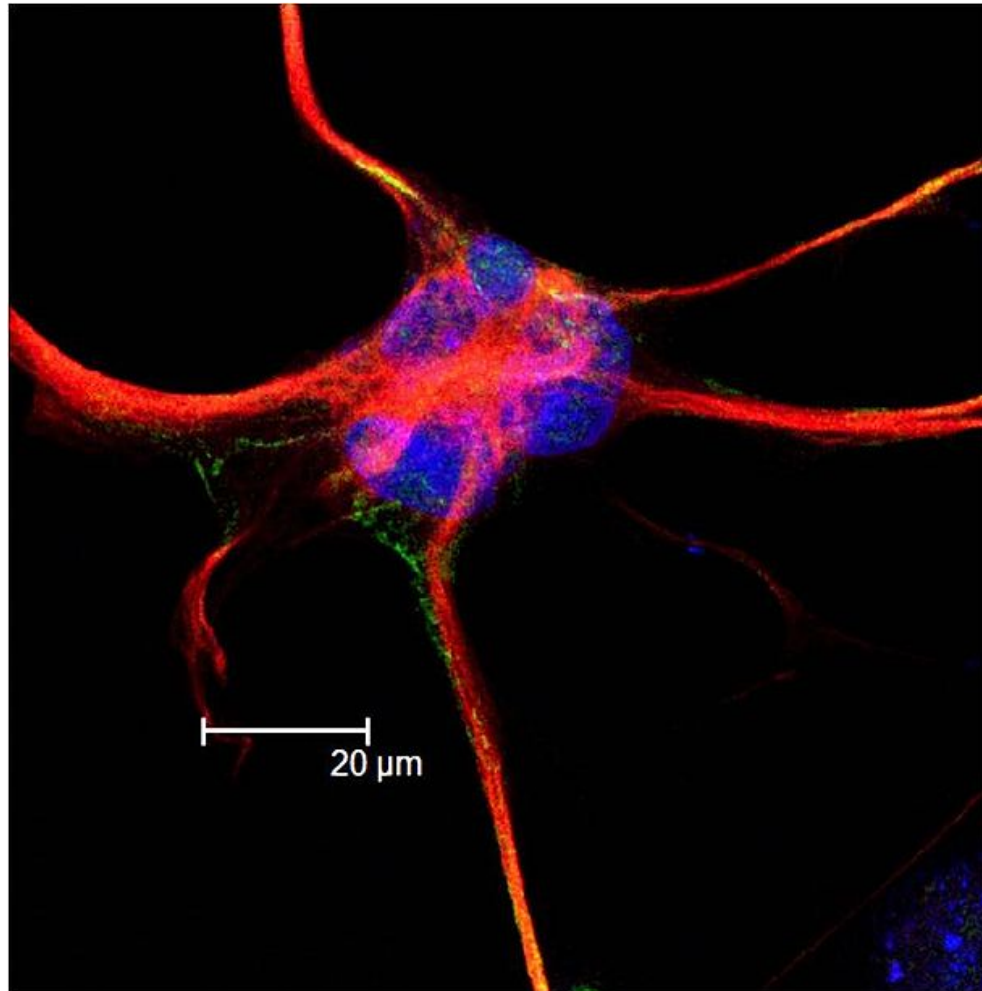
Fig. 3: Astròcit

Font: WIKIPEDIA. Astrocyte.
http://commons.wikimedia.org/wiki/File:Astrocy
tre.jpg [Consulta: 15.05.2013]

---

[5] Barrera hematoencefàlica: barrera entre els vasos sanguinis i el SNC. Impedeix que moltes substàncies tòxiques s'infiltrin al sistema nerviós, a la vegada que permet el pas d'O_2 i nutrients. Si no existís, moltes substàncies nocives arribarien al cervell, alterant el seu funcionament. Les cèl·lules que la componen disposen de proteïnes específiques que transporten activament substàncies nutritives, com ara la glucosa.
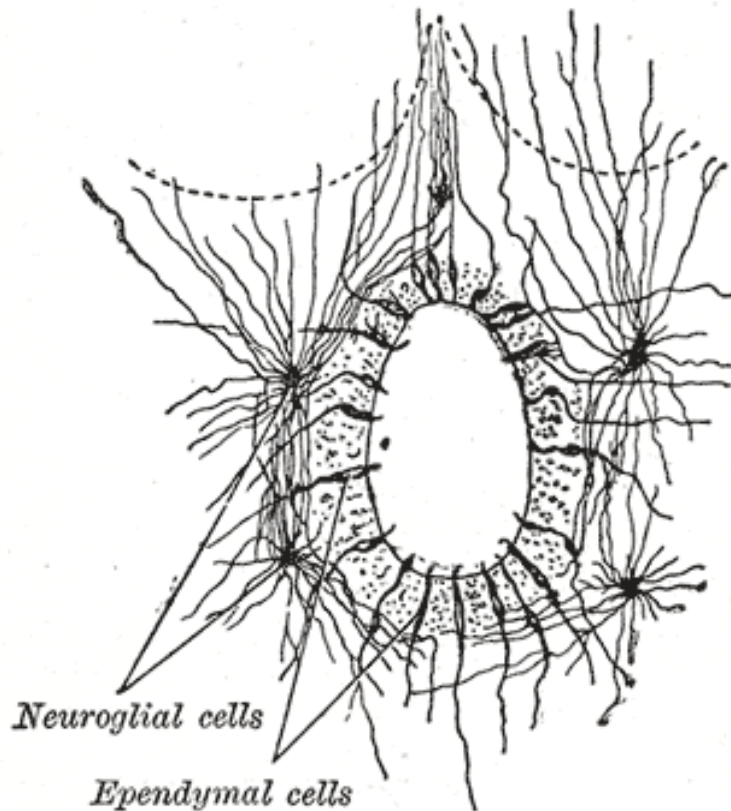
Fig. 4: Cèl·lula glial.

Font: WIKIPEDIA. Célula glial.
*http://upload.wikimedia.org/wikipedia/comm
ons/0/0b/Gray667.png*. [Consulta:
15.05.2013]

Altres funcions que fan són netejar substàncies de rebuig del cervell, mantenir el nivell de pH[6] del SNC i l'equilibri iònic extracel·lular, sostenir les neurones al seu lloc, digerir part de les neurones mortes, regular el contingut de l'espai intercel·lular, unir les neurones als capil·lars sanguinis, participar en els processos de regeneració del teixit nerviós, implicar-se en la regulació de la funció vascular i també amb els processos de neurogènesi del SNC, actuant com a precursors neutrals.

Quan els astròcits perden la capacitat de morir-se per tal de deixar espai a les cèl·lules filles, és quan parlem de cèl·lules tumorals. Aquests provenen

---

[6] El pH és una mesura quantitativa de l'acidesa o basicitat d'una dissolució, que és donada per l'activitat dels cations hidroni, H_3O^+, en dissolució.

de les cèl·lules mare del sistema nerviós, que alhora donen lloc a les neurones i a les oligodendrites.

Quan aquestes *stem cells*[7] no es troben diferenciades, en un medi de cultiu especial, formen unes estructures anomenades neurosferes, que són agrupacions de cèl·lules procedents de la mitosi d'una mateixa cèl·lula mare. Cada cèl·lula mare es divideix successivament donant lloc a una altra cèl·lula mare i a una cèl·lula normal i corrent. Alhora, aquestes últimes es divideixen en dues cèl·lules filles també sense capacitat d'*stem cell*.
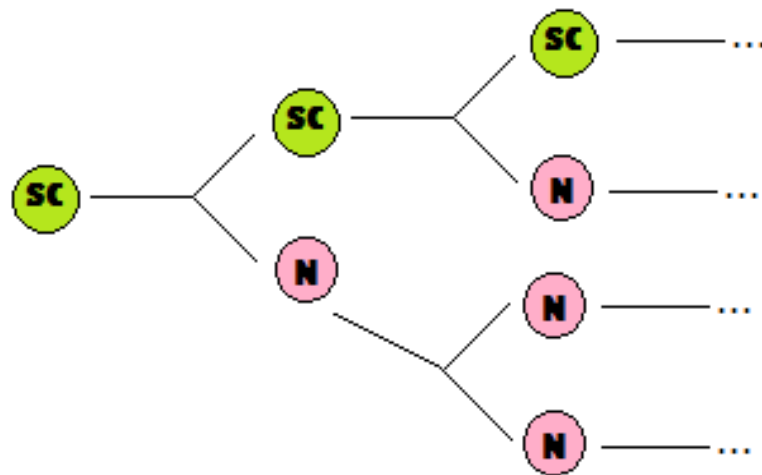
Fig. 5: Reproducció per mitosi d'una *stem cell* del sistema nerviós. El conjunt forma una neurosfera.

Font: Pròpia.

2.1.2. Simptomatologia

Els símptomes i limitacions dels pacients afectats per aquesta malaltia varien i evolucionen en funció dels parells cranials i el nombre de fibres nervioses afectades pel creixement del tumor.

No obstant, solen ser comuns els problemes de coordinació, equilibri, dificultats o incapacitat de caminar, moviment de braços i/o de mans,

---

[7] Cel·lules mare, en anglès.

paralització dels músculs facials, i en últim extrem, incapacitat de parlar o empassar qualsevol tipus d'aliment, ja sigui sòlid o líquid. També es pot incloure un moviment limitat o anormal de l'ull, somriur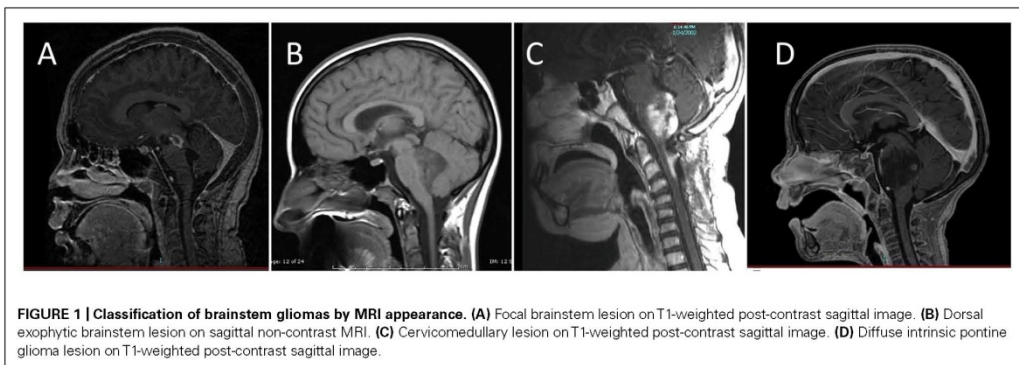e asimètric, debilitat, dificultats escolars i terrors nocturns sobtats, diplopia (visió doble) i atàxia (descoordinació en el moviment). Aquesta simptomatologia apareix quan la malaltia està en un estadi molt avançat, ja que les cèl·lules tumorals han infiltrat bona part del cervell, com ara el cerebel[8], responsable de l'equilibri i de les vies motores de l'organisme, o bé el pons cerebral, que conté nuclis de nervis cranials, alguns d'ells crítics (necessaris) per la vida.

2.1.3. Diagnòstic

El DIPG es diagnostica mitjançant escàners i altres proves radiològiques, com ara ressonàncies magnètiques, que en aquest cas particular són les més efectives gràcies a la seva gran sensibilitat.

Les ressonàncies magnètiques (a partir d'ara, MRI[9]) han permès classificar els tumors de tronc cerebral segons les característiques d'imatge (*Epstein and Farmer, 1993*).

1

FIGURE 1 | Classification of brainstem gliomas by MRI appearance. (A) Focal brainstem lesion on T1-weighted post-contrast sagittal image. **(B)** Dorsal exophytic brainstem lesion on sagittal non-contrast MRI. **(C)** Cervicomedullary lesion on T1-weighted post-contrast sagittal image. **(D)** Diffuse intrinsic pontine glioma lesion on T1-weighted post-contrast sagittal image.
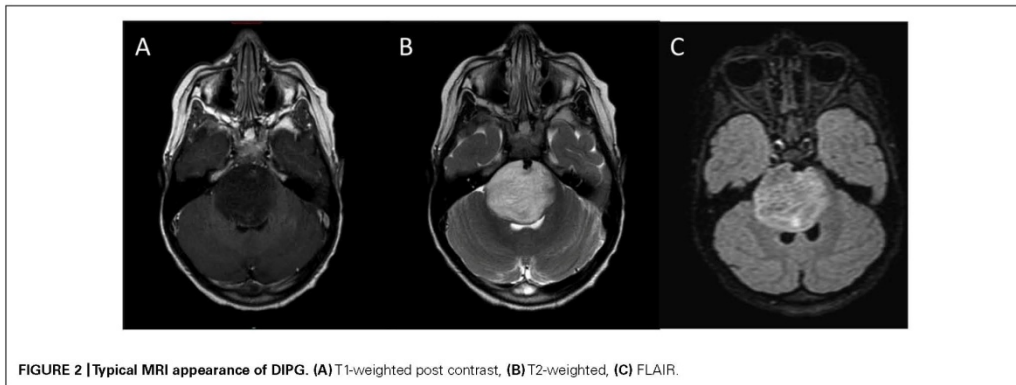
---

[8] El cerebel processa informació provinent d' altres àrees del cervell, de la medul·la espinal i dels receptors sensorials amb l'objectiu d'indicar el temps exacte necessari per realitzar moviments coordinats i suaus del sistema muscular esquelètic.

[9] Magnetic Resonance Imaging

2

FIGURE 2 | **Typical MRI appearance of DIPG. (A)** T1-weighted post contrast, **(B)** T2-weighted, **(C)** FLAIR.

Fig. 6: (1) Classificació dels gliomes segons la seva aparença a la MRI. La última imatge correspon a un DIPG. (2) Aparença típica del DIPG en una MRI.

Font: Diffuse intrinsic pontine glioma: poised for progress *(Warren, K.E., et al. 2012).* [Consulta: 15.05.2013]

A l'MRI, el DIPG apareix com una gran massa expansiva amb origen al tronc cerebral. Algunes altres característiques del DIPG en aquesta prova inclouen l'afectació ventral del pons cerebral i el recobriment de l'artèria basilar[10]. També podem observar-hi un increment de la densitat dels vasos sanguinis, com també un augment en la seva permeabilitat. Un augment del corrent sanguini en una regió d'"interès" pot ser indicatiu d'un increment del creixement vascular, associat amb el grau tumoral, o a la seva transformació en tumor maligne.

Tot i que l'MRI no és 100% específica, la majoria dels pacients diagnosticats de DIPG mitjançant aquesta tècnica presenten realment la lesió. Per tal de confirmar el diagnòstic, es fa una biòpsia, que consisteix a extreure part del teixit afectat i observar, al laboratori d'anatomia patològica, que conté cèl·lules tumorals. Aquest procés es basa en introduir les coordenades del lloc d'on es pretén obtenir la mostra a un programa informàtic. Això permet que una "agulla-pinça" d'entre un i dos mil·límetres de diàmetre accedeixi al focus principal del tumor i n'obtingui teixit (els processats de la biòpsia s'explicaran detalladament més endavant: al punt *3.1.*).

---

[10] Artèria que s'origina en la unió de las artèries vertebrals dreta i esquerra i que proporciona sang oxigenada al cervell.

En aquest cas, les biòpsies són relativament difícils d'obtenir, degut al complicat accés a l'epicentre tumoral, posicionat en un lloc de difícil aproximació. És per aquest motiu que solen obtenir-se de l'àrea més accessible, que pot no ser representativa de la totalitat de la lesió, ja que presenten variabilitat segons la zona d'on s'obté la mostra (veure annex 3: *Warren et al., 2011c*).

2.1.4.   Tractaments actuals

Els tractaments actuals es basen en els utilitzats en els gliomes adults, ja que la biologia d'aquest tumor era considerada, fins fa poc, semblant a la del DIPG. No obstant aquesta proposta està bastant refutada dins la comunitat científica, ja que s'ha descobert que els DIPGs tenen la seva pròpia identitat.

Actualment, doncs, no hi ha cap tractament efectiu contra el DIPG i cal destacar que fins i tot en alguns centres recomanen no iniciar cap tipus de cura pels pacients. Tot i així s'està aconseguint, gràcies a alguns tractaments com ara la quimioteràpia i la radioteràpia (citats al punt *2.1.1.)*, millorar tant la qualitat de vida dels pacients, com intentar reduir els símptomes que la malaltia provoca.

Hi ha dos tipus de tractament: el d'abans i el de després de *l'estat bombolla* (més detall al punt *2.1.1.*).

El tractament que actualment és més utilitzat abans d'aquest període és la radioteràpia[11] combinada, en alguns centres sanitaris (mai a l'Hospital Sant Joan de Déu de Barcelona), amb un tipus de quimioteràpia oral anomenada Temozolamida (4-methyl-5-oxo- 2,3,4,6,8-pentazabicyclo [4.3.0] nona-2,7,9-triene- 9-carboxamide). La Temozolamida és un radio-sensibilitzador que té com a objectiu potenciar els efectes de la radioteràpia i aconseguir que aquesta sigui més efectiva. Una vegada finalitzada la radioteràpia, es segueix subministrant mensualment, com a manteniment. No obstant això, no existeix

---

[11] Dosis total=54-60 Gy (Gray), administrada durant 6 setmanes diàriament, en fraccions de 180-200 cGY

una evidència científica sòlida que demostri que la Temozolamida millori el pronòstic dels pacients amb DIPG, ni tampoc en altres tipus de tumors cerebrals.

Alternativament, a l'Hospital Sant Joan de Déu de Barcelona, els pacients amb DIPG reben un tractament quimioteràpic experimental amb Irinotecan i Cisplatí, prèviament a la radioteràpia. L'activitat d'aquest tractament experimental, actiu contra altres tumors cerebrals infantils, encara no s'ha pogut demostrar fefaentment a DIPG. La manca d'activitat dels tractaments de quimioteràpia en DIPG sembla ser deguda a la impermeabilitat de la barrera hematoencefàlica davant de molècules no específiques per la nutrició o la fisiologia de les cèl·lules del cervell, com a els fàrmacs subministrats, que són de naturalesa "estranya" (xenobiòtics) per al cervell. Així, la barrera hematoencefàlica els impedeix entrar des de la sang al parènquima (teixit que fa funcional l'òrgan en qüestió).

Amb aquest tractament de radioteràpia, la gran majoria dels pacients (75%) milloren en quant a simptomatologia i s'aconsegueix allargar l'esperança de vida (de mitjana) uns tres mesos (*Haas-Kogan et al., 2011*). No obstant, al cap de sis o nou mesos, com s'ha citat al punt *2.1.1.*, el tumor progressa de nou i els símptomes tornen a aparèixer en més del 90% dels casos.

Aquesta recaiguda podria ser deguda a l'evolució natural (i bastant desconeguda) del tumor, la malignitat del qual augmenta després d'adquirir resistència a la radioteràpia.

Un cop es confirma que el tumor torna a progressar, els diferents tractaments varien molt segons l'hospital, el país, l'especialista i el seu grau d'especialització. Una de les propostes és seguir administrant nous fàrmacs o combinacions de quimioteràpia per tal d'intentar reestabilitzar el tumor.

L'ús d'esteroides[12] com a tractament d'aquesta malaltia és ja un fet acceptat pels professionals. Com més avança el tumor, hi ha més pressió intracranial deguda al bloqueig dels canals de circulació del líquid cefaloraquidi (a vegades també a causa de la radioteràpia, que sol inflamar la zona on s'aplica gairebé en la totalitat dels casos). Això provoca un intens dolor, que es veu pal·liat pels afectes d'aquest tipus de cortisona. La part negativa d'aquest tractament és que un ús prolongat pot provocar un augment de pes, propensió a les infeccions, canvis de caràcter… És per això que es limita el seu ús tant com sigui possible.

Sempre hi ha l'opció d'utilitzar teràpies alternatives com a últim recurs davant de famílies desesperades. Actualment, també s'estan duent a terme diferents assajos clínics (veure annex 9) amb l'objectiu de trobar un tractament efectiu per al DIPG.

2.1.4.1. Radioteràpia

La radioteràpia consisteix en la utilització de rajos d'alta energia per destruir o reduir les cèl·lules tumorals d'una zona específicament delimitada, interferint en el seu creixement. Trobem també la tipologia loco-regional, si s'hi inclouen els ganglis propers al tumor. En conclusió, podem dir que tracta el tumor al seu lloc d'origen. Sol ser específica per a cada pacient i el tipus del càncer que pateix.

---

[12] S'administra cortisol, un tipus d'esteroides produïts de forma natural pel propi organisme. Sovint s'administra una versió sintètica d'aquesta molècula (cortisona, hidrocortisona, prednisona, metilprednisolona, dexametasona...) . Contribueixen al tractament de diverses maneres, com per exemple reduint nàusees, formant part de la quimioteràpia, reduint la inflamació causada per la radioteràpia i les reaccions al·lèrgiques en cas de transfusió, disminuint el dolor causat per tumors cerebrals…

L'aparell que s'usa en aquest tractament és l'anomenat accelerador lineal (a partir d'ara, LINAC).

Fig. 7: Aparell de radioteràpia, LINAC

Font: IONACTIVE CONSULTING. Linac. *http://www.ionactive.co.uk/blog.html?page=2.*
[Consulta: 10.11.2013]

Aquesta màquina subministra raigs X d'alta energia a la regió on es troba el tumor del pacient. Aquests tractaments estan dissenyats de manera que no es destrueixin els teixits sans circumdants. El LINAC utilitza tecnologia de microones per tal d'accelerar els electrons i després permetre que aquests xoquin contra un blanc de metall pesat. Com a resultat d'aquests xocs, es produeixen els raigs X d'alta energia. Aquests són modelats en abandonar la màquina per formar un feix que s'assembli a la forma de la lesió a la qual es dirigeix. El feix surt d'una part de l'accelerador anomenat *gantry* (veure glossari), que pot ser rotada al voltant del pacient. Alhora, la butaca de tractament on està estirat el pacient (s'utilitzen uns rajos làser per assegurar que aquest està en la posició correcta) es pot moure en diferents direccions. Així doncs, la radiació es pot subministrar des de qualsevol angle fent girar el *gantry* i movent la butaca de tractament.

La radioteràpia s'empra com a tractament únic o en combinació amb altres teràpies, abans o després d'aquestes (com la cirurgia o la quimioteràpia) amb el propòsit de reduir la mida del tumor abans que sigui operat i/o destruir les cèl·lules tumorals que encara restin vives.

Hi ha diferents tipus de radioteràpia:

- *Externa:* La radiació s'administra des de l'exterior del cos mitjançant una màquina anomenada accelerador lineal. L'accelerador emet la radiació específicament sobre el lloc on es vol aplicar el tractament. Per aconseguir-ho, la màquina pot fer diversos moviments durant la sessió de tractament. S'aplica diàriament (cinc dies a la setmana) de forma ambulatòria, durant diverses setmanes.

- *Braquiteràpia:* També anomenada radioteràpia interna. Consisteix en l'administració de la radiació a través de materials radioactius especials (radioisòtops), anomenats "llavors" o "fonts", que es dipositen a prop o dins del tumor. S'utilitzen normalment agulles, fils, etc.

- *Radioteràpia d'intensitat modulada (IMRT):* És una tècnica que permet administrar altes dosis de radiació sobre una zona específica, i així reduir l'afectació dels teixits del voltant. Segons els casos, aquesta tècnica pot substituir la radioteràpia externa convencional.

Aquest tractament pot fer aparèixer efectes secundaris, ja que tot i estar dirigida a les cèl·lules tumorals, sovint afecta els teixits propers, tot i que en menor intensitat. Segons la zona del cos irradiada, els efectes secundaris són diferents. Els més comuns són: fatiga o cansament, pèrdua del pèl a la zona irradiada, alteracions locals de la pell (més seca, sensible o envermellida)... No obstant, solen ser temporals i controlables. Cal tenir molt clar, però, que el fet de que aquests apareguin, no significa necessàriament que el tractament estigui essent efectiu.

2.1.4.2. Quimioteràpia

Juntament amb la hormonoteràpia i les teràpies biològiques (veure glossari) la quimioteràpia s'empra per curar[13] el càncer (funció curativa) o per millorar la qualitat de vida en els casos en què la curació completa no és possible i cal conviure amb la malaltia (funció pal·liativa).

La quimioteràpia actua sobre les cèl·lules que es divideixen ràpidament, com és el cas de les cèl·lules canceroses, però també en algunes cèl·lules sanes. Per a alguns tipus de càncer, com ara el DIPG, es fa servir només un medicament, per a d'altres com ara el càncer d'ovaris se'n combinen diversos.

La quimioteràpia s'administra de diferents formes:

- *Intravenosa:* és el mètode més comú. El medicament s'administra directament a través de la vena. En alguns casos es posa un catèter en una de les venes de més calibre, més ampla, i es deixa fix connectat a un disc sota la pell. Això permet que cada vegada que calgui administrar la quimioteràpia es connecti directament el tractament mitjançant el disc. Aquest catèter es coneix com *port-a-cath*[14]. També hi ha un altre tipus de catèter que es deixa posat, però en aquest cas la connexió és externa.

- *Oral:* els medicaments són administrats en forma de píndola, càpsula o líquid.

La quimioteràpia s'aplica en períodes de temps d'entre quatre i sis mesos aproximadament, en intervals de dies, setmanes o mesos, també anomenats

---

[13] El càncer es considera curat quan no hi ha evidències de presencia de cèl·lules tumorals a l'organisme del pacient

[14] Un Port-a-cath és un dispositiu que proporciona un accés venós permanent, és a dir, permet l'accés repetit al sistema vascular, facilitant tant l'extracció de mostres de sang com l'administració de medicacions, nutrients, productes sanguinis, etc reduint les molèsties associades a les puncions repetides o la incomoditat d'un catèter extern.

cicles. Cada cicle es compon de dos períodes: quan es rep el tractament i el temps de recuperació abans d'iniciar el següent cicle.

En general, la freqüència de la quimioteràpia depèn de diversos factors com són el tipus de càncer, el tipus de quimioteràpia utilitzada, la resposta del tumor al tractament i el nivell de l'estat general de salut amb el tractament.

Igualment que en la radioteràpia, es produeixen efectes secundaris en alguns pacients, tot i que amb menys freqüència. La majoria d'ells són temporals i controlables. El fet que apareguin alguns efectes secundaris no implica que hagin d'aparèixer tots ni que siguin un signe del funcionament del tractament.

Els més comuns són els següents:

- Fatiga o cansament
- Pèrdua del cabell o canvi de color i consistència.
    - Disminució del nivell de cèl·lules de la sang (glòbuls vermells[15], glòbuls blancs[16] i plaquetes[17]) que pot provocar un augment del risc d'infeccions hematomes o sagnat. Aquest fet també pot provocar feblesa o cansament.
- Nàusees i vòmits, pèrdua de gana, diarrea, estrenyiment, alteració de la mucosa de la boca...
- Canvis en el cicle menstrual, en les dones

- Esterilitat en alguns casos

Depenent del moment del tractament en què s'administra, la quimioteràpia pot ser de diferents tipus:

- *Quimioteràpia d'inducció o neoadjuvant:* la quimioteràpia s'administra abans de qualsevol altre tractament. Amb això es pretén disminuir la

---

[15] La seva disminució pot provocar anèmia
[16] La seva disminució pot provocar neutropènia: risc de tenir infecció per baixada de defenses
[17] La seva disminució pot provocar trombocitopènia, risc de sagnats o hematomes

mida del tumor, permetent que es realitzin després, tractaments menys agressius i reduir el risc de recaiguda. D'altra banda també es positiu des del punt de vista d'eliminar petites metàstasis[18] detectades prematurament.

- *Quimioteràpia concomitant:* s'administra de forma simultània a la radioteràpia. Es pretén augmentar l'eficàcia terapèutica.

- *Quimioteràpia adjuvant o complementaria a un altre tractament:* és generalment local i pretén reduir el risc de recaiguda.

2.2. El *Rotarod*

2.2.1.   Antecedents

La prova de *Rotarod* CITI s'utilitza per avaluar l'efecte dels fàrmacs sobre la coordinació motora o resistència a la fatiga en ratolins i rates utilitzant una unitat d'una manera segura i ètica.

A causa de la preocupació pel deteriorament del comportament motor humà per l'ús de medicaments receptats, la prova *Rotarod* s'utilitza amb freqüència en les primeres etapes del desenvolupament de fàrmacs, per tal de detectar precoçment problemes i/o efectes secundaris que aquest puguin causar, i que podrien no ser detectats en humans fins molt més endavant.

El *Rotarod*, alhora, proporciona una manera fàcil de provar l'activitat motora en rosegadors. L'administració de drogues, els efectes dels danys o la fatiga del SNC sobre la coordinació motora poden ser determinants mesurant el temps durant el qual l'animal es manté sobre un rodet que gira. Així doncs s'ha convertit en un indicador sensible de traumes induïts per lesions cerebrals en animals de laboratori.

---

[18] Cèl·lules tumorals que hagin pogut emigrar a altres òrgans del cos

També s'ha utilitzat per avaluar els efectes de malalties neurodegeneratives en ratolins, com podria ser la malaltia de Pàrkinson, l'ELA[19] o també per l'Esclerosi Múltiple (EM).
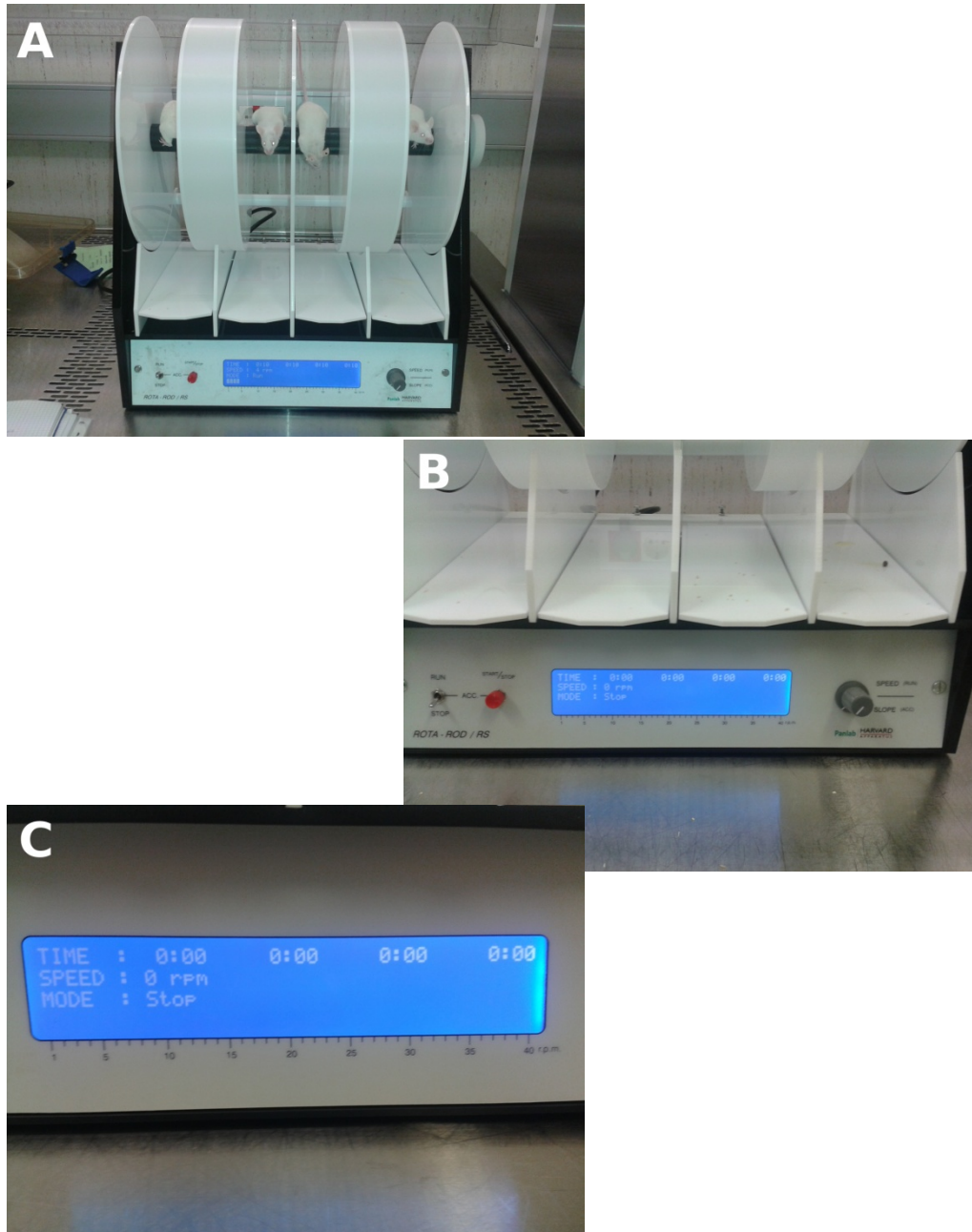
Fig. 8: *Rotarod.* (A)*Rotarod* en funcionament durant l'assaig. (B)Panell de control del *Rotarod.* (C)Pantalla de presa de dades.

Font: Pròpia

---

[19] Esclerosi Lateral Amiotròfica

2.2.2. Funcionament

L'aparell té unes mides de 362 x 240 x 400 mm.

Els animals es col·loquen a la bateria de textura per evitar que rellisquin. Quan un animal cau sobre una de les plataformes amb sensors, els resultats dels assaigs es registren digitalment i es mostren en el panell frontal.

Aquesta prova té la capacitat per avaluar els canvis de mobilitat de fins a cinc animals (depenent del model de l'aparell) en un estàndard de temps. Així doncs, l'usuari pot seleccionar d'un a cinc carrils que s'han d'incloure en un experiment.

En experiments amb ratolins els tambors fan 3,175cm de diàmetre, mentre que si l'experiment es fa amb rates, els tambors fan 9,525cm de diàmetre.

La pantalla LED mostra els resultats de la prova per a cada posició dels animals, que són:

- Aturar rpm[20]
- Durada de la prova
- Distància recorreguda

Aquest aparell permet regular la velocitat (de 4 a 11 rpm), si es vol avaluar la prova a velocitat constant, o bé l'acceleració, regulant el temps (30 segons, 1 minut, 2 minuts, 3 minuts o 10 min) i la velocitat màxima a la què es vol arribar si es pretén que hi hagi un augment de velocitat.

Els paràmetres que aquest aparell avalua és tant el temps que l'animal triga a caure, com la velocitat que l'aparell portava quan ha caigut.

---

[20] Revolucions per minut

2.3. Els animals

2.3.1.   La immunodeficiència

La immunodeficiència és un estat patològic en el qual el sistema immunitari és incapaç de desenvolupar una resposta immunològica adequada davant la presència d'un antigen estrany (virus, bacteris i fins i tot cèl·lules cancerígenes) i per tant aquest no és eliminat del cos. Aquest fet és molt important quan es tracta de microorganismes invasors perquè l' organisme és vulnerable i pot patir infeccions recurrents més o menys greus segons el grau d'immunodeficiència.

Les immunodeficiències poden ser degudes a la manca de maduració dels limfòcits B i T i també a defectes dels mecanismes efectors tant de l'immunitat innata com immunitat específica

Hi ha diferents tipus d'immunodeficiències:

- *Defectes dels limfòcits T :* Els limfòcits T, també anomenats cèl·lules T, s'activen quan el receptor T és activat pels limfòcits B. Són cèl·lules centrals en la funció i regulació del sistema immunitari adaptatiu i/o cel·lular dels vertebrats. La seva funció és atacar i destruir cèl·lules pròpies tumorals o infectades. A més de tenir funcions directes, com la citotoxicitat o la citòlisi, regulen el funcionament del seu propi llinatge i el d'altres mitjançant contactes cel·lulars i mediadors solubles, denominats citocines. Els limfòcits T que provenen de les cèl·lules mare s'originen a la medul·la òssia i d'allà passen al tim, on maduren. És per aquesta raó, que se'ls anomena limfòcits T.

- *Defectes dels limfòcits B:* Els limfòcits B són limfòcits que tenen un paper important en la resposta immunitària humoral (veure glossari). Les funcions   principals   dels   limfòcits   B   són

fabricar anticossos contra antígens, funcionar com a cèl·lules presentadores d' antigen[21] i eventualment transformar-se en cèl·lules de memòria B després de ser activats per la interacció amb antigen. Els limfòcits B són un component essencial del sistema immunitari adaptatiu.

- *Defectes fagòcits:* Els fagòcits són els glòbuls blancs que protegeixen el cos fagocitant proteïnes alienes nocives, bacteris i cèl·lules mortes o moribundes. Juguen un paper essencial en la defensa contra les infeccions, i en la immunitat posterior. Per consegüent, els fagòcits són vitals a l'hora de combatre les infeccions, així com a l'hora de mantenir els teixits sans mitjançant l'eliminació de cèl·lules mortes i moribundes que han arribat a la fi de la seva vida.

- *Defectes del sistema del complement:* El sistema del complement és una cascada bioquímica que contribueix a eliminar els organismes patògens d'un organisme. És una part del sistema immunitari que no és adaptable i que no canvia al llarg de la vida d'un individu; pertany al sistema immunitari innat.

  El sistema del complement consisteix en una sèrie de petites proteïnes presents a la sang, que normalment circulen com a zimògens (veure glossari). Quan són estimulades per un d'entre diversos senyals, proteases del sistema fragmenten unes proteïnes específiques per a alliberar citocines i iniciar una cascada creixent de fragmentacions addicionals.

  El resultat final d'aquesta cascada d'activació és una amplificació massiva de la resposta i una activació del complex d'atac a la membrana, que mata cèl·lules.

---

[21] Són un grup divers de cèl·lules del sistema immunitari la funció és la de captar, processar i, com el seu nom els indica, presentar molècules antigèniques sobre les seves membranes perquè siguin reconeguts, especialment per limfòcits T.

- *Defectes de les molècules del complex d'histocompatibilitat*: El terme complex d'histocompatibilitat principal (MHC[22]) engloba a un gran grup de glicoproteïnes de membrana altament polimòrfiques, implicades en el reconeixement de l'antigen i més concretament en la presentació de l'antigen. L'acció de l'MHC és essencial en el desenvolupament tant de la resposta immunitària humoral[23] com cel·lular. Aquestes proteïnes tenen un paper cabdal en el sistema immunitari, l'autoimmunitat i l'èxit reproductiu. També en la discriminació entre allò que és propi i allò que és estrany i cal combatre, funció que quan es veu alterada desencadena processos d'autoimmunitat.

    Les proteïnes codificades per l'MHC són expressades a la superfície de les cèl·lules en tots els vertebrats mandibulats i presenten tant antígens propis (fragments peptídics de la pròpia cèl·lula) com antígens aliens (per exemple, fragments de microorganismes invasors) als limfòcits. Aquests reconeixen l'antigen com a estrany i coordinen l'eliminació dels patògens i/o de les cèl·lules infectades o no funcionals.

Els ratolins i rates de laboratori són animals immunodeficients artificialment. Aquest procés es duu a terme per tal de que a l'hora d'inocular-los, el seu sistema no rebutgi i elimini les cèl·lules tumorals que se l'hi han implantat i per què el tumor desitjat es reprodueixi sense problemes.

---

[22] Major Histocompatibility Complex

[23] La immunitat humoral és el principal mecanisme de defensa contra els microorganismes extracel·lulars i les seves toxines.

2.3.2.   Els model utilitzat

Els ratolins *nod-scid* són un excel·lent model de malaltia autoimmune i una eina important per a la dissecció dels mecanismes de tolerància.

Fig. 9: Ratolí *nod-scid*

Font: Pròpia.

Aquesta soca de ratolí presenta una immunodeficiència severa que afecta al normal desenvolupament dels limfòcits T i B. Alhora tenen reduïdes, tant funcionalment com de desenvolupament, les cèl·lules NK[24], macròfags[25] i granulòcits[26]. Paral·lelament a l'envelliment dels animals, un percentatge

---

[24] Tipus de limfòcit citotòxic que constitueix un component principal del sistema immunitari innat. Les cèl·lules NK tenen un paper important en el refús de tumors i cèl·lules infectades per virus.

[25] Cèl·lula amb capacitat immunològica present al teixit conjuntiu.

[26] Un granulòcit és un tipus de cèl·lula de la sang, i més concretament un tipus de leucòcit (glòbul blanc), amb enzims i que es caracteritza per contenir gràduls en el citoplasma i un nucli cel·lular irregular o segmentat. Són els glòbuls blancs considerats com a "no específics" en el sentit que no estan especialitzats en un sol antigen ni generen anticossos específics per a cada patògen.

variable presenta un degoteig en el desenvolupament de limfòcits T i B funcionals.

Desenvolupa diabetis autoimmune espontània, que comparteix moltes similituds amb la diabetis autoimmune en humans, incloent la presència d'anticossos específics de pàncrees, CD4+ (veure glossari) auto reactius i cèl·lules T CD8+ (veure glossari).

Degut a totes aquestes deficiències, els ratolins *Nod-Scid* són altament susceptibles a les infeccions oportunistes víriques i bacterianes.

Durant els últims deu anys, els investigadors han utilitzat una àmplia varietat d'eines per estudiar aquests ratolins. A més, han desenvolupat recentment una sèrie d'intervencions terapèutiques en aquest model animal, que s'han acabat traduint en teràpies humanes.

3. Metodología

Com ja s'ha citat a la introducció d'aquest treball, la recerca en la qual es centra el meu projecte, dins d'una de les línies d'investigació del laboratori d'oncologia de l'Hospital Sant Joan de Déu, encapçalada pel Dr. Angel Montero Carcaboso, es basa en provar l'efectivitat d'un mètode de diagnòstic pioner a nivell mundial en el context del DIPG, que podria permetre un avenç en el temps del diagnòstic d'aquesta malaltia a nivell de laboratori en models animals i que alhora possibilitaria un avenç, també a nivell temporal, en l'inici de possibles nous tractaments probablement augmentant-ne l'efectivitat.

Per dur a terme el meu projecte, la investigació ha estat dividida en tres parts diferenciades: *in vitro*, *in vivo* i proves immunohistoquímiques.

3.1.   In vitro

Durant aquesta part del treball, he après les tècniques bàsiques per fer créixer un cultiu cel·lular a partir de línies ja processades, com també a partir d'una biòpsia.

Cal dir que jo vaig treballar només amb *stem cells* del tumor originat al sistema nerviós, és a dir cèl·lules mare que en diferenciar-se donen lloc a cèl·lules del tumor. Les cèl·lules mare del sistema nerviós, en diferenciar-se, donen lloc a oligodendrites, astròcits i les ja més conegudes neurones (més informació al punt *2.1.1.1.*). Aquest tipus de cèl·lules mare, es troben en forma de neurosfera (més informació *2.1.1.1.*). En els tumors cerebrals es poden seleccionar, de manera similar, cèl·lules mare del tumor, de naturalesa maligna, el creixement de les quals en medis de cultiu especials formen "tumorsferes", que en diferenciar-se forma cèl·lules tumorals d'aparença d'oligodendrites i astròcits, però també de naturalesa maligna.

Per fer créixer el cultiu cel·lular, evitant que les neurosferes es diferenciïn, es cultiven utilitzant uns processos i un medi de cultiu especials.

Quan arriba la biòpsia al laboratori, procedent d'anatomia patològica de l'hospital, després que el diagnòstic clínic del pacient sigui confirmat, el teixit, dipositat en un tub de plàstic estèril i contingut en sèrum fisiològic, s'ha de processar el més ràpid possible, per què les cèl·lules que el componen no es malmetin, en trobar-se fora d'un medi no adient per el seu normal desenvolupament.

No totes les mostres biopsiades es cultivaran al mateix moment en què arriben procedents de l'hospital.

Pel què fa el teixit sòlid, una part es criopreserva (veure glossari). Criopreservant part del teixit ens assegurem que si el teixit processat es contaminés o no creixés de la manera esperada, tenim teixit suficient per poder tornar a començar el procés des del principi.

Posem el teixit en un tub/vial amb PBS (Tampó Fosfat Salí), per tal de netejar la mostra. Centrifuguem el tub/vial durant tres minuts a 300 RCF[27]. Seguidament aspirem el PBS i resuspenem el teixit amb el reactivo per la seva criopreservació, denominat comercialment *synth-a-freeze*. Posem el tub/vial en gel durant una mitja hora; després les col·loquem en un Mr. Frosty, un dispositiu de plàstic que conté una solució d'isopropanol (C_3H_8O) que ens permet reduir un grau centígrad (ºC) cada minut. Aquest fet ens permet congelar la mostra en un congelador a -80ºC. Després de dues setmanes de tenir-lo a aquesta temperatura, hem de traslladar els vials a nitrogen líquid, que es troba a una temperatura de -196ºC.

La resta de teixit sòlid es cultivarà. Per processar-lo, s'hi afegeix un enzim anomenat col·lagenasa, que trenca els enllaços peptídics del col·lagen, una molècula proteica fibrosa i que és la base del teixit conjuntiu, present en gairebé tots els teixits de l'organisme. Aquest procés permet desnaturalitzar el teixit i per tant, ens permet obtenir les cèl·lules i vesícules que el formen. Després d'afegir-hi aquest enzim i de deixar-lo reposar una estona, s'afegeix PBS (tampó fosfat salí) al tub on hi ha el teixit amb l'enzim, per tal de rentar la mostra, ja que la col·lagenasa podria lisar les cèl·lules si l'hi deixéssim massa estona degut a la seva toxicitat. Un cop afegit el PBS centrifuguem la mostra per tal de formar un "pel·let" cel·lular (sediment) i així poder aspirar

---

[27] 1 RCF (Relative Centrifugal Force) = 97 rpm

tota la part líquida (PBS i col·lagenasa). Aquest procés es durà a terme diverses vegades intercalant-lo amb resuspensions cel·lulars mitjançant un pipeteig per assegurar-nos que s'ha fet una bona neteja. Un cop aquest procés està acabat, afegim medi de cultiu (amb factors de creixement específics per cèl·lules mare), que permetrà que totes les cèl·lules diferenciades del cultiu no sobrevisquin, i que per tant, obtinguem un cultiu estrictament de cèl·lules mare.

En el cas de les mostres líquides, el sèrum que conté les mostres biopsiades també es processen, ja que poden contenir cèl·lules del teixit tumoral.
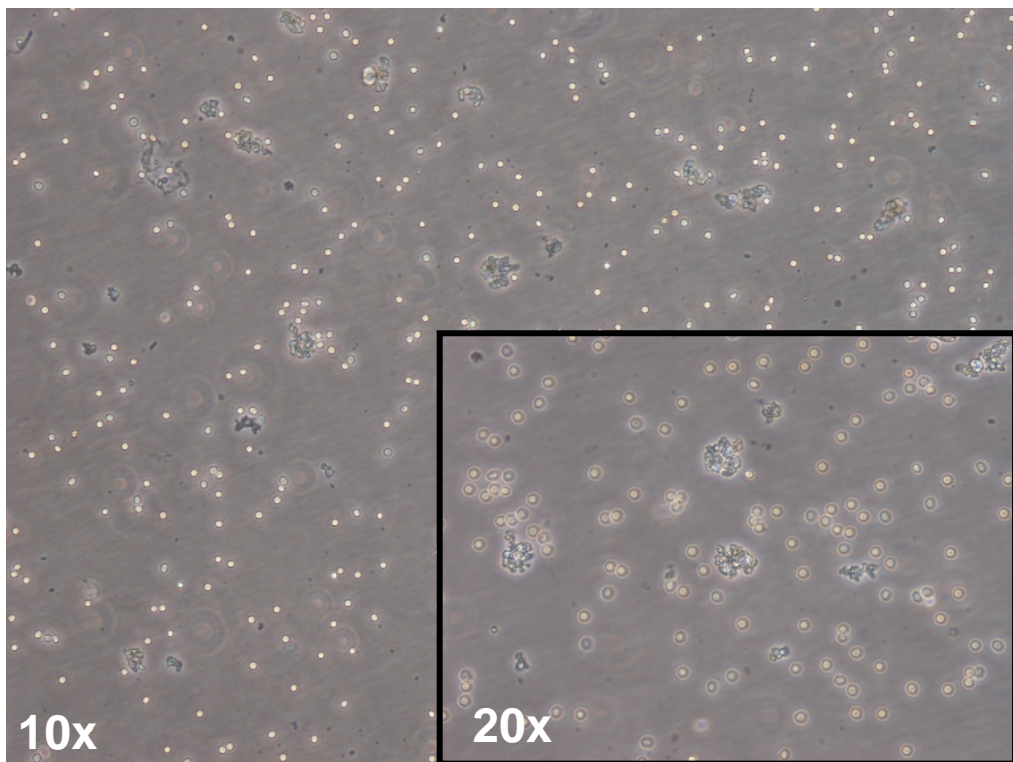

Fig. 10: Processat d'un fragment de teixit biopsiat a l'Hospital Sant Joan de Déu. Primers "passos". Hi podem observar principalment vesícules cerebrals i eritròcits (glòbuls vermells).

Font: Pròpia

Un cop les biòpsies han estat processades i distribuïdes en flascons de cultiu petits, degut a la poca quantitat de cèl·lules mare que hi trobem en un principi, s'ha de fer créixer el cultiu, que permetrà eliminar les cèl·lules i vesícules que no ens interessen i alhora conservar les *stem cells* que hi ha i augmentar-ne el nombre, aconseguint que formin neurosferes cel·lulars.

Per fer créixer el cultiu, doncs, utilitzem un procés denominat de forma comuna *passe*/pas (veure glossari). Aquest procés consisteix en trencar les neurosferes quan aquestes assoleixen una mida bastant gran (en el cas que el cultiu ja estigui bastant avançat), tamany que pot arribar a ser perjudicial pel normal desenvolupament cel·lular, com també en el cas d'obtenir una nova línia cel·lular a partir d'una biòpsia. Normalment es duu a terme cada dues-tres setmanes, depenent de l'evolució del cultiu. En trencar les neurosferes fem possible que el cultiu s'expandeixi, ja que les cèl·lules mare tenen més espai per créixer i reproduir-se.
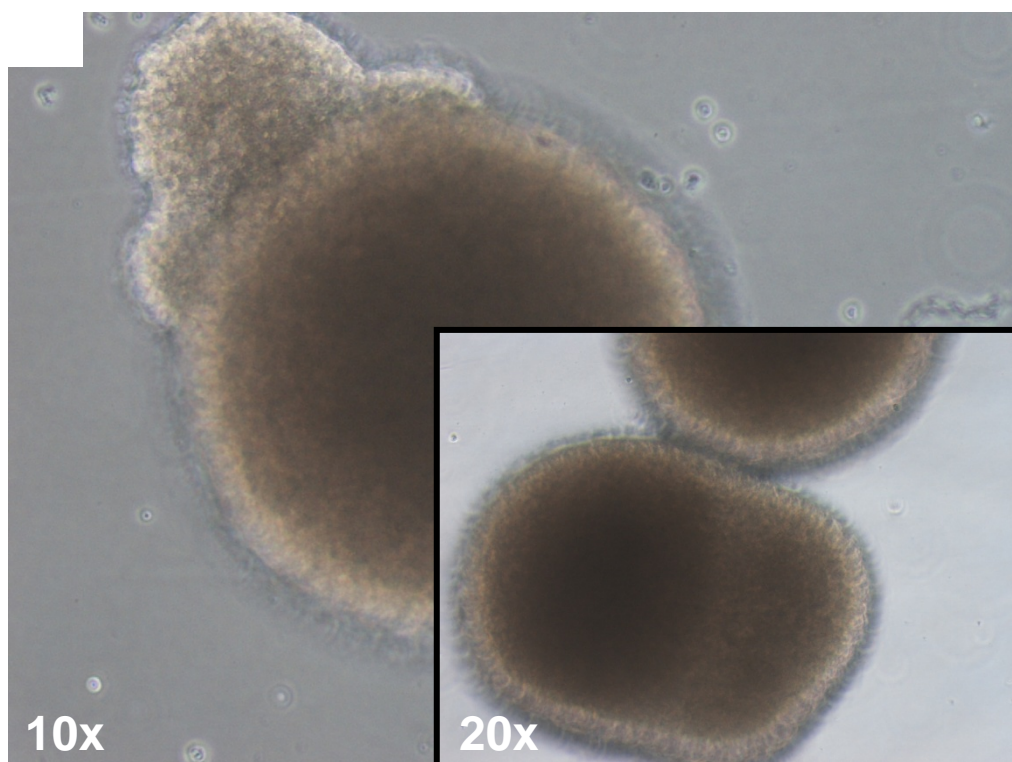
Fig. 11: Neurosferes en un pas avançat. S'aprecien les malformacions que aquestes adopten quan hi ha una presència massiva de cèl·lules, per tant, després de prendre aquestes imatges es va realitzar un pas per evitar possibles problemes de creixement de les *stem cells*.

Font: Pròpia

Aquest procés consisteix en aspirar, mitjançant una pipeta, tot el contingut del flascó de cultiu. A continuació és diposita en un o més tubs de 25mL (segons la quantitat de cultiu que tinguem), que es centrifuguen durant tres minuts a 300 RCF. Seguidament n'aspirem el medi, que substituïm per 3-4mL de TrypLE Expres s[28]. Deixem actuar aquest compost enzimàtic mentre pipetegem el *pel·let* (agregat de cèl·lules) del fons del tub, trencant així les unions de la neurosfera tant químicament com mecànicament. Seguidament hi afegim 10mL TSM (veure glossari) per tal de neutralitzar la toxicitat del TrypLE i tornem a centrifugar el/s tub/s. Aspirem el TSM i el Tryple, i hi afegim part del medi on ja teníem les cèl·lules i la mateixa quantitat de TSM complet (veure glossari) nou. Resuspenem les cèl·lules del *pel·let*, que ja no es trobaran amb forma de neurosfera, i les tornem al flascó de cultiu (indicant sempre el nº de pas i el dia en què aquest procés hagi estat realitzat).

Quan obtenim un gran nombre de neurosferes en un flascó petit, passem el cultiu a un flascó gran, i més endavant, segons els nostres interessos podem dividir el cultiu en dos o més flascons grans.

Per aconseguir un bon desenvolupament cel·lular també utilitzarem el procés de canvi de medi, que repetirem cada cop que el medi que hi ha al flascó canviï de color, ja que significarà que aquest ha perdut les propietats necessàries per nodrir correctament les cèl·lules que conté.

Aquest procés consisteix en aspirar mitjançant una pipeta tot el contingut del flascó, que dipositem en un o més tubs de 25mL. Aquest serà centrifugat durant tres minuts a 300 RCF. Aspirem el medi i el reservem en un tub apart.

Introduïm TSM complet al tub (el mateix volum o 1mL més que el que hem extret al pas anterior) i també la meitat del TSM, també complet, que hem guardat.

En tot moment, els flascons, després de treballar-hi, s'han de guardar en un incubador estèril i humidificat, a 37 ºC i 5% de CO_2.

---

[28] TrypLE ™ Express és un enzim recombinant animal d'origen lliure, utilitzat per dissociar un ı àmplia gamma de cèl·lules adherents de mamífer, inclosos CHO, cèl·lules HEK 293, A529, queratinòcits humans primaris i cèl·lules mare embrionàries. Aquest compost enzimàtic trenca els enllaços peptídics de les cues C-terminal de la lisina i arginina, i és un reemplaçament directe per la tripsina.
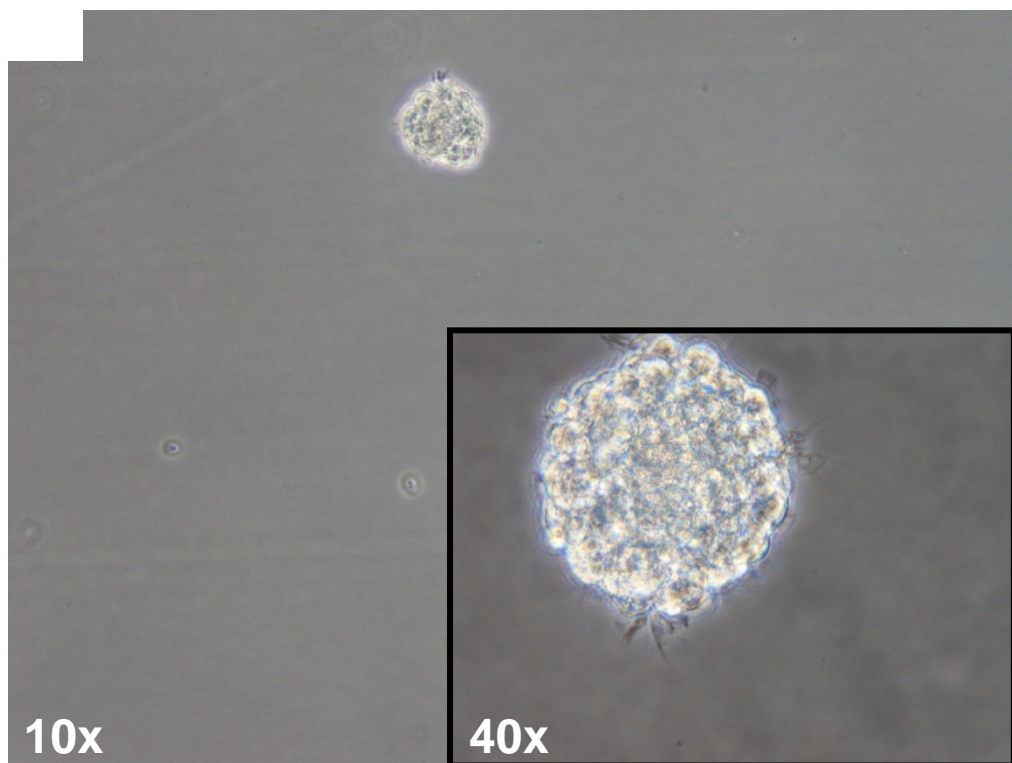
Fig. 12: Neurosfera formada poc temps després d'un pas (s'aprecia en la mida).

Font: Pròpia
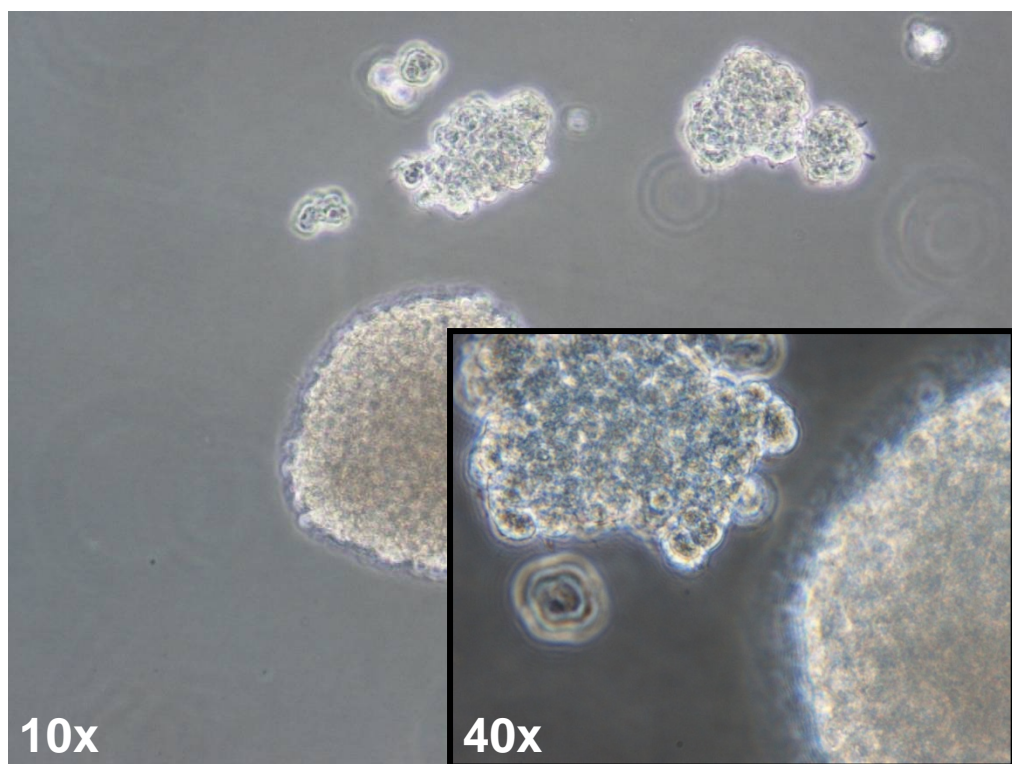
Fig. 13: Cultius avançats de neurosferes procedents de biòpsies de DIPG de pacients de l'hospital.

Font: Pròpia

Un cop les línies cel·lulars contenen un gran nombre de neurosferes, visibles a simple vista, és el moment per inocular els animals.

La quantitat de cèl·lules que s'inoculen es l'estimada per tal de fer créixer un tumor al cervell de l'animal immunodeprimit, en general i aproximadament, mig milió de cèl·lules. El procés de recompte cel·lular (veure annex 8) es fa gràcies a la Càmera de Neubauer (veure glossari).
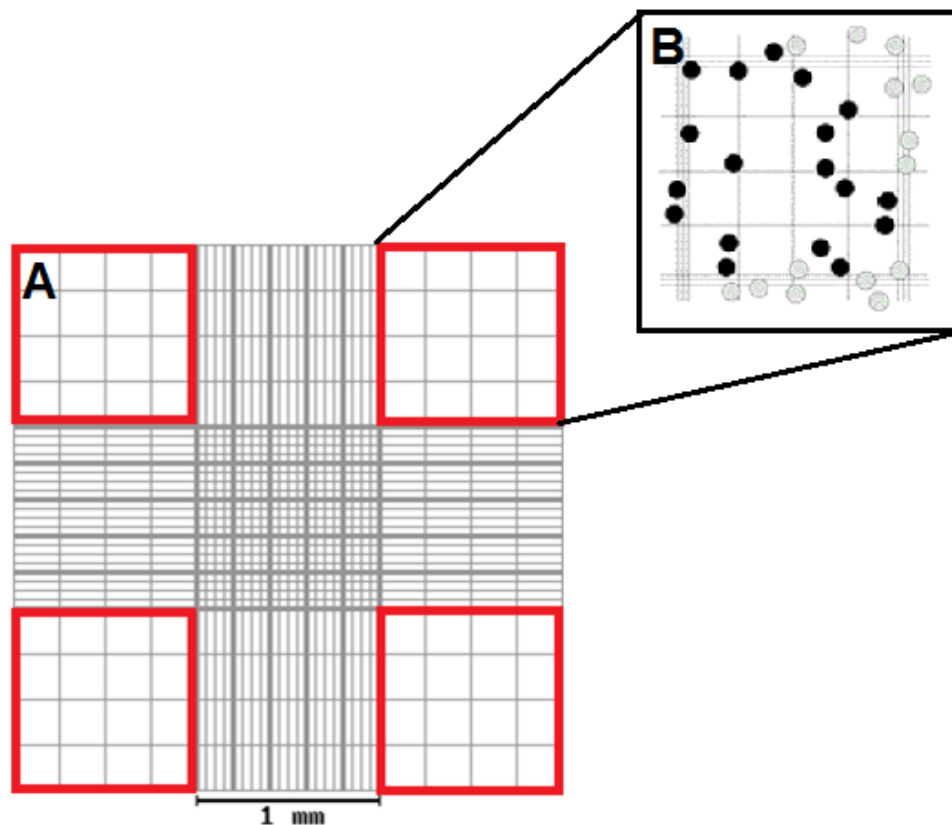
Fig. 14: Càmera de Neubauer. (A) En vermell, els quatre quadrants on comptarem les cèl·lules. (B) Ampliació d'un dels quadrants de recompte amb cèl·lules

Font: *Technical Note - Neubauer Chamber Cell Counting, Oscar Bastidas* (veure annex 8).

Aquest procediment consisteix en realitzar, primer de tot, els mateixos passos que hem utilitzat per expandir el cultiu (procés explicat en el mateix punt: *3.1.*). Un cop hem disgregat les neurosferes i per tant hem obtingut cèl·lules mare soltes en comptes d'afegir-hi medi de cultiu, hi incorporem 1 mL de PBS. D'aquesta dissolució n'agafem 25µL, que posem en un vial d'un mL. Seguidament hi afegim 25µL de Tryptan Blue, i pipetegem les dues solucions

juntes per tal d'homogeneïtzar la mescla, de la qual n'utilitzarem 10µL. Aquests 10µL els dipositarem sobre la quadrícula de la Càmera de Neubauer, que cobrirem amb un cobreobjectes.

El Tryptan Blue té la propietat de tenyir de color blau només les cèl·lules mortes de manera que, a l'hora de comptar, només tindrem en compte les cèl·lules de color blanquinós.

Per facilitar la tasca de comptatge cel·lular ens ajudem d'un comptador de mà. Seguidament, i un cop hem comptat les cèl·lules dels quatre quadrants, passem a realitzar els càlculs corresponents:

$$\frac{n^{\circ}\ \text{cèl·lules comptades}}{4} \cdot 2 \cdot 10^4 = X\ \text{cèl·lules/mL}$$

Mitjana de cèl·lules dels quatre quadrants

Les cèl·lules han estat diluïdes dues vegades (PBS i Tryptan Blue)

Volum total dels quatre quadrants

$$N^{\circ}\ \text{de cèl·lules total que necessitem per inocular els animals (ja establert)} \cdot \frac{1\ \text{mL}}{X\ \text{cèl·lules/mL}} = \text{mL (µL) totals que necessitem del tub on hi ha la resta de cèl·lules per inocular-ne el n}^{\circ}\ \text{desitjat}$$

Quan s'han realitzat els càlculs corresponents, es procedeix a preparar les cèl·lules per la corresponent inoculació (procés que no és competència d'aquest TR).

Seguidament es procedeix a inocular els animals. Per fer-ho s'utilitzen unes coordenades (X, Y i Z) establertes amb l'ajuda d'un atles del cervell del ratolí ("Atles Paxinos") que ens permeten injectar les cèl·lules, disperses en 5 µLs de matrigel (un líquid biocompatible), al punt que a nosaltres ens interessa del cervell dels animals. Aquestes coordenades són confidencials i pertanyen estrictament al grup d'investigació.
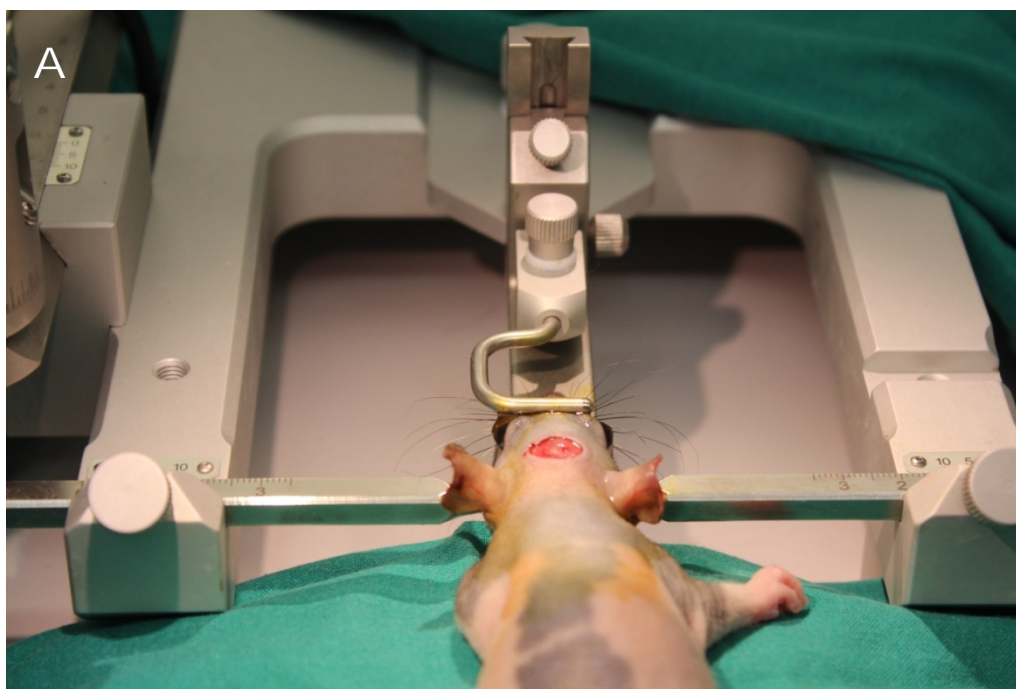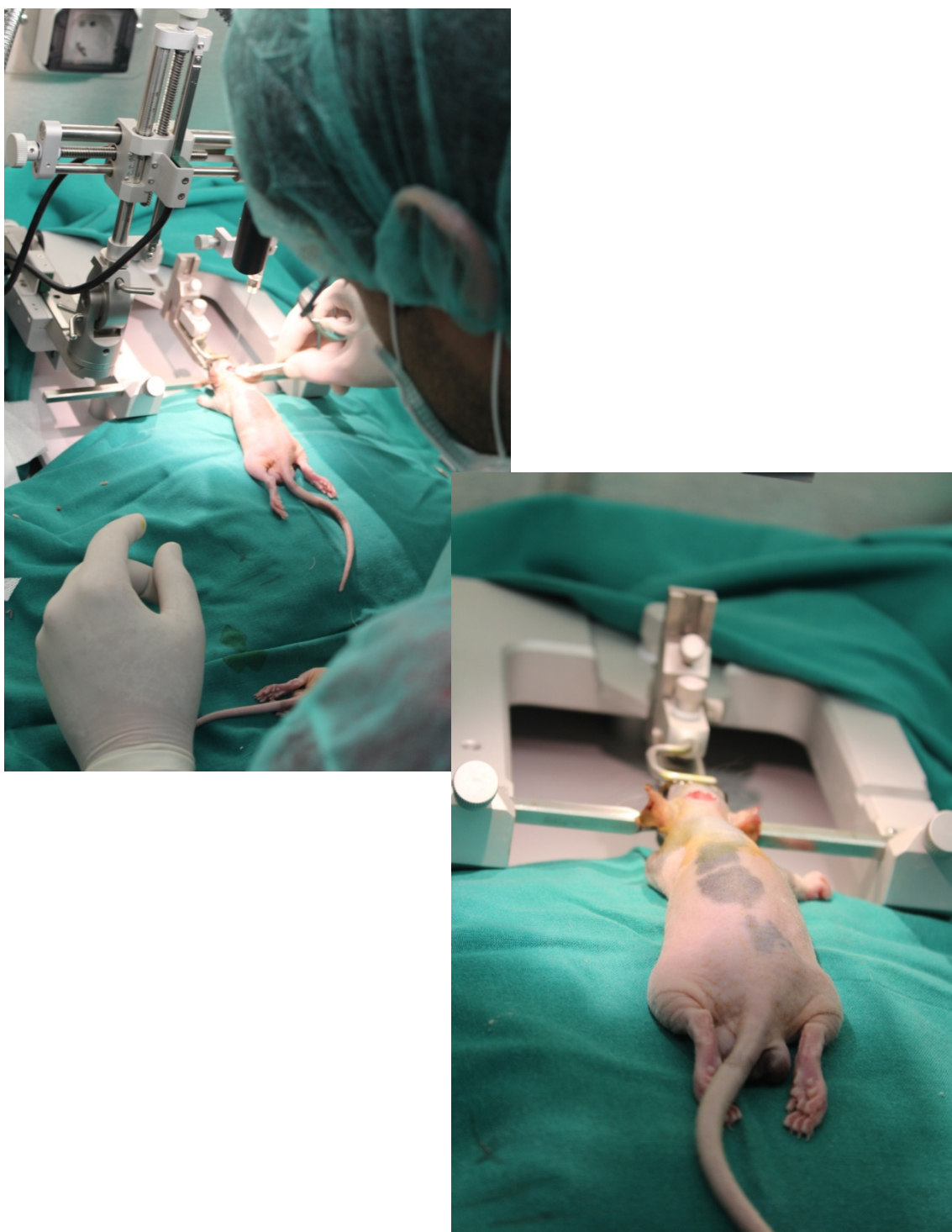
Fig. 15: Operació d'inoculació de les rates; s'empra la mateixa metodologia en ratolins. (A) Incisió cranial prèvia a la inoculació de cèl·lules tumorals. (B) Introducció de les cèl·lules mitjançant una agulla a la que se li han introduït les coordenades X, Y i Z.

Font: Pròpia

3.2.   In vivo

Anteriorment a aquest projecte, s'ha comprovat que els primers símptomes greus i apreciables a simple vista, s'evidencien després d'uns cinc - sis mesos de la inoculació (de forma subjectiva). El meu propòsit és, mitjançant el Rotarod® (definit en el punt *2.2.*), objectivitzar l'aparició de la malaltia molt abans que aquests símptomes apareixin. És per aquest motiu, doncs, que he treballat amb ratolins inoculats uns tres mesos abans que jo arribés a les instal·lacions.

Per aquest treball només s'ha utilitzat una part del total de la població que s'inclouen en l'estudi. Aquesta reducció de població pel meu treball consta de quinze individus, tots inoculats el mateix mes amb cèl·lules procedents de la mateixa línia cel·lular, i per tant, del mateix pacient.

Perquè els resultats de l'estudi siguin rellevants, s'ha de fer un seguiment dels animals un cop per setmana mitjançant aquest mètode.

4. Resultats

4.1. Estudi preliminar

Per portar a terme aquest projecte i establir unes condicions òptimes per la realització de l'experiment del *Rotarod*, es va fer un estudi previ.

Aquest va consistir en: durant les sis setmanes posteriors a la inoculació, es van fer córrer els ratolins a l'aparell i s'observà quin era el temps òptim a partir del qual la majoria de ratolins aguantava sense caure'n, fins a un màxim de tres minuts (180s). També es van determinar els intents que els ratolins necessitaven, de mitjana, per a acomplir els temps establerts anteriorment.

Aquesta investigació prèvia va constar de vint-i-dos individus, set dels quals no estan inclosos en el meu estudi posterior.

Els resultats s'exposen en el següent gràfic:
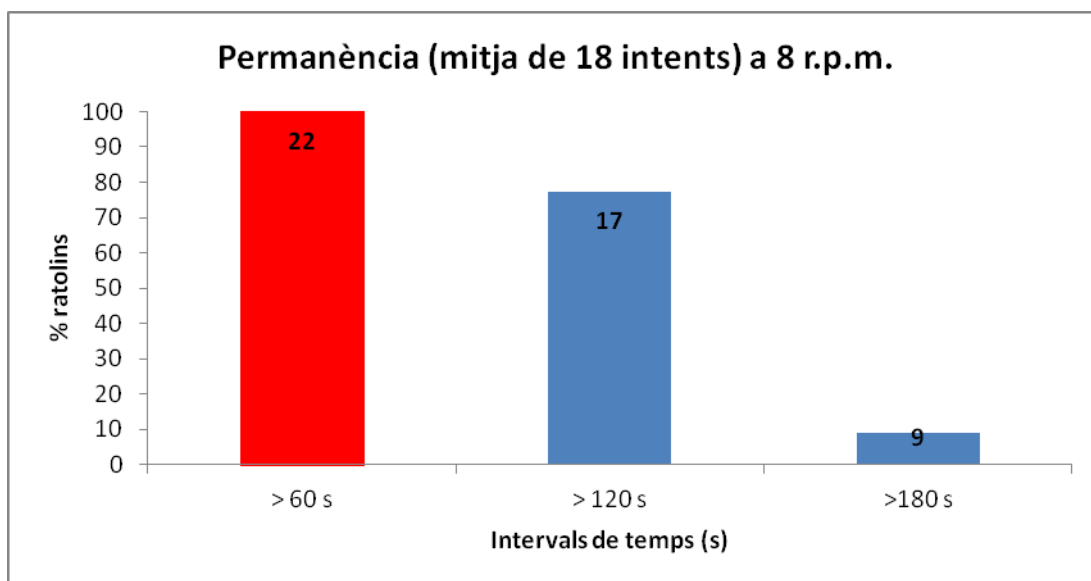
Gràfic 1: Percentatge d'individus (eix Y) enfront el temps que aguanten sobre el Rotarod® (eix X)

Font: Pròpia

Aquest gràfic reflecteix el percentatge (%) d'individus que compleixen l'1, els 2 i els 3 minuts. Com s'aprecia, els ratolins compleixen amb un percentatge del 100% el primer minut, mentre que com més temps passa, menys ratolins sans aguanten sobre l'aparell.

Com s'aprecia al Gràfic 1, el millor valor de compliment és d'un minut (de color vermell), i per tant és la condició temporal que s'utilitzarà en l'estudi definitiu.

Aquest segon gràfic és acumulatiu, i s'hi mostra el número d'intents necessaris, de mitjana, per tal que els ratolins es mantinguin sobre el *Rotarod* durant més d'un minut.
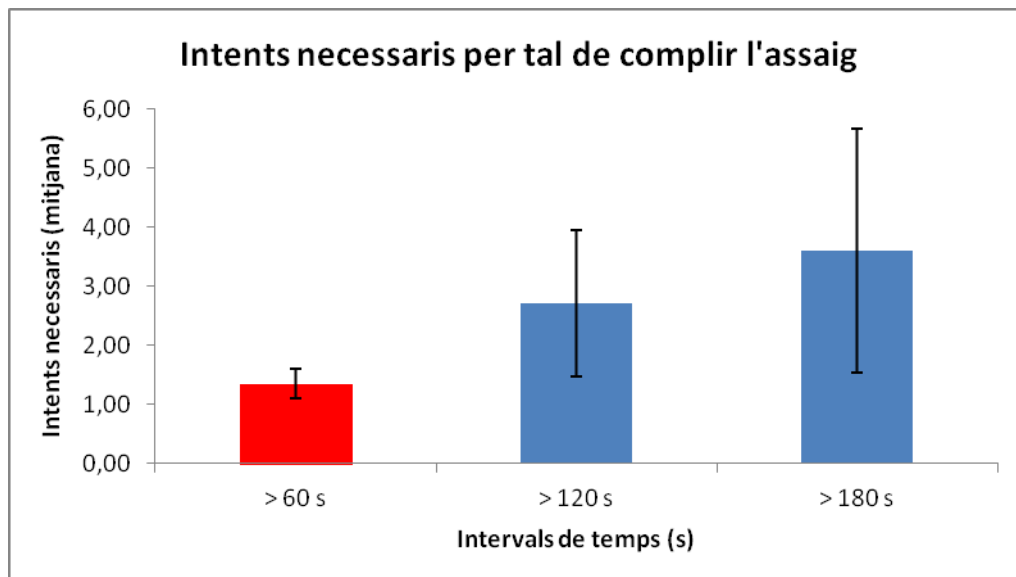
Gràfic 2: Gràfic indicador del nombre d'intents necessaris que necessiten els ratolins, de mitjana, per a acomplir les condicions preliminars establertes.

Font: Pròpia

Al tractar-se de mitjanes hi ha un marge d'error en les dades contingudes. Es mostren amb unes ratlles verticals sobre cada una de les barres. Comprovem que com més estona aguanten sobre el rodet, més intents necessiten per a acomplir les condicions.

Cal dir que la velocitat acordada en un principi per l'estudi era de 11 rpm -el màxim que ofereix el *Rotarod*- però vam adornar-nos, observant el comportament dels animals sobre l'aparell, que si la reduíem fins a 8 rpm, els ratolins complien molt millor l'experiment.

D'aquest estudi se'n van deduir unes condicions òptimes per tal que els ratolins acomplissin l'assaig que es va dur a terme a continuació:

Velocitat (rpm)	Temps (s)		Nº d'intents
8	30 (0 rpm)	60	5

Fig. 16: Condicions definitives utilitzats en l'estudi posterior.

Font: Pròpia

Així doncs, es va decidir que per realitzar el següent estudi, els ratolins romandrien durant trenta segons damunt el rodet de l'aparell aturat. Després d'aquest temps s'augmentaria la velocitat a 8 rpm, durant un minut. A més a més, cada ratolí repetiria l'assaig fins que no aconseguís acomplir les condicions, un màxim de cinc vegades.

També es va determinar que un no compliment de l'assaig estaria considerat com a tal si es repetia durant tres dies seguits en què es realitzava la presa de dades.

4.2. Estudi amb condicions definitives

Un cop vam haver trobat les condicions més òptimes per tal de poder realitzar l'experiment satisfactòriament, es va procedir a recollir els resultats en un full de càlcul, i a analitzar-los. Aquest procés es realitzà de tres maneres diferents:

- *Compliment de l'experiment al llarg de les setmanes:* consisteix en un seguiment del comportament dels ratolins sobre el *Rotarod*, un cop per setmana.

- *Supervivència dels animals al llarg de les setmanes (OS, Overage Survival):* comprèn tant els casos de mort inesperada per efecte del tumor com els casos de sacrifici per símptomes evidents de la presència de tumor (pèrdua de pes, inactivitat o dèficit motor greu). Els ratolins són sacrificats mitjançant un procés de desnucació (prèviament anestesiats amb isoflurà, $C_3H_2ClF_5O$), en el qual el seu sofriment és mínim. Aquest procés només es duu a terme com a conseqüència de tres paràmetres diferents:

  - Pèrdua de pes significativa: Els ratolins sans solen pesar uns 24 grams, així que quan arriben a pesar menys de 18 grams se'ls sacrifica.

  - Un mal estat del pelatge pot ser significatiu alhora de decidir sacrificar un animal de laboratori, ja que pot ser indicatiu de la seva mala salut.

  - Aspecte moribund: poca mobilitat o activitat i poca sociabilitat amb els altres animals de la gàbia per part de l'individu és motiu de sacrifici.

- *Aparició dels primers símptomes (EFS, Event Free Survival)*: Supervivència sense símptomes. Els símptomes són determinats de manera visual durant l'inspecció setmanal dels animals.

Els resultats dels animals inoculats han estat comparats en tot moment amb els de cinc ratolins control; és a dir, que han estat operats però no inoculats amb tumor sinó amb el vehicle de les cèl·lules tumorals (matrigel).

Cal remarcar que el projecte no està finalitzat i que les dades i conclusions compreses en aquest projecte són provisionals.

Aquests gràfics mostren, comparativament, el percentatge de mortalitat al llarg de les setmanes després de la inoculació entre ratolins amb tumor i ratolins sans.

A l'eix Y del gràfic número tres hi trobem representat el percentatge de ratolins supervivents a l'estudi. Aquest es contraposa a l'eix X, que ens representa les setmanes posteriors a la inoculació, considerant aquesta data com a valor zero.
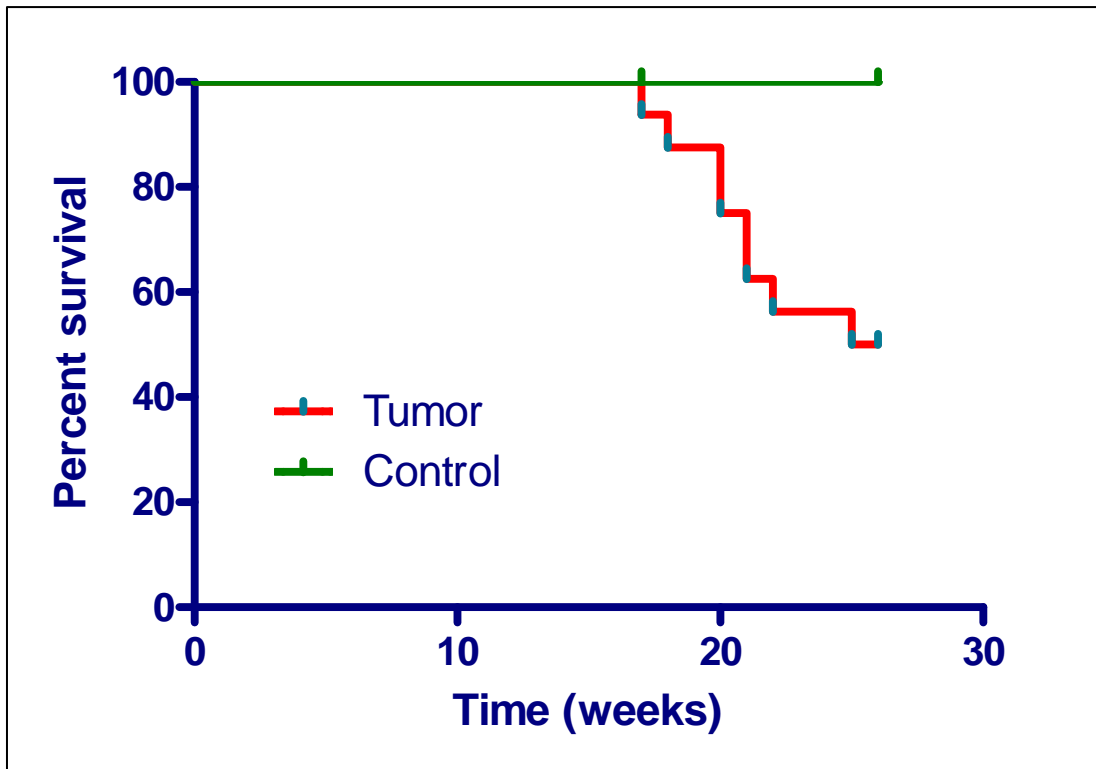
Gràfic 3: Gràfic comparatiu de l'OS entre ratolins control i ratolins inoculats des de la setmana d'inoculació (setmana 0).

Font: Pròpia

Com s'observa al gràfic, el projecte segueix actualment en curs, amb gairebé la meitat dels animals que encara sobreviuen a la malaltia. Pel què fa els ratolins control (representats en verd), al llarg de les setmanes no hi ha cap mort. En comparació als ratolins sans, a partir de la setmana 18 posterior a la operació i la corresponent inoculació dels animals, s'aprecia un esgraó al gràfic, i que significa la primera mort dins el grup d'animals inoculats.

Entre les setmanes 17 i 18 després de la operació observem al gràfic 3 els primers esdeveniments importants en el comportament dels ratolins ja que algun individu comença a estar més quiet que els altres animals, prenent-los com a punt de referència; algun animal comença a perdre pes i a caminar arrossegant lleument una de les extremitats posteriors. És en aquest moment, i degut als paràmetres concretats al punt *4.2.*, que alguns dels individus són sacrificats una setmana més tard.

D'altra banda, i molt lligat al gràfic 3, el gràfic 4 ens representa a l'eix Y el % de ratolins que NO presenten simptomatologia percebuda durant les inspeccions setmanals al llarg de les setmanes posteriors a la inoculació, representades a l'eix X i prenent com a valor zero el dia de l'operació.
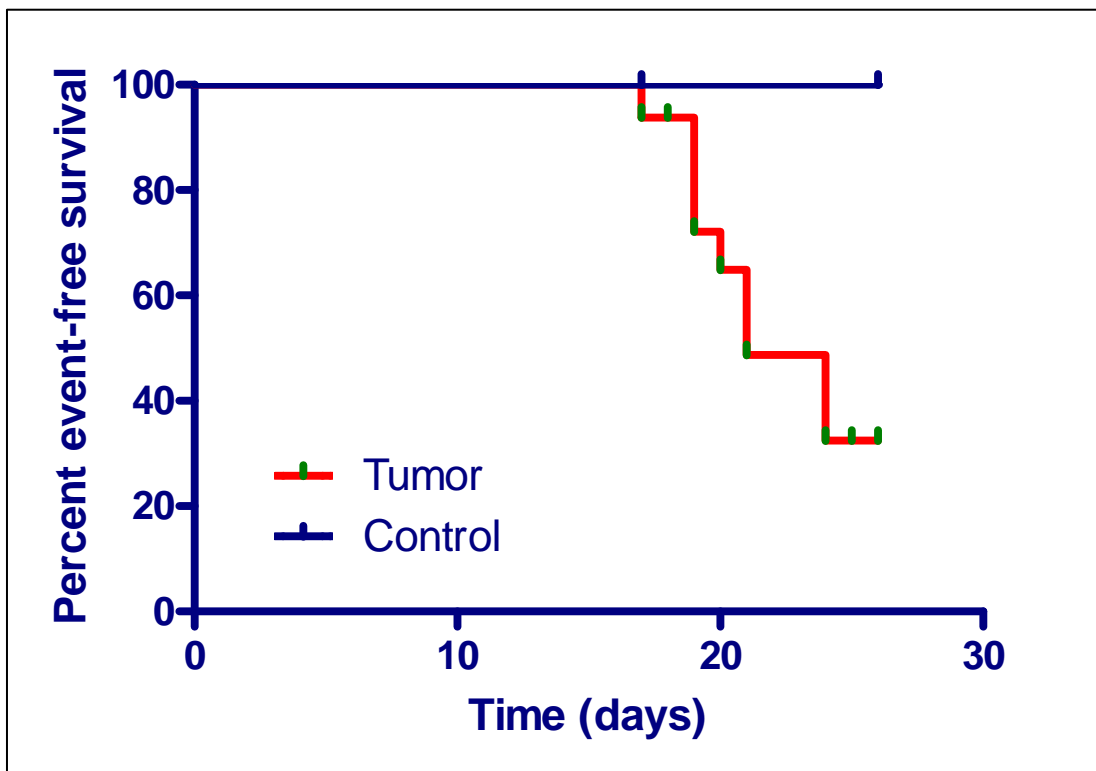
Gràfic 4: Gràfic comparatiu de l'EFS entre ratolins control i ratolins inoculats des de la setmana d'inoculació (setmana 0).

Font: Pròpia

Aquest gràfic ens permet determinar una diferència important entre el grup control i el grup de ratolins inoculats ja que ens sosté la idea que només els ratolins inoculats moririen.

Igual que el gràfic anterior al 4, només els ratolins inoculats presenten la simptomatologia pròpia de la malaltia, principalment atàxia (descoordinació en el moviment) i paralització d'una de les extremitats inferiors, a partir de la 17 setmana .

Aquest gràfic ens mostra, comparativament, el compliment de les condicions determinades anteriorment (punt *4.2.*) en l'assaig del *Rotarod*, al llarg de les setmanes següents a la inoculació.
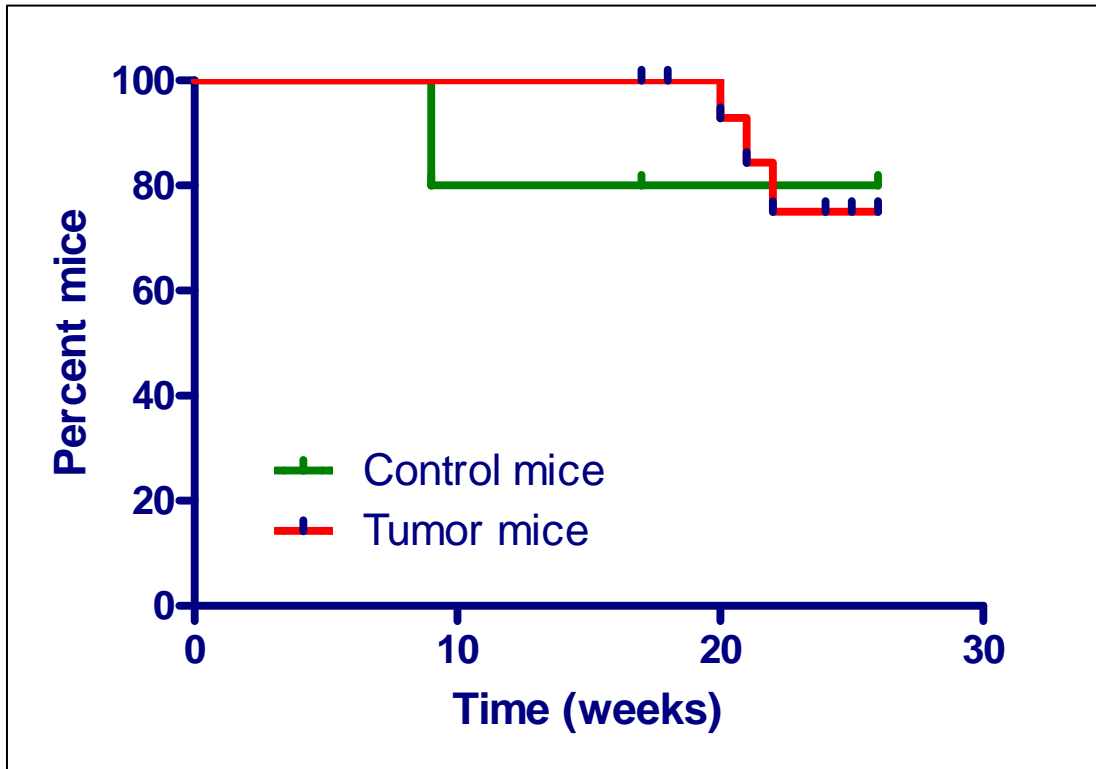
Gràfic 5: Gràfic comparatiu del compliment al *Rotarod* entre ratolins amb tumor i ratolins sans, des de la setmana d'inoculació (setmana 0).

Font: Pròpia

Com s'aprecia, un dels ratolins control no compleix d'experiment la setmana nou, i segueix sense fer-ho a partir d'aquesta.

A partir de la setmana vint, alguns dels ratolins inoculats deixen de complir l'experiment setmana rere setmana.

En resum, els gràfics 6 i 7 mostren l'aparició dels primers esdeveniments en la vida dels individus, ja siguin la mort, els primers símptomes indicadors de l'avançament de la malaltia o bé els primers incompliments de les condicions determinades anteriorment (*4.2.*) en l'assaig del *Rotarod*.

Aquests són alhora els més importants del treball, ja que recullen tots els paràmetres estudiats: EFS (color verd), OS (blau clar) i compliment de l'assaig del Rotarod® (blau fosc).

En aquest primer gràfic s'hi recullen les dades preses del grup de ratolins malalts durant les vint-i-set setmanes posteriors a la inoculació.
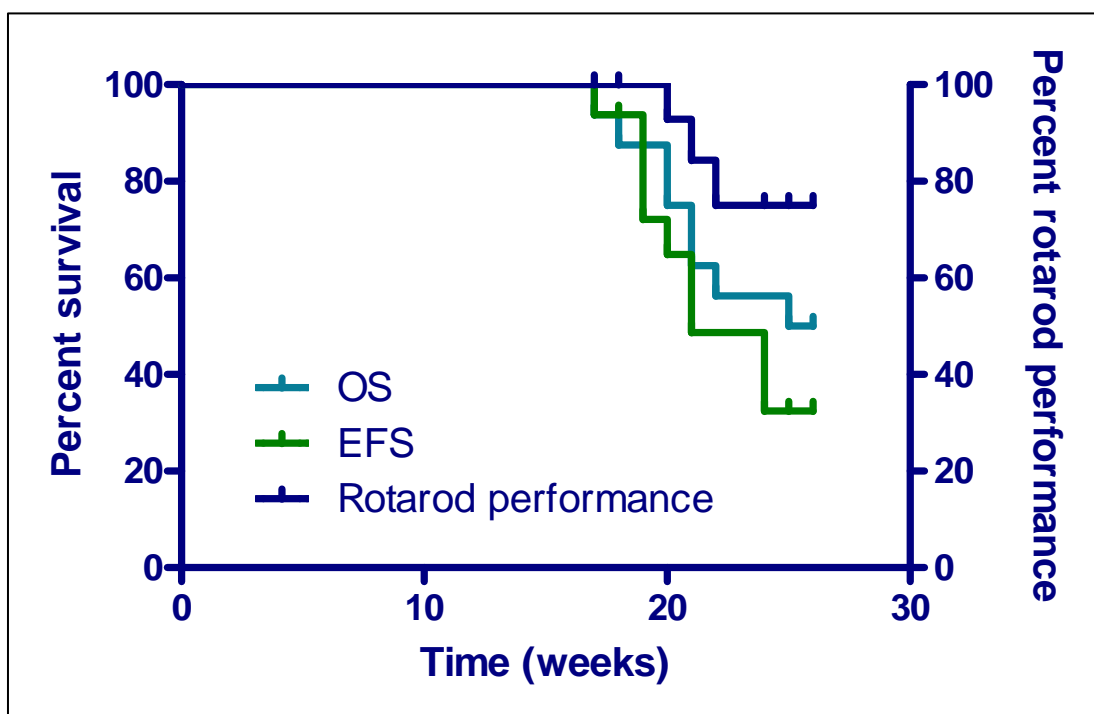
Gràfic 6: Gràfic comparatiu de l'OS, l'EFS i el compliment al *Rotarod* en ratolins amb tumor, des de la setmana d'inoculació (setmana 0).

Font: Pròpia

S'observa que els esdeveniments a les vides del grup d'animals són, cronològicament: símptomes (setmana 17), mort (setmana 18) i incompliment de l'assaig del *Rotarod* (setmana 20).
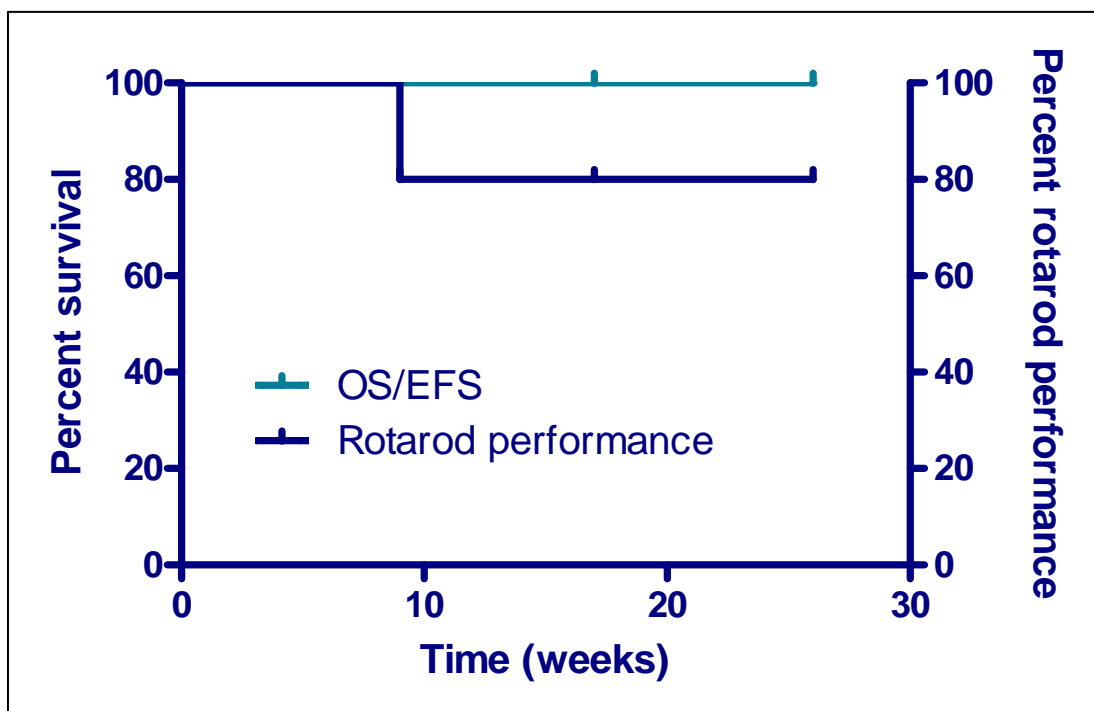
Gràfic 7: Gràfic comparatiu de l'OS, l'EFS i el compliment al *Rotarod* en ratolins sans, des de la setmana d'inoculació (setmana 0).

Font: Pròpia

Aquest gràfic ens mostra el recull dels mateixos paràmetres que en l'anterior, dos dels quals resten sense variacions al llarg de les setmanes (EFS i OS). No obstant hi ha un ratolí control que no compleix l'assaig del *Rotarod*.

Una conseqüència important derivada d'aquesta comparació és que d'incompliment de l'assaig *Rotarod* no serveix per detectar precoçment els símptomes de DIPG en aquesta soca de ratolí, *Nod-Scid*. Per tant, la resposta principal a la nostra hipòtesi de treball és que el mètode *Rotarod* no és un mètode adequat, en aquest soca animal, per als nostres fins. No és un mètode sensible per a la detecció precoç del DIPG en aquests ratolins. A més, atès que alguns ratolins del grup control (no tumor) també van fallar l'assaig *Rotarod* (gràfic 7), podem concloure que aquest mètode no és prou específic, perquè ratolins sans també fallen l'assaig. Els resultats són fins a cert punt decebedors, però conclusius a causa del nostre disseny experimental amb un suficient nombre de ratolins, condicions de l'assaig optimitzades i freqüència apropiada dels assajos.

Després del sacrifici, es va procedir a analitzar els cervells dels ratolins morts per confirmar la infiltració de les cèl·lules mare tumorals procedents d'una biòpsia humana de DIPG i que són les que provoquen aquesta simptomatologia als animals.

Aquest procés va dur-se a terme realitzant unes proves immunohistoquímiques, i que no són competència d'aquest treball, mitjançant les quals un anticòs que només reacciona amb una proteïna fabricada per les cèl·lules humanes, tenyia d'un color marronós les cèl·lules inoculades i les cèl·lules filles d'aquestes, també tumorals.
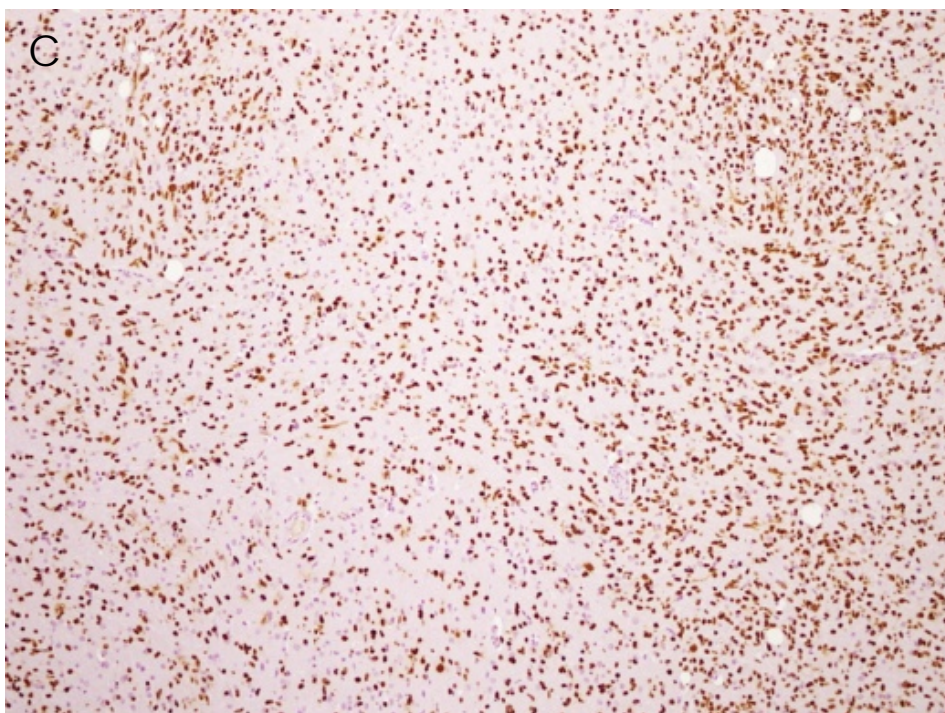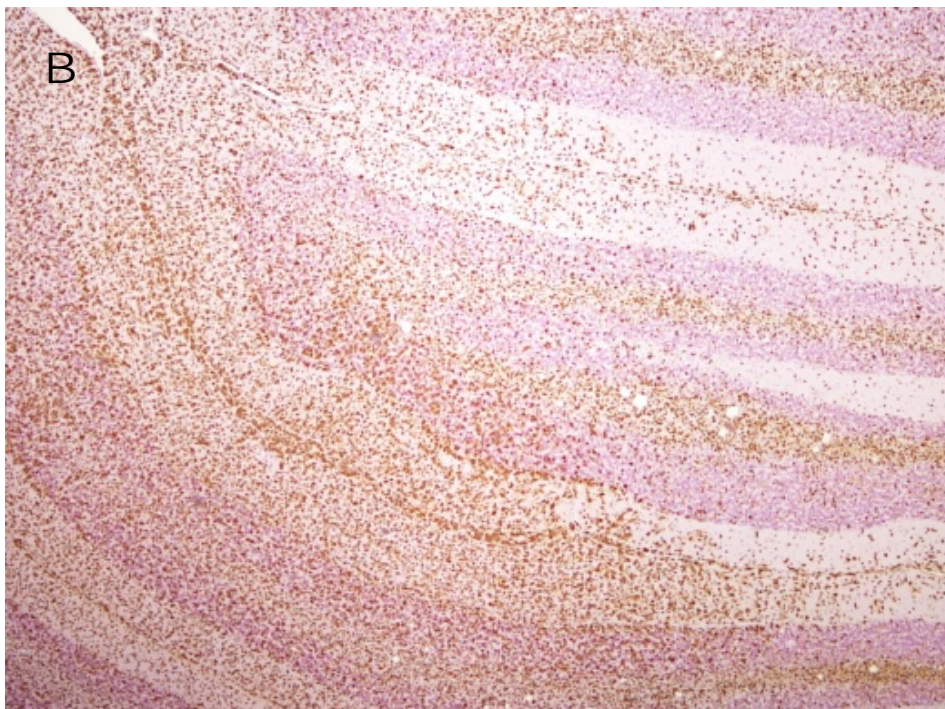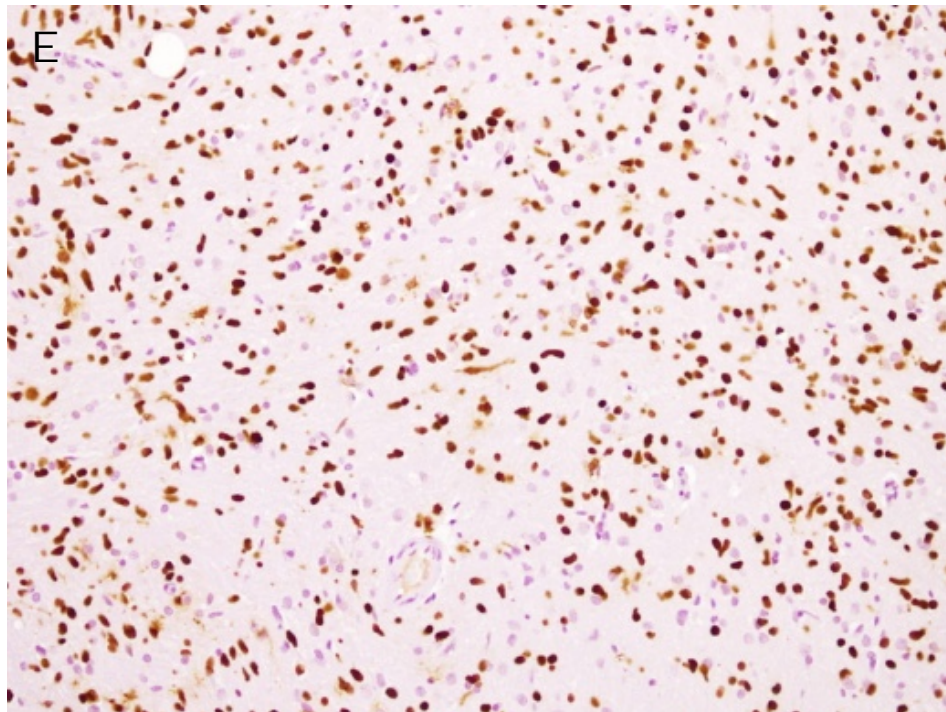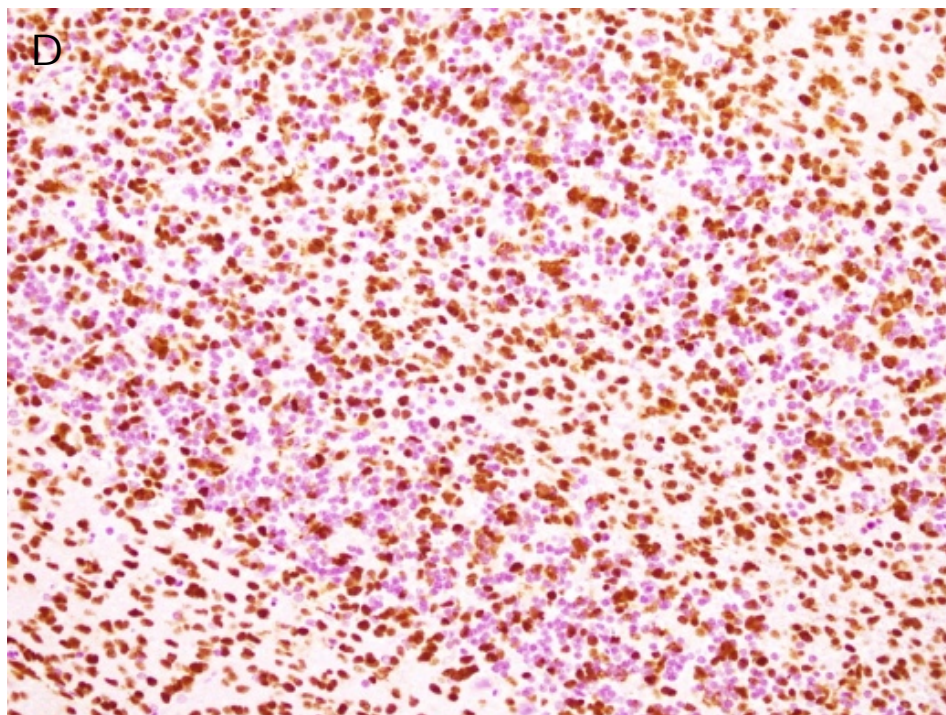
Fig. 17: (A, B, C, D, E) Fotografies microscòpiques d'un tall transversal d'un cervell dels ratolins sacrificats durant l'estudi per tal d'apreciar-hi el grau d'infiltració tumoral.

Font: Pròpia

Com s'observa a les fotografies microscòpiques, el cervell dels ratolins està completament infiltrat per cèl·lules tumorals d'una manera 100% difusa. Podem concloure, doncs, que la inoculació s'ha realitzat correctament i de forma efectiva.

Aquesta conclusió ens permet saber que el procés utilitzat (coordenades d'inoculació i concentració cel·lular) ha estat el correcte. De cara a un futur, doncs, aquest es podrà repetir de manera que s'obtinguin més animals que reprodueixin a la perfecció el DIPG humà i que seran destinats a altres projectes d'investigació.

5. Conclusions

De la recerca pràctica d'aquest treball se n'han obtingut tres conclusions principals:

Conclusió 1:

Els símptomes de la malaltia (pèrdua de pes, pèrdua d'activitat motora, mal aspecte del pelatge), detectats visualment en la inspecció setmanal, precedeixen en poc temps (una setmana aproximadament) al punt en que l'animal ha de ser sacrificat, segons els criteris de punt final de l'experiment.

El gràfic 3 ens mostra les primeres morts o sacrificis, mentre que en el gràfic 4 hi trobem recollides les aparicions dels primers símptomes. Els ratolins control, no obstant això, no presenten cap símptoma durant tot el període del nostre estudi.

Conclusió 2:

Degut al fet que els primers ratolins que no compleixen l'assaig del Rotarod® ho fan posteriorment a l'*OS* i l'*EFS* (definits al punt *4.2.*) exactament a la setmana 20 i per tant amb sis i quatre setmanes de diferència, respectivament, podem concloure que el Rotarod® no serveix per predir, de forma objectiva, l'aparició del DIPG abans que la malaltia es faci evident a simple vista (símptomes) en ratolins. Aquesta conclusió refuta la meva hipòtesi general ja que la contradiu totalment.

Si analitzem el Gràfic 5, observem que tot i ser animals no inoculats, hi ha un ratolí control que no compleix el *Rotarod*.

Aquest fet serveix per confirmar la conclusió anterior, ja que les condicions sobre l'aparell tampoc són acomplertes per ratolins sans. Un sol incompliment per part d'un ratolí sa es considerà significatiu en l'estudi, ja que el nostre objectiu era que l'assaig només fos fallat per ratolins inoculats a causa de la afectació del seu SNC per culpa de la malaltia. Per corroborar que aquest ratolí control està completament sa, va realitzar-se-li una autòpsia cerebral, que va descartar la presencia de tumor, al contrari dels cervells necropsiats dels ratolins inoculats (veure *Fig: 17)*.

Conclusió 3:

Hem de proposar mètodes alternatius pel seguiment de la malaltia i l'avaluació de l'efecte dels tractaments en els ratolins *Nod-Scid*. Dels assajos que actualment s'estan realitzant al laboratori s'ha pogut determinar que la implantació del tumor és d'un 100% (tots els ratolins inoculats el desenvolupen), i la supervivència mitja està al voltant de les 26 setmanes. Per tant, a partir d'aquestes dades establirem els temps durant el qual administrarem els tractaments als animals, probablement al voltant de les 16 setmanes des de la inoculació.

6. Projectes futurs

Paral·lelament a aquest estudi se n'estan realitzant d'altres de tipologia diversa dins del mateix Hospital Sant Joan de Déu de Barcelona.

El que està més relacionat amb aquest treball és el de l'execució del mateix estudi, amb condicions diferents, amb rates immunodeprimides. Actualment aquest estudi està obtenint molt bons resultats. Sembla clar que el model animal es clau per tal de poder aplicar el mètode *Rotarod*. No obstant, mentre que aquest no ha pogut aplicar-se amb èxit als ratolins de la soca *Nod-Scid,*les rates de la soca *Nude* són extremadament dòcils en les condicions seleccionades per elles en l'assaig (diferents a les dels ratolins), els seus símptomes d'atàxia són més evidents a simple vista que en ratolins, i aquests es tradueixen en un incompliment precoç de l'assaig del *Rotarod*. Aquest estudis estan actualment molt avançats al laboratori.

D'altra banda també s'estan provant nous fàrmacs en cultiu cel·lular (tant de tumorsfera com de cèl·lula diferenciada) mitjançant assajos de citotoxicitat, per tal que en un futur aquests puguin ser testant en models animals.

Molt lligat hi va l'estudi futur relacionat amb la utilització de nanopartícules i virus com a vectors inductors de les teràpies.

Per acabar s'està analitzant la possible expressió d'un gen lligat amb l'aparició de la malaltia. Aquest projecte està en els seus inicis.

7. Glossari

CD4+: Els limfòcits T col·laboradors o limfòcits T cooperadors (de l'anglès "T helper cells"), també coneguts com a limfòcits T efectors o simplement limfòcits Th, són un subgrup de limfòcits (al seu torn un tipus de leucòcit) que tenen un paper molt important en establir i maximitzar les capacitats de defensa del sistema immunitari.

CD8+: Molècula que s'expressa en la superfície d'algunes cèl·lules T, conegudes com citolítiques. És una glicoproteïna dimèrica de 65-70kDa que creua la membrana i participa com a correceptor en l'estabilització de l'adhesió del receptor de limfòcits T a molècules del Complex Major d'Histocompatibilitat tipus I (MHC I). Implicada també en la maduració tímica de limfòcits T i en la transmissió de senyals intracel·lulars durant l'activació de l'HLA I.

Criopreservar: Aquest procés de congelació ens permet conservar teixits i/o cèl·lules a temperatures molt baixes, assegurant la supervivència d'aquests, i per tant, poder utilitzar aquest material en futures ocasions.
Per tal de criopreservar el material, utilitzem un criopreservador anomenat "synth-a-freeze".

Hormonoteràpia: És un tractament que actua sobre algunes hormones concretes del cos que alguns tumors necessiten per créixer, com ara alguns tipus de càncer de mama i de pròstata. L'hormonoteràpia atura l'activitat de les hormones en el cos o bé en canvia la seva quantitat per evitar o limitar el creixement del tumor.

Immunitat humoral: La immunitat humoral és l'aspecte del sistema immunitari que és mitjançat per la secreció d'anticossos produïts a les cèl·lules dels limfòcits B. Els anticossos produïts s'uneixen a la superfície dels antígens com ara virus i bacteris.
La immunitat humoral es refereix a la producció d'anticossos i a tots els processos que l'acompanyen.

Medi de cultiu per cèl·lules mare: Es diferencia dels altres medis de cultiu perquè en comptes de portar vitamines, que fan que les cèl·lules es diferenciïn, conté proteïnes.

Per fer-lo necessitem:

- 250mL Neurobasal-A Medium (1X), liquid
- 250mL N-MEM/F-12 (1X), liquid, 1:1
- 5mL HEPES Buffer Solution (1M)
- 5mL MEM Sodium Pyruvate Solution 100mM (100X), liquid
- 5mL MEM Non- Essential Amino acids Solution 10mM (100X), liquid
- 5mL GlutaMAX-l Supplement
- 5mL Antibiotic-Antimyotic (100X), liquid

} TSM

- 50µ H-EFG (20ng/mL)
- 50µ H-FGF-basic-154 (20ng/mL)
- 25µ H-PDGF-AA (10ng/mL)
- 25µ H-PDGF-BB (10ng/mL)

} Proteïnes. Un cop s'afegeixen al TSM, aquest passa a estar complet i llest per a utilitzar-lo en cultius de cèl·lules mare, Aquest, però s'ha de consumir amb un límit de 24 hores.

El TSM es pot conservar indefinidament a 4ºC.

"Passe"/pas: Tècnica emprada per expandir cultius cel·lulars, és a dir, per fer-los créixer i obtenir un nombre més elevat de cèl·lules.

Teràpies biològiques: Les teràpies biològiques actuen ajudant el sistema immunològic (les defenses del cos) a lluitar contra el càncer. Només actuen contra les cèl·lules malignes i no sobre les sanes, per tant hi ha menys efectes secundaris i generalment són ben tolerats. S'utilitzen vacunes o bé anticossos monoclonals (substàncies produïdes al laboratori amb l'objectiu que trobin i ataquin un determinat lloc de la superfície de les cèl·lules tumorals). Des d'aquí ataquen la proteïna que està generant el creixement de les cèl·lules canceroses).

Timus/tim: El tim o timus és un òrgan limfoide que consta de dos lòbuls i es localitza al mediastí, darrere de l'estèrnum. La principal funció del tim és oferir un

espai per a la maduració de les cèl·lules T, i és vital en la protecció contra la autoimmunitat.

Zimogen: Un zimogen o proenzim és un precursor enzimàtic inactiu en què són sintetitzats una part important d'enzims. Es tracta d'una molècula que necessita ser activada per a convertir-se en un enzim actiu que pugui intervenir en reaccions de l'organisme, augmentant la velocitat de reacció.

8. Bibliografia

8.1. Articles

Diffuse intrinsic pontine glioma: poised for progress *(Warren, K.E., et al. 2012)*

Difuse intrinsic pontine gliomas: A systematic update on clinical trials and biology (*Jansen, M.H.A., et al. 2012*)

Hedgehog-responsive candidate cell of origin for diffuse intrinsic pontine glioma *(Monje, M., et al. 2011)*

Identification of human brain tumorinitiating cells *(Singh, S.K., et al. 2004)*

Isolation and Characterization of Tumorigenic, Stem–like Neural Precursors from Human Glioblastoma (*Galli, R., et al. 2012*)

Technical note-Neubauer Chamber Cell Counting *(Oscar Bastidas)*

8.2. Webs

AMERICAN COLLEGE OF RADIOLOGY AND RADIOLOGICAL SOCIETY OF NORTH AMERICA, Prueba/tratamiento, Radioterapia, Accelerador lineal (LINAC).
http://www.radiologyinfo.org/sp/info.cfm?pg=linac [Consulta: 02.07.2013]

ASSOCIACIÓN ESPAÑOLA CONTRA EL CÁNCER, Sobre el cáncer, Tratamientos, Tipos de Radioterapia.
https://www.aecc.es/SobreElCancer/Tratamientos/Radioterapia/Paginas/tipos deradioterapia.aspx [Consulta: 26.05.2013]

ASSOCIACIÓN ESPAÑOLA CONTRA EL CANCER, Sobre el cáncer, Tratamientos, Tipos de Quimioterapia.
https://www.aecc.es/SobreElCancer/Tratamientos/Quimioterapia/Paginas/Que es.aspx [Consulta: 26.05.2013]

CÉNTRO MÉDICO TÉKNON, Dr. Xavier Centeno, Port-a-Cath

http://www.teknon.es/ca_ES/web/centeno/port-a-cath [Consulta: 06.11.2013]

CHARLES RIVER LABORATORIES, Nod-Scid mouse.

http://www.criver.com/products-services/basic-research/find-a-model/nod-scid-mouse [Consulta: 29.05.2013]

DIPG REGISTRY, Ensayos clínicos activos.

http://dipgregistry.creativestaging.biz/es/profesionales-medicos/ensayos-clinicos-activos/ -[Consulta: 29.07.13]

FONDO ALICIA PUEYO.

http://www.fondoaliciapueyo.org/ [Consulta: 15.5.2013]

GENERALITAT DE CATALUNYA, Càncer, Ciutadans, Tractaments, Hormonoteràpia.

http://www20.gencat.cat/portal/site/cancer/menuitem.6877f76ecea739f796072 d10b0c0e1a0/?vgnextchannel=4fd9ebd5d7b73210VgnVCM1000000b0c1e0aR CRD&vgnextfmt=default&vgnextoid=4fd9ebd5d7b73210VgnVCM1000000b0c 1e0aRCRD [Consulta: 11.07.2013]

GENERALITAT DE CATALUNYA, Càncer, Ciutadans, Tractaments, Quimioteràpia.

http://www20.gencat.cat/portal/site/cancer/menuitem.6877f76ecea739f796072 d10b0c0e1a0/?vgnextoid=a6a9ebd5d7b73210VgnVCM1000000b0c1e0aRCR D&vgnextchannel=a6a9ebd5d7b73210VgnVCM1000000b0c1e0aRCRD&vgne xtfmt=default [Consulta: 26.05.2013]

GENERALITAT DE CATALUNYA, Càncer, Ciutadans, Tractaments, Radioteràpia.

http://www20.gencat.cat/portal/site/cancer/menuitem.6877f76ecea739f796072 d10b0c0e1a0/?vgnextchannel=0859ebd5d7b73210VgnVCM1000000b0c1e0aR CRD&vgnextfmt=default&vgnextoid=0859ebd5d7b73210VgnVCM1000000b0 c1e0aRCRD [Consulta: 26.05.2013]

GENERALITAT DE CATALUNYA, Càncer, Ciutadans, Tractaments, Teràpies biològiques.

http://www20.gencat.cat/portal/site/cancer/menuitem.6877f76ecea739f796072 d10b0c0e1a0/?vgnextoid=fcf9ebd5d7b73210VgnVCM1000000b0c1e0aRCRD &vgnextchannel=fcf9ebd5d7b73210VgnVCM1000000b0c1e0aRCRD&vgnextf mt=default [Consulta: 11.07.2013]

HARLAN LABORATORIES, Products and Services, Research models and services, Nod-scid mice.

http://www.harlan.com/products_and_services/research_models_and_services /research_models/nodscid_mice.hl [Consulta: 23.07.13]

INTERNATIONAL TECHNOLOCY CENTER (IITC), Rotarods & Treadmills.

http://www.iitcinc.com/rotarod.html [Consulta: 29.05.2013]

KIDS HEALTH from NEMOURS, Teens, Cancer Centre, Los esteroides y en tratamiento contra el cáncer.

http://kidshealth.org/teen/cancer_center/cancer_center_esp/treatment-steroids-esp.html [Consulta: 02.07.2013]

MEDLINE PLUS (Biblioteca Nacional de Medicina de EE.UU), **Función del cerebelo.**

http://www.nlm.nih.gov/medlineplus/spanish/ency/esp_imagepages/18008.htm [Consulta: 02.07.2013]

NCBI, The NOD mouse: a model of immune dysregulation.
http://www.ncbi.nlm.nih.gov/pubmed/15771578 [Consulta: 29.05.2013]

NCBI, The SCID mouse mutant: definition, characterization, and potential uses. *http://www.ncbi.nlm.nih.gov/pubmed/1910681* [Consulta: 29.05.2013]

PANLAB HARVARD APPARATUS, Rota-rod.
http://www.panlab.com/panlabWeb/Hardware/php/displayHard.php?nameHard=ROTA-ROD [Consulta: 29.05.2013]

WIKIPEDIA, Arteria basilar.
http://es.wikipedia.org/wiki/Arteria_basilar [Consulta: 22.07.2013]

WIKIPEDIA, Astrocito.
http://es.wikipedia.org/wiki/Astrocito [Consulta: 15.05.2013]

WIKIPEDIA, Barrera hematoencefàlica.
http://es.wikipedia.org/wiki/Barrera_hematoencef%C3%A1lica [Consulta:02.07.2013]

WIKIPEDIA, Cèl·lula Glial.
http://es.wikipedia.org/wiki/C%C3%A9lula_glial [Consulta: 15.5.2013]

WIKIPEDIA, Célula presentadora de antígeno.
http://es.wikipedia.org/wiki/C%C3%A9lula_presentadora_de_ant%C3%ADgeno [Consulta: 06.11.2013]

WIKIPEDIA, Sistema de complement.
http://ca.wikipedia.org/wiki/Sistema_del_complement [Consulta: 22.07.2013]

WIKIPEDIA, Sistema Immunitari.
http://ca.wikipedia.org/wiki/Sistema_immunitari#Limf.C3.B2cits_T_citot.C3.B2xics [Consulta:29.05.2013]

WIKIPEDIA,Complex d'histocompatibilitat.

http://ca.wikipedia.org/wiki/Complex_d%27histocompatibilitat_principal

[Consulta:22.07.2013]

WIKIPEDIA,Puente troncoencefálico.

http://es.wikipedia.org/wiki/Protuberancia_anular [Consulta: 02.07.2013]

8.3. Webs de consulta ràpida

WIKIPEDIA, Fagòcit.

http://ca.wikipedia.org/wiki/Fag%C3%B2cit [Consulta: 22.07.2013]

WIKIPEDIA, Immunitat humoral.

http://ca.wikipedia.org/wiki/Immunitat_humoral [Consulta: 22.07.2013]

WIKIPEDIA, Immunodeficiència.

http://ca.wikipedia.org/wiki/Immunodefici%C3%A8ncia [Consulta:29.05.2013]

WIKIPEDIA, Limfòcits B.

http://ca.wikipedia.org/wiki/Limf%C3%B2cits_B [Consulta: 22.07.2013]

WIKIPEDIA, Limfocito T CD4.

http://es.wikipedia.org/wiki/Linfocito_T_CD4%2B [Consulta: 21.09.2013]

WIKIPEDIA, Meséncefalo.

http://es.wikipedia.org/wiki/Mesenc%C3%A9falo [Consulta: 22.07.2013]

WIKIPEDIA, pH.

http://ca.wikipedia.org/wiki/PH [Consulta: 21.09.13]

WIKIPEDIA, Rotarod performance.

http://en.wikipedia.org/wiki/Rotarod_performance_test [Consulta: 29.05.2013]

WIKIPEDIA, CD8.

http://es.wikipedia.org/wiki/CD8 [Consulta: 21.09.2013]

WIKIPEDIA, Astrocitroma.

http://es.wikipedia.org/wiki/Astrocitoma [Consulta: 15.05.2013]

WIKIPEDIA, Zimogen.

http://ca.wikipedia.org/wiki/Zimogen [Consulta: 22.07.2013]

WIKIPEDIA, Limfòcit.

http://ca.wikipedia.org/wiki/Limf%C3%B2cit_T [Consulta: 22.07.2013]

9. Annexos

9.1. Índex d'annexos

RESULTATS CONDICIONS PRELIMINARS (dades crues 1/2)

Condicions: 3 intents, 300 s màxim, a 8 rpm

(T) = Dades recollides que informen sobre la fracció de temps que els ratolins es mantenen sobre el ROTAROD, amb una durada màxima de 300 segons.
#n = Nombre identificatiu de l'animal inoculat

Setmanes post-inoculació 1	Temps (s)	#5	#6	#7	#8	#9	#10	#12
6	T1	265	52	96	47	88	300	23
6	T2	246	52	84	300	46	87	201
6	T3	300	67	52	300	147	51	87
7	T1	169	206	42	79	26	300	58
7	T2	300	300	107	27	213	8	178
7	T3	300	184	35	83	300	216	112
8	T1	250	64	265	300	69	97	94
8	T2	189	58	197	245	58	165	56
8	T3	299	97	236	26	63	273	199
10	T1	65	89	97	49	74	300	89
10	T2	28	75	300	300	26	256	79
10	T3	79	64	268	300	59	149	136
11	T1	122	84	39	50	15	300	300
11	T2	20	43	38	117	46	300	120
11	T3	80	57	46	98	81	300	300
12	T1	224	46	48	48	27	273	121
12	T2	59	83	77	39	64	75	149
12	T3	40	62	35	20	43	38	144

Setmanes post-inoculació 2	Temps (s)	#13	#14	#15	#16	#17	#18	#19	#20
5	T1	65	126	182	300	289	241	300	45
5	T2	68	71	93	203	69	300	75	219
5	T3	94	261	300	4	149	300	26	97
6	T1	124	69	244	12	300	45	26	63
6	T2	53	73	195	63	300	300	75	105
6	T3	41	58	300	72	300	292	64	74
7	T1	300	60	59	287	125	99	300	25
7	T2	296	31	132	300	300	68	284	101
7	T3	284	46	78	268	164	75	300	67
8	T1	69	237	79	300	99	52	300	146
8	T2	300	96	85	52	74	63	274	121
8	T3	297	300	201	234	89	97	265	206
10	T1	24	131	24	36	61	244	22	158
10	T2	82	X	300	198	131	61	23	123
10	T3	62	164	231	101	112	124	122	103
11	T1	123	18	300	109	55	52	21	15
11	T2	206	49	300	187	103	96	257	89
11	T3	100	276	137	35	300	21	64	168

RESULTATS CONDICIONS PRELIMINARS (dades crues 2/2)

Condicions: 3 intents, 300 s màxim, a 8 rpm

(T) = Dades recollides que informen sobre la fracció de temps que els ratolins es mantenen sobre el ROTAROD, amb una durada màxima de 300 segons.
#n = Nombre identificatiu de l'animal inoculat
Bn = Nombre identificatiu de l'animal control

Setmanes post-inoculació 3	Temps (s)	#21	#22	#23	#24
4	T1	68	75	300	59
	T2	268	59	63	300
	T3	300	25	300	300
5	T1	300	247	24	183
	T2	58	219	87	78
	T3	300	300	75	300
6	T1	300	70	36	300
	T2	249	64	285	69
	T3	288	91	122	72
7	T1	98	300	68	65
	T2	67	34	95	61
	T3	74	278	75	176
9	T1	53	22	99	71
	T2	226	59	90	19
	T3	79	65	110	72
10	T1	82	29	48	29
	T2	23	91	67	13
	T3	99	62	266	58

Setmanes post-inoculació 4	Temps (s)	B2	B3	B4
4	T1	300	253	79
	T2	268	300	653
	T3	184	54	264
5	T1	65	233	98
	T2	87	65	67
	T3	23	98	43
6	T1	64	46	201
	T2	97	210	300
	T3	99	300	97
7	T1	300	284	66
	T2	56	76	300
	T3	300	216	235
9	T1	149	300	68
	T2	87	49	74
	T3	267	78	91
10	T1	300	96	265
	T2	67	300	31
	T3	58	214	300

NÚMERO D'INTENTS NECESSARIS PER A ROMANDRE MÉS DE 60s SOBRE DEL ROTAROD

DADES ANALITZADES (1/3)

I,n = Dades recollides que informen sobre els intents setmanals de permanencia (1), o no (0), sobre el ROTAROD.
#n = Nombre identificatiu de l'animal inoculat
Bn = Nombre identificatiu de l'animal control

Assaigs	Intents	#5	#6	#7	#8	#9	#10	#12	#13	#14	#15	#16	#17	#18	#19	#20	#21	#22	#23	#24	B2	B3	B4	MITJANA	DESVEST
Setmana 1	I.1	1	0	1	0	1	1	0	1	1	1	1	1	1	1	0	1	1	1	0	1	1	1		
	I.2	1	0	1	1	0	1	1	1	1	1	1	1	1	1	1	1	0	1	1	1	1	1		
	I.3	1	1	0	1	1	0	1	1	1	1	0	1	1	0	1	1	0	0	1	1	0	1		
Setmana 2	I.1	1	1	0	1	0	1	0	1	1	1	0	1	0	0	1	1	1	0	1	1	1	1		
	I.2	1	1	1	0	1	0	1	0	1	1	1	1	1	1	1	0	1	1	1	1	1	0		
	I.3	1	1	0	1	1	1	1	0	0	1	1	1	1	1	1	1	1	1	1	0	1	0		
Setmana 3	I.1	1	1	1	1	1	1	1	1	1	0	1	1	1	1	0	1	1	0	1	1	0	1		
	I.2	1	0	1	1	0	1	0	1	0	1	1	1	1	1	1	1	1	1	1	1	1	1		
	I.3	1	1	1	0	1	1	1	1	0	1	1	1	1	1	1	1	1	1	1	1	1	1		
Setmana 4	I.1	1	1	1	0	0	1	1	1	1	1	1	1	1	1	1	0	0	1	1	1	1	1		
	I.2	0	1	1	1	0	1	1	1	1	1	0	1	0	0	1	1	0	1	1	0	1	1		
	I.3	1	1	1	1	0	1	1	1	1	1	1	1	1	1	1	1	1	1	1	1	1	1		
Setmana 5	I.1	1	0	0	0	0	1	1	0		0	0	1	1	0	1	0	0	0	0	1	0	1		
	I.2	0	0	1	1	1	1	1	1	1	1	1	1	1	1	1	1	1	1	1	1	0	1		
	I.3	1	1	0	1	1	1	1	1	1	1	1	1	1	1	1	1	1	1	1	1	1	1		
Setmana 6	I.1	1	0	0	0	0	1	1	1	0	1	1	0	0	0	0	1	0	0	0	1	1	1		
	I.2	0	1	1	0	1	1	1	1	0	1	1	1	1	1	1	0	1	1	0	1	1	0		
	I.3	0	1	0	0	0	0	1	1	1	1	0	1	0	1	1	1	1	1	0	0	1	1		
Intents > 60 s		14	13	10	10	9	15	15	15	12	16	13	17	14	13	15	15	12	15	13	15	15	16		
% del total de intents		0,78	0,72	0,56	0,56	0,50	0,83	0,83	0,83	0,67	0,89	0,72	0,94	0,78	0,72	0,83	0,83	0,67	0,83	0,72	0,83	0,83	0,89	0,76	0,12
Número d'intents necessaris per a fer > 60 s		1,29	1,38	1,80	1,80	2,00	1,20	1,20	1,20	1,50	1,13	1,38	1,06	1,29	1,38	1,20	1,20	1,50	1,20	1,38	1,20	1,20	1,13	1,35	0,24

NÚMERO D'INTENTS NECESSARIS PER A ROMANDRE MÉS DE 120s SOBRE DEL ROTAROD

DADES ANALITZADES (2/3)

I.n = Dades recollides que informen sobre els intents setmanals de permanencia (1), o no (0), sobre el ROTAROD.
#n = Nombre identificatiu de l'animal inoculat
Bn = Nombre identificatiu de l'animal control

Ratolí	Intents	#5	#6	#7	#8	#9	#10	#12	#13	#14	#15	#16	#17	#18	#19	#20	#21	#22	#23	#24	B2	B3	B4	MITJANA	DESVEST
Setmana 1	I.1	1	0	0	0	0	1	0	0	1	1	1	1	1	1	0	0	0	1	0	1	1	0		
	I.2	1	0	0	1	0	0	1	0	0	0	1	0	1	0	1	1	0	0	1	1	1	1		
	I.3	1	0	0	1	1	0	0	0	1	1	0	1	1	0	0	1	0	1	1	1	0	1		
Setmana 2	I.1	1	1	0	0	0	1	0	1	0	1	0	1	0	0	0	1	1	0	1	0	1	0		
	I.2	1	1	0	0	1	0	1	0	0	0	0	1	1	0	0	0	1	0	0	0	0	0		
	I.3	1	1	0	0	1	1	0	0	0	1	0	1	1	0	0	1	1	0	1	0	0	0		
Setmana 3	I.1	1	0	1	1	0	0	0	1	0	0	1	1	0	1	0	1	0	0	1	0	0	1		
	I.2	1	0	1	1	1	1	0	1	0	1	1	1	0	1	0	1	0	1	0	0	1	1		
	I.3	1	0	1	0	0	1	1	1	0	0	1	1	0	1	0	1	0	1	0	0	0	0		
Setmana 4	I.1	0	0	0	0	0	1	0	0	1	0	0	0	1	1	1	0	0	0	0	1	1	0		
	I.2	0	0	1	1	0	1	0	1	0	0	0	0	1	1	1	1	0	0	0	0	0	0		
	I.3	0	0	1	1	0	1	1	1	1	1	1	0	0	1	1	0	0	0	1	1	0	1		
Setmana 5	I.1	1	0	0	0	0	1	1	1	0	0	0	0	0	0	0	0	0	0	0	1	0	1		
	I.2	0	0	0	0	0	0	1	1	0	1	1	0	0	1	0	0	0	0	0	0	1	0		
	I.2	0	0	0	0	0	1	1	0	1	1	0	0	1	0	1	0	0	0	0	0	0	0		
Setmana 6	I.1	1	0	0	0	0	1	1	1	0	1	0	0	0	0	0	0	0	0	0	1	0	1		
	I.2	0	0	0	0	0	1	1	1	0	1	1	1	0	1	0	1	0	0	0	0	1	0		
	I.3	0	0	0	0	0	1	1	0	1	1	0	1	0	0	1	0	0	1	0	0	1	1		
Intents > 120 s		11	3	5	6	3	12	10	8	7	12	9	10	7	9	7	8	5	5	6	8	10	8		
% del total de intents		0,61	0,17	0,28	0,33	0,17	0,67	0,56	0,44	0,39	0,67	0,50	0,56	0,39	0,50	0,39	0,44	0,28	0,28	0,33	0,44	0,56	0,44	0,43	0,14
Número d'intents necesaris per a fer > 120 s		1,64	6,00	3,60	3,00	6,00	1,50	1,80	2,25	2,57	1,50	2,00	1,80	2,57	2,00	2,57	2,25	3,60	3,60	3,00	2,25	1,80	2,25	2,71	1,25

NÚMERO D'INTENTS NECESSARIS PER A ROMANDRE MÉS DE 180s SOBRE DEL ROTAROD

DADES ANALITZADES (3/3)

I.n = Dades recollides que informen sobre els intents setmanals de permanencia (1), o no (0), sobre el ROTAROD.
#n = Nombre identificatiu de l'animal inoculat
Bn = Nombre identificatiu de l'animal control

Ratolí	Intents	#5	#6	#7	#8	#9	#10	#12	#13	#14	#15	#16	#17	#18	#19	#20	#21	#22	#23	#24	B2	B3	B4	MITJANA	DESVEST
Setmana 1	I.1	1	0	0	0	0	1	0	0	0	1	1	1	1	1	0	0	0	1	0	1	1	0		
	I.2	1	0	0	1	0	0	1	0	0	0	1	0	1	0	1	1	0	0	1	1	1	1		
	I.3	1	0	0	1	0	0	0	0	1	1	0	0	1	0	0	1	0	1	1	1	0	1		
Setmana 2	I.1	0	1	0	0	0	1	0	0	0	1	0	1	0	0	0	1	1	0	1	0	1	0		
	I.2	1	1	0	0	1	0	0	0	0	0	0	1	1	1	0	0	1	0	0	1	0	0		
	I.3	1	1	0	0	1	1	0	0	0	1	0	1	1	0	0	1	1	1	1	1	0	0		
Setmana 3	I.1	1	0	1	1	0	0	0	1	0	0	1	0	0	1	0	1	0	0	1	0	0	1		
	I.2	1	0	1	1	0	0	0	1	0	0	1	1	0	1	0	1	0	1	0	0	1	1		
	I.3	1	0	1	0	0	1	1	1	0	0	1	0	0	1	0	1	0	0	0	1	1	0		
Setmana 4	I.1	0	0	0	0	0	1	0	0	1	0	0	0	0	0	0	0	1	0	0	1	0	0		
	I.2	0	0	1	1	0	1	0	1	0	0	0	0	0	1	0	0	0	0	0	0	0	1		
	I.3	0	0	1	1	0	0	0	1	1	1	1	0	0	1	1	0	1	0	0	0	1	1		
Setmana 5	I.1	0	0	0	0	0	1	1	0	0	0	0	0	0	0	0	0	0	0	0	0	1	0		
	I.2	0	0	0	0	0	1	0	0	0	1	1	0	0	0	0	1	0	0	0	0	0	0		
	I.3	0	0	0	0	0	1	1	0	0	1	0	0	0	0	0	0	0	0	0	1	0	0		
Setmana 6	I.1	1	0	0	0	0	1	0	0	0	1	1	0	0	0	0	0	0	0	0	1	0	1		
	I.2	0	0	0	0	0	0	0	1	0	1	1	0	0	1	0	0	0	0	0	0	1	0		
	I.3	0	0	0	0	0	0	0	0	1	0	0	1	0	0	0	0	0	1	0	0	1	1		
Intents > 180 s		9	3	5	6	2	10	4	6	4	10	9	6	6	8	2	8	5	4	5	7	10	8		
% del total d'intents		0,50	0,17	0,28	0,33	0,11	0,56	0,22	0,33	0,22	0,56	0,50	0,33	0,33	0,44	0,11	0,44	0,28	0,22	0,28	0,39	0,56	0,44	0,35	0,14
Número d'intents necessaris per a fer > 180 s		2,00	6,00	3,60	3,00	9,00	1,80	4,50	3,00	4,50	1,80	2,00	3,00	3,00	2,25	9,00	2,25	3,60	4,50	3,60	2,57	1,80	2,25	3,59	2,06

Diffuse intrinsic pontine glioma: poised for progress

Katherine E. Warren*

Pediatric Neuro-Oncology Section, Pediatric Oncology Branch, National Cancer Institute, National Institutes of Health, Bethesda, MD, USA

Diffuse intrinsic pontine gliomas (DIPGs) are amongst the most challenging tumors to treat. Surgery is not an option, the effects of radiation therapy are temporary, and no chemotherapeutic agent has demonstrated significant efficacy. Numerous clinical trials of new agents and novel therapeutic approaches have been performed over the course of several decades in efforts to improve the outcome of children with DIPG, yet without success. The diagnosis of DIPG is based on radiographic findings in the setting of a typical clinical presentation, and tissue is not routinely obtained as the standard of care. The paradigm for treating children with these tumors has been based on that for supratentorial high-grade gliomas in adults as the biology of these lesions were presumed to be similar. However, recent pivotal studies demonstrate that DIPGs appear to be their own entity. Simply identifying this fact releases a number of constraints and opens opportunities for biologic investigation of these lesions, setting the stage to move forward in identifying DIPG-specific treatments. This review will summarize the current state of knowledge of DIPG, discuss obstacles to therapy, and summarize results of recent biologic studies.

Keywords: **pons, glioma, brainstem, DIPG, diffuse, intrinsic, pediatric, pontine**

INTRODUCTION

More than 70% of children with tumors of the central nervous system (CNS) will survive at least 5 years from diagnosis (Smith et al., 2010; Howlader et al., 2011). However, pediatric CNS tumors represent a heterogeneous group of diseases and the dismal survival of select tumor subtypes, such as diffuse intrinsic pontine gliomas (DIPG), is not reflected in this number. The median survival for children with DIPG is less than 1 year from diagnosis (Mandell et al., 1999; Cohen et al., 2011), and no improvement in survival has been realized in more than three decades. The reason for this stagnancy has, at least in part, been attributed to our lack of understanding of the biology of this disease. In the past few years, considerable coordinated and collaborative efforts have been made to address this. Notably, more has been published on the biology and pathophysiology of DIPG in the past 5 years than in all prior years combined, generating a groundswell of excitement and cautious enthusiasm. How to best apply this data to the treatment of children with DIPG remains to be seen, but improved outcome for these patients is anticipated as we move beyond empiric therapy and attempt to bridge the gap between bench and bedside. This review will discuss the current status and our present understanding of this disease.
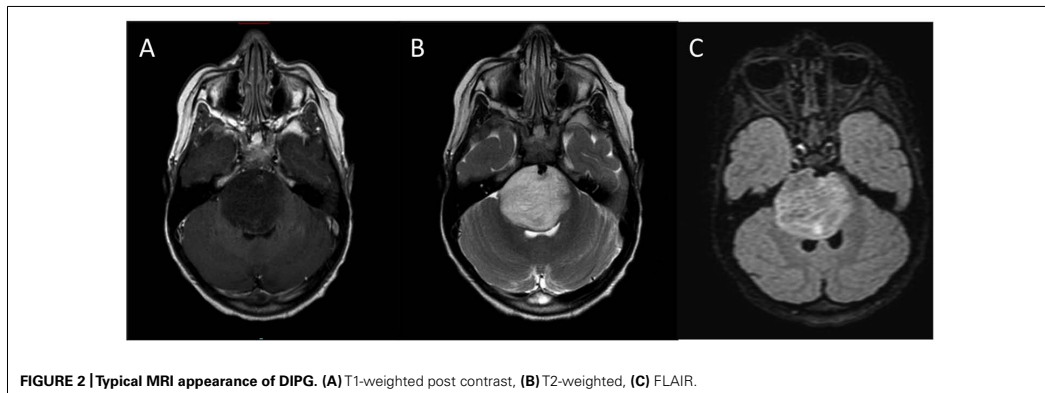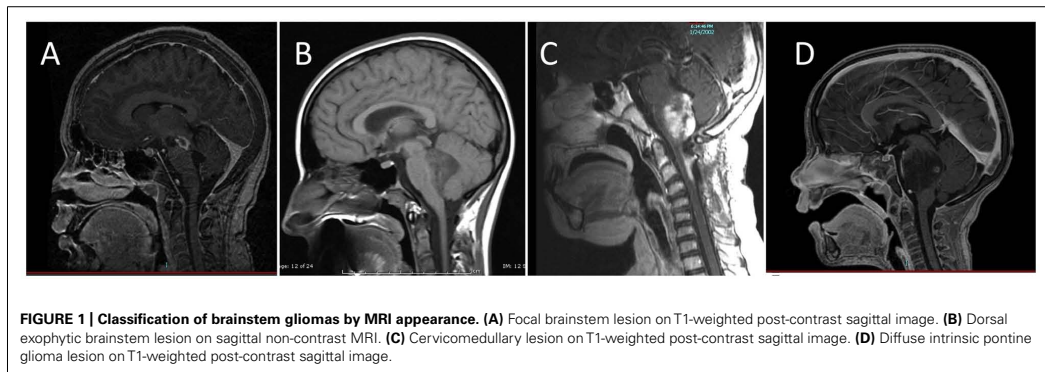
Diffuse intrinsic pontine gliomas are the most common brainstem tumors in children, representing 75–80% of pediatric brainstem tumors, and affecting an estimated 200–300 children in the United States each year. While brainstem tumors have sometimes been grouped together as a single entity, magnetic resonance imaging (MRI) has allowed classification of these tumors into distinct subsets of focal, dorsally exophytic, cervicomedullary, or diffusely infiltrating tumors based on imaging characteristics (Epstein and Farmer, 1993; **Figure 1**). The prognosis for children with diffusely infiltrating pontine gliomas is significantly worse than that of other brainstem tumors. The pons contains cranial nerve nuclei and nuclei critical for life-sustaining function, so damage by the tumor or its treatment has tremendous repercussions. Resection is not an option and the tumors are resistant to other therapeutic measures.

PRESENTATION AND DIAGNOSIS

Diffuse intrinsic pontine glioma is generally a disease of middle childhood, with the majority of children diagnosed between 5 and 10 years of age. Most present with some evidence of brainstem dysfunction or cerebrospinal fluid (CSF) obstruction, although a handful of tumors are identified as incidental findings. Typically, symptoms are present for a short period of time (i.e., <1 month), but it is not unusual to have generalized or subtle symptoms present for several months prior to diagnosis. Commonly reported symptoms include abnormal or limited eye movements, diplopia, an asymmetric smile, clumsiness, difficulty walking, loss of balance, and weakness. Classic findings on clinical examination include the triad of multiple cranial neuropathies, long tract signs (hyperreflexia, clonus, increased tone, presence of a Babinski reflex), and ataxia. Signs and symptoms of increased intracranial pressure may be present due to obstructive hydrocephalus resulting from expansion of the pons. Various other symptoms may occur, including behavioral changes, night terrors, and school difficulties.

The diagnosis of DIPG is based on characteristic MRI findings in the face of this typical clinical presentation (**Figure 2**). On MRI, the tumor appears as a large expansile brainstem mass as opposed to an extrinsic mass compressing the pons. While there may be an exophytic component due to expansion of the tumor via the path of least resistance, the epicenter of DIPG lies within the pons, and the lesion involves the majority of the pons. DIPGs are

FIGURE 1 | Classification of brainstem gliomas by MRI appearance. (A) Focal brainstem lesion on T1-weighted post-contrast sagittal image. (B) Dorsal exophytic brainstem lesion on sagittal non-contrast MRI. (C) Cervicomedullary lesion on T1-weighted post-contrast sagittal image. (D) Diffuse intrinsic pontine glioma lesion on T1-weighted post-contrast sagittal image.

FIGURE 2 | Typical MRI appearance of DIPG. (A) T1-weighted post contrast, (B) T2-weighted, (C) FLAIR.

hypo- or iso-intense on T1- weighted imaging, hyperintense on T2-weighted imaging, and frequently appear relatively homogeneous on fluid attenuated inversion recovery (FLAIR) sequences. Pinpoint intratumoral hemorrhages are not uncommon. Other MRI features of typical DIPG include ventral involvement of the pons, and encasement of the basilar artery. Contrast-enhancement is variable, but these lesions frequently do not significantly enhance at diagnosis.

Prior to the routine use of MRI, it is estimated that up to 15% of patients diagnosed with DIPG actually had a non-tumor process or non-glial tumor (Jenkin et al., 1987; Epstein and Wisoff, 1988), and biopsy procedures were frequently undertaken for histological confirmation. Although MRI is not 100% specific, the vast majority of children diagnosed with DIPG by MRI do have a diffuse infiltrative glioma. Consequently, in the early 1990s when MRI became widely available, it was proposed that obtaining tissue for histologic confirmation was not necessary in children with a typical clinical presentation and distinctive radiographic findings on MRI (Albright et al., 1993; Cartmill and Punt, 1999). This recommendation was rapidly incorporated as standard practice given the perceived surgical risk in this delicate area, particularly for children with concurrent increased intracranial pressure and those

considered poor surgical candidates. Since the available therapies at the time were primarily non-specific cytotoxic agents, the initial repercussions of diagnosis without tissue appeared to be of little consequence.

HISTOLOGY

Because of limited tissue availability, our knowledge of DIPG comes primarily from evaluation of autopsy specimens, small biopsy samples obtained from patients with atypical radiographic findings, and biopsy samples obtained from a small number of institutions such as the Institut Gustave-Roussy where biopsy has been routinely performed on children with suspected DIPG since 2003 (Roujeau et al., 2007). The majority of diffusely infiltrating brainstem tumors are fibrillary astrocytomas, histologically resembling malignant gliomas in other locations. Anaplasia, increased mitotic activity, tumor necrosis, and vascular proliferation are often, but not always, present. DIPGs may therefore be classified histologically as fibrillary astrocytomas, World Health Organization (WHO) Grades II–IV (Schumacher et al., 2007), although the utility of grading has been questioned. When biopsies are indicated, they are generally obtained from the most accessible area and may not be representative of the entire tumor as significant

geographic variability of these tumors has been reported (Warren et al., 2011c; **Figure 3**). In addition, prognosis is not associated with histological grade (Edwards et al., 1989; Grigsby et al., 1989; Hargrave et al., 2006; Laigle-Donadey et al., 2008).

Tumor cells often appear relatively small, with prominent cytoplasmic intermediate filaments and cell processes, similar to fibrillary astrocytomas in other locations of the brain (Maria et al., 1993). In DIPG, tumor cells tend to pervade normal cells, diffusely expanding the pons and distorting, displacing and destroying nerve fiber tracts that normally course through it (Maria et al., 1993). The tumors tend to spread contiguously, extending to involve the midbrain, medulla, and cerebellar peduncles (Mantravadi et al., 1982; Grigsby et al., 1989). Despite this tendency for local spread, CNS metastasis at diagnosis is not uncommon, with up to 20% of patients reported to have leptomeningeal disease at diagnosis (Donahue et al., 1998; Sethi et al., 2011). This may be an underestimate, as spinal disease is not always investigated in asymptomatic patients. Significantly higher numbers of patients (up to 56%) have evidence of spinal metastases or leptomeningeal dissemination at the time of recurrence or autopsy (Donahue et al., 1998; Gururangan et al., 2006; Sethi et al., 2011).

STANDARD THERAPY AND DISEASE COURSE

The standard of care for children with newly diagnosed DIPG is focal radiation therapy, using a 1 cm margin to cover microscopic disease, to a total dose of 54–60 Gy administered over 6 weeks, usually in daily (Monday–Friday) 180–200 cGy fractions. Glucocorticoids are frequently administered in an effort to reduce and control edema associated with the tumor and radiation treatment. About 75% of patients will have some improvement in neurological symptoms in response to radiation therapy and steroids, but many patients suffer concomitant adverse effects primarily attributed to steroids. Radiation therapy appears to control tumor growth for a short period of time, prolonging survival by a mean of ~3 months (Haas-Kogan et al., 2011). Patients receiving doses under 50 Gy have a worse outcome compared to those receiving higher doses (Lee, 1975; Kim et al., 1980; Litman et al., 1980). Total radiation doses higher than 60 Gy have been evaluated. Initial studies utilizing hyperfractionated radiation therapy with total doses up to 72 Gy suggested a modest improvement in survival of children with brainstem gliomas compared to radiation alone, and compared to radiation with neoadjuvant or adjuvant chemotherapy (Edwards et al., 1989; Freeman et al., 1993; Packer et al., 1993). However, subsequent trials using radiation doses up to 78 Gy did not confirm this finding (Freeman et al., 1993; Packer et al., 1994; Mandell et al., 1999). While radiation therapy appears to offer some benefit to children with DIPG, no radiosensitizing agent has improved outcome (Mandell et al., 1999; Marcus et al., 2003; Sanghavi et al., 2003; Bernier-Chastagner et al., 2005).
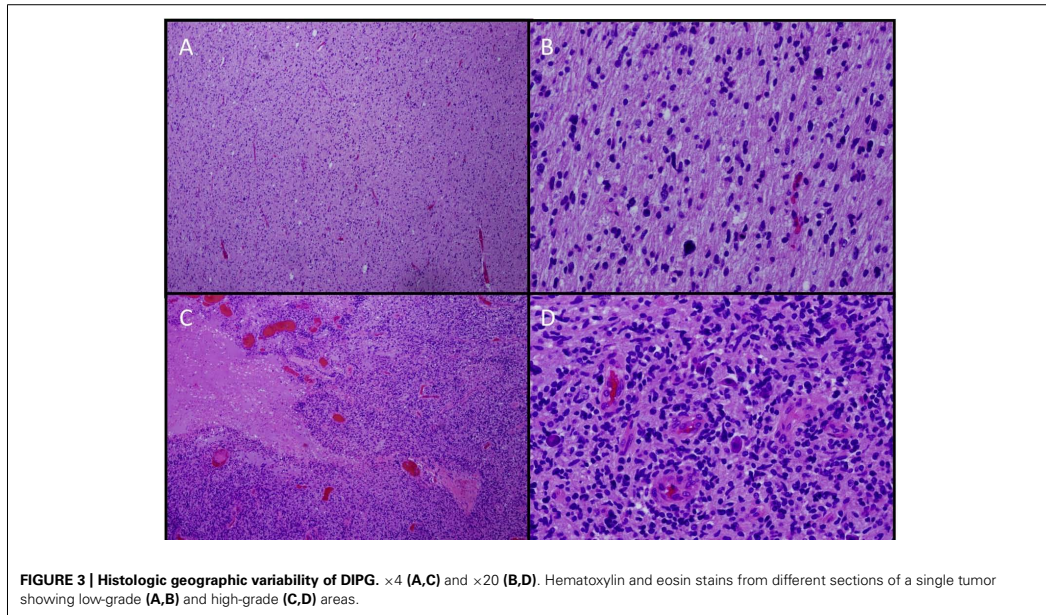
Within 3–8 months after completion of radiation therapy, most children with DIPG will have clinical or radiographic evidence of disease progression. The pattern of failure is generally local. In one study, 25% of cases with disease progression involved the irradiated volume, while 75% involved the margin of the radiation field (Grigsby et al., 1989). Recently, concern

has been raised regarding a suspected increased incidence of distant disease at recurrence with the use of antiangiogenic therapies (Rubenstein et al., 2000; Zuniga et al., 2009), but this has not been clearly demonstrated for patients with DIPG. Additional therapies for DIPG are generally not effective and neurologic deterioration occurs unabated over the ensuing weeks to months.

CHEMOTHERAPY

Because of inevitable disease progression in the vast majority of children with DIPG, many receive adjuvant chemotherapy, frequently as part of a clinical trial, at some point during their disease course in an attempt to improve survival. However, no chemotherapeutic agent has ever demonstrated a significant improvement in outcome beyond that achieved with standard radiation therapy alone. An early prospective, randomized trial performed 25 years ago compared radiation only versus radiation plus post-radiation chemotherapy using prednisone, CCNU, and vincristine (Jenkin et al., 1987). This study was performed prior to the routine use of MRI and included children with brainstem tumors involving the pons or medulla. Five-year survival was not statistically different between the two arms, with 17% 5-year survival noted in the radiation only arm versus 20% in the radiation plus chemotherapy arm. Of note, these survival rates are higher than those reported in more recent trials; this is likely related to the inclusion of non–DIPG patients. DIPG has been studied in a large number of clinical trials including those evaluating cytotoxic agents, high-dose chemotherapy with stem cell rescue (Dunkel et al., 1998; Bouffet et al., 2000), neoadjuvant chemotherapy (Doz et al., 2002), biologic response modifiers (Warren et al., 2006, 2011a,b) and radiation sensitizers, none of which demonstrated significantly improved outcome. Contemporary studies limiting enrollment to patients with DIPG generally report progression-free survival (PFS) of 5–8 months and 2-year overall survival rates of <10% (Pollack et al., 2007, 2011; Gururangan et al., 2010; Haas-Kogan et al., 2011; **Table 1**).

The majority of recent trials are early (i.e., phase I) clinical trials or single-armed phase II studies that rely on historical controls for comparison (Broniscer et al., 2010; Michalski et al., 2010; Cohen et al., 2011; Geoerger et al., 2011; Haas-Kogan et al., 2011; Warren et al., 2011a). Although most, if not all, studies demonstrate the all-too-recognizable ski-slope Kaplan–Meyer survival curve, a true historical cohort has not been defined. Those studies that include younger children, children with a long history of symptoms prior to diagnosis, and children with neurofibromatosis type 1 (NF-1) may favorably bias results, as will those excluding patients with herniation, disseminated disease, and intratumoral hemorrhage. The eligibility criteria for previous and ongoing studies differ, the definition of typical and atypical DIPG is not standardized, and the definition of response or disease progression varies between, and within, pediatric consortia. There is frequently mismatch between clinical and radiographic findings for an individual patient; while some adhere to radiographic definition of response and progression, others adjust treatment based on clinical findings alone (Hayward et al., 2008). Performing DIPG-specific randomized phase II clinical trials that have adequate power to detect modest improvements (e.g., from 10 to 12 months) in outcome

FIGURE 3 | Histologic geographic variability of DIPG. ×4 **(A,C)** and ×20 **(B,D)**. Hematoxylin and eosin stains from different sections of a single tumor showing low-grade **(A,B)** and high-grade **(C,D)** areas.

Table 1 | Results from recent phase II or non-dose-escalating trials (e.g., pilot) for DIPG.

Reference	Year	Treatment	No. of evaluable patients	Median PFS, EFS, or TTP (month)	Median OS (month)	Median 1-year OS (%)	Comment
Warren et al. (2011a)	2012	XRT, PEG-Intron	32	7.8	11.5	46 ± 9	
Chassot et al. (2012)	2012	TMZ + XRT	21	7.5	11.7	50	Biopsy-proven
Cohen et al. (2011)	2011	TMZ + XRT	58	6.1	9.6	40 ± 6.5	
Haas-Kogan et al. (2011)	2011	Tipifarnib + XRT	40	5.9	8.9	35 ± 7.5	
Pollack et al. (2011)	2011	Gefitinib + XRT	43	7.4		56 ± 7.6	
Sharp et al. (2010)	2010	Metronomic TMZ + XRT	15	5.13	9.8	20 ± 10.3	
Kim et al. (2010)	2010	TMZ + thal + XRT	12	7.2	12.7	58.3	
Jalali et al. (2010)	2010	TMZ + XRT	20	6.9	9.15		
Frappaz et al. (2008)	2008	Pre-XRT chemo (BCNU/MTX)			17		11 patients with symptoms >1 month prior to dx
Sirachainan et al. (2008)	2008	TMZ + XRT, then TMZ + cRA	12	10.2 ± 3	13.5 ± 3.6	58 ± 14.2	7 patients <5 years; OS 16.2 ± 0.7 months
Korones et al. (2008)	2007	VCR, VP-16, XRT	30		9	27.7 ± 7	
Turner et al. (2007)	2007	Thal + XRT	12	5	9		
Aquino-Parsons et al. (2008)	2006	Carbogen + XRT	7	8	9.6		
Bernier-Chastagner et al. (2005)	2005	Topotecan + XRT	32		8.3	25.5 ± 8	

DIPG, diffuse intrinsic pontine glioma; DIBG, diffuse intrinsic brainstem glioma; XRT, radiation therapy; PFS, progression-free survival; TMZ, temozolomide; TTP, time to progression; EFS, event-free survival; OS, overall survival; cRA, cis-retinoic acid.

is generally precluded by the relatively small number of patients and the time necessary to reach objective endpoints. Until a more contemporary historical cohort is defined, studies that attempt to identify a modest improvement in survival would therefore require a large number of patients or a randomized control arm involving DIPG patients who receive radiation therapy only, something that is not likely to appeal to patients, families or treating physicians.

OBSTACLES TO CHEMOTHERAPY

A number of obstacles that may contribute to the lack of efficacy of chemotherapeutic agents are known or suspected. For a drug to be effective against a tumor, you need to have an active agent, delivered to its site of activity, and present in its active form in effective concentrations for a long enough period of time. The cells need to be sensitive to the agent, and if it is a molecularly targeted agent, the target must be present. While this may be stating the obvious, from a practical standpoint, much of this information is unknown when treating a patient with DIPG.

There are several factors that can affect drug levels at the brain tumor site. These include the concentration of drug in the bloodstream, the amount of protein and tissue binding (i.e., it is the free or unbound drug that is active), and the degree of CNS penetration (i.e., how much drug crosses the blood:brain or blood:tumor barriers and diffuses across the brain parenchyma to its site of action). The blood:brain barrier (BBB), a layer of specialized endothelial cells comprising the wall of CNS capillaries, re-enforced by its surrounding basal lamina, pericytes, astrocytes, and microglia (Wolburg et al., 2009), serves to protect the CNS from toxins, limits the CNS penetration of large, hydrophilic substances, and thereby hinders delivery of many chemotherapeutic agents to the tumor site. The blood:tumor barrier may be less restrictive due to disrupted and leaky tumor vessels, but even if agents are able to cross, diffusion of agents across the parenchyma remains limited to only a few millimeters (Morrison and Dedrick, 1986).

Given the lack of adequate tumor-bearing animal models and the ethical constraints of sampling brain tumor tissue in children, the degree of drug penetration at the tumor site and therefore adequate drug dosing remains unknown. With empiric cytotoxic agents, the paradigm is to treat with the maximum tolerated dose (MTD), but this may not result in adequate exposure at the tumor site, and is not applicable to molecularly targeted agents for which an MTD may not be identified.

Several strategies have been employed to overcome the BBB and improve drug delivery to the tumor site. These include the use of high dose chemotherapy with stem cell rescue (Finlay and Zacharoulis, 2005), biologic or osmotic BBB disruption (Hall et al., 2006; Warren et al., 2006), and p-glycoprotein inhibition (Greenberg et al., 2005). Most recently, convection-enhanced delivery has been used to deliver agents directly into the tumor of patients with DIPG (Lonser et al., 2007). Using this technique, agents are delivered under continuous low-pressure via a catheter placed directly in the tumor or tumor bed, and clinical trials in children with DIPG are ongoing.

When treating with chemotherapy, it would be advantageous to assess drug activity or inactivity early in the treatment course so treatment options can be reassessed and patients will not be exposed to additional cycles of inactive agents. Determining the acute effects of an agent, particularly a cytostatic agent, and early efficacy on the tumor and its microenvironment can be difficult. In neuro-oncology, activity of an antitumor agent is frequently assessed using MacDonald criteria (MacDonald et al., 1990) or a variant, with decreased tumor size, decreased steroid use, and improved neurologic symptoms indicative of response. However, there are a number of issues with applying these response criteria to patients with DIPG. These criteria were developed primarily for enhancing supratentorial gliomas, and DIPG frequently do not enhance or they may exhibit a heterogeneous pattern of enhancement. Given their invasive nature and indistinct borders, there is significant interobserver variability using standard tumor measurement criteria when measuring DIPG on MRI (Hayward et al., 2008). Even if the tumor size is reduced by a chemotherapeutic regimen, this is generally not sustained and does not translate into improved survival. Standard MRI cannot reliably differentiate tumor and treatment effects, and phenomena such as pseudoprogression and pseudoresponse complicate interpretation of MR images. For children with DIPG, new enhancement months after radiation therapy may represent treatment effect (e.g., radiation necrosis), tumor progression, or both. These cannot be easily distinguished using standard MRI, resulting in a frustrating predicament for both families and caregivers.

Non-invasive evaluation to identify response to antitumor agents continues to be investigated, and some imaging techniques, such as MR perfusion and magnetic resonance spectroscopy (MRS), have shown promise as predictive or surrogate markers of response in this population (Hipp et al., 2011; Steffen-Smith et al., 2011). In one study, evaluating spectroscopy in 38 children with DIPG, the choline:N-acetyl aspartate ratio (CHO:NAA) was shown to be prognostic, with those patients having CHO:NAA higher than the median of 2.1 demonstrating a greater risk of mortality compared to patients with CHO:NAA ≤ 2.1 (Steffen-Smith et al., 2011). This study also showed that changes in CHO:NAA over time were associated with outcome. Any increase in CHO:NAA was inversely associated with survival ($p = 0.009$), while decreasing CHO:NAA was associated with a decreased risk of death. The greater the change, the more significant the observed effect.

Likewise, perfusion studies were evaluated in a group of DIPG patients. In general, tumor growth is associated with increased vessel density and increased vessel permeability, features that can be evaluated on newer MRI sequences. Increased blood flow to a region of interest may be indicative of increased vascular growth, associated with tumor grade, or associated with malignant transformation. In a recent study by Price et al. (2011) relative cerebral blood volume (rCBV) determined on perfusion imaging correlated with cell proliferation in adults with high-grade gliomas. In a study evaluating perfusion imaging in 34 children with DIPG, increased perfusion at *any* single time point was associated with shorter survival (RR = 4.91; Hipp et al., 2011). In addition, increasing perfusion over time was a poor prognostic factor. Additional imaging techniques such as diffusion tensor imaging are being evaluated in children with DIPG although their clinical utility remains to be seen.

LACK OF TISSUE

Because of limited tissue availability, very little information on the biology and pathophysiology of DIPG has been available in the literature (Louis et al., 1993; Cheng et al., 1999; Gilbertson et al., 2003) until recently. The importance of understanding the biology of DIPG has been brought to the forefront with the development of molecularly targeted agents. No molecularly targeted agent has been shown to significantly improve survival in a clinical trial for children with DIPG. This includes therapeutic agents aimed at targets defined in adult high-grade gliomas, including platelet-derived growth factor receptor (PDGFR; Pollack et al., 2007), epidermal growth factor receptor (EGFR; Geoerger et al., 2011; Pollack et al., 2011), vascular endothelial growth factor receptor-2 (VEGFR2) (Broniscer et al., 2010), and farnesyl transferase (Haas-Kogan et al., 2011). Determining why these agents fail is key to advancing the use of molecularly targeted agents in general for the treatment of children with DIPG.

An unprecedented number of studies on the biology of DIPG have been published in the past few years (Joshi et al., 2008; Paugh et al., 2010, 2011; Zarghooni et al., 2010; Barrow et al., 2011; Monje et al., 2011; Warren et al., 2011c). These studies give insight as to the possible cell of origin, genetic profiling, driver mutations, and oncogenic alterations. While the etiology and exact pathophysiology of DIPG remain to be determined, critical pathways and potential treatment targets have been identified, and critical conclusions can be drawn: (1) pediatric DIPGs differ from adult high-grade gliomas, (2) pediatric DIPGs differ from pediatric supratentorial high-grade gliomas, (3) genomic studies of DIPG demonstrate aberrations in druggable targets, (4) significant interpatient and intrapatient variability exists, and (5) the tumor microenvironment appears to play a key role in DIPG tumorigenesis.

An intriguing characteristic of DIPG is the predominant age group affected, with a peak incidence in middle childhood, suggesting an etiology associated with development. In efforts to define a potential cell of origin, Monje et al. (2011) examined the spatial and temporal distribution of neural precursor cells in the human brainstem. They described a distinct cell population in the ventral pons that is Nestin and Vimentin immunopositive (both markers of primitive neuroectodermal cell types in the developing and post-natal CNS); approximately half of these cells are also positive for the basic helix-loop-helix transcription factor Olig2 (classically associated with oligodendroglial lineage precursor cells). They demonstrated that the density of this Nestin+ Vimentin+ Olig2+ cell type normally changes during childhood. It is present in all ventral brainstem structures during infancy, decreases by 2 years of age, and then increases again during middle childhood. What regulates the changing density of this cell population in humans is unknown. However, using a mouse model, Monje et al. (2011) determined that Hedgehog signaling drives proliferation of Olig2+ cells in the ventral pons of mice. In addition, Hedgehog activity and Hedgehog-responsive cells increased in the ventral pons of the mouse during the time period corresponding to middle childhood in humans. These studies suggest that the nature of neural precursor cells in the ventral pons and the

microenvironment within the developing brain may influence the disease process.

Puget et al. (2012) also implicated the Sonic Hedgehog pathway in a trial in which they performed genomic studies on a large number ($n = 61$) of newly diagnosed children with DIPG. In this study, DIPG was distinguished from high-grade gliomas by several genes involved in the Sonic Hedgehog pathway. The authors suggest that the gene expression signatures of DIPG were associated with "differential reprogramming of embryonic signaling organizers." They demonstrated involvement of two distinct oncogenic pathways that resulted in two biological DIPG subgroups, including one group with an oligodendroglial phenotype that was associated with PDGFRA gain or amplification, and another group referred to as the mesenchymal and pro-angiogenic phenotype that was associated with higher expression of STAT3.

Both the Monje and Puget studies implicate altered gene expression during development as potentially key steps in DIPG pathogenesis. Histones play an important role in gene regulation, influencing chromatin structure and accessibility, and post-translational modifications of the histone tail play a role in epigenetic regulation of gene expression. Notably, two recent studies demonstrated somatic mutations in histone H3.3 associated with DIPG (Khuong-Quang et al., 2012; Wu et al., 2012). Wu et al. (2012) performed whole genome sequencing on DNA of seven patients with DIPG and showed that four of these seven had a mutation in *H3F3A* (the gene that encodes the H3.3 protein) or *HIST1H3B* (gene which encodes H3.1) that resulted in a K27M substitution (lysine replaced by methionine at amino acid 27). They expanded this study in 43 additional DIPG patients and found that 78% of DIPG patients demonstrated K27M substitutions in *H3F3A* or *HIST1H3B* compared to only 22% of non-brainstem glioma patients. Similarly, Khuong-Quang et al. (2012) demonstrated that 71% of 42 DIPG patients had the K27M mutation compared to 14% of supratentorial glioblastomas. They also noted that patients with wild type H3.3 had better overall survival. Interestingly, H3.3 is located on Chromosome 1q, an area commonly gained in DIPG (Barrow et al., 2011; Warren et al., 2011c). However, in the study by Wu et al. (2012), there was no significant correlation between the presence of *H3F3A* mutations and gain of chromosome 1q. Lysine 27 of the histone H3 tail is also a key residue for epigenetic regulation of neural precursor cell differentiation (Liu and Casaccia, 2010).

Several genomic studies have identified a number of chromosomal aberrations and targets in DIPG, including PDGFRA, MDM4, MYCN, EGFR, MET, KRAS, CDK4, amongst others (Paugh et al., 2010, 2011; Zarghooni et al., 2010; Barrow et al., 2011; Warren et al., 2011c; Grill et al., 2012; Li et al., 2012). Not surprisingly, many of the identified aberrations involve genes that regulate cell growth, cell death, and repair pathways. Rather than describe each of these in detail, it is important to realize that, although these studies significantly contribute to our knowledge and understanding of the biology of DIPG, the number of samples is relatively small. The glaring fact is that no one target is identified in all tumor cells of all patients with DIPG. Treating a single target will therefore unlikely result in a significantly improved outcome for these patients. Indeed, clinical trials evaluating individual molecularly

targeted agents have been performed in children with DIPG without success. Precise reasons for the lack of efficacy are unknown, but in most, if not all, studies, it is unknown if the target was expressed, was insufficiently expressed, or whether drug exposure at the target site was adequate. Presumably, combinations of several targeted agents will be necessary to observe an effect given the multiple chromosomal alterations found in individual patient samples.

BIOPSY

In contrast to the majority of centers in the United States, routine biopsy of children with suspected DIPG has been performed in Europe since 2003 (Roujeau et al., 2007). In the initial report detailing their experience in 24 children, the investigators report morbidity in 2 children (cranial nerve palsy, worsening hemiparesis) which was reversible, and no incidents of mortality, concluding that the procedure was relatively safe in experienced hands using modern neurosurgical technique (Roujeau et al., 2007). Given this demonstration of relative safety, along with the significant information obtained, the ability to perform genomic testing on small tissue samples, the identification of potentially druggable targets and known interpatient heterogeneity, there is a movement within the pediatric neuro-oncology community to push for routine biopsy of patients with suspected DIPG (Mac-Donald, 2012; Rutka, 2012) although this remains under debate (Boop, 2011).

Because the vast majority of samples biopsied are malignant gliomas, the primary purpose of the biopsy in patients with a typical clinical presentation and typical radiographic appearance would not necessarily be for histologic confirmation, although this would be important for those with atypical features, particularly since brainstem PNET can mimic DIPG radiographically (Sufit et al., 2012). Rather, the major question to be addressed is whether or not treatment chosen based on biopsy results can improve the outcome of these children. Intrapatient heterogeneity of DIPG has been demonstrated, and defining where to biopsy and how representative these results are of the tumor need to be broached. At the very least, routine biopsy would supply additional tissue for study, may enhance our understanding of the disease, and enrich the datasets gleaned from clinical trials.

CONCLUSION

An unprecedented number of biologic and genomic studies, generating considerable novel and exciting data, have been performed on DIPG over the past few years, primarily due to a number of collaborative efforts. We now know that DIPGs are a distinct entity, biologically different from both adult high-grade gliomas and pediatric supratentorial high-grade gliomas. We know that genomic mutations occur in DIPG, resulting in a number of druggable targets. However, we also know that no single target defines DIPG, and significant inter- and intrapatient variability exists. Our challenge now is to select appropriate targets, treat with agents at doses that will result in adequate exposure at the site of action, and rapidly identify drug efficacy or lack of response in individual patients. Until we are able to non-invasively identify targets, obtaining tissue from patients will be important for selecting appropriate agents, so that children with DIPG will only be exposed to those agents that have any chance of benefit. Tumor assessment, identification of tumor targets, selection of appropriate agents, and determination of adequate dosing should inform treatment selection, and pre-treatment determination of this data may become the new study paradigm for the next generation of DIPG clinical trials.

It is imperative that we continue to embrace global collaborations given the relatively small numbers of patients. It is key to be able to perform trials and identify efficacious treatment paradigms quickly. We need to be able to compare results from different clinical trials; to do this, similar eligibility and response criteria are necessary, and it is important to identify an appropriate historical cohort. Finally, it is necessary to change our mindset, and not be mired in historical outcomes for children with DIPG, as recent data opens a host of avenues for promising approaches.

ACKNOWLEDGMENTS

REFERENCES

Albright, A., Packer, R., Zimmerman, R., Rorke, L., Boyett, J., and Hammond, G. (1993). Magnetic resonance scans should replace biopsies for the diagnosis of diffuse brain stem gliomas: a report from the Children's Cancer Group. *Neurosurgery* 33, 1026–1029.

Aquino-Parsons, C., Hukin, J., and Green, A. (2008). Concurrent carbogen and radiation therapy in children with high-risk brainstem gliomas. *Pediatr. Blood Cancer* 50, 397–399.

Barrow, J., Adamowicz-Brice, M., Cartmill, M., Macarthur, D., Lowe, J., Robson, K., et al. (2011). Homozygous loss of ADAM3A revealed by genome-wide analysis of pediatric high-grade glioma and diffuse intrinsic pontine gliomas. *Neuro Oncol.* 13, 212–222.

Bernier-Chastagner, V., Grill, J., Doz, F., Bracard, S., Gentet, J., Marie-Cardine, A., et al. (2005). Topotecan as a radiosensitizer in the treatment of children with malignant diffuse brainstem gliomas: results of a French Society of Paediatric Oncology Phase II study. *Cancer* 104, 2792–2797.

Boop, F. (2011). Brainstem gliomas. *J. Neurosurg. Pediatr.* 8, 537–538.

Bouffet, E., Raquin, M., Doz, F., Gentet, J., Rodary, C., Demeocq, F., et al. (2000). Radiotherapy followed by high dose busulfan and thiotepa: a prospective assessment of high dose chemotherapy in children with diffuse pontine gliomas. *Cancer* 88, 685–692.

Broniscer, A., Baker, J., Tagen, M., Onar-Thomas, A., Gilbertson, R., Davidoff, A., et al. (2010). Phase I study of vandetanib during and after radiotherapy in children with diffuse intrinsic pontine glioma. *J. Clin. Oncol.* 28, 4762–4768.

Cartmill, M., and Punt, J. (1999). Diffuse brain stem glioma. A review of stereotactic biopsies. *Childs Nerv. Syst.* 15, 235–237.

Chassot, A., Canale, S., Varlet, P., Puget, S., Roujeau, T., Negretti, L., et al. (2012). Radiotherapy with concurrent and adjuvant temozolomide in children with newly diagnosed diffuse intrinsic pontine glioma. *J. Neurooncol.* 106, 399–407.

Cheng, Y., Ng, H., Zhang, S., Ding, M., Pang, J., Zheng, J., et al. (1999). Genetic alterations in pediatric high-grade astrocytomas. *Hum. Pathol.* 30, 1284–1290.

Cohen, K., Heideman, R., Zhou, T., Holmes, E., Lavey, R., Bouffet, E., et al. (2011). Temozolomide in the treatment of children with newly diagnosed diffuse intrinsic pontine gliomas: a report from the Children's Oncology Group. *Neuro Oncol.* 13, 410–416.

Donahue, B., Allen, J., Siffert, J., Rosovsky, M., and Pinto, R. (1998). Patterns of recurrence in brain stem gliomas: evidence for craniospinal dissemination. *Int. J. Radiat. Oncol. Biol. Phys.* 40, 677–680.

Doz, F., Neuenschwander, S., Bouffet, E., Gentet, J., Schneider, P., Kalifa, C., et al. (2002). Carboplatin before and during radiation therapy for the treatment of malignant brain stem tumours: a study by the Societe Francaise d'Oncologie Pediatrique. *Eur. J. Cancer* 38, 815–819.

Dunkel, I., Garvin, J., Goldman, S., Ettinger, L., Kaplan, A., Cairo, M., et al. (1998). High dose

chemotherapy with autologous bone marrow rescue for children with diffuse pontine brain stem tumors. Children's Cancer Group. *J. Neurooncol.* 37, 67–73.

Edwards, M., Wara, W., Urtasun, R., Prados, M., Levin, V., Fulton, D., et al. (1989). Hyperfractionated radiation therapy for brain-stem glioma: a phase I-II trial. *J. Neurosurg.* 70, 691–700.

Epstein, F., and Farmer, J. P. (1993). Brain-stem glioma growth patterns. *J. Neurosurg.* 78, 408–412.

Epstein, F., and Wisoff, J. (1988). Intrinsic brainstem tumors in childhood: surgical indications. *J. Neurooncol.* 6, 309–317.

Finlay, J., and Zacharoulis, S. (2005). The treatment of high grade gliomas and diffuse intrinsic pontine tumors of childhood and adolescence: a historical – and futuristic – perspective. *J. Neurooncol.* 75, 253–266.

Frappaz, D., Schell, M., Thiesse, P., Marec-Bérard, P., Mottolese, C., Perol, D., et al. (2008). Preradiation chemotherapy may improve survival in pediatric diffuse intrinsic brainstem gliomas: final results of BSG 98 prospective trial. *Neuro Oncol.* 10, 599–607.

Freeman, C., Krischer, J., Sanford, R., Cohen, M., Burger, P., Del Carpio, R., et al. (1993). Final results of a study of escalating doses of hyperfractionated radiotherapy in brain stem tumors in children: a Pediatric Oncology Group study. *Int. J. Radiat. Oncol. Biol. Phys.* 27, 197–206.

Geoerger, B., Kieran, M., Grupp, S., Perek, D., Clancy, J., Krygowski, M., et al. (2011). Phase II trial of temsirolimus inchildren with high-grade glioma, neuroblastoma and rhabdomyosarcoma. *Eur. J. Cancer* 4853–4862.

Gilbertson, R., Hill, D., Hernan, R., Kocak, M., Geyer, R., Olson, J., et al. (2003). ERBB1 is amplified and overexpressed in high-grade diffusely infiltrative brain stem glioma. *Clin. Cancer Res.* 9, 3620–3624.

Greenberg, M., Fisher, P., Freeman, C., Korones, D., Bernstein, M., Friedman, H., et al. (2005). Etoposide, vincristine, and cyclosporin A wth standard-dose radiation therapy in newly diagnosed diffuse intrinsic brainstem gliomas: a pediatric oncology group phase I study. *Pediatr. Blood Cancer* 45, 644–648.

Grigsby, P., Garcia, D., and Ghiselli, R. (1989). Analysis of autopsy findings in patients treated with irradiation for thalamic and brain stem tumors. *Am. J. Clin. Oncol.* 12, 255–258.

Grill, J., Puget, S., Andreiuolo, F., Philippe, C., Macconaill, L., and Kieran, M. (2012). Critical oncogenic mutations in newly diagnosed pediatric diffuse intrinsic pontine glioma. *Pediatr. Blood Cancer* 58, 489–491.

Gururangan, S., Chi, S., Young Poussaint, T., Onar-Thomas, A., Gilbertson, R., Vajapeyam, S., et al. (2010). Lack of efficacy of bevacizumab plus irinotecan in children with recurrent malignant glioma and diffuse brainstem glioma: a Pediatric Brain Tumor Consortium study. *J. Clin. Oncol.* 28, 3069–3075.

Gururangan, S., Mclaughlin, C., Brashears, J., Watral, M., Provenzale, J., Coleman, R., et al. (2006). Incidence and patterns of neuroaxis metastases in children with diffuse pontine glioma. *J. Neurooncol.* 77, 207–212.

Haas-Kogan, D., Banerjee, A., Poussaint, T., Kocak, M., Prados, M., Geyer, J., et al. (2011). Phase II trial of tipifarnib and radiation in children with newly diagnosed diffuse intrinsic pontine gliomas. *Neuro Oncol.* 13, 298–306.

Hall, W., Doolittle, N., Daman, M., Bruns, P., Muldoon, L., Fortin, D., et al. (2006). Osmotic blood–brain barrier disruption chemotherapy for diffuse pontine gliomas. *J. Neurooncol.* 77, 279–284.

Hargrave, D., Bartels, U., and Bouffet, E. (2006). Diffuse brainstem glioma in children: critical review of clinical trials. *Lancet Oncol.* 7, 241–248.

Hayward, R., Bent, R., Steffen-Smith, E., Wiest, J., and Warren, K. (2008). Use of imaging in response criteria for pediatric patients with diffuse intrinsic pontine gliomas. *Neuro Oncol.* 10, 394.

Hipp, S., Steffen-Smith, E., Hammoud, D., Shih, J., Bent, R., and Warren, K. (2011). Predicting outcome of children with diffuse intrinsic pontine gliomas using multiparametric imaging. *Neuro Oncol.* 13, 904–909.

Howlader, N., Noone, A., Krapcho, M., Neyman, N., Aminou, R., Waldron, W., et al. (2011). *SEER Cancer Statistics Review, 1975–2008.* Bethesda, MD: National Cancer Institute.

Jalali, R., Raut, N., Arora, B., Gupta, T., Dutta, D., Munshi, A., et al. (2010). Prospective evaluation of radiotherapy with concurrent and adjuvant temozolomide in children with newly diagnosed diffuse intrinsic pontine glioma. *Int. J. Radiat. Oncol. Biol. Phys.* 77, 113–118.

Jenkin, R., Boesel, C., Ertel, I., Evans, A., Hittle, R., Ortega, J., et al. (1987). Brain-stem tumors in childhood: a prospective randomized trial of irradiation with and without adjuvant

CCNU, VCR, and prednisone. A report of the Childrens Cancer Study Group. *J. Neurosurg.* 66, 227–233.

Joshi, B., Puri, R., Leland, P., Varricchio, F., Gupta, G., Kocak, M., et al. (2008). Identification of Interleukin-13 receptor alpha2 chain overexpression in situ in high-grade diffusely infiltrative pediatric brainstem glioma. *Neuro Oncol.* 10, 265–274.

Khuong-Quang, D.-A., Buczkowicz, P., Rakopoulos, P., Liu, X.-Y., Fontebasso, A., Bouffet, E., et al. (2012). K27M mutation in histone H3.3 defines clinically and biologically distinct subgroups of pediatric diffuse intrinsic pontine gliomas. *Acta Neuropathol.* 124, 439–447.

Kim, C., Kim, S., Phi, J., Lee, M., Kim, I., Kim, I., et al. (2010). A prospective study of temozolomide plus thalidomide during and after radiation therapy for pediatric diffuse pontine gliomas: preliminary results of the Korean Society for Pediatric Neuro-Oncology study. *J. Neurooncol.* 100, 193–198.

Kim, T., Chin, H., Pollan, S., Hazel, J., and Webster, J. (1980). Radiotherapy of primary brain stem tumors. *Int. J. Radiat. Oncol. Biol. Phys.* 6, 51–57.

Korones, D., Fisher, P., Kretschmar, C., Zhou, T., Chen, Z., Kepner, J., et al. (2008). Treatment of children with diffuse intrinsic brain stem glioma with radiotherapy, vincristine and oral VP-16: a Children's Oncology Group phase II study. *Pediatr. Blood Cancer* 50, 227–230.

Laigle-Donadey, F., Doz, F., and Delattre, J. (2008). Brainstem gliomas in children and adults. *Curr. Opin. Oncol.* 20, 662–667.

Lee, F. (1975). Radiation of infratentorial and supratentorial brain-stem tumors. *J. Neurosurg.* 43, 65–68.

Li, G., Mitra, S., Monje, M., Henrich, K., Bangs, C., Nitta, R., et al. (2012). Expression of epidermal growth factor variant III (EGFRvIII) in pediatric diffuse intrinsic pontine gliomas. *J. Neurooncol.* 108, 395–402.

Litman, P., Jarrett, P., Bilaniuk, L., Rorke, L., Zimmerman, R., Bruce, D., et al. (1980). Pediatric brain stem gliomas. *Cancer* 45, 2787–2792.

Liu, J., and Casaccia, P. (2010). Epigenetic regulation of oligodendrocyte identity. *Trends Neurosci.* 33, 193–201.

Lonser, R., Warren, K., Butman, J., Quezado, Z., Robison, R., Walbridge, S., et al. (2007). Real-time image-guided direct convective perfusion of intrinsic brainstem lesions. Technical note. *J. Neurosurg.* 107, 190–197.

Louis, D., Rubio, M., Correa, K., Gusella, J., and Von Diemling, A. (1993). Molecular genetics of pediatric brain stem gliomas. Application of PCR techniques to small and archival brain tumor specimens. *J. Neuropathol. Exp. Neurol.* 52, 507–515.

MacDonald, D., Cascino, T., Schold, S., and Cairncross, J. (1990). Response criteria for phase II studies of supratentorial malignant glioma. *J. Clin. Oncol.* 8, 1277–1280.

MacDonald, T. (2012). Diffuse intrinsic pontine glioma: time to biopsy again? *Pediatr. Blood Cancer* 58, 487–488.

Mandell, L., Kadota, R., Freeman, C., Douglass, E., Fontanesi, J., Cohen, M., et al. (1999). There is no role for hyperfractionated radiotherapy in the management of children with newly diagnosed diffuse intrinsic brainstem tumors: results of a Pediatric Oncology Group phase III trial comparing conventional vs. hyperfractionated radiotherapy. *Int. J. Radiat. Oncol. Biol. Phys.* 43, 959–964.

Mantravadi, R., Phatak, R., Bellur, S., Liebner, E., and Haas, R. (1982). Brain stem gliomas: an autopsy study of 25 cases. *Cancer* 49, 1294–1296.

Marcus, K., Dutton, S., Barnes, P., Coleman, C., Pomeroy, S., Goumnerova, L., et al. (2003). A phase I trial of etanidazole and hyperfractionated radiotherapy in children with diffuse brainstem glioma. *Int. J. Radiat. Oncol. Biol. Phys.* 55, 1182–1185.

Maria, B., Rehder, K., Eskin, T., Hamed, L., Fennell, E., Quisling, R., et al. (1993). Brainstem glioma: I. Pathology, clinical features, and therapy. *J. Child. Neurol.* 8, 112–128.

Michalski, A., Bouffet, E., Taylor, R., Hargrave, D., Walker, D., Picton, S., et al. (2010). The addition of high-dose tamoxifen to standard radiotherapy does not improve the survival of patients with diffuse intrinsic pontine glioma. *J. Neurooncol.* 100, 81–88.

Monje, M., Mitra, S., Freret, M., Raveh, T., Kim, J., Masek, M., et al. (2011). Hedgehog-responsive candidate cell of origin for diffuse intrinsic pontine glioma. *Proc. Natl. Acad. Sci. U.S.A.* 108, 4453–4458.

Morrison, P., and Dedrick, R. (1986). Transport of cisplatin in rat brain following microinfusion: an analysis. *J. Pharm. Sci.* 75, 120–128.

Packer, R., Boyett, J., Zimmerman, R., Albright, A., Kaplan, A., Rorke, L., et al. (1994). Outcome of children with brain stem gliomas after treatment with 7800 cGy of hyperfractionated radiotherapy. A Children's

Cancer Group Phase I/II Trial. *Cancer* 74, 1827–1834.

Packer, R., Boyett, J., Zimmerman, R., Rorke, L., Kaplan, A., Albright, A., et al. (1993). Hyperfractionated radiation therapy (72 Gy) for children with brain stem glioma: a Childrens Cancer Group Phase I/II Trial. *Cancer* 72, 1414–1421.

Paugh, B., Broniscer, A., Qu, C., Miller, C., Zhang, J., Tatevossian, R., et al. (2011). Genome-wide analyses identify recurrent amplifications of receptor tyrosine kinases and cell-cycle regulatory genes in diffuse intrinsic pontine glioma. *J. Clin. Oncol.* 29, 3999–4006.

Paugh, B., Qu, C., Jones, C., Liu, Z., Adamowicz-Brice, M., Zhang, J., et al. (2010). Integrated molecular genetic profiling of pediatric high-grade gliomas reveals key differences with the adult disease. *J. Clin. Oncol.* 28, 3061–3068.

Pollack, I., Jakacki, R., Blaney, S., Hancock, M., Kieran, M., Phillips, P., et al. (2007). Phase I trial of imatinib in children with newly diagnosed brainstem and recurrent malignant gliomas: a Pediatric Brain Tumor Consortium report. *Neuro Oncol.* 9, 145–160.

Pollack, I., Stewart, C., Kocak, M., Poussaint, T., Bronsicer, A., Banerjee, A., et al. (2011). A phase II study of gefitinib and irradiation in children with newly diagnosed brainstem gliomas: a report from the Pediatric Brain Tumor Consortium. *Neuro Oncol.* 13, 290–297.

Price, S., Green, H., Dean, A., Joseph, J., Hutchinson, P., and Gillard, J. (2011). Correlation of MR relative cerebral blood volume measurements with cellular density and proliferation in high-grade gliomas: an image-guided biopsy study. *AJNR Am. J. Neuroradiol.* 32, 501–506.

Puget, S., Philippe, C., Bax, D., Job, B., Varlet, P., Junier, M., et al. (2012). Mesenchymal transition and PDGFRA amplification/mutation are key distinct oncogenic events in pediatric diffuse intrinsic pontine gliomas. *PLoS ONE* 7:e30313. doi: 10.1371/journal.pone.0030313

Roujeau, T., Machado, G., Garnett, M., Miquel, C., Puget, S., Geoerger, B., et al. (2007). Stereotactic biopsy of diffuse pontine lesions in children. *J. Neurosurg.* 107, 1–4.

Rubenstein, J., Kim, J., and Ozaka, T. (2000). Anti-VEGF antibody treatment of glioblastoma prolongs survival but results in increased vascular cooption. *Neoplasia* 2, 306–314.

Rutka, J. (2012). Biopsy of diffuse intrinsic pontine glioma? *J. Neurosurg. Pediatr.* 10, 79–80.

Sanghavi, S., Needle, M., Krailo, M., Geyer, J., Ater, J., and Mehta, M. (2003). A phase I study of topotecan as a radiosensitizer for brainstem glioma of childhood: first report of the Children's Cancer Group-0952. *Neuro Oncol.* 5, 8–13.

Schumacher, M., Schulte-Monting, J., Stoeter, P., Warmuth-Metz, M., and Solymosi, L. (2007). Magnetic resonance imaging compared with biopsy in the diagnosis of brainstem diseases of childhood: a multicenter review. *J. Neurosurg.* 106, 111–119.

Sethi, R., Allen, J., Donahue, B., Karajannis, M., Gardner, S., Wisoff, J., et al. (2011). Prospective neuraxis MRI surveillance reveals a high risk of leptomeningeal dissemination in diffuse intrinsic pontine glioma. *J. Neurooncol.* 102, 121–127.

Sharp, J., Bouffet, E., Stempak, D., Gammon, J., Stephens, D., Johnston, D., et al. (2010). A multi-centre Canadian pilot study of metronomic temozolomide combined with radiotherapy for newly diagnosed paediatric brainstem glioma. *Eur. J. Cancer* 46, 3271–3279.

Sirachainan, N., Pakakasama, S., Visudithbhan, A., Chiamchanya, S., Tuntiyatorn, L., Dhanachai, M., et al. (2008). Concurrent radiotherapy with temozolomide followed by adjuvant temozolomide and *cis*-retinoic acid in children with diffuse intrinsic pontine glioma. *Neuro Oncol.* 10, 577–582.

Smith, M., Seibel, N., Altekruse, S., Ries, L., Melbert, D., O'Leary, M., et al. (2010). Outcomes for children and adolescents with cancer: challenges for the twenty-first century. *J. Clin. Oncol.* 28, 2625–2634.

Steffen-Smith, E., Shih, J., Hipp, S., Bent, R., and Warren, K. (2011). Proton magnetic resonance spectroscopy predicts survival in children with diffuse intrinsic pontine glioma. *J. Neurooncol.* 105, 365–373.

Sufit, A., Donson, A., Birks, D., Knipstein, J., Fenton, L., Jedlicka, P., et al. (2012). Diffuse intrinsic pontine tumors: a study of primitive neuroectodermal tumors versus the more common diffuse intrinsic pontine gliomas. *J. Neurosurg. Pediatri.* 10, 81–88.

Turner, C. D., Chi, S., Marcus, K., Macdonald, T., Packer, R., Poussaint, T., et al. (2007). Phase II study of thalidomide and radiation in children with newly diagnosed brain stem gliomas and glioblastoma multiforme. *J. Neurooncol.* 82, 95–101.

Warren, K., Bent, R., Wolters, P., Prager, A., Hanson, R., Packer, R., et al. (2011a). A phase 2 study of pegylated interferon α-2b (PEG-Intron(®)) in children with diffuse intrinsic pontine glioma. *Cancer* 118, 3607–3613.

Warren, K., Gururangan, S., Geyer, J., Mclendon, R., Poussaint, T., Wallace, J., et al. (2011b). A phase II study of O6-benzylguanine and temozolomide in pediatric patients with recurrent or progressive high-grade gliomas and brainstem gliomas: a Pediatric Brain Tumor Consortium study. *J. Neurooncol.* 106, 643–649.

Warren, K., Killian, K., Suuriniemi, M., Wang, Y., Quezado, M., and Meltzer, P. (2011c). Genomic aberrations in pediatric diffuse intrinsic pontine gliomas. *Neuro Oncol.* 14, 326–332.

Warren, K., Jakacki, R., Widemann, B., Aikin, A., Libucha, M., Packer, R., et al. (2006). Phase II trial of intravenous lobradamil and carboplatin in childhood brain tumors: a report from the Children's Oncology Group. *Cancer Chemother. Pharmacol.* 58, 343–347.

Wolburg, H., Noell, S., Wolburg-Buchholz, K., Mack, A., and Fallier-Becker, P. (2009). Agrin, aquaprin-4, and astrocyte polarity as an important feature of the blood:brain barrier. *Neuroscientist* 15, 180–193.

Wu, G., Broniscer, A., Mceachron, T., Lu, C., Paugh, B., Becksfort, J., et al. (2012). Somatic histone H3 alterations in pediatric diffuse intrinsic pontine gliomas and non-brainstem glioblastomas. *Nat. Genet.* 44, 251–253.

Zarghooni, M., Bartels, U., Lee, E., Buczkowicz, P., Morrison, A., Huang, A., et al. (2010). Whole-genome profiling of pediatric diffuse intrinsic pontine gliomas highlights platelet-derived growth factor receptor α and poly (ADP-ribose) polymerase as potential therapeutic targets. *J. Clin. Oncol.* 28, 1337–1344.

Zuniga, R., Torcuator, R., Jain, R., Anderson, J., Doyle, T., Ellika, S., et al. (2009). Efficacy, safety and patterns of response and recurrence in patients with recurrent high-grade gliomas treated with bevacizumab plus irinotecan. *J. Neurooncol.* 91, 329–336.

Hedgehog-responsive candidate cell of origin for diffuse intrinsic pontine glioma

Michelle Monje[a,b,c,1,2], Siddhartha S. Mitra[c,d,1], Morgan E. Freret[a,b,c], Tal B. Raveh[c], James Kim[b,c], Marilyn Masek[e], Joanne L. Attema[c,3], Gordon Li[d], Terri Haddix[e], Michael S. B. Edwards[d], Paul G. Fisher[a], Irving L. Weissman[c,e], David H. Rowitch[f,g], Hannes Vogel[e], Albert J. Wong[d,h], and Philip A. Beachy[b,c,2]

Departments of [a]Neurology, [b]Developmental Biology, [d]Neurosurgery, [e]Pathology, and [h]Cancer Biology, and [c]Institute for Stem Cell Biology and Regenerative Medicine, Stanford University Medical Center, Stanford, CA 94305; and Departments of [f]Neurological Surgery and [g]Pediatrics, University of California School of Medicine, San Francisco, CA 94143

Contributed by Philip A. Beachy, February 1, 2011 (sent for review July 28, 2010)

Diffuse intrinsic pontine gliomas (DIPGs) are highly aggressive tumors of childhood that are almost universally fatal. Our understanding of this devastating cancer is limited by a dearth of available tissue for study and by the lack of a faithful animal model. Intriguingly, DIPGs are restricted to the ventral pons and occur during a narrow window of middle childhood, suggesting dysregulation of a postnatal neurodevelopmental process. Here, we report the identification of a previously undescribed population of immunophenotypic neural precursor cells in the human and murine brainstem whose temporal and spatial distributions correlate closely with the incidence of DIPG and highlight a candidate cell of origin. Using early postmortem DIPG tumor tissue, we have established in vitro and xenograft models and find that the Hedgehog (Hh) signaling pathway implicated in many developmental and oncogenic processes is active in DIPG tumor cells. Modulation of Hh pathway activity has functional consequences for DIPG self-renewal capacity in neurosphere culture. The Hh pathway also appears to be active in normal ventral pontine precursor-like cells of the mouse, and unregulated pathway activity results in hypertrophy of the ventral pons. Together, these findings provide a foundation for understanding the cellular and molecular origins of DIPG, and suggest that the Hh pathway represents a potential therapeutic target in this devastating pediatric tumor.

Hedgehog pathway | cancer stem cells | brainstem glioma

Brainstem gliomas account for 10–20% of childhood brain tumors (1). Such tumors cluster into two disparate groups with widely divergent outcomes. Gliomas of the ventral pons (basis pontis), hereafter referred to as diffuse intrinsic pontine gliomas (DIPGs) (Fig. 1A), are typically diffusely infiltrative, higher grade [World Health Organization (WHO) II–IV], extremely aggressive cancers, leading to death in less than a year. Those arising in the dorsal pons (pontine tegmentum), midbrain, or medulla, in contrast, tend to be low-grade gliomas (often pilocytic astrocytomas or gangliogliomas) with a markedly more favorable course of survival, sometimes for years or decades (2, 3). DIPGs of the ventral pons peak in incidence in middle childhood (at the age of 6–7 y) and are rare in adulthood (3, 4) (Fig. 1B). The region- and age-specific nature of brainstem gliomas suggests that the underlying pathophysiology involves dysregulation of a postnatal neurodevelopmental process.

Neural stem cells, defined as cells with the capacity for self-renewal and production of multipotential progeny, are well recognized in the postnatal forebrain and spinal cord (5). For example, adult stem cell populations in the postnatal lateral ventricle subventricular zone contribute to olfactory bulb neurogenesis throughout life, and progenitors in the postnatal hippocampus produce granule cell layer neurons throughout life (5, 6). The presence of stem cells throughout the ventricular system of the neuroaxis has been described (7), but little attention has been paid to those in the subventricular zone of the third and fourth (IVth) ventricles. In addition to multipotent stem cells, important populations of more differentiated neural precursor

cells exist throughout the central nervous system but are similarly underexplored in the brainstem.

The relationship of normal neural stem cells to so-called "cancer stem cells" (CSCs) is somewhat controversial, but there is an emerging view that certain brain tumors might arise from stem-like precursor cell populations in both children and adults (8–10). CSCs or tumor-initiating cells, isolated from primary brain tumors, possess many of the characteristics of normal neural stem cells, generate neurospheres in vitro, and can recapitulate the tumor in vitro and in vivo, whereas other cell types from the tumor cannot (8, 11). The glioma-initiating cells studied to date, isolated from other types of glial tumors, resemble normal neural stem cells in some respects, such as immunophenotype and molecular gene expression (8, 12, 13).

The clinical behavior of DIPG suggests it is a unique disease, distinct from typical high-grade gliomas occurring elsewhere in the central nervous system. The study of DIPG biology has been limited by a dearth of available tumor tissue, however. Biopsy of this tumor is rare, because the diagnosis can typically be made by MRI appearance alone and brainstem surgery poses a significant risk of morbidity. With little human tissue available for study and no realistic animal models, few published studies address the underlying biology of DIPG and no advances in treatment have occurred since the application of radiation therapy 35 y ago (4, 14).

Results

Nestin[+] and Olig2^{+} Cell Populations in the Developing Human Ventral Pons. The spatial and temporal specificity of brainstem tumors (Fig. 1 A and B) prompted a close examination of the spatial and temporal distribution of neural precursor cells in the human brainstem throughout postnatal life. To accomplish this, 24 normal postmortem brainstem samples from all three brainstem regions—midbrain, pons, and medulla (Fig. 1A)—were analyzed from subjects lacking evidence of neurological, developmental, or oncological disease.

Immunohistochemical analysis and confocal microscopy revealed two distinct Nestin-immunopositive cell populations in the postnatal human brainstem: one population in the subventricular zone (defined as 50 μm deep to the ependymal layer) of the floor of the IVth ventricle and one population in the ventral pons. The ventral pontine Nestin^{+} cells exhibit a distinct morphology, with

Fig. 1. Spatiotemporal distribution of ventral pontine PPCs and incidence of DIPG. (*A*) Sagittal and axial MRI scans showing normal brainstem anatomy (*Left*) and DIPG (*Right*). The DIPG tumor is indicated by an asterisk. C, cerebellum; M, midbrain; P, pons, S, spinal cord; IV, fourth ventricle. (*B*) Incidence of DIPG expressed at age of diagnosis. Data were drawn from the Stanford University Brain Tumor Database and represent all patients with DIPG cared for at Stanford University Medical Center from 1997–2008 (*n* = 47). (*C*) Ventral PPC visualized on confocal micrograph [*Left*; Nestin (green) and Olig2 (red), magnification 40×] and light micrograph [*Right*; Nestin (brown), magnification 60×]. (Scale bar: 50 μm.) Density of Nestin$^+$ cells in the human ventral pons (*D*) and midbrain (*E*) as a function of postnatal age (*n* = 24). Each data point represents one to two cases; when two cases are represented, the value expressed is an average of the two. The symbol (- -) denotes an age at which no valid tissue samples were available for analysis. Comparable data in the medulla are presented in Fig. S1*E*.
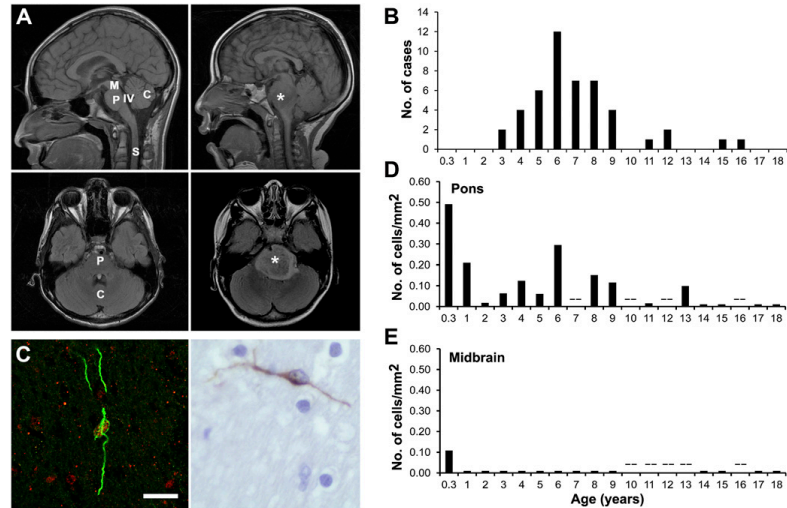
long thin processes in a bipolar arrangement (Fig. 1*C*). These Nestin$^+$ cells also express the primitive neural precursor cell marker Vimentin but not GFAP (Fig. S1 *A* and *B*). In contrast, immunophenotypic neural precursor cells of the floor of the IVth ventricle subventricular zone do not uniformly coexpress Nestin and Vimentin (Fig. S1*C*). Approximately half (40–60%) of the Nestin$^+$/Vimentin$^+$ ventral pontine cells also express the basic helix–loop–helix transcription factor Olig2 (Fig. 1*C*), a marker frequently found in cells that ultimately give rise to oligodendroglial precursors. This cell type is morphologically distinct from Nestin$^+$ cells of the subventricular zone of the IVth ventricular floor, located in dorsal regions of the brainstem (Fig. S1 *C* and *D*).

The density of this Nestin$^+$ cell type in the human midbrain, pons, and medulla was quantified throughout childhood (Fig. 1 *D* and *E* and Fig. S1*E*). During infancy, this cell type is present in all ventral brainstem structures and then wanes by 2 y of age. In the human pons, this cell type again increases in density in middle childhood, peaking around the age of 6 y. This second peak in the ventral pontine Nestin$^+$ population corresponds strikingly with the incidence of DIPG (Fig. 1 *B* and *D*). A similar temporal distribution was observed in the medulla (Fig. S1*E*). In contrast, no such Nestin$^+$ cell population is seen in the midbrain after infancy (Fig. 1*E*).

Hedgehog Signaling Drives Proliferation of Olig2$^+$ Cells in the Murine Ventral Pons. Given the experimental limitations of human tissue, we investigated the occurrence of a correlate pontine precursor-like cell (PPC) population in the mouse. A caveat that should be noted is that murine brainstem anatomy (Fig. 2*A*) does not exactly mirror human brainstem anatomy. For example, some structures present in human medulla, such as the dorsal vagal complex, are instead found in the murine pons. We found Nestin$^+$ cells in the ependymal and subventricular zone of the murine IVth ventricular floor, similar to the floor of the human IVth ventricle. Nestin$^+$ and Vimentin$^+$ cells were extremely rare in the ventral murine brainstem at any time point during postnatal life, however. Nevertheless, we found a robust population of Olig2$^+$ cells in the far ventral pons (Fig. 2*B* and Fig. S2*A*), and some of these cells also expressed SOX2, a marker of primitive cell types (13) (Fig. S2*A*), suggesting precursor cell identity.

The Hedgehog (Hh) pathway is of interest in these candidate PPCs because of its established role in the physiology of other

ventral neural precursor cell populations (15) and because Olig2 is known to be regulated in ventral embryonic spinal cord by Sonic hedgehog (Shh) (16). We therefore used a reporter for Hh pathway activity in which β-galactosidase is expressed under control of the promoter of the Hh pathway target, *Gli1* (*Gli1::LacZ*), and found expression of β-galactosidase concentrated in the far ventral pons (Fig. 2*C*). On closer examination, we found that all β-galactosidase$^+$ ventral pontine cells are also dual-positive for Olig2 and SOX2 expression (Fig. 2*B* and Fig. S2*A*). These Hh-responsive cells emerge around postnatal day (P) 14 and increase dramatically in this region from P14 to P21 (Fig. 2*D*), a time period in the mouse that roughly corresponds to "middle childhood" in humans, based on eye and tooth development. Unbiased stereological quantification reveals a three-fold increase in the total number of Hh-responsive cells in the ventral pons from P14 to P21 (Fig. 2*E*; 5,011 ± 373 at P14 vs. 14,599 ± 812 at P21, *n* = 4 animals per group; *P* < 0.001). These β-galactosidase$^+$ cells in the ventral pons do not coexpress the proliferation marker Ki67 but are intermixed with cells that are copositive for Ki67 and the oligodendrocyte precursor marker PDGF receptor-α (PDGFR-α) (Fig. S2*B*). On the basis of their location and time of emergence, these murine PPCs thus resemble human PPCs (*Discussion*).

Because of the established role for Hh signaling both in normal neural precursor cells (9, 15, 17, 18) and in other brain tumors, such as medulloblastoma (19–22), we postulated that the Hh pathway might play a role in transformation of this ventral PPC population. To test the functional and possibly oncogenic role of the Hh pathway in ventral pontine Olig2$^+$ precursor cells, we used a genetic mouse model in which the Hh pathway is specifically up-regulated in Olig2$^+$ cells. An *Olig2-Cre* mouse was crossed to a Rosa26-*flox-stop-flox-SmoothenedM2* (*R26-lsl-SmoM2*) mouse, such that Cre recombination results in expression of the constitutively active SmoothenedM2 protein, thus constitutively activating the Hh pathway in cells expressing Olig2 and their progeny. In this *Olig2-Cre; R26-lsl-SmoM2* mouse, we observed a 2.8-fold increase in the absolute number of proliferating cells in the ventral pons at P14 detected by Ki67 immunohistochemistry and quantified using unbiased stereology (Fig. 2 *F* and *G*; 18,728 ± 1,887 in control mice vs. 51,757 ± 3,434 in *Olig2-Cre; R26-lsl-SmoM2* heterozygous mice, *n* = 3 animals per group; *P* < 0.005). As in control littermates and in the *Gli1-*

Fig. 2. Hh pathway is sufficient to drive proliferation in the ventral pons during middle childhood. (*A–E*) Hh-responsive Olig2⁺ cells in the murine pons. (*A*) Nissl stain of the mouse pons Allen Mouse Brain Atlas (Seattle, WA): Allen Institute for Brain Science. ©2009. Available at http://mouse.brain-map.org (36). Region of Hh-responsive Olig2⁺ precursor cells is marked with an asterisk. (*B*) Confocal photomicrograph (magnification 40×) illustrating colocalization of Olig2 (red) and β-galactosidase [indicating Gli1 expression (green)] in the *Gli1::LacZ* reporter mouse. DAPI expression (blue) is also shown. An arrowhead marks an example of an Olig2- and β-galactosidase–colabeled cell; an asterisk marks an example of a cell that is not colabeled. (*C*) Fluorescent micrograph (magnification 2.5×) showing Hh-responsive cells (white) in the *Gli1::LacZ* mouse. Note the cluster of Hh-responsive cells in the ventral pons (*). (*D*) Middle childhood peak in Hh-responsive cell density in the pons of the *Gli1::LacZ* transgenic reporter mouse. Data are expressed as the number of β-galactosidase–immunopositive cells per 10× field. Note the dramatic increase in Hh-responsive cells in the P14–P21 time frame, which represents the mouse equivalent of middle childhood. Data are mean ± SEM (*n* = 3 animals per time point). (*E*) Unbiased stereological quantification of the total number of Hh-responsive cells on one side of the ventral pons on P14 compared with P21. Data are mean ± SEM (*n* = 3 animals per time point; *P < 0.001). (*F* and *G*) Hh pathway activity increases proliferation in the ventral pons. (*F*) Confocal photomicrographs (magnification 10×) of Ki67⁺ cells (red) in control and Olig2::Cre × SmoM2 heterozygote mouse ventral pons at P14. PDGFR-α (green) is shown. (Scale bar: 20 μm.) (*G*) Unbiased stereological quantification of Ki67⁺ cells in the ventral pons at P14 in the *Olig2::Cre × SmoM2* mouse pons vs. littermate controls. Data are mean ± SEM (*n* = 3 animals per group; *P < 0.005). (*H* and *I*) Hh pathway upregulation results in ventral pontine hypertrophy. (*H*) Light micrographs (magnification 1.5×) of the ventral pons at P21 from *Olig2::Cre × SmoM2* heterozygote and littermate control mice. Images shown represent a reconstruction of the entire coronal brain section from multiple images taken at 1.5× magnification. (*I*) Volume of the ventral pons at P21 in *Olig2::Cre × SmoM2* heterozygotes vs. littermate controls. Data are expressed as the dorsal − ventral dimension × transverse dimension × rostrocaudal dimension in cubic millimeters. Data are mean ± SEM (*n* = 3 animals per group; *P < 0.05).
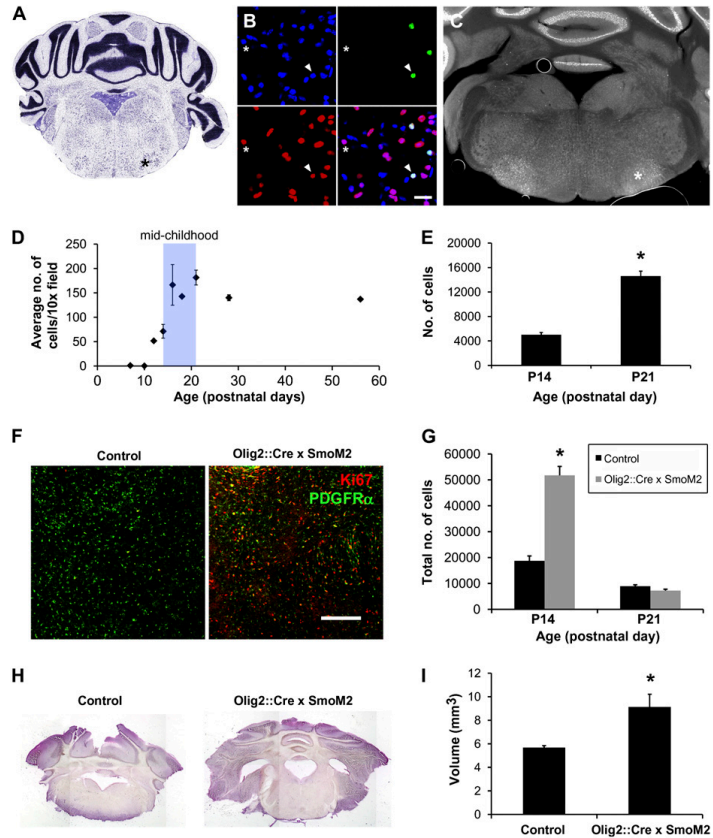
LacZ mice, proliferation at P14 in the *Olig2-Cre; R26-lsl-SmoM2* heterozygous mice was largely limited to this ventral pontine germinal zone and to PDGFR-α⁺ oligodendrocyte precursor cells (Fig. 2*F*; the proportion of dividing cells that coexpress PDGFR-α and Ki67 was 88 ± 3% in *Olig2-Cre; R26-lsl-SmoM2* mice vs. 84 ± 5% in control mice; *P* = 0.49). This burst of proliferation in the ventral pons of *Olig2-Cre; R26-lsl-SmoM2* heterozygous mice ends by P21; at that time, unbiased stereological quantification of Ki67⁺ cells reveals equal numbers of proliferating cells in control and *Olig2-Cre; R26-lsl-SmoM2* heterozygous mice (Fig. 2*G*; 9,696 ± 541 in control mice vs. 7,224 ± 543 in *Olig2-Cre; R26-lsl-SmoM2* heterozygous mice, *n* = 3 animals per group; *P* = 0.09).

By P21, hypertrophy of the ventral pons was evident in the *Olig2-Cre; R26-lsl-SmoM2* mice compared with control littermates (Fig. 2*H*). Measurement of the dorsal-ventral, transverse, and rostrocaudal dimensions of the pons in a one in four series of 40-μm tissue sections revealed an increase in volume of 50% (Fig. 2*I*; *P* < 0.05). Histological analysis on H&E-stained sections did not reveal dysplasia at P21 (Fig. S2*C*). Because these mice develop medulloblastoma during the postnatal period (10), all analyses carefully excluded regions of frank medulloblastoma present in the cerebellum and subarachnoid space, and careful

examination of the pons at P14 and P21 revealed no infiltration of the brainstem by medulloblastoma cells. These mice die of medulloblastoma in early adulthood, thereby limiting later analysis of dysplasia in the pons.

Establishment of Previously Undescribed DIPG Cell Culture and Xenograft Models. A major obstacle in the study of DIPG has been a lack of available tumor tissue for research. To overcome this impasse, an early postmortem tissue harvest strategy was used. DIPG tumor tissue was donated by a 5-y-old boy who had received minimal treatment (clinical details are presented in *SI Materials and Methods*). Histopathology was consistent with a WHO grade III anaplastic astrocytoma (Fig. 3 *A*, *C*, *E*, *G*, and *I* and Fig. S3 *A*, *B*, and *F*) that was intensely immunopositive for Nestin (Fig. S3*A*) and GFAP (Fig. S3*F*).

Cells cultured on a nonadherent plate in serum-free medium supplemented with FGF and EGF formed tumor neurospheres (Fig. 4*A*) and secondary tumor neurospheres after dissociation and replating at low density (10 cells/μL). Limiting dilution analysis (23) of unsorted cells indicated an in vitro self-renewing frequency of 1 in 79 cells (1 in 64–1 in 98 cells, 95% confidence interval). Subsequent supplementation of PDGF-AB to the medium resulted in qualitative improvement of neurosphere

culture growth; the neurosphere culture expanded more rapidly after this addition, but the change in growth rates was not quantified at the time.

Using cultures with a low passage number (<10), the immunophenotype of neurosphere-forming cells was assessed using fluorescent immunocytochemistry and confocal microscopy. We found that all cells in the culture expressed the intermediate filament proteins Nestin, GFAP, and Vimentin (Fig. 4 B and C), which are classically found in neural stem or precursor cells and more recently described in many glial tumors (24). Nestin and Vimentin also mark endothelial cells, which is a potential source of culture contamination. Endothelial cells, however, were not present as assessed by immunostaining or FACS analysis for the endothelial cell-specific marker CD31. Sox2, a marker expressed in both normal embryonic and postnatal stem cells and in poorly differentiated CSCs (13), was also expressed to varying degrees in all DIPG neurosphere cells (Fig. 4D). A small subset of cultured DIPG neurosphere cells express Olig2 (Fig. 4F). Taken together, this immunophenotype of cultured DIPG neurosphere cells is consistent with a primitive neural precursor cell type.

Brain tumor-initiating cells are classically identified with the cell surface marker CD133 (also known as prominin 1 or Prom1) (11). Recently, it has become clear that CD133 may only mark a subset of the self-renewing cancer-propagating cells in a glioma (25). CD133 is also expressed on normal neural stem cells, although the expression of CD133 is similarly nonuniform in normal neural stem cells and may be restricted to the actively proliferating fraction of stem cells (26). Increasing CD133$^+$ fractions of brain tumor cultures correlates with higher tumor grade (11). Examining the proportion of cells in the DIPG neurosphere culture that express CD133, we found that 37% of cells are CD133$^+$ by FACS (Fig. S3C) and that a similar fraction are positive by immunocytochemistry (approximately one-third of cells, Fig. 4E). Examination of the original tumor tissue revealed CD133$^+$ cells sparsely distributed throughout the tumor (Fig. S3B).

To test for tumor-initiating capacity and to establish a xenograft mouse model, dissociated neurosphere cells were stereotactically transplanted to the brains of immunodeficient (nonobese diabetic/SCID/IL2γ-chain–deficient) mice on P2. Two transplantation strategies were used, and cells were transplanted either to the lateral ventricles (LV, three mice) or to the IVth ventricle (IV, eight mice). Mice were routinely examined for neurological deficits. Twenty-six weeks following neurosphere cell transplantation, all three mice in the LV group and four of eight mice in the IV group exhibited clinical symptoms, such as poor grooming and hemiparesis. Two-thirds of the mice from both groups were sacrificed, and the brains were processed for histology; one-third of the mouse brains were processed for serial transplantation of the xenograft. In the LV group, all brains demonstrated large tumors, evident by eye (Fig. 3B) and on H&E-stained sections (Fig. 3 D and F and Fig. S3 D and H). Tumor histopathology was characteristic of a high-grade glioma (Fig. 3 D and F and Fig. S3 D, E, G, and H). Infiltrating tumor cells were found throughout the mouse brain, including the cortex, cerebellum, and pons (Fig. 3 D and F and Fig. S3 D and H). Invasion of the brainstem following LV tumor cell injection has not been observed by our group in this orthotopic mouse transplant model with any other tumor type, including multiple cases of glioblastoma and medulloblastoma. This highlights the unique biology of DIPG, as distinct from other high-grade gliomas. In the IVth ventricle group, 50% of brains exhibited tumors evident by eye as enlarged hindbrains and histologically on H&E-stained sections (Fig. 3 H and J and Fig. S3I). Like the LV xenografted brains, diffuse infiltration of the brainstem, cerebellum, and cerebrum was observed (Fig. 3 H and J and Fig. S3I). In comparison with xenografts to the LVs, xenografting to the IVth ventricle resulted in pontine histopathology more similar to that of DIPG (Fig. 3F vs. H and J).

Functional Role for Hh Signaling in DIPG. Using the newly established DIPG cell culture model, we tested the role of Hh signaling in human DIPG. To test for Hh pathway activity, a Gli reporter construct was used in which red fluorescent protein (RFP) expression is under control of Gli binding sites within a lentiviral
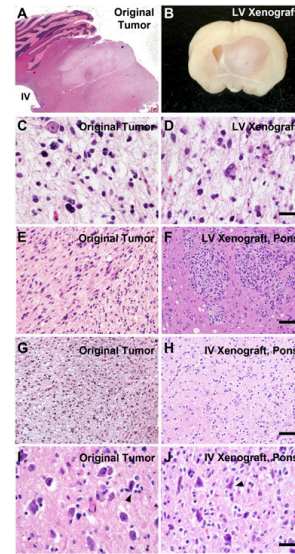
Fig. 3. DIPG xenograft. H&E-stained light micrographs (A, C–J) and bright-field image of mouse brain (B). (Left) Original DIPG tumor. (A) Light micrograph (magnification 2×) of H&E-stained sagittal section through the pons of the tumor tissue donor. Diffuse infiltration of tumor in the ventral pons is visualized as lighter staining, notably sparing the dorsal region of pons that is closest to the IVth ventricle. The cerebellum is seen in the dorsolateral relationship to the pons in this plane of section. Additional images of the original tumor are shown at magnifications of 40× (C and I), 20× (E), and 10× (G). (Right) Mouse DIPG xenografts. (B) Following stereotactic transplantation of dissociated neurospheres from a human DIPG to the LV, examination of brains from immunodeficient mice reveals a large tumor and marked midline shift evident on a gross coronal section. (D) Diffuse infiltration by tumor is seen throughout the brain in H&E-stained sections (magnification 40×). (F) Although the DIPG cells were transplanted to the LVs, infiltration was seen in the hindbrain, including the pons (magnification 20×). (H and J) Transplantation of dissociated neurospheres from a human DIPG to the IVth ventricle resulted in diffuse infiltration of the pons. Note the perineuronal satellitosis (arrowheads) of tumor cells around pontine neurons (larger cells) seen in the xenograft (J) and original tumor (I). The histopathology of the mouse xenograft was indistinguishable from that of the original tumor. (Scale bars: C, D, and I–J, 50 μm; E–H, 100 μm; G and H, 250 μm.)

vector. To validate this Hh pathway reporter system, National Institutes of Health (NIH) 3T3 cells were transduced with the Gli binding site::RFP reporter and exposed to the Shh protein ligand (ShhN) alone or together with the Hh antagonist 3-keto-N-(aminoethyl-aminocaproyl-dihydrocinnamoyl)-cyclopamine (KAAD-cyclopamine, 200 nM). At baseline, NIH 3T3 cells did not express RFP (Fig. S4A), but RFP was expressed in transduced NIH 3T3 cells when exposed to ShhN (Fig. S4B). RFP expression in transduced NIH 3T3 cells exposed to ShhN was blocked by simultaneous exposure to KAAD-cyclopamine (Fig. S4C).

Dissociated DIPG neurosphere cells from the initial culture described above, as well as primary tumor cells from a second tumor tissue donation, were transduced with lentivirus containing either the WT Gli binding site-RFP construct (Fig. 5A) or a negative control construct with mutated Gli binding sites (Fig. 5B). As a positive control, 293 cells expressing Gli1 were also transduced with the Gli binding site-RFP reporter construct. RFP expression indicated Hh pathway activity in both the primary DIPG tumor cell culture and the dissociated neurosphere cells (Fig. 5A). To determine the source of Hh ligand in this culture, immunocytochemistry for Shh was performed. DIPG neurosphere cells uniformly
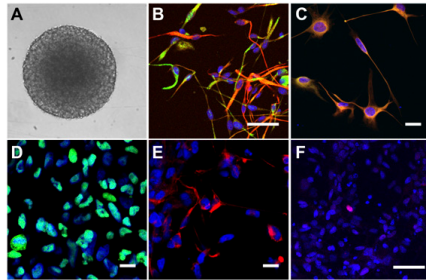
Fig. 4. DIPG neurosphere culture. (*A*) Tumor neurosphere is shown on a light micrograph (magnification 10×). Immunocytochemistry and confocal microscopy (magnification 40×) reveal DIPG tumor neurosphere cells that are uniformly immunopositive for GFAP (*B*, red), Nestin (*B* and *C*, green) Vimentin (*C*, red), and Sox2 (*D*, green). Immunocytochemistry for CD133 (*E*, red) reveals a CD133+ fraction of about one-third of cells. Rare cells are immunopositive for Olig2 (*F*, red). DAPI (blue) was used as a nuclear counterstain in images *B–F*. (Scale bars: 50 μm.)

express Shh ligand, indicating an autocrine and/or paracrine Hh signaling mechanism (Fig. 5*C*). Semiquantitative real-time RT-PCR confirmed expression of Gli1, Patched (PTCH) receptor, and Shh ligand in DIPG neurosphere cells (Fig. S4*D*).

To test the functional significance of the Hh pathway on DIPG tumor neurosphere cell self-renewal capacity, we used a secondary neurosphere assay. Dissociated DIPG tumor neurosphere cells were plated at low density (100 cells per well in a 96-well plate format) using FACS sorting of live cells and then cultured in the presence or absence of added processed and purified Shh (ShhNp) or the Hh pathway antagonist KAAD-cyclopamine. Neurosphere formation (Fig. 5*D*) was quantified at 14 d following plating of dissociated cells. Exposure to KAAD-cyclopamine (200 nM) resulted in a 67% reduction in the average number of secondary neurospheres per well ($P < 0.001$) compared with control wells treated with methanol vehicle alone (Fig. 5*E*). The addition of ShhNp increased secondary neurosphere formation by 200% ($P < 0.05$; Fig. 5*E*).

Discussion

DIPGs are aggressive tumors of childhood that are poorly understood and nearly always fatal. The lack of a faithful experimental model system together with a limited understanding of the normal neural precursor cell biology of the postnatal brainstem has limited study of this devastating disease and prevented development of effective treatment strategies.

We now report the identification of a neural precursor-like cell population in the normal human ventral pons that is linked both anatomically and temporally to the incidence of DIPG (Fig. 1). The frequency of this cell type during middle childhood mirrors the bell-shaped incidence curve of DIPG (Fig. 1 *B* and *D*). These cells are notably absent after early infancy in the midbrain (Fig. 1*E*), where high-grade gliomas are virtually nonexistent. This PPC is restricted to the ventral pons and medulla during childhood (Fig. 1*D* and Fig. S1*E*). High-grade gliomas primarily occur in the ventral pons but are sometimes found in the medulla as well. The predilection for the ventral pons may reflect not only the presence of a susceptible cell of origin but a signaling microenvironment favorable for tumor formation (27–29). Differences in brainstem cell populations and in their behavior may relate to the different developmental origins of each brainstem region, with the human midbrain, pons, and medulla arising from three different neuroembryonic vesicles (the mesencephalon, metencephalon, and myelencephalon, respectively).

The human PPC population comprises primitive Nestin+ and Vimentin+ cells with long bipolar processes (Fig. 1*C* and Fig. S1 *A* and *B*), with a significant subset of these cells coexpressing

Olig2 (Fig. 1*C*). We note that although coexpression of Nestin with Olig2 occurs in this human cell population, coexpression of these two markers has not previously been described and appears not to occur in the mouse. The Olig2+ precursor population that we have found in the mouse ventral pons does not express Nestin, and the murine correlate to this human PPC that we have characterized is thus similar but not identical in a manner consistent with precedent. Olig2+ precursor cells frequently represent cells that ultimately form myelinating oligodendroglia, although differentiation along astroglial and even neuronal lineages is also described (30). In the mouse, Hh-responsive Olig2+ precursors in the ventral pons are intermixed with dividing PDGFR-α–immunopositive oligodendrocyte precursor cells (Fig. S2*B*), suggesting that this population forms myelinating oligodendrocytes during middle childhood (P14–P21 in the mouse). The majority of postnatal myelination is complete by this time point, but ongoing myelination is known to occur in the human pons through the first decade of life (31). The precise tracts that are myelinating and why this may occur specifically during middle childhood are unknown.

Similar to human PPCs, DIPG neurosphere cells are Nestin+ and Vimentin+, with a subset expressing Olig2 (Fig. 4 *C* and *F*). In contrast to the normal human PPC, the DIPG tumor neurosphere cells also express GFAP (Fig. 4*B*), a marker expressed in many glial tumors regardless of the cell of origin (32). Taken together with the anatomical and temporal correlates of their occurrence, the immunophenotypic characteristics of these cell populations suggest the hypothesis that this PPC could be the DIPG cell of origin.

Our results show that driving unregulated Hh pathway activity in the murine counterpart of this population results in ventral pontine hyperplasia (Fig. 2 *F–I*), indicating that the PPC might be susceptible to transformation and may represent the cell of origin for DIPG. The absence of dysplasia in this model suggests that an additional "hit" may be necessary for transformation to DIPG. That Hh pathway dysregulation alone may not be sufficient for DIPG oncogenesis is supported by the observation that patients with Gorlin syndrome (a genetic syndrome of susceptibility to unregulated Hh pathway activity caused by heterozygous germline mutation of the PTCH gene and characterized by de-
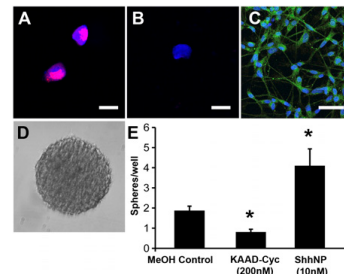
Fig. 5. Hh pathway activity in DIPG. (*A*) DIPG tumor cells transduced with a lentiviral Hh pathway reporter construct, Gli1::RFP. A confocal photomicrograph (magnification 40×) illustrates RFP (red) and a DAPI nuclear counterstain (blue). (*B*) Confocal photomicrograph (magnification 40×) illustrates lack of RFP (red) signal in negative control tumor cells transduced with a mutated Gli1 binding site::RFP construct and a DAPI nuclear counterstain (blue). (Scale bar: 30 μm.) (*C*) Confocal photomicrograph (magnification 40×) demonstrates Shh ligand expression (green) in DIPG tumor neurosphere cells. A DAPI nuclear counterstain (blue) is also shown. (*D*) Light micrograph (magnification 10×) of a secondary tumor neurosphere at 14 d following dissociation and FACS sorting of live cells at low density (100 cells per well in a 96-well plate format). (*E*) Quantification of secondary tumor neurospheres (such as that seen in *D*) at 14 d following dissociation and FACS sorting of live cells at low density (100 cells per well) and exposed to either KAAD-cyclopamine (200 nM), ShhNp (10 nM), or methanol vehicle control. Data are expressed as the average number of tumor neurospheres per well ± SEM ($n = 10–16$ wells per condition; *$P < 0.05$).

NEUROSCIENCE

velopment of basal cell nevi and medulloblastoma) do not classically develop DIPG. Our results indicate that the Hh pathway is one important component in both the normal physiology of the PPC and the pathophysiology of DIPG, because Hh pathway activation increases and Hh pathway blockade decreases the self-renewal capacity of cells in DIPG tumor neurospheres (Fig. 5E).

Dysregulation of the Hh pathway alone is not enough to cause both hyperplasia and dysplasia (i.e., cancer) in the ventral brainstem by P21 in the mouse model used here, as we also previously reported (10), and transformation to DIPG likely involves additional hits. Indeed, recent work has highlighted the PDGF pathway as important in brainstem tumors, with genomic analysis of DIPG samples demonstrating copy number alterations in PDGFR-α (33). In addition, up-regulation of PDGF signaling in Nestin+ cells of the IVth ventricle subventricular zone (22) or nonspecifically in cells of the dorsolateral pons (34) causes dorsal pontine glioblastoma in mouse models. A putative role for PDGF signaling in DIPG pathophysiology fits well with our observations, because the candidate cell of origin appears to give rise to a dividing oligodendrocyte precursor cell type that expresses PDGFR-α, and is therefore likely to be responsive to PDGF. Furthermore, we found qualitatively that the addition of recombinant PDGF to our human DIPG cell culture resulted in improved culture yield.

We present here a postmortem cell culture strategy that has generated DIPG culture and xenograft models (Figs. 3 and 4), representing a previously undescribed resource for the research community and enabling studies to probe the underlying biology of DIPG. Within this DIPG cell culture, we have demonstrated a capacity for self-renewal and tumor initiation as well as an immunophenotype similar to that of a neural stem cell, suggesting the presence of a putative DIPG CSC. The characteristics of this neurosphere culture are consistent with those of an aggressive brain tumor, because a CD133+ cell fraction of 37% is relatively high compared with that previously reported for other aggressive brain tumors, such as medulloblastoma and glioblastoma (6–21% and 19–29%, respectively) (35). Adjusting for the enrichment of CD133+ cells by FACS in published secondary

neurosphere assays, the self-renewing frequency found in this study (1 in 79 cells) is in line with that of similar studies of medulloblastoma tumor neurospheres (11).

The human PPC population we have described is temporally and anatomically restricted to the time and place that DIPGs form and is immunophenotypically similar to DIPG, suggesting that this cell is a candidate for the DIPG cell of origin. This hypothesis is strengthened by the demonstration that up-regulation of the Hh pathway in mouse ventral PPCs results in ventral pontine hyperplasia during the middle childhood window when such tumors form in humans. A role for Hh signaling in DIPG tumor propagation is confirmed by the positive effects of Hh pathway activity on self-renewal of DIPG neurosphere cells in our DIPG cell culture model. Together, these findings provide insights into DIPG pathogenesis and may ultimately result in unique therapeutic avenues to treat DIPG.

Materials and Methods

Full methodological details are found in the *SI Materials and Methods* including methods for cell culture, xenografting, archival human autopsy case selection and quality control, histological processing, quantitative microscopy, FACS analysis, generation of the lentiviral-based Gli binding site-RFP reporter, real time PCR and statistics. Clinical details of the human postmortem tissue donation are also provided.

1. Central Brain Tumor Registry of the United States (2010) *CBTRUS Statistical Report: Primary Brain and Central Nervous System Tumors Diagnosed in the United States in 2004-2006* (Central Brain Tumor Registry of the United States, Hinsdale, IL).
2. Barkovich AJ, et al. (1990-1991) Brain stem gliomas: A classification system based on magnetic resonance imaging. *Pediatr Neurosurg* 16:73–83.
3. Fisher PG, et al. (2000) A clinicopathologic reappraisal of brain stem tumor classification. Identification of pilocytic astrocytoma and fibrillary astrocytoma as distinct entities. *Cancer* 89:1569–1576.
4. Donaldson SS, Laningham F, Fisher PG (2006) Advances toward an understanding of brainstem gliomas. *J Clin Oncol* 24:1266–1272.
5. Zhao C, Deng W, Gage FH (2008) Mechanisms and functional implications of adult neurogenesis. *Cell* 132:645–660.
6. Shors TJ, et al. (2001) Neurogenesis in the adult is involved in the formation of trace memories. *Nature* 410:372–376.
7. Weiss S, et al. (1996) Multipotent CNS stem cells are present in the adult mammalian spinal cord and ventricular neuroaxis. *J Neurosci* 16:7599–7609.
8. Hemmati HD, et al. (2003) Cancerous stem cells can arise from pediatric brain tumors. *Proc Natl Acad Sci USA* 100:15178–15183.
9. Yang ZJ, et al. (2008) Medulloblastoma can be initiated by deletion of Patched in lineage-restricted progenitors or stem cells. *Cancer Cell* 14:135–145.
10. Schüller U, et al. (2008) Acquisition of granule neuron precursor identity is a critical determinant of progenitor cell competence to form Shh-induced medulloblastoma. *Cancer Cell* 14:123–134.
11. Singh SK, et al. (2003) Identification of a cancer stem cell in human brain tumors. *Cancer Res* 63:5821–5828.
12. Taylor MD, et al. (2005) Radial glia cells are candidate stem cells of ependymoma. *Cancer Cell* 8:323–335.
13. Ben-Porath I, et al. (2008) An embryonic stem cell-like gene expression signature in poorly differentiated aggressive human tumors. *Nat Genet* 40:499–507.
14. Laigle-Donadey F, Doz F, Delattre JY (2008) Brainstem gliomas in children and adults. *Curr Opin Oncol* 20:662–667.
15. Ahn S, Joyner AL (2005) In vivo analysis of quiescent adult neural stem cells responding to Sonic hedgehog. *Nature* 437:894–897.
16. Lu QR, et al. (2000) Sonic hedgehog—Regulated oligodendrocyte lineage genes encoding bHLH proteins in the mammalian central nervous system. *Neuron* 25:317–329.
17. Lai K, Kaspar BK, Gage FH, Schaffer DV (2003) Sonic hedgehog regulates adult neural progenitor proliferation in vitro and in vivo. *Nat Neurosci* 6:21–27.
18. Breunig JJ, et al. (2008) Primary cilia regulate hippocampal neurogenesis by mediating sonic hedgehog signaling. *Proc Natl Acad Sci USA* 105:13127–13132.
19. Goodrich LV, Milenković L, Higgins KM, Scott MP (1997) Altered neural cell fates and medulloblastoma in mouse patched mutants. *Science* 277:1109–1113.
20. Pomeroy SL, et al. (2002) Prediction of central nervous system embryonal tumour outcome based on gene expression. *Nature* 415:436–442.
21. Ehtesham M, et al. (2007) Ligand-dependent activation of the hedgehog pathway in glioma progenitor cells. *Oncogene* 26:5752–5761.
22. Becher OJ, et al. (2010) Preclinical evaluation of radiation and perifosine in a genetically and histologically accurate model of brainstem glioma. *Cancer Res* 70:2548–2557.
23. Quintana E, et al. (2008) Efficient tumour formation by single human melanoma cells. *Nature* 456:593–598.
24. Ma YH, et al. (2008) Expression of stem cell markers in human astrocytomas of different WHO grades. *J Neurooncol* 86:31–45.
25. Clément V, Dutoit V, Marino D, Dietrich PY, Radovanovic I (2009) Limits of CD133 as a marker of glioma self-renewing cells. *Int J Cancer* 125:244–248.
26. Sun Y, et al. (2009) CD133 (Prominin) negative human neural stem cells are clonogenic and tripotent. *PLoS ONE* 4:e5498.
27. Gilbertson RJ, Gutmann DH (2007) Tumorigenesis in the brain: Location, location, location. *Cancer Res* 67:5579–5582.
28. Calabrese C, et al. (2007) A perivascular niche for brain tumor stem cells. *Cancer Cell* 11:69–82.
29. Gilbertson RJ, Rich JN (2007) Making a tumour's bed: Glioblastoma stem cells and the vascular niche. *Nat Rev Cancer* 7:733–736.
30. Zhou Q, Anderson DJ (2002) The bHLH transcription factors OLIG2 and OLIG1 couple neuronal and glial subtype specification. *Cell* 109:61–73.
31. Yakovlev PI (1967) The myelogenetic cycles of regional maturation of the brain. *Regional Development of the Brain in Early Life*, ed Minkowski A (Blackwell Scientific, Oxford), pp 3–70.
32. Lindberg N, Kastemar M, Olofsson T, Smits A, Uhrbom L (2009) Oligodendrocyte progenitor cells can act as cell of origin for experimental glioma. *Oncogene* 28:2266–2275.
33. Zarghooni M, et al. (2010) Whole-genome profiling of pediatric diffuse intrinsic pontine gliomas highlights platelet-derived growth factor receptor alpha and poly (ADP-ribose) polymerase as potential therapeutic targets. *J Clin Oncol* 28:1337–1344.
34. Masui K, et al. (2010) Glial progenitors in the brainstem give rise to malignant gliomas by platelet-derived growth factor stimulation. *Glia* 58:1050–1065.
35. Singh SK, et al. (2004) Identification of human brain tumour initiating cells. *Nature* 432:396–401.
36. Lein ES, et al. (2007) Genome-wide atlas of gene expression in the adult mouse brain. *Nature* 445:168–176.

Tumour Review

Diffuse intrinsic pontine gliomas: A systematic update on clinical trials and biology

M.H.A. Jansen [a,c,*], D.G. van Vuurden [a,c,1], W.P. Vandertop [b,c,2], G.J.L. Kaspers [a,c,3]

[a] Department of Pediatrics, Division of Pediatric Oncology/Hematology, VU University Medical Center, Amsterdam, The Netherlands
[b] Neurosurgical Center Amsterdam, VU University Medical Center, Amsterdam, The Netherlands
[c] Neuro-Oncology Research Group, Cancer Center Amsterdam, VU University Medical Center, Amsterdam, The Netherlands

ARTICLE INFO

ABSTRACT

Patients with diffuse intrinsic pontine gliomas (DIPG) have a poor prognosis. Although DIPG constitute only 10–15% of all pediatric brain tumors, they are the main cause of death in this group. Despite 26 clinical trials in newly diagnosed DIPG in the past 5 years (including several targeted agents), there is no clear improvement in prognosis. However, knowledge on DIPG biology is increasing, mainly due to the (re)introduction of biopsies and autopsies, the possibility of gene expression profiling, and the development of in vivo models. Translation of this knowledge into clinical trials in combination with improved drug distribution methods may eventually lead to more effective treatment of this devastating disease.

© 2011 Elsevier Ltd. All rights reserved.

Background

Effective treatment of diffuse intrinsic pontine gliomas (DIPG) in children remains elusive. DIPG comprise 10–15% of childhood brain tumors but are the main cause of death in this young group. Despite several treatment regimens being studied over the last 25 years, prognosis has not improved and <10% of patients are alive two years after diagnosis.[1]

In 2006, Hargrave et al. reviewed all clinical studies performed in DIPG patients from 1984 to 2005: 29 studies were reported including a total of 973 patients.[1] Most studies were non-randomized and comparison was difficult due to unclearly defined inclusion criteria. In these studies, the median overall survival (OS) ranged from 7–16 months; when only studies with detailed clinical and radiological eligibility criteria were included, the median

OS ranged from 8–11 months with a progression-free survival (PFS) of 5–9 months. The use of hyperfractionated radiotherapy, pre-irradiation chemotherapy, concurrent chemo-radiotherapy and radiosensitizers has not increased long-term OS. In addition, adjuvant chemotherapy and high-dose chemotherapy regimens have also failed to improve long-term prognosis.

Historically, DIPG were diagnosed radiologically and biopsies were not performed due to perceived morbidity.[2] This was later shown to be overestimated and biopsies are now more widely practiced.[3–5] Biopsies, together with autopsy material, have paved the way for biological studies in DIPG. Studies published in the past five years will probably be the basis for a more rational drug treatment of these tumors.

The present study is an update on the clinical trials (including recently completed and ongoing studies) and presents current knowledge on DIPG biology with regard to potential future targeted therapy.

Methods

A search was made in PubMed, the Cochrane Central Register of Controlled Trials and Embase covering the period from 1 January 2005 until 1 March 2011. The following terms were used (with synonyms and closely related words): "brain stem" and "gliomas" or "tumors" and "RCT's" or "reviews" or "meta-analyses" or "systematic reviews" and "children". Two reviewers (MJ and GJK) independently screened the references for eligible articles by reading

the title and abstract. Full-text versions of these articles were then obtained. The full search strategy can be requested from the first author.

Inclusion criteria: only prospective clinical trials including and separately analyzing pediatric patients (aged 0–19 years) with newly diagnosed DIPG were eligible for review. Investigated parameters were: inclusion criteria of the studies, baseline characteristics (age, gender, life expectancy at diagnosis, symptoms at diagnosis and duration of symptoms, performance scores, percentage of tumor involving the pons, histological diagnosis) and outcome (response on MRI, progression-free and overall survival time). Overall rates were composed of the range of the medians.

To evaluate ongoing trials, a search was done using the search terms "brain stem glioma" "brainstem glioma" and pontine glioma on http://apps.who.int/trialsearch/ and http://clinicaltrials.gov/ and the Abstract Books of ISPNO, SNO, SIOP, AACR and EACR from 2005–2010.

Results

The systematic search on clinical trials yielded 584 publications dating from 2005 (Fig. 1). Unfortunately, although some studies included newly diagnosed DIPG patients, they did not analyze them separately and were therefore excluded from this review.[6,7]

Table 1 summarizes the inclusion criteria and baseline characteristics, and Table 2 the survival time and response rates for all published clinical studies.

Inclusion criteria and baseline characteristics

In total, 26 prospective clinical trials, including 561 children (40% boys and 60% girls) with newly diagnosed DIPG, were published in 23 manuscripts and were eligible for review.[8–30] The median number of patients per study was 20 (range 7–63). The median age was 6.2 (range 2.5–9.2) years; one study included patients up to age 3 years only.[15] There was considerable inter-study variability in eligibility criteria, including performance state, life expectancy, symptoms at diagnosis and laboratory findings. A Karnofsky performance state of ⩾40% was requested in two stud-

ies,[10,28] ⩾50% in seven studies,[9,11,14,16,17,21,25] ⩾60% in one study,[26] and ⩾70% in two studies.[13,19] A life expectancy of six weeks or more was requested in five studies.[9,11,13,22,28] The presence of one typical symptom at diagnosis (cranial nerve deficits, long tract signs or ataxia) was an inclusion criteria in two studies[23,28] and five studies requested two or more of these symptoms.[8,17,18,21,26] Seven studies also restricted the period of symptom duration at diagnosis in an attempt to exclude less aggressive tumors.[8,18,21,23,26,28,30] In total, 18 studies stated that only typical DIPG patients were included based on MRI criteria, but only eight of these further specified the MRI criteria, i.e. six requested tumor involvement of ⩾50% of the pons[8,9,17,18,24,30] and two stated a minimal involvement of 67%.[11,21] Seven studies also included gliomas other than DIPG: four included newly diagnosed pediatric high-grade glioma (HGG),[14,28–30] one included recurrent pediatric HGG,[25] and two included other (refractory) brain tumors.[13,15] However, in all these studies DIPG patients were analyzed separately.

Biopsies were generally obtained in case of uncertainty about MRI diagnosis. In one study, biopsy was an inclusion criterion. Thirteen studies reported a total of 108 biopsies; pathology showed 20 (WHO grade II) diffuse astrocytomas, 1 oligodendroglioma grade II, 1 oligoastrocytoma grade II, 37 (WHO grade III) anaplastic astrocytomas, 3 oligoastrocytoma grade III, 27 (WHO grade IV) glioblastoma multiforme, 15 not further specified malignant gliomas, and 4 were undefined.[8,10–13,17–20,24,25,28,30]

Survival rates

The median OS ranged from 4–17 months, but was not reported in three studies.[10,14,16] The 1-, 2- and 3-year OS ranged from 14–70%, 0–25% and 0–10%, respectively. Median PFS ranged from 3–10 months. If only studies which specified MRI criteria for DIPG (>50% pontine involvement) were included, median OS ranged from 7–14 months and PFS from 5–8 months.[8,9,11,17,18,21,24,30]

Hypofractionation of radiotherapy

Two studies on hypofractionation of radiotherapy, focusing on non-inferiority with shorter treatment duration, reported median OS rates of 8 and 9 months; this is at the lower end of the published range.[18,24]

Neo-adjuvant chemotherapy

The study accomplishing the highest median OS (17 months (95% C.I. 11–20)) was conducted by Frappaz et al. In that study, neo-adjuvant high-dose methotrexate, BCNU, cisplatin and tamoxifen was given in cycles to DIPG patients until progressive disease occurred, then followed by radiotherapy.[12] One toxic death was reported. When survival was estimated from the start of radiotherapy, Kaplan–Meier curves were comparable with historical controls (median OS 9 months), suggesting that the 8-month improvement in survival duration was due to upfront chemotherapy. However, the long-term survival was poor, with a 3-year OS of 4%. In addition, Massimino et al. reported on three neo-adjuvant chemotherapy protocols, including one high-dose chemotherapy regimen followed by autologous stem cell transplantation.[22] The median OS ranged from 9–13 months. Remarkably, in the study in which vinorelbine was used, two long-term survivors were reported: both alive at 31 and 48 months post-diagnosis, respectively.[22]

Temozolomide

Addition of temozolomide to radiotherapy has not resulted in an improved survival rate in DIPG, in contrast to adult glioblastoma multiforme.[31] The median OS ranged from 9 to 10 months.[11,17,26] Importantly, no long-term survivors were present in the 63 pa-
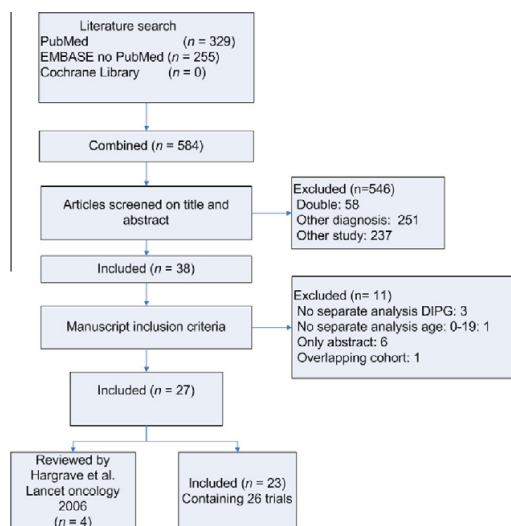

Fig. 1. Flow chart (according to PRISMA) of the systematic search.

Table 1
Inclusion criteria and baseline characteristics of published studies including newly diagnosed DIPG patients from 2005.

Therapy	Phase	DIPG only	Symptoms[a]	Lab	Symptom duration	Karnofsy/ Lansky	Life exp.	Tumor > 50% pons	NF excl.	N	Age (yr)	Range (yr)	Boys/ girls	Symptom (mths)	Biopsy	Gr 2	Gr 3	Gr 4	MG[b]	Ref No.
Pre-irradiation therapy																				
HDC (and adj) VCR-lomustine)	II	y	n	n	n	n	n	n	n	10	6	–	37%	–	30	6	18	6	–	22
Cisplatin, VP-16 (and adj isotretinoin)	II	y	n	n	n	n	n	n	n	17	6	–	37%	–					–	22
Vinorelbine	II	y	n	n	n	n	n	n	n	14	6	–	37%	–						22
BCNU, cisplatin, tamoxifen, HD-MTX	II	y	n	n	n	n	n	n	n	23	9	3–20	50%	2	4[c]	–	–	–	–	12
Carboplatin, VCR, MTX, cyclophosphamide, cisplatin	II	BT	n	n	n	n	n	n	n	7	3	0–3	57%	–	–	–	–	–	–	15
Radiotherapy																				
Hypofractionation	Pilot	y	≥2	n	<3 mths	n	n	y	y	9	6	3–13	44%	2	4	–	–	4	–	18
Hypofractionation	–	y	n	n	n	n	n	y	n	22	6	3–13	55%	1	4	–	3	1	–	24
Chemo-radiotherapy																				
TMZ	II	y	≥2	y	n	≥50%	n	y	n	20	8	3–18	75%	–	8	6	–	–	2	17
TMZ	II	y	≥2	y	<6 mths	≥60%	n	n	n	15	6	2–12	40%	–	–	–	–	–	–	26
TMZ	II	y	n	y	n	≥50%	>2mths	y>67%	n	63	8	3–16	48%	–	3	–	1	2	–	11
TMZ and cis-retinoic acid	II	y	n	n	n	≥70%	n	n	n	12	4	3–9	25%	1.5	3	–	–	–	–	27
TMZ and thalidomide	I/II	y	n	y	n	n	n	n	n	17	8	3–16	35%	–	1	–	1	1	–	19
Cisplatin, VP-16, VCR, ifosfamide	II	HGG	n	n	<6 mths	n	n	y	n	37	8	–	57%	–	16	4	8	4	–	30
Tamoxifen	II	y	≥1	n	<6 mths	n	n	n	n	31	7	2–16	42%	0.7	–	–	–	–	–	23
VCR and oral VP-16	II	y	≥2	n	<6 mths	≥50%	>6 wks	y>67%	y	30	8	3–14	40%	–	–	–	–	–	–	21
VP-16, cytarabin, ifosfamide, cisplatinum, dactinomycin	II	y	n	n	n	n	n	y	n	21	6	–	37%	–	–	–	–	–	–	22
Radiosensitizers																				
Carbogen	Pilot	y	≥2	n	<3 mths	n	n	y	y	10	9	–	–	1	3	–	–	–	3	8
Motexafin gadolinium	I	y	n	y	n	≥50%	>8 wks	y	n	44	6	2–20	36%	–	–	–	–	–	–	9
Adjuvant chemotherapy																				
Interferon Ý and cyclofosfamide	I/II	HGG	n	n	n	n	n	n	n	19	–	–	–	–	–	–	–	–	–	29
Anti-angiogenesis therapy																				
Thalidomide	II	GBM	≥1	n	<3 mths	≥40%	>8 wks	n	n	12	6	2–14	31%	–	1	–	–	–	1	28
Topotecan, adjuvant thalidomide, celecoxib, etoposide	II	y	n	n	n	n	n	n	n	8	8	3–13	–	–	5	2	3	–	–	20
Targeted therapy Tipifarnib	I	y	n	y	n	≥50%	n	n	n	17	6	4–14	35%	–	–	–	–	–	–	16
Imatinib	I	refr HGG	n	y	n	≥50%	n	n	n	27	7	3–19	51%	–	5	–	1	1	–	25
Gefitinib	I	HGG	n	n	n	≥50%	n	n	n	20	7	3–21	30%	–	2	–	2	–	–	14
Vandetanib	I	y	n	y	n	≥40%	n	n	n	35	6	3–16	43%	–	1	–	–	1	–	10
Erlotinib	I	refr BT	n	n	n	≥70%	>8 wks	n	n	21	6	2–16	33%	–	21	4[d]	4[e]	7	6	13

n = no inclusion criterion, y = yes, inclusion criterion, lab = normal liver, renal and bone marrow function, mths = months, wks = weeks, yr = years, exp = expectancy, NF = neurofibromatosis, N = number of patients, Gr = glioma grade, BT = brain tumors other than ependymoma, GBM = glioblastoma multiforme HGG = high-grade glioma, refr = refractory, Ref = reference, HDC = high-dose chemotherapy with autologous stem cell reinfusion. BCNU = carmustine, HD = high-dose, MTX = methotrexate, VCR = vincristine, TMZ = temozolomide, VP-16 = etoposide.
[a] Cranial nerve deficits, long tract signs, or ataxia.
[b] Malignant glioma no grade reported.
[c] No tumor grade reported.
[d] 1 Oligodendroglioma grade II and 1 oligoastrocytoma grade II.
[e] 3 Oligoastrocytoma grade III.

Table 2
Response and survival rates of published studies including newly diagnosed DIPG patients from 2005.

Therapy	CR	PR	SD	PD	MOS (mths)	CI	1-year OS	2-year OS	3-year OS	PFS (mths)	1-year PFS	Ref. No.
Pre-irradiation therapy												
HDC (and adj VCR-lomustine)	–	–	–	–	13	–	70%	10%	–	10	40%	22
Cisplatin, VP-16 (and adj isotretinoin)	–	–	–	–	9	–	29%	12%	–	5	12%	22
Vinorelbine	–	–	–	–	9	–	43%	21%	–	7	21%	22
Carmustine, cisplatin, tamoxifen, HD-MTX	–	–	–	–	17	11–20	65%	22%	4%	–	–	12
Carboplatin, VCR, MTX, cyclophosphamide, cisplatin	–	–	–	–	3.6	–	14%	0%	0%	2.5	0%	15
Radiotherapy												
Hypofraction	–	–	–	–	8.6	–	–	–	–	5	–	18
Hypofraction	–	–	–	–	7.6	–	–	–	–	5.7	–	24
Chemo-radiotherapy												
TMZ	–	–	–	–	9.2	–	35%	15%	10%	6.9	–	17
TMZ	–	–	–	–	9.8	–	20%	7%	–	5.1	7%	26
TMZ	0%	31%	34%	14%	9.6	–	40%	3.6%	0%	6.1	14%	11
TMZ and cis-retinoic acid	0%	58%	33%	9%	13.5	6–22	58%	–	–	10.2	–	27
TMZ and thalidomide	0%	83%	8%	8%	12.7	10–15	58%	25%	–	7.2	17%	19
Cisplatin, VP-16, VCR, ifosfamide	3%	22%	46%	30%	13.6	–	–	–	–	4.8	0%	30
Tamoxifen	–	–	–	–	6.3	–	16%	6%	6%	3.9	3%	23
VCR and oral VP-16	–	–	–	–	12	–	45%	18%	–	7	30%	21
VP-16, cytarabin, ifosfamide, cisplatinum, dactinomycin	0%	26%	67%	7%	9	–	27%	3%	0%	–	–	22
Radiosensitizers												
Carbogen	–	–	–	–	9.6	–	–	–	–	8	–	8
Motexafin gadolinium	–	–	–	–	7	8–3	–	–	–	–	–	9
Adjuvant chemotherapy												
Interferon Ý and cyclofosfamide	–	–	–	–	9.6	–	–	0%	0%	–	–	29
Anti-angiogenesis therapy												
Thalidomide	0%	54%	15%	23%	9	–	–	0%	0%	5	–	28
Topotecan, adjuvant thalidomide, celecoxib, etoposide	–	50%[a]	–	–	12.5	–	63%	–	–	11	–	20
Targeted therapy Tipifarnib	–	–	–	–	–	–	36%	–	–	–	–	16
Imatinib	0%	6%	–	–	11	–	45%	–	–	–	24%	25
Gefitinib	–	–	–	–	–	–	48%	–	–	–	16%	14
Vandetanib	–	–	–	–	–	–	38%	21%	–	–	–	10
Erlotinib	0	17%	50%	33%	12	–	50%	19%	–	8	–	13

mths = months, CR = complete response, PR = partial response: >50% decrease, SD = stable disease: <50 decrease and <25% increase, PD = progressive disease: >25% increase, MOS = median overall survival, PFS = progression-free survival, OS = overall survival, Ref. = reference, HDC = high-dose chemotherapy with autologous stem cell transfusion, MTX = methotrexate, VCR = vincristine, TMZ = temozolomide, VP-16 = etoposide.

[a] Partial response was defined as >20% decrease in this study.

tients cohort reported by Cohen et al.[11] The combination of radiotherapy, temozolomide and either thalidomide or retinoic acid, resulted in a median OS of 13 (95% CI, 10–15) months and 14 (95% CI, 6–21) months, respectively.[19,27] Temozolomide was dosed at 75–90 mg/m^2 daily during radiotherapy and at 200 mg/m^2, 5 days per 28-day cycle of adjuvant temozolomide[17,19,27] in all but one study.[26] This latter study had a metronomic schedule: 85 mg/m^2 daily concurrent with radiotherapy and adjuvant in 6-week cycles with a 1-week break.[26] Main temozolomide related toxicity was bone marrow suppression, especially grade III lymphopenia up to 87%.[26]

Other chemoradiotherapy

Studies on concurrent chemotherapy other than temozolomide (including a vincristine-etoposide, a tamoxifen and an intensified chemotherapy protocol) reported median OS rates ranging from 6 to 14 months, with the best outcome for the intensified chemotherapy trial by Wolff et al.[21,23,30] However, with regard to the latter protocol (consisting of cisplatin, etoposide, vincristine and ifosfamide) the authors concluded that there was no improvement compared to their historical Hirntumor-glioblastoma multiforme DIPG cohorts (a prospective German language multicenter study cohort).[30]

Non-cytotoxic radiosensitizers

Two non-cytotoxic radiosensitizers have been investigated: inhaled carbogen, a potential radiosensitizer of hypoxic tumors, and motexafin gadolinium, an expanded metalloporphyrin with radiosensitizing activity based on depletion of DNA repair enzymes.[8,9]

The carbogen trial was discontinued after 10 patients because of lack of efficacy; for motexafin gadolinium, a phase II trial has been initiated.

Anti-angiogenic therapy

Thalidomide, a drug with antiangiogenic activity, was studied as a single agent in a phase II trial.[28] None of the 12 patients completed the 12 months of treatment, mainly due to progressive disease or toxicity (23%). Prolonged steroid usage was noted in patients enrolled on this study: 11 patients required steroids for at least 6 weeks and 8 patients for more than 12 weeks. The median OS was 9 months (C.I. not reported). Two trials in which thalidomide was studied in combination with other drugs (either temozolomide or celecoxib-etoposide) both had a median OS of 13 months.[19,20]

Targeted therapy

In the past 5 years several tyrosine kinase inhibitors and other targeted agents have been introduced in DIPG, mostly in phase I trials; therefore, survival rates should be interpreted with caution. A phase I trial on the farnesyltransferase inhibitor tipifarnib (inhibiting rat sarcoma; Ras) reported a maximum tolerated dose of 125 mg/m^2/dose twice daily concurrent with radiotherapy and 200 mg/m^2/dose as adjuvant treatment[16]; the 1-year OS rate was 36% (SE 17%). In addition, the platelet-derived growth factor receptor (PDGFR) and C-KIT inhibitor imatinib was studied in a phase I trial[25]; the 1-year OS rate was 46% (SD 9%). Importantly, the 6-month estimate of cumulative incidence of intratumoral hemorrhage (ITH) was high (33%) and led to a study amendment. How-

ever, three patients not receiving imatinib also developed ITH, which suggests that ITH is a spontaneously occurring phenomenon in the course of this disease. ITH was also observed in a phase I trial on gefitinib, an inhibitor of the epidermal growth factor receptor (EGFR).[14] Because ITH occurred in 25% of the patients at a dose of 375 mg/m^2, the recommended dose for phase II studies is 250 mg/m^2. In the gefitinib study the 1-year OS for patients with DIPG was 48% (SE 11%).[14] Additionally, erlotinib (another EGFR inhibitor), was studied in a phase I trial in newly diagnosed DIPG and recurrent HGG.[13] Most frequently reported toxicity was skin toxicity, diarrhea and asthenia, with ITH occurring only in non-pontine gliomas. The maximum tolerated dose was established at 125 mg/m^2 with and without radiotherapy. The median OS was 12 months in the DIPG subgroup of this study, being the only study in which histological confirmation was required for inclusion. The availability of tumor samples enabled EGFR expression and amplification analysis. EGFR expression in patients with DIPG showed a trend to correlation with PFS (median PFS of 10 months in EGFR + - patients; $n = 6$) versus 6 months in EGFR patients ($n = 11$) (HR: 0.35; $p = 0.06$). Recently, a phase I trial reported on vandetanib, a tyrosine kinase inhibitor of the EGFR and vascular endothelial growth factor (VEGFR).[10] The maximum tolerated dose was 145 mg/m^2, with a caveat that blood pressure should be monitored; two patients developed hypertension with reversible posterior encephalopathic syndrome, both in combination with steroid use. The 1-year OS was 38% (SD 11%), with two long-term survivors.

Non-published completed and ongoing trials

Several trials in newly diagnosed DIPG are ongoing and/or have not yet been published; these are summarized in Table 3.

Results of the HEAD-start protocols, neo-adjuvant high-dose chemotherapy followed by autologous stem cell transplantation, have not yet been published (Patel et al., Neuro Oncol 2008; 10:427: abstract). Temozolomide is still being studied in metronomic and traditional dose schedules in multiple trials (Chassot, 2010, Kramm, 2010, Bailey, 2007; clinicaltrials.gov).Studies with motexafin and capecitabine are ongoing in DIPG. Capecitabine is an oral family member of the fluoropyrimidine (5-FU) group, a widely used cytostatic drug which appears to have radiosensitizing capacity in vitro.[32,33]

Several trials with targeted agents are currently ongoing in DIPG. EGFR inhibition has been mainly studied with the humanized monoclonal antibody nimotuzumab. Preliminary results of the first nimotuzumab trial in progressive DIPG were encouraging (150 mg/m^2 once weekly i.v.), since 10/22 DIPG patients experienced stable disease or partial responses. (Fleischhack et al., Pediatr Blood Cancer 45:444, 2005: abstract). However, preliminary results of the subsequent phase II/III trial in newly diagnosed patients showed a median OS of 10 (±1) months which provided no benefit compared to historical controls (Fleischhack et al., Neuro Oncol 12(6):9, 2010: abstract). VEGF inhibition with the monoclonal antibody bevacizumab is currently being studied in newly diagnosed DIPG, either with irinotecan or with valproic acid (Fouladi, Blaney, 2009; clinicaltrials.gov). One trial is investigating a multi-targeted therapy approach with nimotuzumab, bevacizumab and valproic acid combined with radiotherapy, following a neo-adjuvant window phase with cisplatinin-irinotecan (Cruz et al., Neuro Oncol 12(6):10, 2010: abstract). Additionally, PDGFR inhibition by dasatinib is being studied in combination with vandetanib (Broniscer, 2009; clinicaltrials.gov). Finally, the first molecular target-based trial is planned in which patients are treated with radiotherapy with concomitant bevacizumab, followed by bevacizumab maintenance therapy with either temozolomide and/or erlotinib. Maintenance therapy stratification will be based on MGMT pro-

moter methylation status and EGFR expression in tumor biopsy samples taken at diagnosis (Kieran, 2011; clinicaltrials.gov).

Currently, a study is recruiting patients in which IL-13 pseudo-monas exotoxin is infused by convection enhanced delivery in children with recurrent DIPG and high-grade gliomas (NIHCC, 2009; clinicaltrials.gov). Convection enhanced delivery is a method in which drugs are administered directly into the tumor under a continuous high-pressure gradient. It has thus far been applied in the brainstem in two patients, of which one had progressive DIPG and the other Gaucher disease.[34] Reported morbidity was mild and transient in both procedures. The patient with DIPG received IL-13 bound to pseudomonas exotoxin and survived 4 months after administration.[34]

Biology

Knowledge on DIPG biology was limited until recently, mainly due to a lack of available tumor tissue. Historically, biopsies were not regularly performed on DIPG, since diagnosis on MRI was found to be reliable and a histological diagnosis would not change therapy for the individual patient. In addition, a stereotactic biopsy was considered to be a dangerous procedure.[2] However, the question regarding tumor tissue has been raised again; an FDA meeting (2009) and a European meeting (2011) were organised to discuss biopsies in DIPG (Pena et al. www.fda.gov/AdvisoryCommittees). In France (Paris) and the UK (Nottingham), where patients with DIPG have been biopsied regularly in the past few years, only transient morbidity and no mortality have occurred.[3–5] Furthermore, biopsies have been performed as part of a clinical trial to enable correlation of specific kinase expression to response to molecular targeted therapy.[13]

Autopsies are another important source of DIPG tissue. Two recent studies evaluated the feasibility of DIPG sample collection from autopsy.[35,36] In both studies, about 50% of the informed parents consented to autopsy. In the study by Broniscer et al. DNA and RNA, suitable for genome-wide analysis could be obtained from 100% to 63% of the tumor samples, respectively.[36] Several research groups are working on culturing DIPG tumor cells obtained via biopsy or even post-mortem material.[37] This will enable multiple drug screening and xenografting of DIPG cell lines, which may give direction to future trials. Although brainstem glioma animal models exist, they are thus far based on adult glioma cell lines, with a different biological signature or genetically engineered (=PMID 20197468).[38,39] Our group has developed a human DIPG mouse model that closely resembles the clinical pathomorphology of human DIPG, with diffusely infiltrating tumor cells, whereas previous models have shown a more focal pattern of tumor growth.[40]

This recent paradigm shift to obtain tissue from DIPG, has resulted in improved knowledge on DIPG biology. One of the first studies on DIPG biology was by Gilbertson et al. who examined EGFR expression in 28 brainstem glioma samples (18 biopsy and 10 post-mortem specimens). The samples showed significant increase in EGFR expression with increasing tumor grade: of the glioblastomas, almost half overexpressed EGFR extensively and 28% also had high-level gene amplification of EGFR.[41] Other studies showed high EGFR expression in 27–40% of the DIPG samples. However, these studies did not report EGFR amplification in DIPG, although chromosome 7 polysomy, harbouring the EGFR gene, was reported in 25% of the DIPG samples in one study.[13,42–44] However, PDGFRα amplification in DIPG has been reported in multiple studies, in up to 36% of the patient samples.[42,44,45] In general, PDGFRα was found to be amplified much more frequently in childhood HGG than in adult HGG.[45] In one study, high PDGFRα protein expression was present in 63% of the samples.[44] In that study, the phospho-mammalian target of rapamycin, a protein downstream of the PDGFR and EGFR pathway, was immunopositive in all 11 samples

Table 3
Non-published completed and ongoing studies in DIPG.

Ongoing studies	Therapy	Patient group	Current status	N	Age (yr)	P.I.	Phase	Start year
Neo-adjuvant Chemoradiotherapy	HEAD-protocols[a]	DIPG	Completed	15	<7	Finlay	II	2001
	Temozolomide	DIPG	Not recruiting	18	3–18	Chassot	II	2005
	Temozolomide	DIPG and HGG	Recruiting	135	3–18	Kramm	II	2009
	Temozolomide	DIPG	Not recruiting	41	2–21	Bailey	II	2007
	Paclitaxel	DIPG	Not recruiting	12	3–21	Belasco	I	2002
	Irinotecan, adj. irinotecan & BCNU	DIPG	Not reported	9	3–21	Larrier	II	–
	Thalidomide and Carboplatin	DIPG	Completed	47	3–21	Goldman	II	1999
	ACNU and VCR, followed by etoposide	DIPG	Completed	12	5–20	Sugiyama	II	2003
	Lenalidomide	DIPG and HGG	Recruiting	30	<18	Warren	I	2010
	Capecitabine	DIPG and HGG	Not recruiting	18	3–21	Blaney	I	2006
	Capecitabine	DIPG	Recruiting	44	3–21	Hoffman-La Roche	II	2007
Radiosensitizers	Motexafin Gadolinium	DIPG	Completed	60	<21	Bradley	II	2006
	Topotecan, G-CSF	DIPG	Suspended	72	3–21	Robertson	II	2005
	Arsenic trioxide	DIPG and HGG	Suspended	36	3–21	Cohen	I	2004
Histone deacetylase inhibitor	Vorinostat and RT	DIPG	Recruiting	80	3–21	Su	I–II	2011
EGFR monoclonal antibodies	Nimotuzumab	DIPG	Not recruiting	41	3–20	Bode	III	2007
	Nimotuzumab	DIPG	Not recruiting	44	3–18	Bouffet, Bartels	II	2008
	Nimotuzumab	DIPG	Recruiting	–	3–18	Cabanas	II	2007
	Neo-adj. cisplatin and irinotecan, RT and temozolomide, adj. nimotuzumab, bevacizumab and valproic acid	DIPG	Recruiting	15	0.5–18	Cruz	II	2006
	Nimotuzumab	DIPG	Not open yet	40	3–18	Epelman	III	2010
	Nimotuzumab and vinorelbine	DIPG	Recruiting	–	3–18	Massimino	II	2009
	Cetuximab and irinotecan	DIPG	Recruiting	51	3–21	Dunkel	II	2010
VEGF-monoclonal antibodies	RT and valproic acid, adjuvant bevacizumab and valproic acid	DIPG	Recruiting	56	3–21	Blaney	II	2009
VEGFR and PDGFR-TKI	RT and bevacizumab and TMZ, adj bevacizumab, TMZ and irinotecan	DIPG and HGG	Recruiting	35	3–30	Fouladi	I–II	2009
	Vandetanib and dasatinib	DIPG	Recruiting	28	1.5–21	Broniscer	I	2009
Molecular based therapy	Temozolomide/erlotinib/bevacizumab	DIPG	Not open yet	100	3–18	Kieran	II	2011
$\alpha_v\beta_3$ & $\alpha_v\beta_5$ integrins inhibitor	Cilengitide	DIPG	Recruiting	40	0.5–21	Le Blond	I	2010
Immunotherapy	HLA-A2-restricted synthetic glioma antigen peptides vaccine	DIPG and HGG	Recruiting	36	1.5–20	Jakacki	I	2009
	PI EGFRvIII Peptide vaccination	DIPG	Not open yet	15	≤18	Fisher	I	2010
	Interferon α 2b	DIPG	Not recruiting	32	<21	Warren	II	2002
Convection enhanced delivery	Interleukin-13-PE38QQR	Progressive DIPG and HGG	Recruiting	20	≤17	NIHCC	I	2009

N = estimated inclusion number, yr = years, P.I. = principal investigator, EGFR = epidermal growth factor receptor, VEGF = vascular endothelial growth factor, VEGFR = vascular endothelial growth factor receptor, TKI = tyrosine kinase inhibitor, PDGFR = platelet-derived growth factor receptor, TMZ = temozolomide, VCR = vincristine, RT = radiotherapy, HGG = high-grade glioma, LGG = low-grade glioma, PE = pseudomonas exotoxin.
[a] 3–5 cycles of: vincristine, etoposide, cisplatin, and cyclophosphamide (regimen A); or prednisone, lomustine, vincristine, and carboplatin (regimen B); or vincristine, carboplatin, and temozolomide (regimen C).

Table 4
Drugable targets in DIPG.

Target	Expression/amplification	% of samples	Targeted by drugs[a]
EGFR	Protein expression	27–50%	Erlotinib, gefitinib, nimotuzumab, cetuximab, vandetanib (also VEGFR)
	Amplification	0%	
PDGFR	Protein expression	63–100%	Imatinib, dasatinib
	Amplification	36%	
VEGF(R)	NA	NA	Vandetanib (also EGFR), bevacizumab
MTOR	Protein expression	100%	Everolimus, sirolimus
	Amplification	NA	
PARP	Expression	36%	ABT-888 (study ongoing)
	Amplification	27%	
MGMT	Protein expression	0%	O6-benzylguanine
RAS	NA	NA	Lonofarnib, tipifarnib
avβ3 and avβ5	NA	NA	Cilengitide (EMD121974)
IL-13	NA	NA	IL13-PE38QQR

NA = not analyzed, EGFR = epidermal growth factor receptor, VEGF(R) = vascular endothelial growth factor (receptor), PDGFR = platelet-derived growth factor receptor, MTOR = mammilian target of rapamycin, PARP = poly (ADP-ribose) polymerase, MGMT = methylguanine methyltransferase, RAS = RAt Sarcoma, PE = pseudomonas exotoxin.
  [a] The enumeration of drugs is not exhaustive.

(strong in two, moderate in five and weak in four samples).[44] PARP-1 gene amplification was reported in 27% of the samples. Furthermore, genes involved in double-strand break repair were frequently deleted or subjected to loss of heterozygosity. Additionally, PTEN loss (rare in supratentorial childhood HGG) was found to be common in DIPG, which is associated with a worse prognosis in gliomas.[13,46] Drugable targets are listed in Table 4.

Multiple studies have shown that DIPG differ from non-brainstem HGG. Barrow et al. showed 17p loss (associated with the loss of p53 in adult HGG) and 14q loss to be much more frequent, and 10q loss to be much less frequent, in DIPG compared to non-brainstem HGG.[42] Zarghooni et al. using single nucleotide polymorphism arrays, observed clear differences in the regions of copy number alterations between both groups, indicating a different genetic profile.[44] An abstract from Puget et al. reports on comparative genomic hybridization and gene expression profiling of 35 frozen DIPG samples. (Puget et al., Neuro Oncol 12(6):8-9, 2010 abstract). Gains of chromosome 1q (34%), Xq (25%), 2p and 7p (22%), losses of chromosomes 14q (31%), 10q (28%) and 17p (25%), and amplifications for numerous genes including PDGFRα locus, RNH1, LRP1 and MET, were found. A molecular subgroup characterized by the appearance of gains or amplifications in PDGFRα showed a shorter survival compared to a subgroup characterized by angiogenic and adhesion genes.

Discussion

The prognosis of DIPG has not improved during the past six years. Only one study, by Frappaz et al. clearly showed an improvement in survival duration: pre-irradiation therapy consisting of high-dose methotrexate, BCNU, cisplatin and tamoxifen until progressive disease occurred, then followed by radiotherapy.[12] In that study, the improved survival may have been influenced by the relatively long duration of symptoms (60 days), which may indicate a less aggressive tumor type. The drug combination may be potential therapy; however, high-dose MTX and tamoxifen separately did not improve survival in previous studies.[23,47,48] Another explanation is that radiotherapy retains its activity in patients developing progressive disease under chemotherapy. It should be noted that Frappaz et al. reported a prolonged hospitalization duration compared to historical controls (57 versus 25 days).[12] In addition, it is less likely that this approach of consecutive treatment elements will eventually lead to cure: there was no increase of long-term survivors in their study.[12] However, the strategy of combining drugs deserves further investigation in future trials.

The high expectations of temozolomide could not be realized. It has been hypothesized that temozolomide resistance is due to unmethylated O6-methylguanine DNA methyltransferase (MGMT), but this does not seem to apply to DIPG, since Zarghooni et al. did not find MGMT expression in any of their eleven DIPG samples.[44]

Although biopsies have been reintroduced in some hospitals, this is not yet regular policy. The attitude towards collection of tumor tissue via biopsy and autopsy needs to change. Parents should become more involved with the pros and cons of these procedures, which raise challenging ethical and technical questions. By means of biopsies and autopsies, new potential treatment targets in DIPG have been identified, such as PDGFRα. Drugs targeting the downstream pathway phospho-mammalian target of rapamycin are also of interest. Single-agent therapy with the PDGFR inhibitor imatinib did not improve prognosis, but in that study tumor tissue was not obtained and no PDGFRα gene/protein expressing subgroup could be identified.[25] The high rate of ITH in the imatinib trial warrants investigating other PDGFRα inhibitors, such as dasatinib.[25] ITH was a commonly observed phenomenon in targeted therapy trials in DIPG, necessitating intensive monitoring in future trials. In addition, PARP-1 is an interesting target in DIPG. As was shown by Zarghooni et al., DIPGs harbour multiple deficits in double-strand break repair genes, either by loss of heterozygosity or deletion. As in other tumor types that have loss of these repair mechanisms, PARP inhibition could potentiate synthetic lethality in DIPG.[49] PTEN loss, in this respect, has also been related to deficient DNA double-strand break repair.[50] EGFR may still be a rational target since it is highly expressed in a subgroup of DIPG patients, and gene amplification is present in a subset of patients. However, single-agent EGFR-inhibition by nimotuzumab, erlotinib or gefitinib has not improved the prognosis. Expression of VEGFR, which is known to stimulate angiogenesis and is frequently overexpressed in adult gliomas, has not yet been investigated in DIPG.[51] Also, Ras mutations have not yet been studied in DIPG. Adult gliomas rarely show Ras mutations, but aberrations in several tyrosine kinase receptors can activate Ras; therefore, Ras is attractive for targeting. Indeed, human glioma cell lines overexpressing EGFR showed enhanced response rates to farnesyl transferase inhibitors regardless of Ras mutational status.[52]

In general, the complex biology and drug resistance of these tumors render an unselected single-agent approach less likely to be effective. Instead, a multi-targeted approach seems to be required to improve the prognosis. We believe that treatment stratification based on target expression is debatable. As in adult cancer, wild-type target expression often does not correlate with survival. Autophosphorylated or mutated proteins are considered to be better targets for therapy. Furthermore, the heterogeneity of gliomas with

target determination based on a single biopsy sample imposes the risk of decisions being made that either overestimate/underestimate the effect of a targeted therapy or wrongly include/exclude patients from treatment strata. Reduction of this potential sample error, by obtaining multiple samples, should be advocated. The small number of patients also hampers molecular target stratified trials, emphasizing the need for larger studies conducted by collaborative groups.

A major challenge in DIPG is drug distribution. Penetration of drugs in DIPG seems to be poor, likely due to an intact blood–brain barrier and/or high pressure in the pons. This is illustrated by the lack of gadolinium enhancement in at least 50% of the patients with DIPG.[53] The question of drug penetration may be answered by PET imaging of drug-labelled positron emitters. This technique enables to monitor drug distribution in multiple adult cancers.[54–56] Moreover, labelling monoclonal antibodies and small molecules will give insight into expression of biological targets which may lead to effective personalized treatment and help prevent the administration of inactive drugs with their accompanying side effects.[57] From a therapeutic point of view, improving tumor drug distribution is crucial. This may be accomplished either by disrupting the blood–brain barrier or with permeability-increasing agents (e.g. mannitol, morphine or (met)amphetamine).[58–60] Another opportunity is local delivery, including local tumor injection and convection enhanced delivery, enabling high drug concentrations in the pons, including drugs that normally do not pass the blood–brain barrier.[34,61] Although not yet under study in DIPG, nanoparticles may play an important role in local drug delivery drugs in the future.[62,63]

Finally, it is emphasized that international collaboration in preclinical and clinical research is essential in order to accelerate progress in the acquisition of knowledge and, ultimately, improvement of the prognosis in DIPG. Recent collaborative efforts have resulted in the establishment of a European DIPG Network, focusing on centralization of clinical data, standardization of imaging criteria and the collection of tumor tissue for European research projects.

Conclusion

No clear improvement in survival has been achieved in DIPG during recent years. Trials still show a wide variation in their inclusion criteria. However, with ever-increasing biological data from in vitro studies, genome-wide analyses and in vivo models, a better basis for future clinical trials has been established. Translation of this knowledge into clinical trials in combination with improved drug distribution and response prediction methods may lead to more effective treatment of this devastating disease.

Conflict of interest

None declared.

Acknowledgments

References

1. Hargrave D, Bartels U, Bouffet E. Diffuse brainstem glioma in children: critical review of clinical trials. *Lancet Oncol* 2006;**7**(3):241–8.
2. Epstein F, McCleary EL. Intrinsic brain-stem tumors of childhood: surgical indications. *J Neurosurg* 1986;**64**(1):11–5.
3. Cartmill M, Punt J. Diffuse brain stem glioma. A review of stereotactic biopsies. *Childs Nerv Syst* 1999;**15**(5):235–7.
4. Pincus DW, Richter EO, Yachnis AT, Bennett J, Bhatti MT, Smith A. Brainstem stereotactic biopsy sampling in children. *J Neurosurg* 2006;**104**(2 Suppl): 108–14.
5. Roujeau T, Machado G, Garnett MR, et al. Stereotactic biopsy of diffuse pontine lesions in children. *J Neurosurg* 2007;**107**(1 Suppl):1–4.
6. Nakagawa Y, Kageji T, Mizobuchi Y, Kumada H, Nakagawa Y. Clinical results of BNCT for malignant brain tumors in children. *Appl Radiat Isot* 2009;**67** (7–8 suppl.):S27–30.
7. Wolff JE, Kortmann RD, Wolff B, et al. High dose methotrexate for pediatric high grade glioma: results of the HIT-GBM-D Pilot study. *J Neurooncol* 2011;**102**(3):433–42.
8. Aquino-Parsons C, Hukin J, Green A. Concurrent carbogen and radiation therapy in children with high-risk brainstem gliomas. *Pediatr Blood Cancer* 2008;**50**(2):397–9.
9. Bradley KA, Pollack IF, Reid JM, et al. Motexafin gadolinium and involved field radiation therapy for intrinsic pontine glioma of childhood: a Children's Oncology Group phase I study. *Neuro Oncol* 2008;**10**(5):752–8.
10. Broniscer A, Baker JN, Tagen M, et al. Phase I study of vandetanib during and after radiotherapy in children with diffuse intrinsic pontine glioma. *J Clin Oncol* 2010;**28**(31):4762–8.
11. Cohen KJ, Heideman RL, Zhou T, et al. Temozolomide in the treatment of children with newly diagnosed diffuse intrinsic pontine gliomas: a report from the Children's Oncology Group. *Neuro Oncol* 2011;**13**(4):410–6.
12. Frappaz D, Schell M, Thiesse P, et al. Preradiation chemotherapy may improve survival in pediatric diffuse intrinsic brainstem gliomas: final results of BSG 98 prospective trial. *Neuro Oncol* 2008;**10**(4):599–607.
13. Geoerger B, Hargrave D, Thomas F, et al. Innovative Therapies for Children with Cancer pediatric phase I study of erlotinib in brainstem glioma and relapsing/refractory brain tumors. *Neuro Oncol* 2011;**13**(1):109–18.
14. Geyer JR, Stewart CF, Kocak M, et al. A phase I and biology study of gefitinib and radiation in children with newly diagnosed brain stem gliomas or supratentorial malignant gliomas. *Eur J Cancer* 2010;**46**(18):3287–93.
15. Grundy RG, Wilne SH, Robinson KJ, et al. Primary postoperative chemotherapy without radiotherapy for treatment of brain tumours other than ependymoma in children under 3 years: results of the first UKCCSG/SIOP CNS 9204 trial. *Eur J Cancer* 2010;**46**(1):120–33.
16. Haas-Kogan DA, Banerjee A, Kocak M, et al. Phase I trial of tipifarnib in children with newly diagnosed intrinsic diffuse brainstem glioma. *Neuro Oncol* 2008;**10**(3):341–7.
17. Jalali R, Raut N, Arora B, et al. Prospective evaluation of radiotherapy with concurrent and adjuvant temozolomide in children with newly diagnosed diffuse intrinsic pontine glioma. *Int J Radiat Oncol Biol Phys* 2009;**77**(1):113–8.
18. Janssens GO, Gidding CE, Van Lindert EJ, et al. The role of hypofractionation radiotherapy for diffuse intrinsic brainstem glioma in children: a pilot study. *Int J Radiat Oncol Biol Phys* 2009;**73**(3):722–6.
19. Kim CY, Kim SK, Phi JH, et al. A prospective study of temozolomide plus thalidomide during and after radiation therapy for pediatric diffuse pontine gliomas: preliminary results of the Korean Society for Pediatric Neuro-Oncology study. *J Neurooncol* 2010;**100**(2):193–8.
20. Kivivuori SM, Riikonen P, Valanne L, Lonnqvist T, Saarinen-Pihkala UM. Antiangiogenic combination therapy after local radiotherapy with topotecan radiosensitizer improved quality of life for children with inoperable brainstem gliomas. *Acta Paediatr* 2011;**100**(1):134–8.
21. Korones DN, Fisher PG, Kretschmar C, et al. Treatment of children with diffuse intrinsic brain stem glioma with radiotherapy, vincristine and oral VP-16: a Children's Oncology Group phase II study. *Pediatr Blood Cancer* 2008;**50**(2):227–30.
22. Massimino M, Spreafico F, Biassoni V, et al. Diffuse pontine gliomas in children: changing strategies, changing results? A mono-institutional 20-year experience. *J Neurooncol* 2008;**87**(3):355–61.
23. Michalski A, Bouffet E, Taylor RE, et al. The addition of high-dose tamoxifen to standard radiotherapy does not improve the survival of patients with diffuse intrinsic pontine glioma. *J Neurooncol* 2010;**100**(1):81–8.
24. Negretti L, Bouchireb K, Levy-Piedbois C, et al. Hypofractionated radiotherapy in the treatment of diffuse intrinsic pontine glioma in children: a single institution's experience. *J Neurooncol* 2011. Epub ahead of print.
25. Pollack IF, Jakacki RI, Blaney SM, et al. Phase I trial of imatinib in children with newly diagnosed brainstem and recurrent malignant gliomas: a Pediatric Brain Tumor Consortium report. *Neuro Oncol* 2007;**9**(2):145–60.
26. Sharp JR, Bouffet E, Stempak D, et al. A multi-centre Canadian pilot study of metronomic temozolomide combined with radiotherapy for newly diagnosed paediatric brainstem glioma. *Eur J Cancer* 2010;**46**(18):3271–9.
27. Sirachainan N, Pakakasama S, Visudithbhan A, et al. Concurrent radiotherapy with temozolomide followed by adjuvant temozolomide and cis-retinoic acid in children with diffuse intrinsic pontine glioma. *Neuro Oncol* 2008;**10**(4):577–82.
28. Turner CD, Chi S, Marcus KJ, et al. Phase II study of thalidomide and radiation in children with newly diagnosed brain stem gliomas and glioblastoma multiforme. *J Neurooncol* 2007;**82**(1):95–101.
29. Wolff JE, Wagner S, Reinert C, et al. Maintenance treatment with interferon-gamma and low-dose cyclophosphamide for pediatric high-grade glioma. *J Neurooncol* 2006;**79**(3):315–21.
30. Wolff JE, Driever PH, Erdlenbruch B, et al. Intensive chemotherapy improves survival in pediatric high-grade glioma after gross total resection: results of the HIT-GBM-C protocol. *Cancer* 2010;**116**(3):705–12.

31. Stupp R, Mason WP, van den Bent MJ, et al. Radiotherapy plus concomitant and adjuvant temozolomide for glioblastoma. *N Engl J Med* 2005;**352**(10):987–96.
32. Glynne-Jones R, Dunst J, Sebag-Montefiore D. The integration of oral capecitabine into chemoradiation regimens for locally advanced rectal cancer: how successful have we been? *Ann Oncol* 2006;**17**(3):361–71.
33. Sawada N, Ishikawa T, Sekiguchi F, Tanaka Y, Ishitsuka H. X-ray irradiation induces thymidine phosphorylase and enhances the efficacy of capecitabine (Xeloda) in human cancer xenografts. *Clin Cancer Res* 1999;**5**(10):2948–53.
34. Lonser RR, Warren KE, Butman JA, et al. Real-time image-guided direct convective perfusion of intrinsic brainstem lesions. Technical note. *J Neurosurg* 2007;**107**(1):190–7.
35. Angelini P, Hawkins C, Laperriere N, Bouffet E, Bartels U. Post mortem examinations in diffuse intrinsic pontine glioma: challenges and chances. *J Neurooncol* 2011;**101**(1):75–81.
36. Broniscer A, Baker JN, Baker SJ, et al. Prospective collection of tissue samples at autopsy in children with diffuse intrinsic pontine glioma. *Cancer* 2010;**116**(19):4632–7.
37. Monje M, Mitra SS, Freret ME, et al. Hedgehog-responsive candidate cell of origin for diffuse intrinsic pontine glioma. *Proc Natl Acad Sci U S A* 2011;**108**(11):4453–8.
38. Hashizume R, Ozawa T, Dinca EB, et al. A human brainstem glioma xenograft model enabled for bioluminescence imaging. *J Neurooncol* 2009 [Epub ahead of print].
39. Liu Q, Liu R, Kashyap MV, et al. Brainstem glioma progression in juvenile and adult rats. *J Neurosurg* 2008;**109**(5):849–55.
40. Caretti V, Zondervan I, Meijer DH, et al. Monitoring of tumor growth and post-irradiation recurrence in a diffuse intrinsic pontine glioma mouse model. *Brain Pathol* 2010. Epub ahead of print.
41. Gilbertson RJ, Hill DA, Hernan R, et al. ERBB1 is amplified and overexpressed in high-grade diffusely infiltrative pediatric brain stem glioma. *Clin Cancer Res* 2003;**9**(10 Pt 1):3620–4.
42. Barrow J, mowicz-Brice M, Cartmill M, et al. Homozygous loss of ADAM3A revealed by genome-wide analysis of pediatric high-grade glioma and diffuse intrinsic pontine gliomas. *Neuro Oncol* 2011;**13**(2):212–22.
43. Cheng Y, Ng HK, Zhang SF, et al. Genetic alterations in pediatric high-grade astrocytomas. *Hum Pathol* 1999;**30**(11):1284–90.
44. Zarghooni M, Bartels U, Lee E, et al. Whole-genome profiling of pediatric diffuse intrinsic pontine gliomas highlights platelet-derived growth factor receptor alpha and poly (ADP-ribose) polymerase as potential therapeutic targets. *J Clin Oncol* 2010;**28**(8):1337–44.
45. Paugh BS, Qu C, Jones C, et al. Integrated molecular genetic profiling of pediatric high-grade gliomas reveals key differences with the adult disease. *J Clin Oncol* 2010;**28**(18):3061–8.
46. Thorarinsdottir HK, Santi M, McCarter R, et al. Protein expression of platelet-derived growth factor receptor correlates with malignant histology and PTEN with survival in childhood gliomas. *Clin Cancer Res* 2008;**14**(11):3386–94.
47. Dunkel IJ, Garvin Jr JH, Goldman S, et al. High dose chemotherapy with autologous bone marrow rescue for children with diffuse pontine brain stem tumors. Children's Cancer Group. *J Neurooncol* 1998;**37**(1):67–73.
48. Wagner S, Reinert C, Schmid HJ, et al. High-dose methotrexate prior to simultaneous radiochemotherapy in children with malignant high-grade gliomas. *Anticancer Res* 2005;**25**(3c):2583–7.
49. Carey LA, Sharpless NE. PARP and cancer – if it's broke, don't fix it. *N Engl J Med* 2011;**364**(3):277–9.
50. McEllin B, Camacho CV, Mukherjee B, et al. PTEN loss compromises homologous recombination repair in astrocytes: implications for glioblastoma therapy with temozolomide or poly(ADP-ribose) polymerase inhibitors. *Cancer Res* 2010;**70**(13):5457–64.
51. Reardon DA, Wen PY. Therapeutic advances in the treatment of glioblastoma: rationale and potential role of targeted agents. *Oncologist* 2006;**11**(2):152–64.
52. Feldkamp MM, Lau N, Roncari L, Guha A. Isotype-specific Ras.GTP-levels predict the efficacy of farnesyl transferase inhibitors against human astrocytomas regardless of Ras mutational status. *Cancer Res* 2001;**61**(11):4425–31.
53. Hargrave D, Chuang N, Bouffet E. Conventional MRI cannot predict survival in childhood diffuse intrinsic pontine glioma. *J Neurooncol* 2008;**86**(3):313–9.
54. Borjesson PK, Jauw YW, Boellaard R, et al. Performance of immuno-positron emission tomography with zirconium-89-labeled chimeric monoclonal antibody U36 in the detection of lymph node metastases in head and neck cancer patients. *Clin Cancer Res* 2006;**12**(7 Pt 1):2133–40.
55. Perik PJ, Lub-de Hooge MN, Gietema JA, et al. Indium-111-labeled trastuzumab scintigraphy in patients with human epidermal growth factor receptor 2-positive metastatic breast cancer. *J Clin Oncol* 2006;**24**(15):2276–82.
56. Zalutsky MR. Potential of immuno-positron emission tomography for tumor imaging and immunotherapy planning. *Clin Cancer Res* 2006;**12**(7 Pt):1958–60.
57. van Dongen GA, Visser GW, Lub-de Hooge MN, de Vries EG, Perk LR. Immuno-PET: a navigator in monoclonal antibody development and applications. *Oncologist* 2007;**12**(12):1379–89.
58. Hall WA, Doolittle ND, Daman M, et al. Osmotic blood-brain barrier disruption chemotherapy for diffuse pontine gliomas. *J Neurooncol* 2006;**77**(3):279–84.
59. Kast RE. Using blood brain barrier disruption by methamphetamine for drug delivery. *J Neurooncol* 2007;**85**(1):109–10.
60. Sharma HS, Ali SF. Alterations in blood–brain barrier function by morphine and methamphetamine. *Ann NY Acad Sci* 2006;**1074**:198–224.
61. Jenkinson MD, Smith TS, Haylock B, et al. Phase II trial of intratumoral BCNU injection and radiotherapy on untreated adult malignant glioma. *J Neurooncol* 2010;**99**(1):103–13.
62. Invernici G, Cristini S, Alessandri G, et al. Nanotechnology advances in brain tumors: the state of the art. *Recent Pat Anticancer Drug Discov* 2011;**6**(1):58–69.
63. Xin H, Jiang X, Gu J, et al. Angiopep-conjugated poly(ethylene glycol)-co-poly(epsilon-caprolactone) nanoparticles as dual-targeting drug delivery system for brain glioma. *Biomaterials* 2011;**32**(18):4293–305.

Cancer Research

AACR

Isolation and Characterization of Tumorigenic, Stem-like Neural Precursors from Human Glioblastoma

Rossella Galli, Elena Binda, Ugo Orfanelli, et al.

Updated Version	Access the most recent version of this article at: doi:10.1158/0008-5472.CAN-04-1364

Cited Articles	This article cites 53 articles, 21 of which you can access for free at: http://cancerres.aacrjournals.org/content/64/19/7011.full.html#ref-list-1
Citing Articles	This article has been cited by 100 HighWire-hosted articles. Access the articles at: http://cancerres.aacrjournals.org/content/64/19/7011.full.html#related-urls

E-mail alerts	Sign up to receive free email-alerts related to this article or journal.
Reprints and Subscriptions	To order reprints of this article or to subscribe to the journal, contact the AACR Publications Department at pubs@aacr.org.
Permissions	To request permission to re-use all or part of this article, contact the AACR Publications Department at permissions@aacr.org.

Isolation and Characterization of Tumorigenic, Stem-like Neural Precursors from Human Glioblastoma

Rossella Galli,[1] Elena Binda,[1] Ugo Orfanelli,[1] Barbara Cipelletti,[1] Angela Gritti,[1] Simona De Vitis,[2] Roberta Fiocco,[1] Chiara Foroni,[1] Francesco Dimeco,[3,4] and Angelo Vescovi[1,5]

[1]Stem Cell Research Institute and [2]Laboratory of Molecular Diagnostics, H. S. Raffaele, Milan, Italy; [3]National Neurological Institute "C. Besta," Milan, Italy; [4]Department of Neurological Surgery, Johns Hopkins Medical School, Baltimore, Maryland; and [5]Department of Biological Sciences and Biotechnology, University of Milano-Bicocca, Milan, Italy

ABSTRACT

Transformed stem cells have been isolated from some human cancers. We report that, unlike other brain cancers, the lethal glioblastoma multiforme contains neural precursors endowed with all of the critical features expected from neural stem cells. Similar, yet not identical, to their normal neural stem cell counterpart, these precursors emerge as unipotent (astroglial) *in vivo* and multipotent (neuronal-astroglial-oligodendroglial) in culture. More importantly, these cells can act as tumor-founding cells down to the clonal level and can establish tumors that closely resemble the main histologic, cytologic, and architectural features of the human disease, even when challenged through serial transplantation. Thus, even cells possessing all of the characteristics expected from tumor neural stem cells seem to be involved in the growth and recurrence of adult human glioblastomas multiforme.

INTRODUCTION

Cancer arises from a series of mutations occurring in few or single founder cells. From a therapeutic standpoint, a critical issue regards the elucidation of the identity and physiology of the cell(s) responsible for tumor formation, progression, and recurrence (1). With some exceptions (2), the identity of tumorigenic cells within many cancers remains unclear, but recent observations point to the involvement of somatic stem cells in oncogenesis (3). Embryonic and fetal stem cells may accumulate mutations during their expansion/growth phase throughout development and may form full-blown tumors in adulthood (3), whereas adult stem cells and their progeny may represent the direct target of oncogenic transformation in mature tissues (1). Accordingly, the involvement of cells displaying a stem cell phenotype in cancer formation and progression (1) has been confirmed in acute myeloid leukemia (4–6) and breast cancer (2).

If stem cells and/or their progeny represent the main target of neoplastic transformation, it is then reasonable to infer that the main foci of malignant transformation ought to coincide with those tissue regions that embody somatic stem cells. Indeed, the main areas of distribution of certain brain tumors overlap specific regions of the central nervous system (CNS; refs. 7 and 8) that comprise glia-like neural stem cells and their progeny (9, 10). Accordingly, deregulation of specific proto-oncogenes such as Ink4A/Arf, epidermal growth factor (EGF) receptor, and c-myc (11–13) or expression of SV40 T antigen (14) in glial fibrillary acidic protein (GFAP)- or nestin-expressing neural cells induces high-grade gliomas in brain areas that contain neural stem cells.

Recently, transformed, stem-like neural progenitors have been isolated and cultured from human brain tumor tissues (15–17), which

raises fundamental issues concerning their actual ability to drive cancer growth and recurrence (18).

Here, we report the initial finding that glioblastoma multiforme, the most malignant among the adult human CNS tumors, comprises transformed precursors that bear the full complement of functional characteristics expected from stem cells (19), including the capacity for tumor generation. In fact, these cells can establish tumors with all of the classical features of human glioblastomas multiforme, even upon serial transplantation and, therefore, can be identified as tumor neural stem cells (20).

MATERIALS AND METHODS

Sample Classification. All of the samples were classified according to World Health Organization guidelines. Lines 0627, 0821, 0913, 1022, and 1205 were obtained from patients with diagnosis of primary glioblastoma; line 1030 was derived from a patient suffering from secondary glioblastoma. Patients from whom lines 0627, 0821, 0913, and 1022 were established underwent recurrence after 6 to 12 months post-surgery.

Primary Culture, Culture Propagation, Population Analysis, and Cloning. Tumor samples, either derived from patients or from orthotopic transplantation of glioblastoma multiforme–derived cell lines, were processed as by Gritti *et al.* (21). Primary cells were plated in 25 cm^2 tissue culture flasks plated at clonal density (2500–5000 cells/cm^2) in Dulbecco's modified Eagle's medium/F-12 medium containing 20 ng/mL of both EGF and fibroblast growth factor (FGF2; Peprotech, Rocky Hill, NY). As reference cell lines, normal human fetal neural stem cells (22) and the glioblastoma cell line U87MG were used in all of the assays. Population and serial subclonogenic analysis were performed as by Galli *et al.* (23).

Differentiation of Stem Cell Progeny and Immunocytochemistry. To assess for multipotency, cells were plated at a density of 2.5×10^4 cells/cm^2 onto Matrigel-coated glass coverslips (12 mm diameter) in the presence of leukemia inhibitory factor (10 ng/mL; ref. 24) for 7 to 10 days. Multiple immunofluorescence assays for neural antigens were performed as described by Gritti *et al.* (21) and Galli *et al.* (23).

Evaluation of Tumorigenicity by Subcutaneous Injection and by Orthotopic Injection. Tumorigenicity was determined by injecting glioblastoma multiforme–derived neural stem cells, U87, and human fetal neural stem cells, either subcutaneously (s.c.) or orthotopically. Cells (3×10^6) in 100 μL of PBS were s.c. injected into the right flank of *Scid/bg* mice while 2 μL of a 1×10^8 cells/mL cell suspension in PBS were delivered into the right striatum (0.2 μL/min) by stereotactic injection through a glass electrode connected to a Hamilton syringe. The following coordinates were used: antero-posterior = 0; medio-lateral = +2.5 mm; dorso-ventral = −3.5 mm. Mice were sacrificed at different times between 1 and 10 weeks post-injection, according to the cell line originally injected. Hematoxylin and eosin staining and immunohistochemistry were performed on 15-μm-thick cryostat sections. Sections were processed as by Vescovi *et al.* (22). Antibodies/antisera used were as follows: mouse antivimentin (1:200; Chemicon, Temecula, CA), mouse antihuman mitochondria (1:20; Chemicon), mouse antihuman nuclei (1:20; Chemicon), mouse anti-Galactocerebroside C (Gal C; 1:20; Chemicon), mouse antineuronal class III β-tubulin (Tuj1; 1:500; Babco, Richmond, CA), rabbit anti-GFAP (1:1000; Dako Corporation, Carpinteria, CA), rabbit antilaminin (1:200; Sigma, St. Louis, MO), and rabbit anti-Ki67 (1:1000; NovoCastra, Newcastle, UK).

Chromosome Analysis. Cells were treated with medium containing 10 μg/mL Colcemid (Irvine Scientific, Santa Ana, CA) for 1 to 2 hours and resuspended in hypotonic 1% sodium citrate at room temperature for 30

7011

GLIOBLASTOMA-FOUNDING HUMAN NEURAL PRECURSORS

minutes. The cells were then washed in methanol-acetic acid (3:1, v/v) fixative solution for 30 minutes and spread onto clean dry slides. Q-banding staining was then performed, and 10 metaphases were analyzed for each sample.

Telomeric Repeat Amplification Protocol and Telomere Length Assessment. Telomerase activity was detected using the PCR-based TRAPeze Telomerase Detection kit (Intergen, Purchase, NY), according to the manufacturer's instructions. Total proteins (150 ng) were loaded into each lane. For the telomere length assay, the length of the telomeres was determined using TeloTAGGG Telomere Length Assay (Roche, Gipf-Oberfrick, Switzerland) according to the manufacturer's instructions. Two μg of genomic DNA of each sample were digested with a *Hin*fI/*Rsa*I mixture for 2 hours at 37°C and then loaded into a 0.8% agarose gel.

Molecular Analysis. One μg of total RNA from tumor neural stem cells, U87, and human fetal neural stem cells, extracted using the RNeasy Mini kit (Qiagen, Chatsworth, CA), was primed with oligo(dT) for cDNA synthesis and reverse-transcribed by using Superscript RNase H$^-$ Reverse Transcriptase (Life Technologies, Rockville, MD). All cDNAs used as templates were previously normalized throughout a β-Actin reverse transcriptase-PCR. Sequence of primers and PCR conditions are available on request.

RESULTS

Selection and Expansion of Neural Precursors from Adult Human Brain Tumors. To assess for the presence of neural precursors within human brain tumors, cells from post-surgery specimens of low-grade gliomas, glioblastoma multiformes, or high-grade medulloblastomas were plated at clonal density (21) in serum-free medium, containing EGF and FGF2. This provides a stringent, low-density system ($<5 \times 10^3$ cells/cm^2), which selects away differentiated/differentiating cells in primary CNS cultures, leaving neural stem cells free to proliferate and expand exponentially (25, 26).

Twenty to 40 days after plating, phase-bright clones resembling the classical neurospheres formed *in vitro* by normal neural stem cells (ref. 27; Fig. 1*A* and *B*) were detected in all of the cultures established from high-grade glioblastoma multiformes and medulloblastomas. Clonal frequency was between 0.5 and 31% of the total cells plated for glioblastomas multiforme ($n = 12$) and 50 and 80% for medulloblastomas ($n = 4$). Conversely, clone formation was never observed in cultures from either World Health Organization grade I gliomas or World Health Organization grade II oligodendrogliomas ($n = 5$; up to 90 days *in vitro*). These data confirm and extend previous findings (15–17), which show that EGF/FGF2-responsive precursors are specifically found in glioblastomas multiforme and medulloblastomas.

Glioblastomas Multiforme Contain Multipotent Precursors Endowed with Long-term Self-renewal. The generation of clones from disaggregated primary cancers provides an index of the cancer clonogenicity (20). However, the sole formation of neurospheres in cultured CNS tumors does not provide, *per se*, the demonstration of
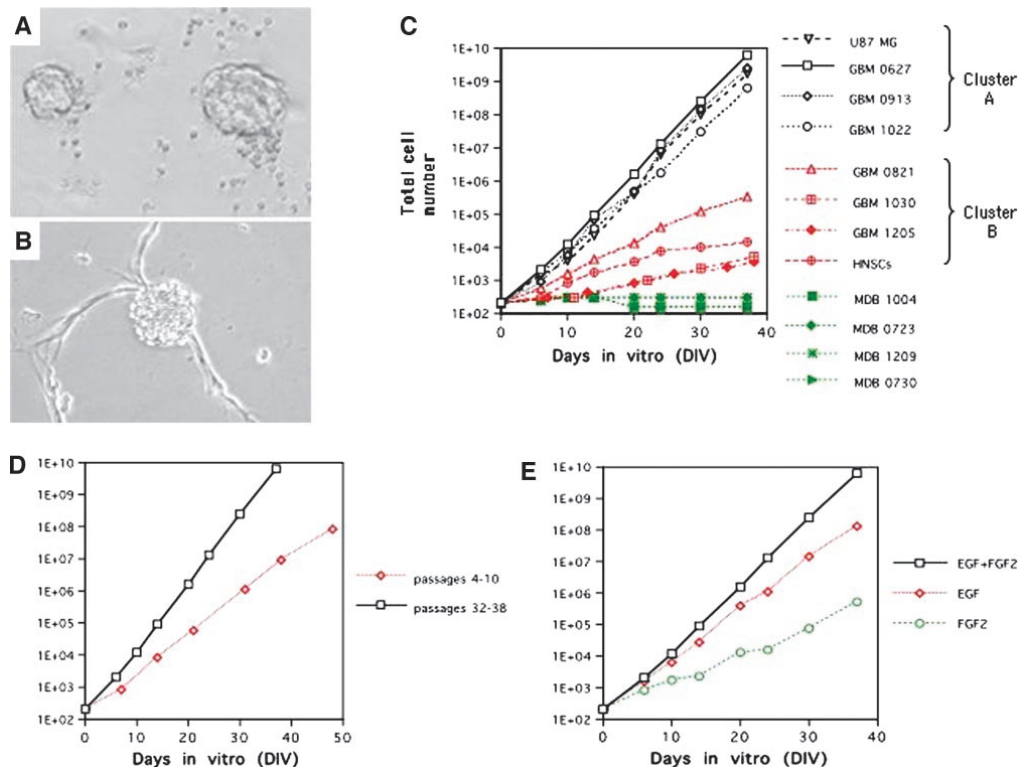

Fig. 1. Analysis of long-term proliferation in glioblastoma multiforme–derived tumor neural stem cells. Phase-bright microphotographs showing examples of glioblastoma multiforme–derived (*A*) and medulloblastoma-derived (*B*) neurospheres; ×20 objective. *C.* Intrinsic differences in the growth rate were observed among cluster A, consisting of faster-growing tumor neural stem cells such as 0627, 0913, and 1022 (*black lines*), and cluster B, comprising slower-expanding glioblastoma multiforme (*GBM*) cell lines 0821, 1030, and 1205 (*red lines*). Although medulloblastoma (*MDB*) tissues displayed the highest content of clonogenic cells (up to 80%), they never established tumor neural stem cell lines (*green lines*). *D.* Differently from normal human fetal neural stem cells (22), glioblastoma multiforme–derived tumor neural stem cells displayed different rates of amplification at low- and high-subculturing stages, as shown for cell line 0627. *E.* The exposure of cell line 0627 to EGF or FGF2 influenced the proliferation rate, which was higher in the presence of both mitogens and lower when using only one factor, as shown previously for normal human fetal neural stem cells (22).

7012

GLIOBLASTOMA-FOUNDING HUMAN NEURAL PRECURSORS

the presence of tumor neural stem cells therein. Transiently amplifying precursors are also known to produce neurospheres in this system, and they can even undergo a limited number of passages in culture (20, 28). In addition, neurosphere formation may also result from spontaneous cell aggregation, usually as the consequence of excessive plating density (29).

Hence, we determined whether the clonogenic cells in our primary glioblastoma multiforme and medulloblastoma cultures represented transient clonogens as generated by short-term proliferating, transit amplifying cells or possessed the cardinal properties expected from cultured tumor neural stem cells (20). To this end, we assessed their capacity for long-term proliferation, self-renewal, multipotency (the ability to generate the three major neural cell types, *i.e.*, neurons, astroglia, and oligodendroglia) and their tumorigenicity (27, 30–32), by combining cloning, subcloning, and population analysis followed by orthotopic, heterotopic, and serial transplantation assays.

One of the primary consequences of dealing with candidate stem cells endowed with extensive self-renewal capacity is the establishment of steadily expanding, stable lines (19, 28). Surprisingly, although medulloblastoma cultures displayed the highest clonogenic capacity, they failed in establishing long-term cell lines (four of four specimens) under the conditions normally used for neural stem cells expansion. In agreement with previous findings (16, 17), medulloblastoma cultures could be propagated for a few passages (Fig. 1*C*), although in our hands, they could only generate Tuj1-immunoreactive cells when triggered to differentiate (data not shown). Conversely, under identical culture conditions, one-half of the 12 cultures established from glioblastomas multiforme comprised multipotent precursors, which established long-term expanding cultures. These six different glioblastoma multiforme–derived lines were expanded for more than 80 passages, with an average doubling time of 3 to 4 days (*i.e.*, 180–280 days *in vitro*), and were characterized as tumor neural stem cells through the comparison with normal human fetal neural stem cells (22) and with the well-characterized human glioblastoma cell line U87MG.

Human glioblastoma multiforme cell lines were named after the date of surgery: 0627, 0821, 0913, 1022, 1030, and 1205. When their growth rate was assessed, significant differences between specific lines emerged (Fig. 1*C*). Nonetheless, despite the fact that the kinetics of expansion was characteristic for each tumor cell line and clearly depended upon the specimen of origin, all of the lines exponentially expanded in number, similarly to normal human fetal neural stem cells and U87 cells and as opposed to their medulloblastoma counterpart (Fig. 1*C*). Based on growth properties, two distinct clusters emerged: cluster A, comprising faster-growing lines 0627, 0913, and 1022; and cluster B, consisting of slower-expanding lines 0821, 1030, and 1205 (Fig. 1*C*). Of note, whereas normal human fetal neural stem cells displayed steady growth capacity over long-term culturing (22, 33), the proliferative activity of glioblastoma multiforme–derived cell lines increased at very late subculturing stages (120–150 days *in vitro*) compared with earlier passages (15–35 days *in vitro*; Fig. 1*D*, in reference to line 0627). This may reflect their progressive enrichment in cells endowed with aberrant proliferative advantage, the tumor cell adaptation to the culture conditions, or the intrinsic, genetic fluctuation expected from tumor cells. Nonetheless, this phenomenon was the only hint as to a possible, latent instability of glioblastoma multiforme–derived cell lines, which displayed an otherwise remarkably stable cellular and molecular phenotype and karyotype (see next sections).

Additional proof that tumor neural stem cells were the likely founders of glioblastoma multiforme–derived cell lines came from the observation that single glioblastoma multiforme cells could give rise to clonal cell lines, which behaved identically to their parental (*i.e.*,

bulk culture) cell lines (not shown). These clonal tumor neural stem cells were used in all of the experiments described from now on.

We continued by analyzing the response of our candidate tumor neural stem cells to mitogens that regulate proliferation in normal neural stem cells (22, 34, 35). As described for adult rodent neural stem cells (34), glioblastoma multiforme–derived cell lines expanded slowly in the presence of the sole FGF2, switched to a faster growth mode when exposed to EGF alone, and expanded even faster when exposed to both mitogens simultaneously (Fig. 1*E*, cell line 0627). Thus, glioblastoma multiforme cells respond to the same mitogenic cues that control the fate of normal neural stem cells.

We then assessed tumor neural stem cell multipotency by determining the ability of clonal glioblastoma multiforme–derived cells to generate neurons, astrocytes, and oligodendrocytes. Early passage (passages 10–15) clonally derived glioblastoma multiforme cells underwent terminal differentiation upon removal of mitogens (34, 36) and the subsequent addition of leukemia inhibitory factor to the medium, as shown previously for human fetal neural stem cells (24). Similar to normal neural stem cells (34), all of the glioblastoma multiforme clonal lines differentiated into GFAP-positive astrocyte-like cells (Fig. 2*B* and *F*) but also into neuron-like cells, which were immunoreactive for Tuj1 (Fig. 2*A* and *E*), MAP5 (Fig. 2*I*), MAP2 (Fig. 2*J*), neurofilament M_r 200,000 (NF200; Fig. 2*K*), glutamate (Fig. 2*L*), and γ-aminobutyric acid (Fig. 2*M*) and into GalC-immunoreactive oligodendrocyte-like cells (Fig. 2*D* and *H*). Conversely, U87 cells never gave rise to cells immunoreactive for any of the above pan-neural antigens, thus demonstrating that multipotency is a unique property of glioblastoma multiforme–derived cells. Such multipotency was maintained unaltered even after extensive culturing, up to passage 80 (not shown). Notably, glioblastoma multiforme–derived, differentiated cultures comprised a fraction of cells, which colabeled, promiscuously, with neuronal and glial markers (Fig. 2*C* and *G*). This abnormal type of cells was never observed in normal human fetal neural stem cells and likely reflects the activation of an aberrant differentiation program in tumor neural stem cells, as expected from developmentally deregulated tumor cells. Intriguingly, this same fraction of promiscuously double-labeled cells varied between each cell line and correlated with the proliferation capacity index, with cluster A glioblastoma multiforme cells (fast-growing), showing the highest content of abnormal end cells, and cluster B lines (slow-growing), displaying a smaller proportion and a behavior somewhat reminiscent of normal human fetal neural stem cells (Fig. 2, *table*).

Ultimately, the self-renewal capacity of glioblastoma multiforme cells was assessed directly, using subcloning experiments by which the number of stem cells in a given clonal neurosphere can be determined by assessing the number of secondary neurospheres generated after dissociation of the clone itself (23, 28, 34). This measure also provides both an estimate of the relative frequencies between symmetric proliferative divisions and symmetric differentiative divisions and an indirect index of the capacity of the stem cell population for size expansion (23, 28, 37). The generation of multiple secondary clones could be observed in all of the lines tested (line 0627, 68.0 ± 5.0; line 0913, 55.3 ± 4.0; line 1022, 85.0 ± 5.0; line 0821, 28.0 ± 8.0; line 1030, 26.1 ± 2.2; line 1205, 63.8 ± 4.0; human fetal neural stem cells, 37.9 ± 6.0; U87, 90.0 ± 5.0; means ± *SEM*, $n = 4$, Student's *t* test, * = $P < 0.001$). When the six different cell lines were compared with each other, a significantly lower frequency of proliferative symmetric divisions was detected in some of the slow-growing cell lines (0821 and 1030) compared with the other lines. This is indicative of an inherent difference in the self-renewal capacity between the different glioblastoma multiforme–derived tumor neural stem cell lines, which strictly correlates with their clonogenic ability and their growth profile.

7013

DOI:10.1158/0008-5472.CAN-04-1364
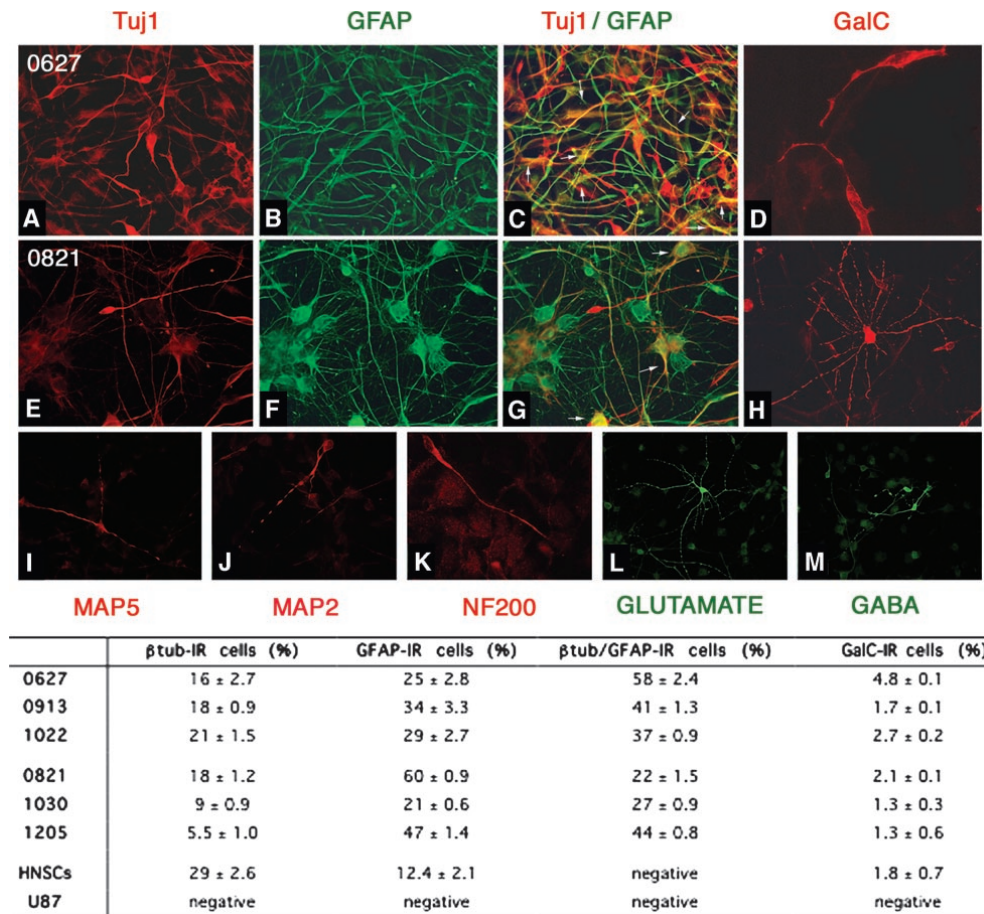
GLIOBLASTOMA-FOUNDING HUMAN NEURAL PRECURSORS

	βtub-IR cells (%)	GFAP-IR cells (%)	βtub/GFAP-IR cells (%)	GalC-IR cells (%)
0627	16 ± 2.7	25 ± 2.8	58 ± 2.4	4.8 ± 0.1
0913	18 ± 0.9	34 ± 3.3	41 ± 1.3	1.7 ± 0.1
1022	21 ± 1.5	29 ± 2.7	37 ± 0.9	2.7 ± 0.2
0821	18 ± 1.2	60 ± 0.9	22 ± 1.5	2.1 ± 0.1
1030	9 ± 0.9	21 ± 0.6	27 ± 0.9	1.3 ± 0.3
1205	5.5 ± 1.0	47 ± 1.4	44 ± 0.8	1.3 ± 0.6
HNSCs	29 ± 2.6	12.4 ± 2.1	negative	1.8 ± 0.7
U87	negative	negative	negative	negative

Fig. 2. Differentiation potential of fast- and slow-expanding tumor neural stem cells. Analysis of the multipotency of the fast-growing line 0627 (representative of cluster A, passage 13; A–D) and slow-growing line 0821, (representative of cluster B, passage 15; E–H) by immunofluorescence for neuronal (Tuj1; red in A, C, E, and G), glial (GFAP; green in B, C, F, and G) and oligodendroglial (GalC; red in D and H) markers. Additional markers of neuronal differentiation were also detected [line 0821, MAP5, MAP2, and NF200, red in I, J, and K; glutamate and γ-aminobutyric acid (GABA), green in L and M]. Cells that colabeled promiscuously with both neuronal and glial markers (arrows in C and G) could be observed in all of the cell lines established; magnification, ×20. The table shows a quantitative analysis of the differentiation capacity of the various glioblastoma multiforme–derived tumor neural stem cell lines, normal human fetal neural stem cells, and U87 cells with respect to their ability to generate cells of the three major neural lineages and to cells that display aberrant, promiscuous neuronal/astroglial colabeling.

These findings show that glioblastoma multiformes contain multipotent, long-term self-renewing, population-expanding cells that satisfy all of the defining criteria expected from tumor neural stem cells in vitro. Nonetheless, because the most critical attribute of tumor stem cells is their capacity to generate and perpetuate their tumor of origin (20), we sought to verify whether our glioblastoma multiforme–derived tumor neural stem cells could function as tumor-founding cells by assessing their actual ability to give rise to tumors in vivo.

The In vivo Tumorigenic Potential of Tumor Neural Stem Cells. When injected into immunosuppressed animals, both s.c. and intracranially (i.c.), all of the six tumor neural stem cell lines reproducibly established tumors, with a take efficiency of 50% s.c and 100% orthotopically, whereas normal human fetal neural stem cells always failed. When compared with classical U87-derived tumors, tumor neural stem cell–derived gliomas developed at a much slower rate. The first appearance of well-defined tumor masses could be observed after 1 week s.c. and 3 weeks i.c. in U87-treated animals, whereas it took at least 6 weeks s.c. and 7 weeks i.c. to observe the same extent of tumorigenesis in glioblastoma multiforme–derived, tumor neural stem cell–transplanted animals.

Histopathologic analysis of s.c. generated tumor neural stem cell–derived tumors demonstrated an unprecedented, striking glioblastoma-like tissue pattern. This was characterized by the presence of (1) several areas of necrosis surrounded by typical pseudo-palisade structures (Fig. 3A), (2) elevated vascular proliferation as demonstrated by laminin staining (Fig. 3B), (3) GFAP immunoreactivity (Fig. 3C), and (4) many mitotic figures, as measured by Ki67 (not shown), which were significantly higher than U87-derived tumors ($3.68 \pm 0.58\%$ for line 0627-derived tumor versus $1.38 \pm 0.13\%$ for U87-derived tumor; $n = 4$, $P < 0.01$, Student's t test). Notably, tumors derived from U87 implantation never displayed any glioblastoma-specific feature. Rather, they were characterized by the presence of cells with globoid

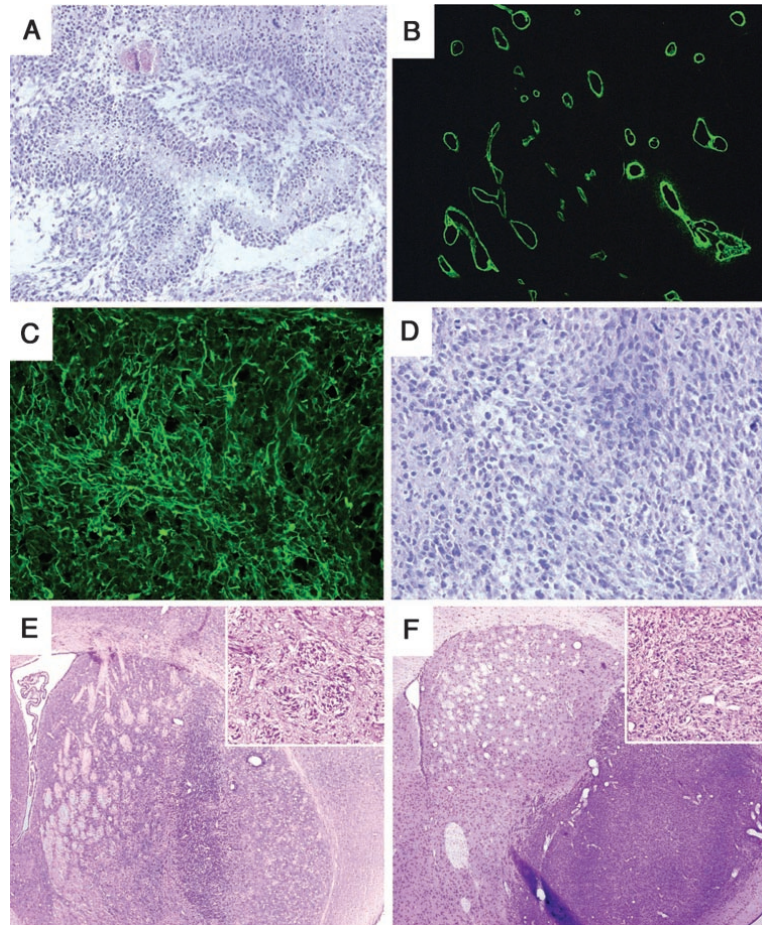7014

110

GLIOBLASTOMA-FOUNDING HUMAN NEURAL PRECURSORS

Fig. 3. Histopathologic features of tumor neural stem cell–derived s.c. and i.c. tumors. *A.* Large areas of necrosis surrounded by highly packed tumor cells ("pseudopalisade") were identified within the tumors generated by s.c. transplantation of tumor neural stem cells into *scid/bg* mice. Extensive neovascularization of the tumor tissue by laminin staining (*B*; ×10 objective) as well as widespread and intense GFAP immunoreactivity (*C*; ×20 objective) could be retrieved. *D.* U87-derived tumors did not display any of the peculiar histomorphologic features, typical of highly malignant gliomas. Tumor neural stem cell–generated i.c. tumors were characterized by a peculiar morphology (*E*; ×4 objective), and nest-like formations, reminiscent of mitotically active anomalous glial cells, could be identified in the core of the lesion (*inset* in *E*), as opposed to U87-derived tumors (*F*), which consisted of highly packed undifferentiated small rounded single mitotic elements (*inset* in *F*).

cytoplasm, which lacked fibrillary structures and hyperchromatic nuclei, the typical hallmarks of highly malignant gliomas (Fig. 3*D*).

Strikingly, when transplanted orthotopically, tumor neural stem cells were able to form i.c. tumors, which displayed an elevated extent of proliferation and an exacerbated migratory and infiltration capability, distinctive of human glioblastomas multiforme. As shown by hematoxylin and eosin staining, tumor neural stem cells generated highly anaplastic tumors, characterized by marked nuclear atypia and high mitotic index (hematoxylin and eosin in Fig. 3*E*). Conversely, unlike any typical glioblastoma, U87 cells gave rise to enormous but well-delimitated tumor masses, which developed strictly within the area of injection (hematoxylin and eosin in Fig. 3*F*). On the same line, the i.c. tumors derived from tumor neural stem cells displayed a very peculiar histomorphology. Six weeks after implantation, peculiar nest-like structures, composed of highly mitotic polymorphic cell nuclei, identified as aberrant glial elements, could be retrieved especially in the center of the lesion (Fig. 3*E*, *inset*). Due to the physical constraints imposed by the walls of the skull, the maximum level of growth reached by i.c. tumor neural stem cell–derived tumors did not allow the formation of clear areas of necrosis (pseudo-palisades), as opposed to s.c. tumors, which were allowed to grow up to 5 cm^3. In agreement

with findings on s.c. tumors, also orthotopic U87-derived lesions did not show any cyto-architectural similarity with the actual human disease (Fig. 3*F*, *inset*).

Most importantly, by staining with human-specific antimitochondria, tumor neural stem cell–derived tumor cells were shown to escape the site of transplantation, infiltrating both the adjacent parenchyma and the corpus callosum, even extending into the contralateral hemisphere, as bipolar migrating cells (Fig. 4*A*). Consistent with our *in vitro* findings and with the study of Hemmati *et al*. (17), when passage seventh medulloblastoma-derived cells were transplanted orthotopically, after 6 weeks from transplantation, no sign of tumor formation could be observed, and the transplanted cells did not migrate significantly from the graft (Fig. 4*B*). The same noninfiltrative behavior could be observed in U87-derived tumors (Fig. 4*C*).

Notably, when i.c. tumors generated by glioblastoma multiforme–derived tumor neural stem cells were characterized for the expression of specific antigens, they displayed an intense mitotic activity as shown by Ki67 staining (Fig. 4*D*, double-labeled cells in *yellow*), whereas the graft established by medulloblastoma cells contained fewer proliferating cells (Fig. 4*E*). Moreover, the tumors established by glioblastoma multiforme–derived tumor neural stem cells were

7015

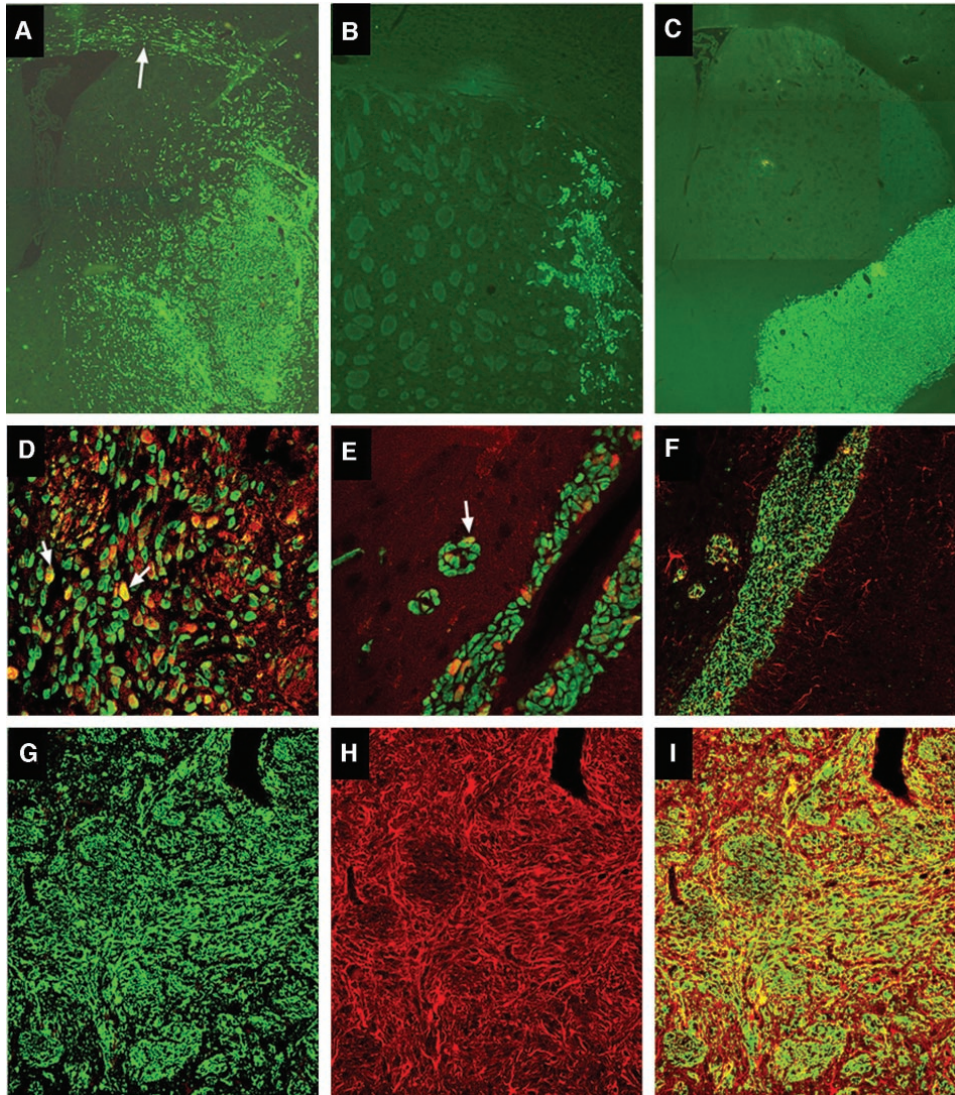GLIOBLASTOMA-FOUNDING HUMAN NEURAL PRECURSORS

Fig. 4. Tumor neural stem cells xenografted i.c. generate tumors, which reproduce the intraparenchymal invasion pattern, typical of human glioblastoma multiformes. Six weeks after orthotopic implantation, tumor neural stem cell–derived tumors (*A*; human-specific antimitochondria staining in *green*) were characterized by an expanding area of growth, located in the center of the tumor mass and by a surrounding "penumbra," from which highly migratory cells departed, infiltrating the adjacent parenchyma and white matter (*A*, *arrow*; ×4 objective). At the same time point, medulloblastoma–derived grafts (*B*; human-specific antinuclei staining in *green*; ×10 objective) exhibited very poor capacity for migration, spreading, and invasion, if any. Notably, U87-derived tumors (*C*; human-specific antimitochondria staining in *green*; ×4 objective) were quite large in size, but cells did not exhibit any migratory capacity, so that these tumors consisted of a progressively enlarging, well-defined cell mass, which remained confined to the site of injection. An elevated mitotic index was exhibited by i.c. tumor neural stem cell tumors (*D*; Ki67 in *red* and human nuclei in *green*; ×40 objective; *arrows* point to examples of double-labeled cells), whereas very few cells within the medulloblastoma-derived grafts were indeed proliferating (*E*; Ki67 in *red* and human nuclei in *green*; ×40 objective; *arrow* pointing to a double-labeled cell). In medulloblastoma grafts, we could never find cells that expressed astroglial markers [*F*; GFAP in *red* and human mitochondria in *green*; ×20 objective; note that GFAP immunoreactivity (*red*) is confined outside the graft mass (*green*)]. Conversely, some cells in glioblastoma multiforme–derived tumor neural stem cell–generated tumors were found to label with the anti-GFAP antibody (*G*, human mitochondria in *green*; *H*, anti-GFAP in *red*; merged confocal image in *I*; ×20 objective).

immunoreactive for the astroglial-specific marker GFAP (Fig. 4*G*–*I*) and vimentin (not shown) and negative for neuronal (Tuj1) and oligodendroglial antigens (GalC), just like typical human glioblastomas multiforme (not shown). Similar to grafted U87 cells, medullo-

blastoma implants did not display immunoreactivity for astroglial (Fig. 4*F*), neuronal, or oligodendroglial antigens (not shown).

Serial Transplantation of Tumor Neural Stem Cells. To conclusively demonstrate the stemness of glioblastoma multiforme–

7016

GLIOBLASTOMA-FOUNDING HUMAN NEURAL PRECURSORS

derived tumor neural stem cells, we performed sequential transplantation experiments. This was done in analogy with the classical hemopoietic serial repopulation paradigm used to identify true hemopoietic stem cells (38). Cultured tumor neural stem cells (primary tumor neural stem cells) were transplanted into the mouse CNS to establish a tumor from which secondary tumor neural stem cells were recultured and then transplanted into new recipients. The successful, sequential generation of brain tumors provided evidence that we had isolated *bona fide* tumor neural stem cells.

Tumor neural stem cells, isolated from post-surgery specimens, were expanded, cloned, and injected orthotopically, giving rise to brain tumors. At the first sign of neurologic impairment (8–10 weeks after transplantation), as produced by the expanding tumor mass (Fig. 5A and E), animals were sacrificed. The tumor was explanted by

careful dissection, which excluded the periventricular region of the forebrain, highly enriched for stem cells and progenitors (ref. 9; Fig. 5B–D), and the cells were cultured under the same conditions used to establish the original tumor neural stem cell cultures. Clonal neurospheres were readily detected in these secondary cultures, which exclusively contained cells that labeled positive with human-specific markers and that were named post-transplantation–tumor neural stem cells (Fig. 5F). Generation of primary spheres from tumor neural stem cell–induced tumors occurred much faster than parental, primary spheres, established from the original patient's specimen (3 days for post-transplantation–tumor neural stem cells compared with 20–40 days for primary, parental tumor neural stem cell lines). Cell lines established from the post-transplantation–tumor neural stem cells also expanded at a faster rate than their parental tumor neural stem cells
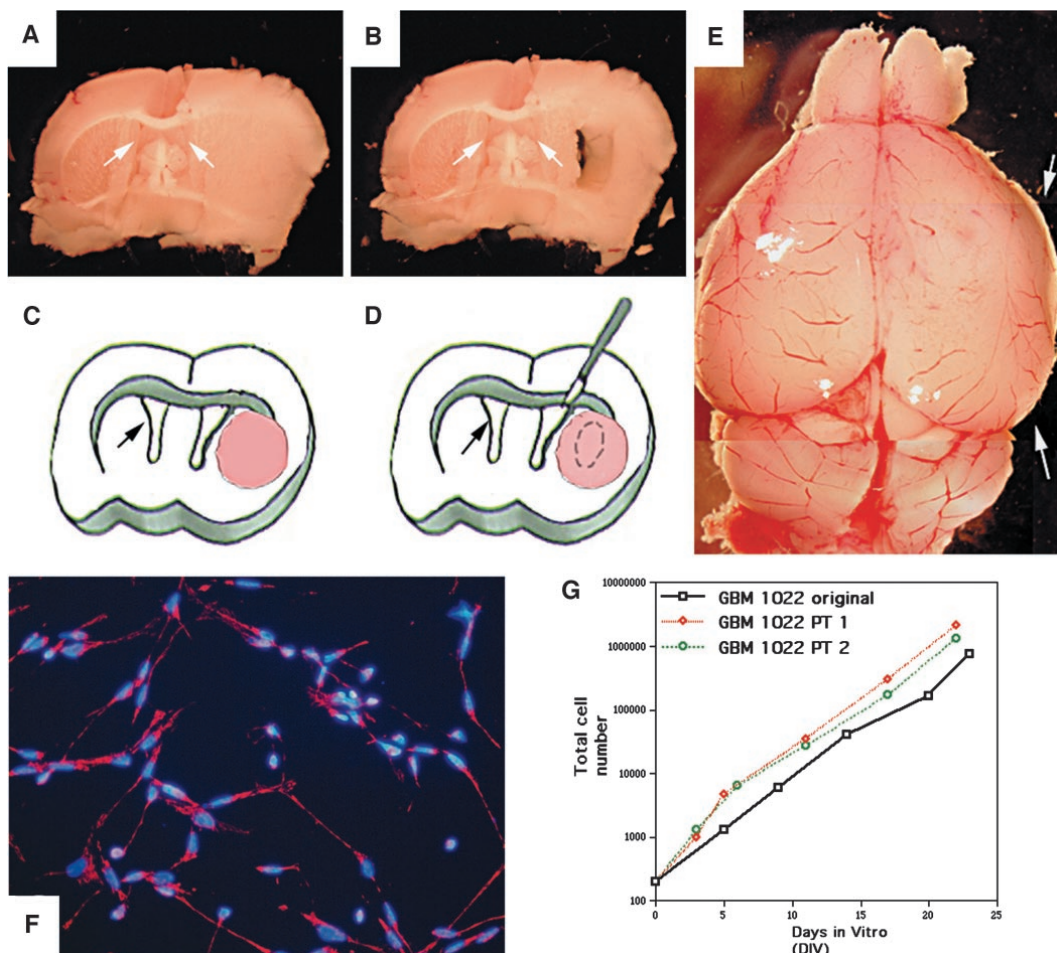

Fig. 5. Tumor neural stem cells self-renew *in vivo*, upon serial transplantation. The tumor mass established from the transplanted human tumor neural stem cells was dissected out at the first sign of neurologic impairment, taking particular care of not including the stem cell–enriched periventricular region (*arrows* in A–D). This procedure was facilitated by the large size of the in-growing tumor mass, which produced a macroscopic enlargement of the injected cerebral hemisphere (E, *arrows*). The tumor cells were then dissociated and placed in culture under conditions identical to those used to establish tumor neural stem cell lines from the original human specimen. This resulted in the establishment of secondary tumor neural stem cell (*PT-TNSCs*) lines, which contained exclusively cells of human origin, with no sign of rodent cell contamination (F; human-specific mitochondria staining in *red* and nuclear 4′,6-diamidino-2-phenylindole staining in *blue*; ×20 objective). G, Post-transplantation–tumor neural stem cells were able to long-term expand in culture, even faster than the original, parental tumor neural stem cell line. *GBM*, glioblastoma multiforme.

7017

GLIOBLASTOMA-FOUNDING HUMAN NEURAL PRECURSORS

(line glioblastoma multiforme 1022 as reference; Fig. 5G). This suggests that the malignancy of serially transplanted post-transplantation–tumor neural stem cells might have been exacerbated by the exposure to the *in vivo* environment or that particularly aggressive cells had been selected upon transplantation, tumor growth, and reculturing.

When post-transplantation–tumor neural stem cell lines were differentiated under the same conditions of their parental ones, all of the three cell types could be detected. Thus, post-transplantation–tumor neural stem cells retained multipotency after transplantation and reculturing ($20 \pm 2.1\%$ of Tuj1-IR cells; $52 \pm 5.4\%$ of GFAP-IR cells; $24 \pm 0.7\%$ of Tuj1/GFAP cells, $n = 10$, two different secondary glioblastoma multiforme 1022 cell lines analyzed). Furthermore, post-transplantation–tumor neural stem cells maintained the same karyotypic features (not shown) and molecular signature of their parental lines (see Fig. 6D, line 1022 and 1022PT), and when retransplanted orthotopically, they were still capable of giving rise to new glioblastoma multiforme–like tumors, with characteristics identical to those generated by primary tumor neural stem cells (not shown). In con-

clusion, tumor neural stem cells satisfy all of the critical criteria to be defined as multipotent tumor neural stem cell lines, both *in vitro* and *in vivo* (20).

Tumor Neural Stem Cells Display Tumor-Specific Properties. In addition to the exacerbated growth rate displayed by most of the glioblastoma multiforme–derived lines when compared with normal human fetal neural stem cells (Fig. 1C), tumor neural stem cells were also expected to bear tumor-specific features, such as highly unbalanced karyotypes and telomerase reactivation.

Karyotypic analysis was performed on all of the six lines, on U87 cells and on human fetal neural stem cells (Fig. 6A). Many different numerical and structural chromosomal aberrations could be detected in tumor neural stem cells and in U87 but not in human fetal neural stem cells, which revealed a normal complement of chromosomes and no genetic abnormalities. Intriguingly, aneuploidy of specific autosomes and sex chromosomes (monosomy 1, trisomy 7 and 22, and disomy X) was retrieved most frequently in the three tumor neural stem cell lines with the highest expansion potential (cluster A), suggesting that peculiar aberrations may confer a certain degree of

A

Cell line	Losses	Gains	Markers
010627	1, 2, 13 and 14	7, 20, 22 and XX	3
020913	1, 13 and 14	7, 19, 20, 22 and XX	5
021022	1, 2, 13 and 15	7, 19, 20, 22 and XX	3
020821	9, 15	3, 17, 18 and 20	3
021030	1, 4, 9, 10, 13, 14 and 22	21	7
021205	6, 10, 14, and 22	7	2
U87	1, 9,10, 11, 12, 14, 13, 16,19, 20,22 and X	negative	11
HFNSCs	negative	negative	0

B

C

D

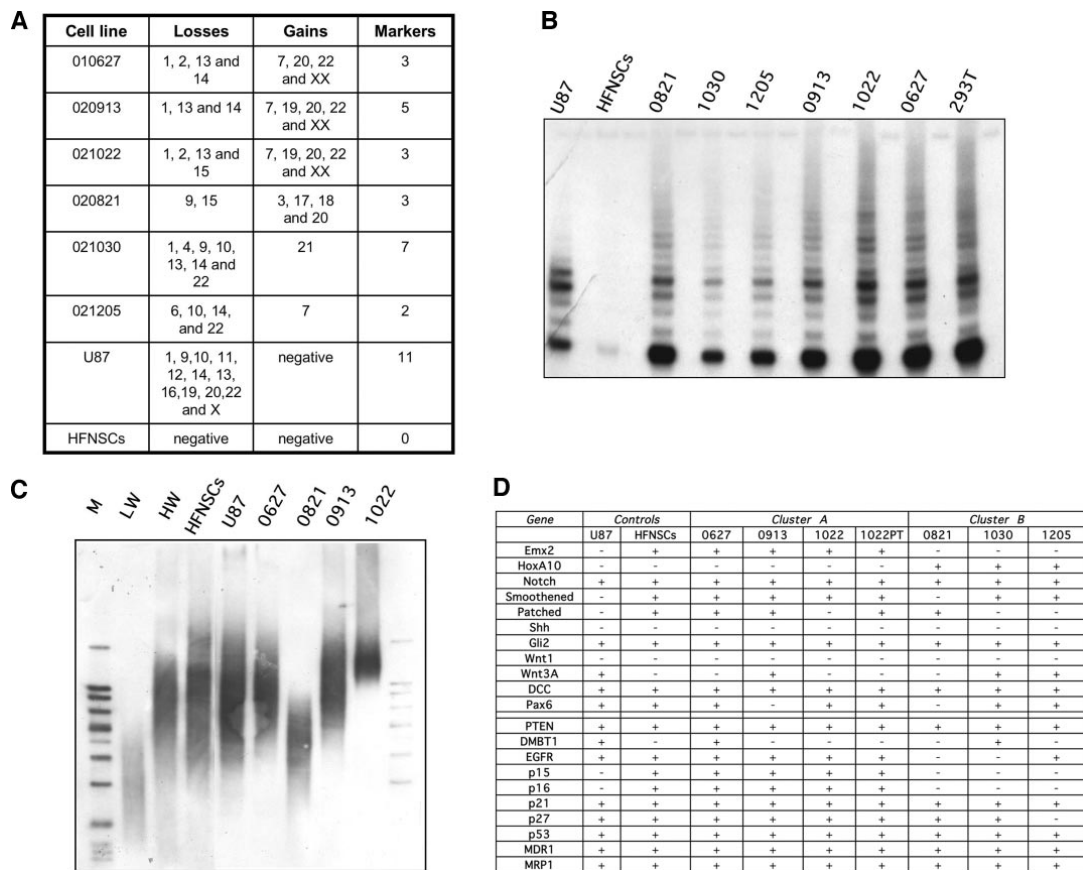| Gene	Controls		Cluster A				Cluster B		
	U87	HFNSCs	0627	0913	1022	1022PT	0821	1030	1205
Emx2	-	+	+	+	+	+	-	+	+
HoxA10	-	-	-	-	-	-	+	+	+
Notch	+	+	+	+	+	+	+	+	+
Smoothened	-	+	+	+	+	+	-	+	+
Patched	-	+	+	+	-	+	+	-	+
Shh	-	-	-	-	-	-	-	-	-
Gli2	+	+	+	+	+	+	+	+	+
Wnt1	-	-	-	-	-	-	-	-	-
Wnt3A	+	-	-	+	-	-	-	+	+
DCC	+	+	+	+	+	+	+	+	+
Pax6	+	+	+	-	+	+	-	+	+
PTEN	+	+	+	+	+	+	+	+	+
DMBT1	+	-	+	-	-	-	-	+	-
EGFR	+	+	+	+	+	+	-	-	+
p15	-	+	+	+	+	+	-	-	+
p16	-	+	+	+	+	+	-	-	-
p21	+	+	+	+	+	+	+	+	+
p27	+	+	+	+	+	+	+	+	-
p53	+	+	+	+	+	+	+	+	+
MDR1	+	+	+	+	+	+	+	+	+
MRP1	+	+	+	+	+	+	+	+	+

Fig. 6. Karyotypic imbalance, telomerase reactivation, and molecular fingerprint characterize all glioblastoma multiforme–derived tumor neural stem cells. A, summary of the chromosomal aberrations found in all of the different tumor neural stem cell lines. HFNSC, human fetal neural stem cell. B, the enzymatic activity of the RNA catalytic subunit of telomerase as assessed by telomeric repeat amplification protocol assay in the different cell lines, normal human neural stem cells, and U87 glioma cells; C, telomere length, as measured by Southern blotting in glioblastoma multiforme cell lines, normal human neural stem cells, and U87 glioma cells. M, marker; LW, low-weight standard; HW, high-weight standard. D, a preliminary gene expression profile on tumor neural stem cells and control cell lines by semiquantitative reverse transcription-PCR. Tumor neural stem cell lines are displayed as clustered into fast-growing (cluster A) or slow-growing (cluster B) cell lines.

7018

GLIOBLASTOMA-FOUNDING HUMAN NEURAL PRECURSORS

proliferation advantage to tumor neural stem cells. Conversely, slow-growing lines (cluster B) showed line-specific, chromosomal aberrations. Notably, long-term culturing did not affect the karyotypic signature of tumor neural stem cells, which remained constant even at high passages in culture (not shown).

Malignant transformation entails the acquisition of an immortal phenotype, which requires active telomere-maintenance mechanisms (39). We tested whether the catalytic subunit of the human ribonucleoprotein enzyme telomerase reverse transcriptase, which provides tumor cells with unlimited proliferation capacity by telomere lengthening, was at work in glioblastoma multiforme–derived cell lines. By means of the telomeric repeat amplification protocol assay, high human telomerase reverse transcriptase activity was retrieved in all of the glioblastoma multiforme–derived cell lines and in the corresponding original tumor specimens (not shown), whereas normal human fetal neural stem cells were telomerase negative (Fig. 6B), as shown previously (40). We also assessed telomere length and detected significant differences among the various tumor neural stem cell lines, with lines 0821 and 1030 displaying very short telomeres, even shorter than human fetal neural stem cells (Fig. 6C). Our observations suggest that tumor neural stem cells, isolated from glioblastoma multiforms, although displaying typical stem cell features, possess line-intrinsic, tumor-related functional properties.

Molecular Phenotyping of Tumor Neural Stem Cells. To assess whether the heterogeneity detected at the cellular and biochemical level in various tumor neural stem cells could also be retrieved at the molecular level (Fig. 6D), the gene expression profiles of the six different lines were analyzed by semiquantitative reverse transcription-PCR. The candidate genes for reverse transcription-PCR were selected and clustered taking into account their restricted pattern of expression in (1) normal neural progenitors; (2) brain tumors; (3) CNS development. Normal human fetal neural stem cells, the glioblastoma cell line U87MG, and human fetal whole brain tissue were used as specimens of reference for the above gene clusters 1, 2, and 3, respectively.

As expected, based on their cellular phenotype, the genetic profiles of the different tumor neural stem cells could readily be clustered based on the expression of specific gene sets. The fast-growing cell lines 0627, 0913, and 1022 were characterized by similar gene expression patterns, whereas each one of the slow-growing lines 0821, 1030, and 1205 displayed a unique molecular signature. Nonetheless, fast-growing lines (0627, 0913, and 1022) also showed cell-line–specific variations in their gene expression profile, confirming that despite the evidence for overlapping cellular and molecular characteristics, each tumor neural stem cell line was ultimately, inherently unique and phenotypically different from all of the others.

Intriguingly, the widest body of heterogeneity in terms of gene expression occurred at the level of developmentally regulated genes, which displayed line-specific, modulation patterns. For instance, the homeobox gene *Emx2*, a regulator of self-renewal in neural stem cells (23), also implicated in cortical development (41, 42), and its repressor *HOXA10* (43) were transcriptionally regulated in a reciprocal fashion, with lines 0627, 0913, and 1022 (cluster A) displaying high levels of Emx2 transcript and no detectable *HOXA10* mRNA and lines 0821, 1030, and 1205 (cluster B) showing the opposite trend. Similarly, genes such as *Patched* and *Pax6* demonstrated a scattered distribution across the different tumor neural stem cell lines, although not correlated to any clear functional clustering. Conversely, a higher degree of homogeneity between lines was retrieved when analyzing tumor-related genes such as *PTEN*, *p21*, *p27*, *p53*, and *MDR1*. In perspective, the line-specific molecular signature and the identification of genes that play a key role in a given type of tumor neural stem cell may be exploited to develop custom-fit therapies, by taking into account the unique genetic background of the specific tumor cells found in the glioblastoma multiforme of a specific patient.

DISCUSSION

This work reports on the isolation and identification of tumor neural stem cells from human adult glioblastoma multiforme, which possess the capacity to establish, sustain, and expand these tumors, even under the challenging settings posed by serial transplantation experiments. These data identify tumor neural stem cells as one of the cell lineages involved in establishing the malignant, aggressive profile of this lethal brain tumor.

Glioblastoma multiforme represents one of the most frequent brain cancers and either may develop from lower grade astrocytic tumors (secondary or progressive glioblastoma multiforme) or may arise very rapidly *de novo* (primary glioblastoma multiforme; ref. 44). In both cases, neither chemotherapy nor radiotherapy has been effective in managing these cancers (45). Glioblastomas multiforme display a rather heterogeneous cellular composition, as indicated by the term "multiforme," with some of the tumor cells bearing significant migratory capacity. This results in invasive spread, in the formation of multiple secondary foci, and in frequent, recurrent growth. Therefore, the identification of the cell type(s) involved in some or all of these phenomena is critical from both a scientific and therapeutic standpoint.

To date, three studies have indicated the presence of undifferentiated neural precursors within pediatric or adult human brain tumors. The initial study by Ignatova *et al.* (15) described the isolation of neurosphere-forming, bipotent (neuronal/astroglial) precursors from glioblastomas multiforme and was subsequently extended by Singh *et al.* (16), who also demonstrated that bipotent progenitors from CNS tumors (mostly medulloblastomas) displayed short-term self-renewal (three passages in culture). The latter work also proposed that oligodendrocytes might have been generated from tumor cells, but the use of a promiscuous marker such as platelet-derived growth factor receptor α, which simultaneously labels both oligodendrocytes and neurons in culture (46), precluded any conclusion in this direction. Similar findings were later reported by Hemmati *et al.* (17), who described the absence of oligodendrocytes and the lack of tumorigenic ability after intracerebral transplantation of tumor-derived cells.

Collectively, these studies show that cells endowed with some of the characteristics expected from stem cells can be found within brain tumors, thus raising some intriguing issues. First and foremost, can aberrant neural precursors be involved in the establishment, expansion, and recurrence of CNS cancers (*i.e.*, are they tumorigenic?) or, rather, do they emerge as the byproduct of the uncontrolled proliferation of the actual tumorigenic cells, which are developmentally deranged? Second, if these precursors are tumorigenic, do they possess all of the features to qualify as tumor neural stem cells (20)?

The data presented here provide answers to these questions. They describe the isolation and identification of human glioblastoma multiforme cells, which possess all of the defining features of somatic stem cells, including *ex vivo* multipotency (*i.e.,* the potential to simultaneously generate cells displaying antigenic reactivity for neuronal, astroglial, and oligodendroglial markers in culture; refs. 47–49) and the ability to establish and expand glioblastoma multiforme–like tumors. The latter contain exclusively cells expressing astroglial markers, as in typical human glioblastomas multiforme. Notably, these cells can perpetuate glioblastoma multiforme–like tumors even under the critical settings imposed by serial transplantation, thus satisfying the most rigorous criteria to be classified as tumor neural stem cells (20).

These findings were highly reproducible when analyzing tumor

7019

GLIOBLASTOMA-FOUNDING HUMAN NEURAL PRECURSORS

neural stem cells established from different specimens, regardless of significant functional, karyotypic, and molecular differences between the various tumor neural stem cells. This may account for the presence within different glioblastoma multiforme specimens of tumor neural stem cells with common general stem cell properties that, however, are also characterized by unique, specimen-related, specific functional and molecular attributes.

Our data seem to suggest that tumor neural stem cells are found mainly within glioblastomas multiforme, although such a conclusion should be taken with caution. In fact, although our findings are consistent with those from Hemmati *et al.* (17) and show that cells from medulloblastomas expand poorly *in vitro* and do not establish tumors upon intracerebral grafting, they should not be construed as evidence that tumor neural stem cells are not present in medulloblastomas. It is possible that medulloblastomas contain cells that elicit their full stem cell potential under different settings than those used to date. Thus, it is intriguing that Kondo *et al.* (50) have reported on the presence of tumorigenic stem-like cells in a rodent glioma cell line (C6) that require different growth factors than those used in previous studies to expand in culture.

The knowledge that cells with stem cell characteristics may be involved in glioblastoma multiforme tumorigenesis is of paramount importance for our understanding of how these tumors form and expand and may provide an indication as to the key cellular and molecular mechanism to be investigated and tackled for diagnostic and therapeutic purposes. Unfortunately, it remains unclear whether tumor neural stem cells in glioblastomas multiforme derive from the transformation of normal human neural stem cells or whether their presence therein reflects the result of the transformation and de-differentiation of a more mature brain cell, which brought about otherwise silent/latent stem cell properties (5). Nonetheless, the demonstration of the existence within glioblastomas multiforme of tumor neural stem cells with the capacity of establishing this type of tumor, together with previous reports showing the existence within similar cancers of bipotent, stem-like cells (15–17), lends to the hypothesis that a hierarchical model of cell genesis may be at work within malignant brain cancers.

To date, only a few glioblastoma multiforme cell lines have been established (51–53) and used for studies on basic glioma biology or to perfect therapy for glioblastoma multiforme (54–57). The tumor neural stem cells described here can be used to routinely establish adult human glioblastoma multiforme cell lines in a quick and reproducible fashion. Of note, these cells reproduce the overall behavior of glioblastomas multiforme closer than any other previously available cell line. For example, when transplanted into immunosuppressed mice, the most widely used human glioblastoma multiforme cell line, the U87MG, gave rise to tumors that did not mimic the typical glioblastoma multiforme characteristics. Conversely, upon orthotopic transplant, all of the glioblastoma multiforme–derived, tumor neural stem cell lines formed tumors bearing all of the primary traits of human glioblastomas multiforme. Most importantly, cells in tumor neural stem cell–founded tumors displayed, *in vivo*, the typical migratory capacity expected from glioblastoma multiforme malignant cells, which was not observed when using U87, and, most importantly, retained their distinctive, line-specific proliferation and differentiation attributes. Thus, the identification of tumor neural stem cells also makes available cell lines of glioblastoma multiforme–initiating cells, which may retain specimen-specific and, thus, patient-specific traits. This may open new avenues to identify novel tumor cell markers for therapeutic and diagnostic purposes and to develop patient-tailored pharmacologic approaches for the cure of glioblastomas multiforme, aiming to target what may very well be the most aggressive cell type found in glioblastomas multiforme, to date, which is the tumor neural stem cell.

ACKNOWLEDGMENTS

REFERENCES

1. Reya T, Morrison SJ, Clarke MF, Weissman IL. Stem cells, cancer, and cancer stem cells. Nature 2001;414:105–11.
2. Al-Hajj M, Wicha MS, Benito-Hernandez A, Morrison SJ, Clarke MF. Prospective identification of tumorigenic breast cancer cells. Proc Natl Acad Sci USA 2003;100: 3983–8.
3. Frank SA, Nowak MA. Cell biology: developmental predisposition to cancer. Nature 2003;422:494.
4. Bonnet D, Dick JE. Human acute myeloid leukemia is organized as a hierarchy that originates from a primitive hematopoietic cell. Nat Med 1997;3:730–7.
5. Passegue E, Ailles LE, Weissman IL. Normal and leukemic hematopoiesis: are leukemias a stem cell disorder or a reacquisition of stem cell characteristics? Proc Natl Acad Sci USA 2003;100:11842–9.
6. Hope KJ, Jin L, Dick JE. Acute myeloid leukemia originates from a hierarchy of leukemic stem cell classes that differ in self-renewal capacity. Nat Immunol 2004; 5:738–43.
7. Rubinstein LJ, Herman MM, VanderBerg SR. Differentiation and anaplasia in central neuroepithelial tumors. Prog Exp Tumor Res 1984;27:32–48.
8. Recht L, Jang T, Savarese T, Litofsky NS. Neural stem cells and neuro-oncology: quo vadis? J Cell Biochem 2003;88:11–9.
9. Alvarez-Buylla A, Seri B, Doetsch F. Identification of neural stem cells in the adult vertebrate brain. Brain Res Bull 2002;57:751–8.
10. Sanai N, Tramontin AD, Quinones-Hinojosa A, et al. Unique astrocyte ribbon in adult human brain contains neural stem cells but lacks chain migration. Nature 2004;427: 740–4.
11. Holland EC, Hively WP, Gallo V, Varmus HE. Modeling mutations in the G_1 arrest pathway in human gliomas: overexpression of CDK4 but not loss of INK4a-ARF induces hyperploidy in cultured mouse astrocytes. Genes Dev 1998;12:3644–9.
12. Bachoo RM, Maher EA, Ligon KL, et al. Epidermal growth factor receptor and Ink4a/Arf: convergent mechanisms governing terminal differentiation and transformation along the neural stem cell to astrocyte axis. Cancer Cell 2002;1:269–77.
13. Jensen NA, Pedersen KM, Lihme F, et al. Astroglial c-Myc overexpression predisposes mice to primary malignant gliomas. J Biol Chem 2003;278:8300–8.
14. Danks RA, Orian JM, Gonzales MF, et al. Transformation of astrocytes in transgenic mice expressing SV40 T antigen under the transcriptional control of the glial fibrillary acidic protein promoter. Cancer Res 1995;55:4302–10.
15. Ignatova TN, Kukekov VG, Laywell ED, Suslov ON, Vrionis FD, Steindler DA. Human cortical glial tumors contain neural stem-like cells expressing astroglial and neuronal markers in vitro. GLIA 2002;39:193–206.
16. Singh SK, Terasaki M, Bonn VE, Hawkins C, Squire J, Dirks PB. Identification of a cancer stem cell in human brain tumors. Cancer Res 2003;63:5821–8.
17. Hemmati HD, Nakano I, Lazareff JA, et al. Cancerous stem cells can arise from pediatric brain tumors. Proc Natl Acad Sci USA 2003;100:15178–83.
18. Oliver TG, Wechsler-Reya RJ. Getting at the root and stem of brain tumors. Neuron 2004;42:885–8.
19. Potten CS, Loeffler M. Stem cells: attributes, cycles, spirals, pitfalls and uncertainties. Lessons for and from the crypt. Development 1990;110:1001–20.
20. Kummermehr J. Tumour stem cells. In: Potten C, editor. Stem cells. London, UK: Academic Press; 1997. p. 363–99.
21. Gritti A, Parati EA, Cova L, et al. Multipotential stem cells from the adult mouse brain proliferate and self-renew in response to basic fibroblast growth factor. J Neurosci 1996;16:1091–100.
22. Vescovi AL, Parati EA, Gritti A, et al. Isolation and cloning of multipotential stem cells from the embryonic human CNS and establishment of transplantable human neural stem cell lines by epigenetic stimulation. Exp Neurol 1999;156:71–83.
23. Galli R, Fiocco R, De Filippis L, et al. Emx2 regulates the proliferation of stem cells of the adult mammalian central nervous system. Development 2002;129:1633–44.
24. Galli R, Pagano SF, Gritti A, Vescovi AL. Regulation of neuronal differentiation in human CNS stem cell progeny by leukemia inhibitory factor. Dev Neurosci 2000; 22:86–95.
25. Reynolds BA, Tetzlaff W, Weiss SA. A multipotent EGF-responsive striatal embryonic progenitor cell produces neurons and astrocytes. J Neurosci 1992;12:4565–74.
26. Wu P, Tarasenko YI, Gu Y, Huang LY, Coggeshall RE, Yu Y. Region-specific generation of cholinergic neurons from fetal human neural stem cells grafted in adult rat. Nat Neurosci 2002;5:1271–8.
27. Reynolds BA, Weiss S. Generation of neurons and astrocytes from isolated cells of the adult mammalian central nervous system. Science 1992;255:1707–10.
28. Loeffler M, Potten C. Stem cells and cellular pedigrees: a conceptual introduction. In: Potten C, editor. Stem cells. London, UK: Academic Press; 1997. p. 1–27.
29. Gritti A, Galli R, Vescovi AL. Cultures of stem cells of the CNS. In: S. Fedoroff, editor. Protocols for neural cell culture. Totowa, NJ: Humana Press; 2000.
30. Reynolds BA, Weiss S. Clonal and population analyses demonstrate that an EGF-responsive mammalian embryonic CNS precursor is a stem cell. Dev Biol 1996;175: 1–13.

7020

DOI:10.1158/0008-5472.CAN-04-1364

GLIOBLASTOMA-FOUNDING HUMAN NEURAL PRECURSORS

31. Caldwell MA, He X, Wilkie N, et al. Growth factors regulate the survival and fate of cells derived from human neurospheres. Nat Biotechnol 2001;19:475–9.

32. Wachs FP, Couillard-Despres S, Engelhardt M, et al. High efficacy of clonal growth and expansion of adult neural stem cells. Lab Invest 2003;83:949–62.

33. Carpenter MK, Cui X, Hu ZY, et al. In vitro expansion of a multipotent population of human neural progenitor cells. Exp Neurol 1999;158:265–78.

34. Gritti A, Frolichsthal-Schoeller P, Galli R, et al. Epidermal and fibroblast growth factors behave as mitogenic regulators for a single multipotent stem cell-like population from the subventricular region of the adult mouse forebrain. J Neurosci 1999;19:3287–97.

35. Svendsen CN, Caldwell MA, Ostenfeld T. Human neural stem cells: isolation, expansion and transplantation. Brain Pathol 1999;9:499–513.

36. Gritti A, Bonfanti L, Doetsch F, et al. Multipotent neural stem cells reside into the rostral extension and olfactory bulb of adult rodents. J Neurosci 2002;22:437–45.

37. Morrison SJ, White PM, Zock C, Anderson DJ. Prospective identification, isolation by flow cytometry, and in vivo self-renewal of multipotent mammalian neural crest stem cells. Cell 1999;96:737–49.

38. Bock TA, Ziegler BL, Buhring HJ, Scheding S, Brugger W, Kanz L. Characterization of purified and ex vivo manipulated human hematopoietic progenitor and stem cells in xenograft recipients. Ann N Y Acad Sci 1999;872:200–7; discussion 207–10.

39. Masutomi K, Hahn WC. Telomerase and tumorigenesis. Cancer Lett 2003;194: 163–72.

40. Ostenfeld T, Caldwell MA, Prowse KR, Linskens MH, Jauniaux E, Svendsen CN. Human neural precursor cells express low levels of telomerase in vitro and show diminishing cell proliferation with extensive axonal outgrowth following transplantation. Exp Neurol 2000;164:215–26.

41. Simeone A, Acampora D, Gulisano M, Stornaiuolo A, Boncinelli E. Nested expression domains of four homeobox genes in developing rostral brain. Nature 1992;358: 687–90.

42. Pellegrini M, Mansouri A, Simeone A, Boncinelli E, Gruss P. Dentate gyrus formation requires Emx2. Development 1996;122:3893–8.

43. Troy PJ, Daftary GS, Bagot CN, Taylor HS. Transcriptional repression of peri-implantation EMX2 expression in mammalian reproduction by HOXA10. Mol Cell Biol 2003;23:1–13.

44. Wechsler-Reya R, Scott MP. The developmental biology of brain tumors. Annu Rev Neurosci 2001;24:385–428.

45. Behin A, Hoang-Xuan K, Carpentier AF, Delattre JY. Primary brain tumours in adults. Lancet 2003;361:323–31.

46. Andrae J, Hansson I, Afink GB, Nister M. Platelet-derived growth factor receptor-α in ventricular zone cells and in developing neurons. Mol Cell Neurosci 2001;17: 1001–13.

47. Kondo T, Raff M. Oligodendrocyte precursor cells reprogrammed to become multi-potential CNS stem cells. Science 2000;289:1754–7.

48. Goldman S. Glia as neural progenitor cells. Trends Neurosci 2003;26:590–6.

49. Belachew S, Chittajallu R, Aguirre AA, et al. Postnatal NG2 proteoglycan-expressing progenitor cells are intrinsically multipotent and generate functional neurons. J Cell Biol 2003;161:169–86.

50. Kondo T, Setoguchi T, Taga T. Persistence of a small subpopulation of cancer stem-like cells in the C6 glioma cell line. Proc Natl Acad Sci USA 2004;101:781–6.

51. Fogh J, Fogh JM, Orfeo T. One hundred and twenty-seven cultured human tumor cell lines producing tumors in nude mice. J Natl Cancer Inst (Bethesda) 1977;59:221–6.

52. Bakir A, Gezen F, Yildiz O, et al. Establishment and characterization of a human glioblastoma multiforme cell line. Cancer Genet Cytogenet 1998;103:46–51.

53. Di Tomaso E, Pang JC, Lam HK, et al. Establishment and characterization of a human cell line from paediatric cerebellar glioblastoma multiforme. Neuropathol Appl Neurobiol 2000;26:22–30.

54. Benedetti S, Pirola B, Pollo B, et al. Gene therapy of experimental brain tumors using neural progenitor cells. Nat Med 2000;6:447–50.

55. Ehtesham M, Kabos P, Gutierrez MA, et al. Induction of glioblastoma apoptosis using neural stem cell-mediated delivery of tumor necrosis factor-related apoptosis-inducing ligand. Cancer Res 2002;62:7170–4.

56. Ehtesham M, Kabos P, Kabosova A, Neuman T, Black KL, Yu JS. The use of interleukin 12-secreting neural stem cells for the treatment of intracranial glioma. Cancer Res 2002;62:5657–63.

57. Ehtesham M, Samoto K, Kabos P, Acosta FL, Gutierrez MA, Black KL, Yu JS. Treatment of intracranial glioma with in situ interferon-γ and tumor necrosis factor-α gene transfer. Cancer Gene Ther 2002;9:925–934.

7021

letters to nature

analysis of spatial patterns in current species distributions could be a powerful approach for estimating levels of threat for the many regions and taxa with limited information on past distributions and landscape change, or with limited ecological information on species' habitat or climate associations. ☐

Methods

Distributions

British distribution sizes and fractal dimensions were calculated with the use of all records for each species in England, Wales and Scotland from 1970–82 (ref. 15) and 1995–99 (ref. 16). Occupied 10-km and 100-km squares were calculated with standard Ordnance Survey grid squares. Distribution maps were based on 65,826 species lists (that is, field visits) for 1970–82 (124,978 species × location distribution records), and 437,690 species lists for 1995–99 (1,548,935 records). Changes in distribution size were calculated by randomly resampling the 1995–99 species lists for each 100-km square to equalize recorder effort between the two periods[17]. Proportional change in distribution size was the number of 10-km squares occupied in 1970–82 subtracted from the number of squares occupied in the resampled 1995–99 data, divided by the number of squares occupied in 1970–82.

The analysis includes all resident butterfly species that have regularly been observed in Britain since 1970, apart from those species for which more than 40% of occupied grid squares in either period were migrants, vagrants or deliberate introductions[16]. Fifty-one species were included, none of which occupied 10% or more of their 100-km squares through migrants or introductions[16] (Supplementary Methods).

Area of occupancy and fractal dimension

Area of occupancy (in km^2) of each British species in each period was calculated at two scales, first by summing the areas of occupied 10-km squares, and second those of occupied 100-km squares. Log_{10}AOO at each scale was plotted against log_{10}(side of grid square (in km)), and the fractal dimension (D_{ij}) was the slope of this scale–area curve, subtracted from 2 (ref. 18). The fractal is used in these analyses as a descriptive measurement of spatial aggregation over a narrow range of scales: we do not imply that these species have 'truly' fractal distributions over multiple scales.

Estimating change

To estimate distribution change independently for each British species, 51 linear regressions of distribution change against D_{ij} and AOO (calculated at 10-km scale) were performed, leaving out each species in turn. Coefficients from the analysis with the remaining 50 species were used to estimate change with the use of D_{ij} and AOO for each omitted species. We tested the predictions by using a linear regression of observed change against estimated change for all 51 species (Fig. 2a, b).

Phylogenetic regression

The main results presented refer to linear regressions with species as independent data points, on the assumption that information on phylogenetic relatedness was not available (as might be typical for poorly recorded taxa). We tested the sensitivity of the results to phylogenetic relatedness with GLS regressions[29] implemented in the software package COMPARE[30] (Supplementary Methods). These analyses suggested that the evolutionary constraint acting on distribution pattern, size and change was small, and gave results consistent with those using species as independent data points. For analyses in which the proportion of variation explained is most important, R^2 from the phylogenetic GLS regression is presented alongside the raw results in the main text. Results from all other phylogenetic regressions are presented in Supplementary Information.

Flanders butterflies and British plants

Details of analyses are presented in Supplementary Methods.

1. Akçakaya, H. R. et al. Making consistent IUCN classifications under uncertainty. Conserv. Biol. 14, 1001–1013 (2000).
2. Groombridge, B. & Jenkins, M. D. World Atlas of Biodiversity (Univ. California Press, Berkeley, CA, 2002).
3. Keith, D. A., Auld, T. D., Ooi, M. K. J. & Mackenzie, D. E. Sensitivity analyses of decision rules in World Conservation Union (IUCN) Red List criteria using Australian plants. Biol. Conserv. 94, 311–319 (2000).
4. Mace, G. M. & Lande, R. Assessing extinction threats: towards a re-evaluation of IUCN threatened species categories. Conserv. Biol. 5, 148–157 (1991).
5. World Conservation Monitoring Centre. Global Biodiversity: Status of the Earth's Living Resources (Chapman & Hall, London, 1992).
6. Hartley, S. & Kunin, W. E. Scale dependency of rarity, extinction risk, and conservation priority. Conserv. Biol. 17, 1559–1570 (2003).
7. Warren, M. S., Barnett, L. K., Gibbons, D. W. & Avery, M. I. Assessing national conservation priorities: an improved red list for British butterflies. Biol. Conserv. 82, 317–328 (1997).
8. World Conservation Union (IUCN). IUCN Red List Categories. Version 3.1. (World Conservation Union, Gland, Switzerland, 2001).
9. Cowley, M. J. R., Thomas, C. D., Thomas, J. A. & Warren, M. S. Flight areas of British butterflies: assessing species status and decline. Proc. R. Soc. Lond. B 266, 1587–1592 (1999).
10. Johnson, C. N. Species extinction and the relationships between distribution and abundance. Nature 394, 272–274 (1998).
11. Brown, J. H., Mehlman, D. W. & Stevens, G. C. Spatial variation in abundance. Ecology 76, 2028–2043 (1995).
12. Rodríguez, A. & Delibes, M. Internal structure and patterns of contraction in the geographic range of the Iberian Lynx. Ecography 25, 314–328 (2002).
13. Channell, R. & Lomolino, M. V. Dynamic biogeography and conservation of endangered species. Nature 403, 84–86 (2000).
14. Shigesada, N. & Kawasaki, K. Biological Invasions: Theory and Practice (Oxford Univ. Press, Oxford, UK, 1997).
15. Heath, J., Pollard, E. & Thomas, J. A. Atlas of Butterflies in Britain and Ireland (Viking Books, Harmondsworth, UK, 1984).
16. Asher, J. et al. The Millennium Atlas of Butterflies in Britain and Ireland (Oxford Univ. Press, Oxford, UK, 2001).
17. Warren, M. S. et al. Rapid responses of British butterflies to opposing forces of climate and habitat change. Nature 414, 65–69 (2001).
18. Kunin, W. E. Extrapolating species abundance across spatial scales. Science 281, 1513–1515 (1998).
19. Ostling, A., Harte, J. & Green, J. L. Self-similarity and clustering in the spatial distribution of species. Science 290 (Suppl.), 671a (2000).
20. Condit, R. et al. Spatial patterns in the distribution of tropical tree species. Science 288, 1414–1418 (2000).
21. Ripley, B. D. Spatial Statistics (John Wiley & Sons, New York, 1981).
22. Brooks, T. M., Pimm, S. L. & Oyugi, J. O. Time lag between deforestation and bird extinction in tropical forest fragments. Conserv. Biol. 13, 1140–1150 (1999).
23. Hill, J. K., Thomas, C. D. & Huntley, B. Climate and habitat availability determine 20th century changes in a butterfly's range margins. Proc. R. Soc. Lond. B 266, 1197–1206 (1999).
24. Hanski, I. Metapopulation Ecology (Oxford Univ. Press, Oxford, 1999).
25. Maes, D. & Van Dyck, H. Butterfly diversity loss in Flanders (north Belgium): Europe's worst case scenario? Biol. Conserv. 99, 263–276 (2001).
26. Thomas, C. D. & Abery, J. C. G. Estimating rates of butterfly decline from distribution maps: the effect of scale. Biol. Conserv. 73, 59–65 (1995).
27. Caughley, G. Directions in conservation biology. J. Anim. Ecol. 63, 215–244 (1994).
28. Linder, E. T., Villard, M.-A., Maurer, B. A. & Schmidt, E. V. Geographic range structure in North American landbirds: variation with migratory strategy, trophic level, and breeding habitat. Ecography 23, 678–686 (2000).
29. Martins, E. P. & Hansen, T. F. Phylogenies and the comparative method: a general approach to incorporating phylogenetic information into the analysis of interspecific data. Am. Nat. 149, 646–667 (1997).
30. Martins, E. P. COMPARE, version 4.6. Computer programs for the statistical analysis of comparative data http://compare.bio.indiana.edu/ (Department of Biology, Indiana University, Bloomington IN, 2004).

....

Identification of human brain tumour initiating cells

Sheila K. Singh[1,2,3], Cynthia Hawkins[1,4], Ian D. Clarke[1,2], Jeremy A. Squire[6], Jane Bayani[6], Takuichiro Hide[1,2], R. Mark Henkelman[5], Michael D. Cusimano[3,7] & Peter B. Dirks[1,2,3]

[1]The Arthur and Sonia Labatt Brain Tumor Research Centre, [2]Program in Developmental Biology, [3]Division of Neurosurgery, [4]Department of Pediatric Laboratory Medicine, and [5]Integrative Biology Program, The Hospital for Sick Children and University of Toronto, 555 University Avenue, Toronto, M5G 1X8, Canada
[6]Ontario Cancer Institute and University of Toronto, 610 University Avenue, Toronto, M5G 2M9, Canada
[7]Division of Neurosurgery, St Michael's Hospital and University of Toronto, 30 Bond Street, Toronto M5B 1W8, Canada

The cancer stem cell (CSC) hypothesis suggests that neoplastic clones are maintained exclusively by a rare fraction of cells with stem cell properties[1,2]. Although the existence of CSCs in human leukaemia is established[3,4], little evidence exists for CSCs in solid tumours, except for breast cancer[5]. Recently, we prospectively isolated a CD133^{+} cell subpopulation from human brain tumours that exhibited stem cell properties in vitro[6]. However,

letters to nature

the true measures of CSCs are their capacity for self renewal and exact recapitulation of the original tumour[1,2,7]. **Here we report the development of a xenograft assay that identified human brain tumour initiating cells that initiate tumours *in vivo*. Only the CD133+ brain tumour fraction contains cells that are capable of tumour initiation in NOD-SCID (non-obese diabetic, severe combined immunodeficient) mouse brains. Injection of as few as 100 CD133+ cells produced a tumour that could be serially transplanted and was a phenocopy of the patient's original tumour, whereas injection of 10^5 CD133− cells engrafted but did not cause a tumour. Thus, the identification of brain tumour initiating cells provides insights into human brain tumour pathogenesis, giving strong support for the CSC hypothesis as the basis for many solid tumours[5], and establishes a previously unidentified cellular target for more effective cancer therapies.**

Several studies have identified stem-like cells in brain tumour cultures[8–10]. By cell sorting for the cell surface antigen CD133 (refs 11–13), we demonstrated that a functional hierarchy exists in the brain tumour cell population *in vitro*[6]. To determine whether the CD133+ human brain tumour cells were capable of tumour initiation *in vivo*, we compared the abilities of CD133+ versus CD133− tumour cells to initiate tumour formation in NOD-SCID mouse brains. Immediately after surgical resection, solid, non-metastatic, brain tumour masses (medulloblastomas from three children, glioblastomas from three adults and one childhood glioblastoma; see Supplementary Table 1) were dissociated into single-cell suspensions. *In vitro* primary sphere formation assays were performed for all uncultured tumours and flow cytometric quantification of CD133 expression was performed on seven acutely dissociated tumours and two corresponding tumour xenografts before serial retransplantation. The CD133+ fraction among highly aggressive glioblastomas (GBMs) ranged from 19 to 29%, and among medulloblastomas ranged from 6 to 21%, and correlated closely with an *in vitro* primary sphere formation assay (which we used to quantify stem cell frequency; see Supplementary Table 2). After dissociation, magnetic bead cell sorting was used to separate the CD133+ brain tumour cells from their CD133− counterparts. Sorted cells were transplanted into the frontal lobe of six-week-old NOD-SCID mice.

Most intracranial xenograft models using human tumour cell lines or primary cultures require 10^5 to 10^6 cells for tumour engraftment and formation[14,15]. Analysis of mouse brains following CD133+ engraftment revealed that as few as 100 CD133+ cells were sufficient for the formation of human brain tumours in NOD-SCID mice that were analysed at 12–24 weeks post-injection (Fig. 1a–c) (see Supplementary Table 3). Injection of 50,000 to 100,000 of CD133− cells did not form tumours in the NOD-SCID brains, and histological examination at 12 weeks revealed only a glial scar tract from initial injection (Fig. 1d). A total of 15 CD133− injections and 19 CD133+ injections were performed. Of the 19 mice injected with CD133+ medulloblastoma or glioblastoma cells, 16 developed brain tumours (see Supplementary Table 3).

CD133+ xenografts from two classic medulloblastomas showed small round blue cell morphology and demonstrated characteristic histologic structures (Homer–Wright rosettes)[16] (Fig. 2). CD133+ xenografts from a third desmoplastic medulloblastoma recapitulated the more primitive cytoarchitecture associated with this subtype (Supplementary Fig. 1).

To further characterize the tumour phenotype of the CD133+ medulloblastoma xenografts, we performed detailed immunohistochemical analyses of each transplanted tumour and of the original patients' tumours that were used for initial histologic diagnosis (see Supplementary Table 3). The CD133+ xenografts from all three medulloblastomas expressed the cytoplasmic primitive intermediate filaments nestin[17] (Fig. 2) and vimentin (data not shown), frequently used as neural precursor cell markers, although they are not definitive neural stem cell markers. All three medulloblastoma

xenografts expressed the neuronal marker βIII-tubulin in a significant number of tumour cells, as did the original tumours from the patients (Fig. 2). Expression of the astrocyte marker GFAP (glial fibrillary acidic protein) was also seen in a minority of the human tumour cells in two of three medulloblastoma xenografts (Fig. 2). The GFAP-positive cells are morphologically neoplastic cells and did not demonstrate hybridization with mouse centromeric probes by interphase fluorescence *in situ* hybridization (FISH, data not shown) supporting that they were derived from the human cell transplant and were not trapped normal mouse astrocytes. Proliferative indices, indicated by MIB-1 (Ki67) immunostaining, were comparable in the xenografts and the original tumours (Fig. 2).

CD133+ xenografts from the adult and childhood GBMs demonstrated classical histopathological features of this tumour type. Both the classical GBM and the diffusely infiltrative GBM (Fig. 3 and Supplementary Fig. 1) possessed the four diagnostic criteria as defined by the World Health Organization[18]. In each case, the phenotype of the mouse xenograft matched that of the patient's original tumour.

CD133+ GBM xenograft phenotype was further studied by immunohistochemistry (Fig. 3). GBM xenografts also expressed nestin, showing a heterogeneous staining pattern that was consistent with the patients' original tumours. MIB-1 immunostaining showed a high degree of proliferation in both xenografts and the original tumours. CD133+ GBM xenografts also demonstrated characteristic expression of GFAP resembling the original patients' tumours, but also showed immunostaining for the neuronal marker MAP2 (microtubule associated protein) in the human tumour cells, which did not label with mouse-specific centromeric probes by FISH (data not shown). This finding of the expression of markers for both neuronal and astrocyte lineages within the CD133+ xenograft reflects an ability of the brain tumour initiating cells (BTIC) for multilineage, albeit cancerous, differentiation *in vivo*. In addition, immunostaining for p53 also revealed a similar increase in nuclear staining pattern for this tumour suppressor protein in the patient tumour and xenograft.
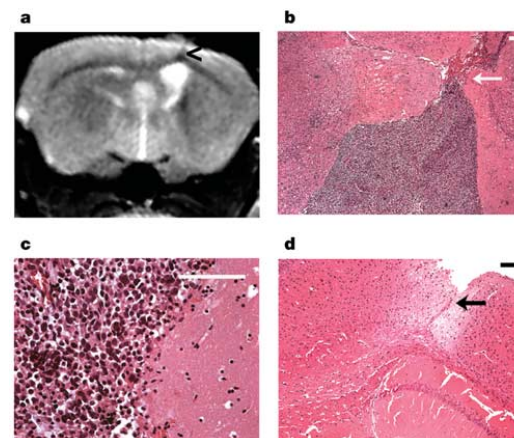

Figure 1 CD133+ tumour cells initiate tumours upon intracranial transplantation into the adult NOD-SCID mouse forebrain. **a**, Magnetic resonance imaging (MRI) scan of a mouse injected with 1,000 CD133+ medulloblastoma cells shows an enhancing mass under the injection tract (arrowheads) 14 weeks post-injection. **b**, **c**, Low (**b**) and high (**c**) magnification histological sections of the xenograft show a highly cellular mass below the injection site (white arrow in **b**). **d**, Histological section of mouse brain injected with CD133− medulloblastoma cells shows the injection tract (black arrow), but no tumour formation. Scale bar on all panels represents 100 microns.

letters to nature

CD133 immunostaining of the GBM xenografts revealed islands of positive cells, or single positive cells, amid large groups of negative cells; this indicates that not every cell in the xenograft is CD133^{+} (Fig. 4a). Double immunostaining for CD133 and GFAP in CD133^{+} xenografts from GBM samples demonstrated that these markers were expressed in different tumour cell subpopulations, suggesting that undifferentiated and differentiated tumour cells coexist within the transplanted tumours (Fig. 4b). A purified but small number of transplanted CD133^{+} cells (Fig. 4c) resulted in a heterogeneous primary xenograft consisting of a minority of CD133^{+} cells (19–22%) and a majority of CD133^{−} cells (78–81%) (Fig. 4d). These results suggest that a tumour hierarchy exists in which the CD133^{+} cells may generate CD133^{−} tumour cells. These data are consistent with our previous observations, which demonstrate that only the CD133^{+} fraction is proliferating and
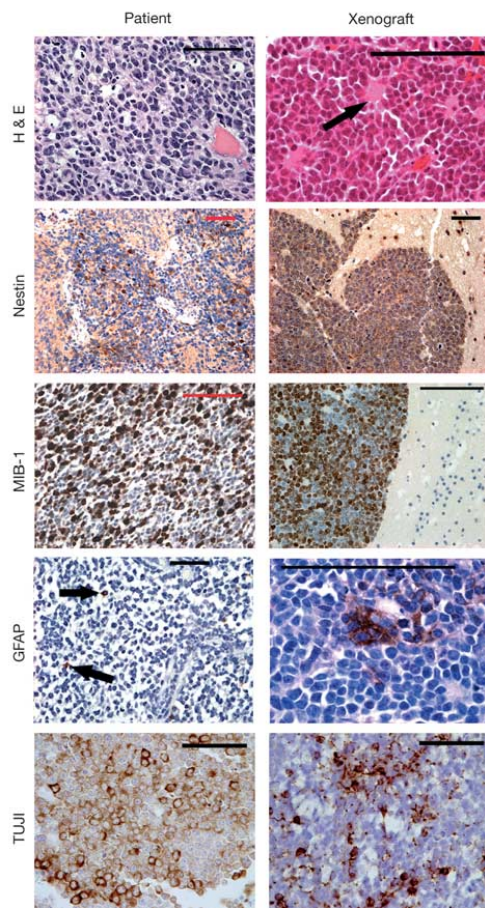
Figure 2 CD133^{+} xenograft from a medulloblastoma (right side) resembles the original patient tumour (left side). H&E of a CD133^{+} xenograft from patient 3 shows classical medulloblastoma cytoarchitecture, resembling the original patient's histology; a Homer–Wright rosette is indicated (arrow). The xenograft and the original tumour both express the neural precursor cell marker nestin (brown) and the neuronal marker βIII-tubulin (TUJI), and show a high proliferative index (MIB-1, brown nuclear staining), which is further increased in the xenograft. The astrocyte cell marker GFAP is also expressed in a small number of cells in the patient tumour and xenograft (brown, see arrows). Scale bar, 100 microns.
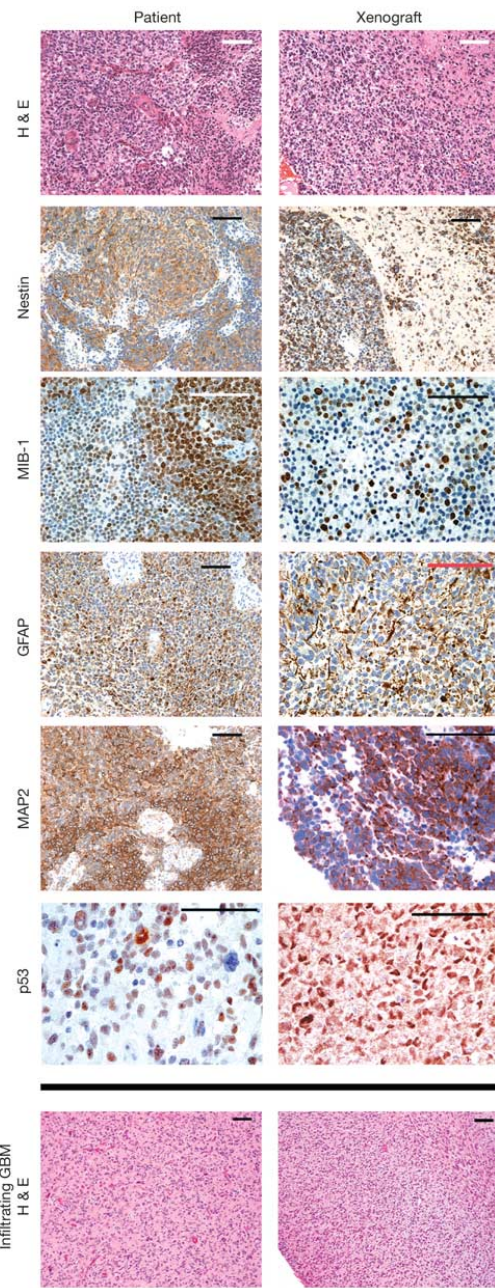
Figure 3 CD133^{+} xenograft from a GBM (right) resembles the original patient tumour (left). H&E section of a CD133^{+} xenograft from patient 5 shows histological features of a GBM, reflecting the patient's original tumour histology. Both the CD133^{+} BTIC xenograft and the patient's original tumour show expression of the neural precursor marker nestin, high proliferative indices (MIB-1), p53 expression, and expression of both neuronal and astrocyte differentiated cell markers (MAP2 and GFAP). There are many invading human-specific nestin-positive tumour cells beyond the tumour borders in the xenograft. A diffusely infiltrative GBM (patient 7) is also depicted by H&E (bottom). Scale bar, 100 microns.

letters to nature
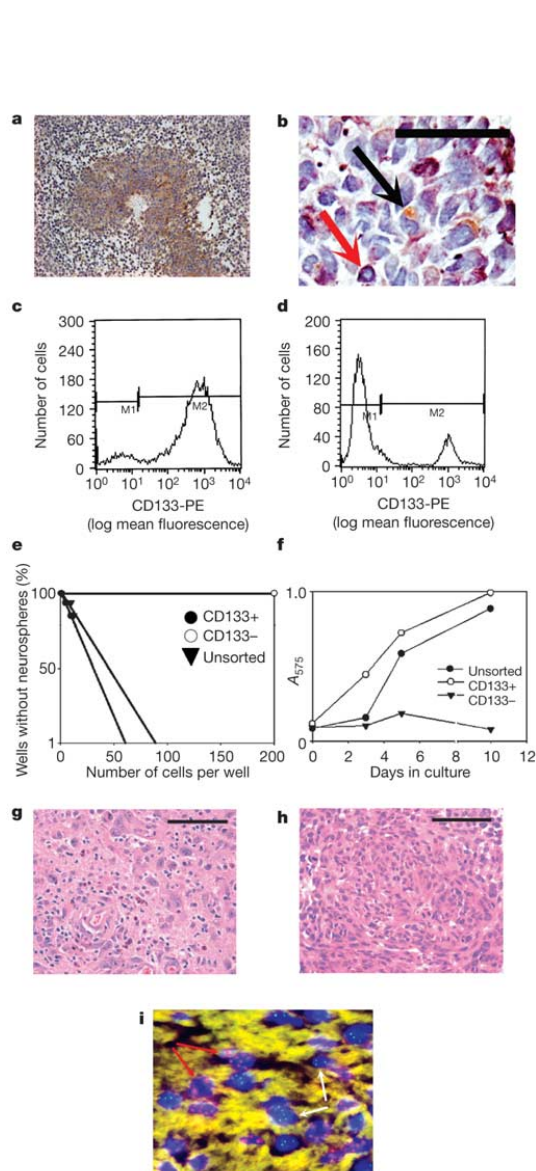
Figure 4 Only the CD133$^+$ BTIC, and not the CD133$^-$ tumour cell, is capable of tumour initiation. **a**, A subpopulation of cells from a CD133$^+$ GBM xenograft are CD133$^+$ (brown). **b**, Undifferentiated CD133$^+$ (brown, black arrow) and differentiated GFAP$^+$ (purple, red arrow) cells coexist in distinct subpopulations in this GBM xenotransplant. **c**, Purity of CD133$^+$ cells (84%) before initial xenotransplantation. M1, CD133$^-$ cells; M2, CD133$^+$ cells. **d**, Example of acutely dissociated primary xenotransplant; 19% CD133$^+$, 81% CD133$^-$. **e**, **f**, Limiting dilution analysis (**e**) and proliferation assays (**f**) of the GBM sorted for CD133 show that CD133$^+$ cells exclusively proliferate and self renew *in vitro*. Absorbance in **f** was measured at 575 nm. **g**, **h**, H&E sections of a recurrent paediatric GBM from the original patient (**g**, patient 6) and from a secondary xenograft from this tumour (**h**). **i**, Paraffin FISH of CD133$^-$ GBM xenograft shows that CD133$^-$ human tumour cells survive after xenotransplant but do not form tumours (human pan-centrometic probes in green, white arrows; mouse pan-centromeric probe in red, red arrows). Scale bar, 100 microns.

demonstrating self renewal *in vitro* (Fig. 4e, f).

A key property of all normal and cancer stem cells is the ability to self renew, a feature that can only be tested by serial passage. To determine whether the CD133$^+$ BTIC had self-renewal capacity, we performed serial retransplantation experiments from primary xenografts derived from a paediatric and an adult GBM (patients 6 and 7) that grew from an initial injection of 1,000 CD133$^+$ cells. After 6 weeks, the primary tumour was excised from the mouse brain and 1,000 CD133$^+$ cells were isolated and then reinjected into secondary mice. After 5 weeks, we observed that two out of two secondarily xenografted mice from the paediatric GBM and three of three mice from the adult GBM had brain tumours that recapitulated the phenotype of the original patient tumour and the primary xenograft (Fig. 4g, h), providing direct evidence for the self-renewal capacity of this population.

Most notably, none of the mice injected with CD133$^-$ tumour cells, purified to near homogeneity, developed brain tumours when analysed at 12 weeks post-injection. On the basis of analysis of flow histograms of tumour cells sorted for CD133, the contaminating CD133$^+$ cells in the purified CD133$^-$ population represent a weakly staining population that has very low CD133 protein expression, rather than the highly staining true CD133$^+$ sorted population (see Methods). To determine whether viable CD133$^-$ human cells had engrafted into the mouse brain but did not form tumours, we performed interphase FISH analysis of murine brain sections using species-specific centromeric probes to detect the presence of human cells at the injection site (Fig. 4i). For each of the CD133$^-$ injections from five medulloblastoma and glioblastoma human brain tumour samples (patients 1–5), human cells could be found in small clusters near the original injection site, but these cells did not form a nodule or mass; this indicates that their inability to form tumours is cell intrinsic, and not owing to an inability to be adequately supported in the brain environment following transplant.

To demonstrate that all engrafted cells have undergone a transformation event and do not represent normal brain cells, we conducted molecular cytogenetic analysis by spectral karyotyping (SKY) and interphase FISH using preparations obtained directly from briefly cultured tumour cells sorted for CD133. We found that both CD133$^-$ and CD133$^+$ tumour cells from a medulloblastoma exhibited chromosomal instability for chromosome 17. The normal signal pattern of two centromere signals and two TP53 signals was detected in less than 4% of sorted cells that were subsequently xenotransplanted, indicating a low rate of potential normal cell contamination (see Supplementary Fig. 2). SKY analysis of GBM specimens bore chromosomal aberrations characteristic of this tumour type (see Supplementary Fig. 3). Further interphase FISH analysis of this GBM using centromere 7 indicated that nearly 80% of both CD133$^+$ and CD133$^-$ cells exhibited an abnormal karyotype, consistent with the SKY findings. Paraffin FISH studies performed on CD133$^+$ xenografts from an adult GBM also indicated that the majority of cells bore evidence of transformation, with amplification of the EGFR gene identical to that of the patient's tumour (see Supplementary Fig. 4). These cytogenetic data indicate that the transplanted cells, whether CD133$^-$ or CD133$^+$, have an abnormal karyotype and aneusomy pattern inconsistent with significant contamination by normal cells. The CD133$^+$ and CD133$^-$ cells have the same cytogenetic alterations, suggesting that they are clonally derived.

Together, these data indicate that the CD133$^+$ human brain tumour cell fraction from tumours of different types, from both adults and children, contain brain tumour initiating cells that exclusively initiate tumour formation in immunodeficient mice. BTIC have potent *in vivo* self-renewal and proliferative capacities, generating tumours that are a phenocopy of the patient's tumour following engraftment with as few as 100 CD133$^+$ cells. Thus, the BTIC possess all the key properties ascribed to a stem cell. These results indicate that brain cancer should not be viewed as blocked or

letters to nature

frozen differentiation; rather, the brain tumour initiating cell clone exhibits patterns of abnormal differentiation. Although our model demonstrates that tumours are initiated by CD133^{+} cells with stem cell properties, whether the cancer-initiating event occurs in a normal stem cell or in normal progenitor or differentiated cells that have reacquired stem cell properties remains to be determined.

Although the frequency of cancer-initiating cells in brain tumours is higher than reported for other cancers[4,5], we suggest that the cancer-initiating frequency may be higher because these tumours are among the most aggressive known human cancers and our patient samples were also derived from within the patient's untreated primary tumour masses. Further *in vivo* limiting dilution analysis will continue to more accurately determine the CSC frequency within the CD133^{+} population.

These results suggest that brain cancers are hierarchically organized and lend strong support for the CSC hypothesis, extending this idea beyond the original studies on human leukaemias[3,4,7,19]. The CSC hierarchy may be functionally elucidated as more surface markers for neural stem cells emerge, and more potent stem cell activity may be found in a CD133^{+} subpopulation. Leukemias have been suggested to originate in stem cell[4] as well as progenitor populations[20,21], and the question of cell of origin remains unclear in brain tumours[22–25].

The identification of an *in vivo* tumour-initiating cell from human brain tumours of different phenotypes provides a powerful tool to investigate the tumorigenic process in the central nervous system. We have also efficiently created a model that can be used to study each individual patient's brain tumour. The cellular heterogeneity of brain tumours dictates that if only a small fraction of cancer stem cells is capable of regenerating the tumour, bulk therapy may fail to target the tumour-initiating cell, allowing for disease progression or relapse. The functional analysis of the BTIC may give new insight into patient prognosis that may then warrant individual tailoring of therapy.

Note added in proof: While our manuscript was under consideration, Galli *et al.*[28] demonstrated that glioblastoma cell lines, established by culture in neurosphere conditions, could proliferate, self renew and differentiate into multiple lineages *in vitro*. Cerebral injection of 200,000 of these tumour sphere cells could also generate tumours *in vivo*, and after repeat culture, could initiate phenotypically similar tumours, in a secondary mouse. □

Methods

Primary tumour sphere culture

Tumour samples were obtained from consenting patients, as approved by the Research Ethics Boards at The Hospital for Sick Children and St Michael's Hospital (Toronto). Tumours were washed, acutely dissociated in oxygenated artificial cerebrospinal fluid (CSF) and subject to enzymatic dissociation. Tumour cells were then briefly placed in tumour sphere media (TSM) to allow for recovery following enzymatic dissociation[6]. On average, each tumour specimen yielded two to five million cells.

Magnetic cell sorting and flow cytometry

Cells were labelled with 1 μL CD133/1 microbeads per 1 million cells using the Miltenyi Biotec CD133 cell isolation kit, as previously described[6], between 1–24 h post-dissociation (median 2.75 h). Tumour cells were generally very adherent and required frequent mechanical and chemical trituration to prevent cell clumping during sorting. Aliquots of CD133^{+} and CD133^{−} sorted cells were evaluated for purity by flow cytometry with a FACSCalibur machine (BD Biosciences), using CD133/2 (293C3)-PE antibody (Miltenyi Biotec). Purities ranged from 70 to 91% for CD133^{+} cells (median 84%), and 87.5 to 99.5% (median 99.5%) for CD133^{−} cells. The small impurity of CD133^{+} cells in the CD133^{−} fraction quantified by FACS showed very low mean fluorescence in comparison to sorted CD133^{+} cells, which had high fluorescence; this suggests that these contaminating CD133^{+} cells in the CD133^{−} fraction are phenotypically different from the sorted CD133^{+} population that were used in our transplantation studies.

Intracranial cell transplantation into NOD-SCID mice

Within 1 to 16 h of magnetic bead cell sorting, purified populations of CD133^{+} and CD133^{−} cells were resuspended in 10 μl of phosphate buffered saline (PBS), in aliquots of 50,000, 10,000, 5,000 and 1,000 CD133^{+} cells (as few as 100 CD133^{+} cells were used for patients 6 and 7) and 50,000 or 100,000 CD133^{−} cells. These aliquots were injected

stereotactically into 6- to 8-week-old NOD-SCID mouse frontal cortex, following administration of general anaesthesia. The injection coordinates were 3 mm to the right of the midline, 2 mm anterior to the coronal suture and 3 mm deep.

Mouse brain fixation and histopathology

Mice were killed and their brains were immediately removed and fixed in 4% paraformaldehyde for 24 h, then transferred to 70% ethanol. Mouse brains were processed on a Tissue-Tek VIP (Sakura) and embedded in paraffin. Brains were sectioned at 5-μm thickness on a Microm HM 200 cryotome (Eryostar), and stained with haematoxylin-and-eosin (H&E) as per standard histopathological technique.

Immunohistochemistry

Paraffin embedded, 5-μm formalin fixed tissue sections were mounted on microscope slides. Tissue sections were then dried overnight at 60 °C, dewaxed in xylene and rehydrated with distilled water. With the exception of sections stained for GFAP, all sections were treated with heat-induced epitope retrieval technique (HIER) using a citrate buffer at pH 6.0. Incubation with the following antibodies was performed for 1 h at room temperature: βIII-tubulin (Chemicon, 1:500), GFAP (DakoCytomation, 1:1,000), MIB-1 (DakoCytomation, 1:20) nestin (Chemicon, 1:200), MAP2 (Sigma, 1:1,000) and p53 (DAKO, 1:20). Immunostaining was performed on a Ventana NEXES auto-immunostainer (Ventana Medical Systems). Double immunostaining for CD133 and GFAP used anti-human CD133 (Miltenyi Biotec, 1:5) incubated overnight at room temperature, followed by anti-human GFAP (DAKO, 1:1,000) for 1 h at room temperature. Human placenta[11,26] and human retinoblastoma specimens were used as positive controls for CD133. Immunodetection was performed using the Elite Vector Stain ABC System (Vector Laboratories). The counterstain of preference was haematoxylin for nuclear detail.

In vitro limiting dilution analysis (primary sphere formation assays)

Limiting dilution assay on tumour cells that had been sorted for CD133 was performed and 0.37 intercepts calculated[6]. Primary sphere formation assays were performed on the entire acutely dissociated tumour cell population on day 0 to quantify stem cell frequency within the tumour, as previously described[6]. Cell proliferation assays were performed on days 0, 3, 5 and 7 post-plating using the Roche MTT-based colorimetric assay cell proliferation kit 1. Cells were plated in 96-well microwell plates in 0.1-ml volumes of TSM, at a density of 1,000 cells per well.

Cytogenetic preparation, FISH analysis and spectral karyotyping of tumour sphere cells

Short-term cultured sorted or unsorted cells were colcemid treated, hypotonically swelled and methanol:acetic acid treated as previously described[27]. Interphase FISH analysis was performed using commercially available probes for centromere 17 and the locus specific probe for p53, as well as the centromere 7 and EGFR probe set (Vysis), and used according to the manufacturer's instructions. Pancentromeric mouse and human specific probes (Cedarlane) were also used. The slides were visualized and imaged using the Quips Imaging System (Vysis). Two-hundred nuclei were scored for each cell population and tabulated. Spectral karyotyping was performed on metaphase spreads using the commercially available probes supplied by Applied Spectral Imaging, and analysed as previously described[27].

1. Reya, T., Morrison, S. J., Clarke, M. F. & Weissman, I. L. Stem cells, cancer, and cancer stem cells. *Nature* **414**, 105–111 (2001).
2. Pardal, R., Clarke, M. & Morrison, S. Applying the principles of stem-cell biology to cancer. *Nat. Rev. Cancer* **3**, 895–902 (2003).
3. Lapidot, T. *et al.* A cell initiating human acute myeloid leukaemia after transplantation into SCID mice. *Nature* **367**, 645–648 (1994).
4. Bonnet, D. & Dick, J. E. Human acute myeloid leukemia is organized as a hierarchy that originates from a primitive hematopoietic cell. *Nature Med.* **3**, 730–737 (1997).
5. Al-Hajj, M., Wicha, M. S., Benito-Hernandez, A., Morrison, S. J. & Clarke, M. F. Prospective identification of tumorigenic breast cancer cells. *Proc. Natl Acad. Sci. USA* **100**, 3983–3988 (2003).
6. Singh, S. K. *et al.* Identification of a cancer stem cell in human brain tumors. *Cancer Res.* **63**, 5821–5828 (2003).
7. Dick, J. E. Breast cancer stem cells revealed. *Proc. Natl Acad. Sci. USA* **100**, 3547–3549 (2003).
8. Ignatova, T. N. *et al.* Human cortical glial tumors contain neural stem-like cells expressing astroglial and neuronal markers *in vitro. Glia* **39**, 193–206 (2002).
9. Hemmati, H. D. *et al.* Cancerous stem cells can arise from pediatric brain tumors. *Proc. Natl Acad. Sci. USA* **100**, 15178–15183 (2003).
10. Kondo, T., Setoguchi, T. & Taga, T. Persistence of a small subpopulation of cancer stem-like cells in the C6 glioma cell line. *Proc. Natl Acad. Sci. USA* **101**, 781–786 (2004).
11. Miraglia, S. *et al.* A novel five-transmembrane hematopoietic stem cell antigen: isolation, characterization, and molecular cloning. *Blood* **90**, 5013–5021 (1997).
12. Corbeil, D., Roper, K., Weigmann, A. & Huttner, W. B. AC133 hematopoietic stem cell antigen: human homologue of mouse kidney prominin or distinct member of a novel protein family? *Blood* **91**, 2625–2626 (1998).
13. Uchida, N. *et al.* Direct isolation of human central nervous system stem cells. *Proc. Natl Acad. Sci. USA* **97**, 14720–14725 (2000).
14. Houchens, D. P., Ovejera, A. A., Riblet, S. M. & Slagel, D. E. Human brain tumor xenografts in nude mice as a chemotherapy model. *Eur. J. Cancer Clin. Oncol.* **19**, 799–805 (1983).
15. Hu, B. *et al.* Angiopoietin-2 induces human glioma invasion through the activation of matrix metalloprotease-2. *Proc. Natl Acad. Sci. USA* **100**, 8904–8909 (2003).
16. Russell, D. & Rubenstein, L. *Pathology of Tumors of the Central Nervous System* (Williams and Wilkins, Baltimore, 1989).

letters to nature

17. Lendahl, U., Zimmerman, L. B. & McKay, R. D. CNS stem cells express a new class of intermediate filament protein. *Cell* **60**, 585–595 (1990).

18. Kleihues, P. *et al.* The WHO classification of tumors of the nervous system. *J. Neuropathol. Exp. Neurol.* **61**, 215–225; discussion 226–229 (2002).

19. Hope, K. J., Jin, L. & Dick, J. E. Acute myeloid leukemia originates from a hierarchy of leukemic stem cell classes that differ in self-renewal capacity. *Nature Immunol.* **5**, 738–743 (2004).

20. Cozzio, A. *et al.* Similar MLL-associated leukemias arising from self-renewing stem cells and short-lived myeloid progenitors. *Genes Dev.* **17**, 3029–3035 (2003).

21. Passegue, E., Jamieson, C. H., Ailles, L. E. & Weissman, I. L. Normal and leukemic hematopoiesis: are leukemias a stem cell disorder or a reacquisition of stem cell characteristics? *Proc. Natl Acad. Sci. USA* **100**(suppl. 1), 11842–11849 (2003).

22. Holland, E. C., Hively, W. P., DePinho, R. A. & Varmus, H. E. A constitutively active epidermal growth factor receptor cooperates with disruption of G1 cell-cycle arrest pathways to induce glioma-like lesions in mice. *Genes Dev.* **12**, 3675–3685 (1998).

23. Holland, E. C. Gliomagenesis: genetic alterations and mouse models. *Nature Rev. Genet.* **2**, 120–129 (2001).

24. Bachoo, R. M. *et al.* Epidermal growth factor receptor and Ink4a/Arf: convergent mechanisms governing terminal differentiation and transformation along the neural stem cell to astrocyte axis. *Cancer Cell* **1**, 269–277 (2002).

25. Oliver, T. G. & Wechsler-Reya, R. J. Getting at the root and stem of brain tumors. *Neuron* **42**, 885–888 (2004).

26. Potgens, A. J., Bolte, M., Huppertz, B., Kaufmann, P. & Frank, H. G. Human trophoblast contains an intracellular protein reactive with an antibody against CD133–a novel marker for trophoblast. *Placenta* **22**, 639–645 (2001).

27. Bayani, J. *et al.* Molecular cytogenetic analysis of medulloblastomas and supratentorial primitive neuroectodermal tumors by using conventional banding, comparative genomic hybridization, and spectral karyotyping. *J. Neurosurg.* **93**, 437–448 (2000).

28. Galli, R. *et al.* Isolation and characterization of tumorigenic, stem-like neural precursors from human glioblastoma. *Cancer Res.* **64**, 7011–7021 (2004).

A FADD-dependent innate immune mechanism in mammalian cells

Siddharth Balachandran*, Emmanuel Thomas* & Glen N. Barber

Department of Microbiology and Immunology and Sylvester Comprehensive Cancer Center, University of Miami School of Medicine, Miami, Florida 33136, USA

* These authors contributed equally to this work

Vertebrate innate immunity provides a first line of defence against pathogens such as viruses and bacteria. Viral infection activates a potent innate immune response, which can be triggered by double-stranded (ds)RNA produced during viral replication[1–3]. Here, we report that mammalian cells lacking the death-domain-containing protein FADD[4,5] are defective in intracellular dsRNA-activated gene expression, including production of type I (α/β) interferons, and are thus very susceptible to viral infection. The signalling pathway incorporating FADD is largely independent of Toll-like receptor 3 and the dsRNA-dependent kinase PKR, but seems to require receptor interacting protein 1 as well as Tank-binding kinase 1-mediated activation of the transcription factor IRF-3. The requirement for FADD in mammalian host defence is evocative of innate immune signalling in

***Drosophila*, in which a FADD-dependent pathway responds to bacterial infection by activating the transcription of antimicrobial genes[6]. These data therefore suggest the existence of a conserved pathogen recognition pathway in mammalian cells that is essential for the optimal induction of type I interferons and other genes important for host defence.**

A major consequence of virus infection is the induction of the type I interferons (IFNs), which are a family of cytokines essential for host defence[3,7]. While investigating the mechanisms of IFN antiviral activity, we noticed that early passage murine embryonic fibroblasts (MEFs) lacking the apoptosis adaptor molecule FADD appeared to be overtly sensitive to virus infection[8]. To examine this phenotype further, we infected $Fadd^{+/-}$ and $Fadd^{-/-}$ MEFs with the IFN-sensitive prototypic rhabdovirus vesicular stomatitis virus (VSV), and observed that VSV replication was markedly increased (>100-fold) in the $Fadd^{-/-}$ MEFs compared with their wild-type counterparts (Fig. 1a–c). Moreover, whereas pre-treatment with type I (α/β) or type II (γ) IFN for 12 h was seen to exert significant antiviral activity in normal cells, these key antiviral cytokines only delayed the onset of viral replication in $Fadd^{-/-}$ MEFs for 24–36 h, whereupon virus replication proceeded unchecked (Fig. 1a–c). The observed susceptibility to infection did not appear to be restricted to VSV, because MEFs lacking FADD were also sensitive to infection by other viruses, including influenza virus and encephalomyocarditis (EMCV) virus (Supplementary Fig. 1). MEFs lacking caspase 8 (refs 9, 10) (or cells treated with caspase inhibitors) exhibited no increased susceptibility to VSV infection compared to control cells, and retained the ability to be protected by IFN, suggesting that FADD exerts its antiviral effects independently of caspase 8 (Supplementary Fig. 2 and data not shown).

Because exposure to type I and II IFNs was unable to effectively protect $Fadd^{-/-}$ MEFs from virus replication, it is plausible that effective IFN-mediated, janus kinase (JAK)-activated STAT (signal transducer and activator of transcription) signalling[11] may require FADD. However, neither nuclear translocation of STAT1 nor the induction of selected type I and II IFN-responsive genes appeared to be impaired in $Fadd^{-/-}$ cells, indicating that IFN signalling *per se* is probably not compromised (Fig. 1d; see also Supplementary Fig. 3).

Despite these observations, it remained possible that the antiviral state initially established by 12 h of pre-exposure to exogenous IFN is short-lived and may require constant *de novo* synthesis of type I IFNs after virus infection (Fig. 1a). Indeed, we noted that continuous supplementation of recombinant type I IFNs to $Fadd^{-/-}$ cells after VSV infection conferred some protection against viral replication and cytolysis (Fig. 1e, f). The continual requirement for IFN induction after virus infection was further emphasized by demonstrating that antibody-mediated neutralization of secreted IFN-α or -β after exposure to VSV rendered normal cells susceptible to infection even after IFN pre-treatment (Fig. 1g, h).

These analyses suggest that an actual defect in the production of type I IFNs after virus/dsRNA detection might be responsible for the susceptibility of $Fadd^{-/-}$ cells to infection. To examine this possibility, we transfected $Fadd^{+/-}$ and $Fadd^{-/-}$ cells with a luciferase reporter construct under control of the IFN-β promoter and subsequently administered poly(I:C), a synthetic mimetic of viral dsRNA thought to be the primary trigger of IFN production after virus infection[3]. Notably, we found that transfected poly(I:C) triggered robust ($\sim$10-fold) induction of the IFN-β promoter in $Fadd^{+/-}$ cells but not in $Fadd^{-/-}$ cells (Fig. 2a). The induction of the IFN-β promoter was not observed using non-transfected, exogenous poly(I:C) alone (Fig. 2a). Poly(I:C)-induced activation of IFN-β promoter-driven luciferase activity could be partially restored by reintroducing murine FADD into $Fadd^{-/-}$ MEFs (Supplementary Fig. 4). A requirement for FADD in dsRNA-induced activation of the IFN-β promoter was further confirmed by short interfering RNA (siRNA)-mediated suppression of FADD in HeLa cells (Supplementary Fig. 4).

401

Conteo Celular con Hematocitómetro
Uso Elemental del Hematocitómetro

Introduction

A pesar del enorme desarrollo tecnológico que ha tenido lugar en los laboratorios científicos, el conteo visual con hematocitómetro sigue siendo el método de conteo más extendido desde el siglo XIX.

El presente artículo se escribe con la intención de ayudar a realizar un conteo celular con un hematocitómetro o cámara de Neubauer a principiantes, y también a técnicos o investigadores experimentados que deseen recordar las bases del mismo.

Primero, describiremos cada una de las partes y los principios de funcionamiento del hematocitómetro.

En una segunda parte, se describe paso a paso cómo realizar un recuento celular con hematocitómetro para obtener unos resultados fiables.

NOTA : Durante

Materiales

Los elementos necesarios para realizar un recuento celular con hematocitómetro son los siguientes:

a) muestra celular a medir
b) hematocitómetro, o cámara de Neubauer
c) microscopio óptico
d) cubre objetos
e) pipeta / micropipeta con puntas
f) buffer para diluciones / PBS, en su caso

LA CÁMARA DE NEUBAUER, O HEMATOCITOMETRO.

Se trata de una gruesa placa de cristal con forma de portaobjetos, de unos 30 x 70 mm y unos 4 mm de grosor.

En una cámara simple, la porción central, que es donde se realiza el conteo, está dividida en 3 partes.

Fig 1. Elementos necesarios para realizar un conteo celular con Hematocitómetro

celeromics

www.celeromics.com

Technical Note - Neubauer Chamber Cell Counting -   Oscar Bastidas   2

En la parte central se encuentra grabada una retícula cuadrangular.

En el caso de cámara dobles, que son las más comunes, existen 2 zonas de conteo, una superior y otra inferior al eje longitudinal de la cámara.
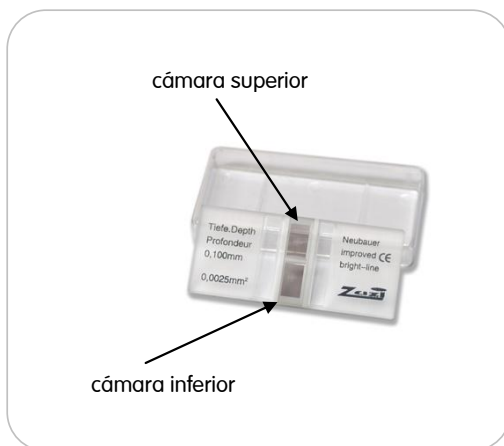

Fig 2. Cámara de Neubauer comercial

Fig 3. Pila de cubreobjetos, y caja.

La reticula completa mide 3 mm x 3 mm de lado. Subdividida a su vez en 9 cuadrados de 1mm de lado cada uno. Fig. 4 – 1

En caso de recuento de sangre, los cuadrados de las esquinas son los destinados al recuento de leucocitos. Al existir estos en menor número que los hematíes, se necesitan menos líneas de referencia para realizar el conteo.

El cuadrado central es el destinado al recuento de hematíes y plaquetas. Se divide en 25 cuadrados medianos de 0,2 mm de lado (Fig.4-2) , y cada uno de estos cuadros se subdivide a su vez en 16 cuadrados pequeños. Fig 4-3

El cuadrado central está por tanto formado por 400 cuadrados pequeños.

CUBREOBJETOS.

El cubreobjetos es un cuadrado de cristal de aproximadamente 22 mm x 22 mm. Debe colocarse sobre la cámara de recuento de forma que cubra la parte central de la cámara, delimitando un espacio entre la cámara y el cubreobjetos de 0,1 mm.

Es común que el cubreobjetos quede ligeramente levantado cuando aplicamos más líquido del necesario a la cámara. Para evitar esto, existen algunas cámaras que tienen dos pinzas especiales para evitar que el cubreobjetos se levante, y la distancia sea mayor de 0,1 mm.

PIPETA

Se trata de un instrumento de laboratorio que permite medir alícuota de líquido con bastante precisión. Tipicamente han sido principalmente de vidrio, pero en la actualidad se utilizan ampliamente las micropipetas, que tienen puntas esterilizadas desechables. Las mas habituales están calibradas para una capacidad máxima de 20, 200 y 1000 uL .

celeromics   www.celeromics.com

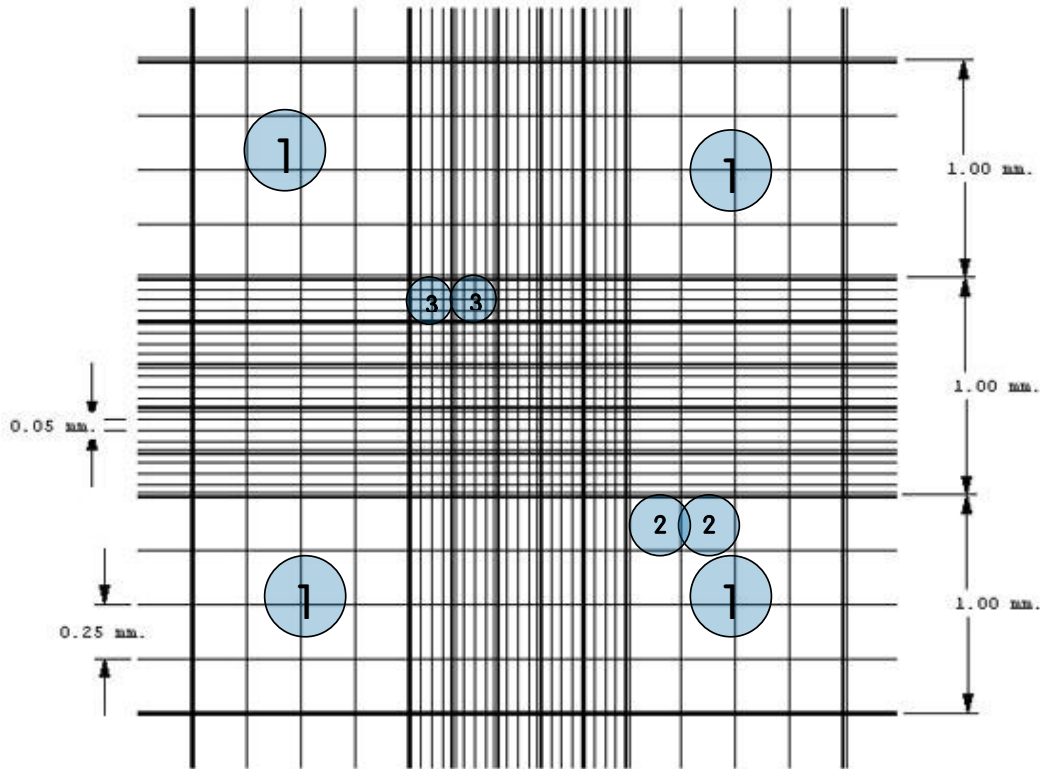Technical Note - Neubauer Chamber Cell Counting -　　Oscar Bastidas　　　3

Fig 4. Detalle de la rejilla de una cámara de Neubauer Improved.

Conteo Celular, paso a paso

PASO 1. Preparación de la muestra.

Dependiendo del tipo de muestra a medir, se ha de habrá de prepararar una muestra con una concentración apta para su recuento.

Típicamente, el rango de concentraciones que permite contar el hematocitómetro está entre 250.000 células y 2,5 millones de células por ml.

Intentaremos que la muestra tenga una concentración en torno a 10^6 (1 millón) aplicando las diluciones correspondientes.

Por debajo de 250.000 células / ml (2,5 * 10^5)la cantidad de células contadas no es suficiente para poder dar una estimación lo suficientemente fiable de la concentración celular [1]

....

La concentración óptima para conteo en hematocitómetro es de 1 millón de células por ml = 10^6 células /ml

....

[1] Ver
http://www.celeromics.com/es/resources/docs/Articles/conteo-celular-con-concentraciones-bajas.htm, para una demostración estadística de por qué ocurre esto.

celeromics　　　　　　　　　　　　www.celeromics.com

Technical Note - Neubauer Chamber Cell Counting -   Oscar Bastidas   4

Por encima de 2,5 millones (2,5 * 10^6) la probabilidad de cometer errores de conteo crece demasiado, y también el tiempo y esfuerzo necesario para realizar un recuento con fiabilidad. Por encima de esta concentración es conveniente diluir la muestra para acercar la concentración al rango óptimo.

PASO 2. Introducción de la muestra en la cámara de Neubauer

Se toman 10 uL de la mezcla preparada en el paso 1 con la micropipeta.

1) Se coloca un cubreobjetos sobre la cámara de Neubauer, y se coloca en posición horizontal sobre la mesa, en un lugar donde nos sea cómodo pipetear.
2) se introduce una punta desechable en el extremo de la micropipeta,
3) se ajusta la micropipeta para succionar 10 uL de líquido. Generalmente este ajuste se realiza guirando el botón del embolo para seleccionar el volumen deseado.
4) se introduce la punta de la micropipeta en la muestra
5) Se pulsa el pistón o embolo superior de la pipeta suavemente hasta que se siente como el pistón llega al final de su recorrido.
6) Se saca la punta de la pipeta de la muestra, y siempre manteniéndola en posición vertical se lleva hasta la cámara de Neubauer.
7) Se coloca la punta de la pipeta en el borde del cubreobjetos, en el extremo de la cámara de Neubauer. Se trata de dejar que el líquido penetre entre la cámara y el cubreobjetos desde el lateral, por capilaridad.
8) Se suelta el pistón suavemente mientras se supervisa que el líquido está entrando correctamente y de forma uniforme en la cámara. (ver Fig.5)
9) En caso de que aparezcan burbujas, el cubreobjetos se haya movido o algo no haya salido bien, repetir la operación

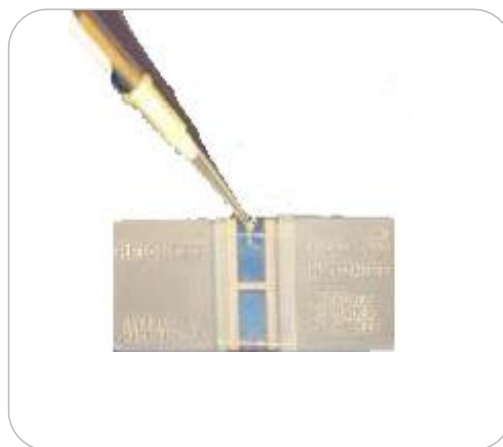Ya tenemos la cámara de Neubauer cargada, lista para el recuento celular.

Fig 5. Introducción de la muestra en la cámara de Neubauer

PASO 3. Preparación y enfoque del microscopio.

1. Colocar la cámara de Neubauer en la bandeja del microscopio. Si el microscopio dispone de pinza de sujeción, fijar la cámara con ella.
2. Encender la luz del microscopio.
3. Enfocar el microscopio hasta que pueden verse nítidas las células mirando por el binocular.
4. Buscar el primer cuadro donde vaya a realizarse el recuento. En este ejemplo vamos a contar 5 cuadros grandes de una cámara de Neubauer Improved de 0,1mm de profundidad. Ver Fig. 8

Ver http://www.celeromics.com/es/resources/docs/Articles/easy-formula-for-manual-cell-counting.htm, para ver las fórmulas a aplicar en cada una de las cámaras de recuento más comunes.

5. Realizar el recuento de células en el primer cuadro.

   Existe una convención por la cual si las células tocan el límite superior o el límite izquierdo del cuadro, deben contabilizarse, pero no se contabilizan si tocan el límite inferior o el límite derecho.

celeromics

www.celeromics.com
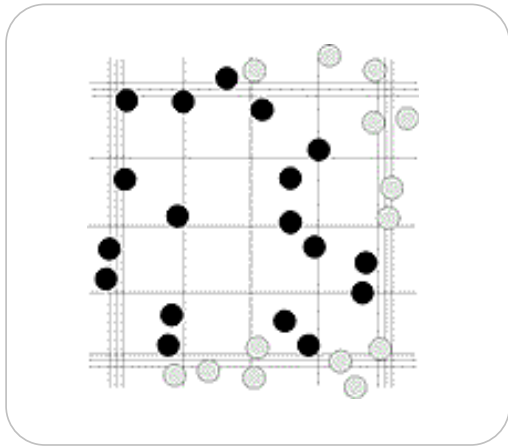
Technical Note - Neubauer Chamber Cell Counting - Oscar Bastidas 5

Fig. 6. Conteo de un cuadro grande de cámara de Neubauer.

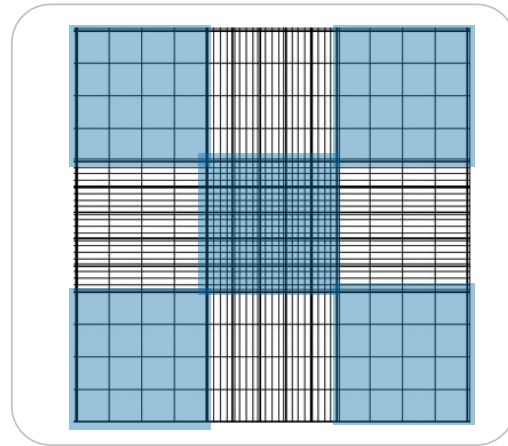Fig. 8. Recuento de 5 cuadros grandes de cámara de Neubauer Improved.

PASO 4. Cálculo de la concentración.

Aplicamos la fórmula del cálculo de concentración celular.

$$\text{Concentración (cel / ml)} = \frac{\text{número de células}}{\text{Volumen (en ml)}}$$

El número de células es la suma de todas las células contadas en todos los cuadros.

El volumen es el volumen total de todos los cuadros donde hemos hecho el recuento.

Como el volumen de 1 cuadro grande es :

0,1 cm x 0,1 cm = 0,01 cm2 de superficie
0,01 cm2 * 0,1 mm (profundidad) =
0,01 cm2 * 0,01 cm = 0,0001 cm3 = 0,0001 ml

La formula para recuento con cuadros grandes en cámara de Neubauer

$$\text{Concentración} = \frac{\text{número de células x 10.000}}{\text{número de cuadros}}$$
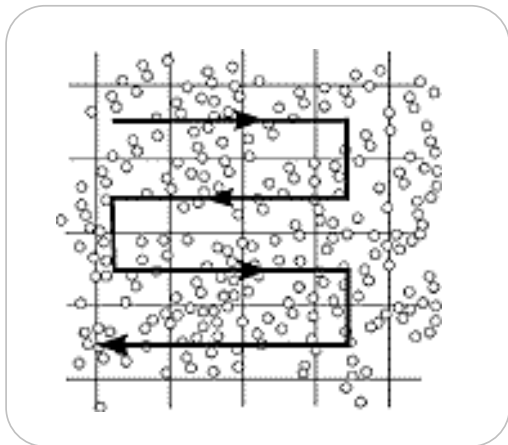

Fig. 7. Recuento con alta concentración celular.

En caso de que la concentración celular sea muy alta, y sea fácil perderse en el recuento, se suele utilizar un orden de conteo en forma de zig-zag, como el descrito en la Fig.7

6. Anotar en una hoja de resultados la cantidad de células contadas en el primer cuadro.

7. Repetir el proceso para el resto de los cuadros que deseamos contar, anotando el resultado de cada uno de ellos. Cuantos más cuadros contemos, más precisión obtendremos en nuestra medida.

En el caso de que hayamos aplicado una dilución, deberemos trasformar la concentración obtenida durante el recuento celular en la concentración de la muestra

celeromics

www.celeromics.com

Technical Note - Neubauer Chamber Cell Counting - Oscar Bastidas 6

original.

En este caso tendremos que dividir el resultado por la dilución aplicada.

La fórmula quedará :

$$\text{Concentración} = \frac{\text{número de células x 10.000}}{\text{número de cuadros x dilución}}$$

Ejemplo:
Para una dilución de 1 : 10. Dilución = 0,1
Para una dilución de 1 : 100, Dilución = 0,01

Error

Errores de hasta 20% y 30% son comunes con este método de recuento debido al pipeteo, a los errores estadísticos por ser la muestra poco representativa, errores del volumen de muestra realmente introducido en la cámara, etc.

Sin embargo, el hematocitómetro sigue siendo uno de los métodos mas ampliamente utilizados en los laboratorios de todo el mundo.

Para acceder a un análisis detallado del error que se está cometiendo en un recuento determinado acceda a:

http://www.celeromics.com/es/resources/docs/Articles/cell-count-error.htm

celeromics

www.celeromics.com

Assajos clínics actuals

Title	Phase	Recruitment	Conditions	Interventions	Sponsors	Expected Completion Date
Clinical Trial Evaluating the Combination of Vandetanib and Dasatinib During and After Radiation Therapy (RT) in Children With Newly Diagnosed Diffuse Intrinsic Pontine Glioma (DIPG)	Phase I	Active, not recruiting	Diffuse Intrinsic Pontine Glioma	Drug: vandetanib and dasatinib	St. Jude Children's Research Hospital	4/1/2013
A Comprehensive and Targeted Therapy Approach in Pediatric Malignant Pontine Gliomas		Recruiting	Pediatric Malignant Pontine Gliomas	Drugs: Gemzar, Ledertepa, Toposin, Alkeran, Avastin, Tarceva, Certican, Campto, Carbosin	VU University Medical Center (The Netherlands)	
An Open Label Dose Escalation Safety Study of Convection-Enhanced Delivery of IL13-PE38QQR in Patients with Progressive Pediatric Diffuse Infiltrating Brainstem Glioma and Supratentorial High Grade Glioma	Phase I	Recruiting	Brain Neoplasm|Glioma	Drug: IL13-PE38QQR	National Institute of Neurological Disorders and Stroke (NINDS)	1/1/2013
A Study of Bevacizumab Therapy in Patients with Newly Diagnosed High-Grade Gliomas and Diffuse Intrinsic Pontine Gliomas		Recruiting	Newly Diagnosed High-Grade Gliomas|Diffuse Intrinsic Pontine Glioma	Drug: Temozolomide|Drug: Bevacizumab|Drug: Irinotecan	Children's Hospital Medical Center, Cincinnati|Genentech	4/1/2012
Phase I Rindopepimut After Conventional Radiation in Children with Diffuse Intrinsic Pontine Gliomas	Phase I	Recruiting	Brain Cancer|Brain Stem Tumors|Pontine Tumors	Biological: Rindopepimut	Stanford University|National Institutes of Health (NIH)|National Cancer Institute (NCI)	12/1/2012
Cilengitide in Combination with Irradiation in Children with Diffuse Intrinsic Pontine Glioma	Phase I	Recruiting	Diffuse Intrinsic Pontine Glioma	Drug: Cilengitide dose escalation|Drug: Cilengitide|Radiation: Concomitant radiotherapy|Biological: Pharmacokinetic|Biological: Pharmacogenetic|Biological: Exploratory investigation	Centre Oscar Lambret	7/1/2015
Molecular Analysis of Samples from Patients with Diffuse Intrinsic Pontine Glioma and Brainstem Glioma		Recruiting	Diffuse Intrinsic Pontine Glioma|Brainstem Glioma		Children's Research Institute	4/1/2014

Phase 2 Study of Nimotuzumab in Pediatric Recurrent Diffuse Intrinsic Pontine Glioma	Phase II	Completed	Recurrent Diffuse Pontine Gliomas	Biological: nimotuzumab (anti EGFR humanized monoclonal antibody)	YM BioSciences	12/1/2010
Molecularly Determined Treatment of Diffuse Intrinsic Pontine Gliomas (DIPG)	Phase II	Recruiting	Diffuse Intrinsic Pontine Glioma	Drug: Bevacizumab|Drug: Erlotinib|Drug: Temozolomide|Radiation: Irradiation	Dana-Farber Cancer Institute|University of California, San Francisco|Children's Hospital Boston|Children's Memorial Hospital|Children's Hospital Los Angeles|University of Utah|Memorial Sloan-Kettering Cancer Center|Seattle Children's Hospital|Children's Hospital Colorad|Doernbecher Children's Hospital|Washington University Children's Hospital|Miami Children's Hospital|Johns Hopkins University|University of Florida|Children's Hospitals and Clinics of Minnesota|Southwestern Regional Medical Center|New York University|University of Rochester|University of Mississippi Medical Center|Louisville Children's Hospital|Children's Healthcare of Atlanta	
Vorinostat and Radiation Therapy Followed by Maintenance Therapy with Vorinostat in Treating Younger Patients with Newly Diagnosed Pontine Glioma	Phase I|Phase II	Recruiting	Brain and Central Nervous System Tumors	Drug: vorinostat|Radiation: 3-dimensional conformal radiation therapy|Radiation: intensity-modulated radiation therapy	Children's Oncology Group|National Cancer Institute (NCI)	

Lenalidomide and Radiation Therapy in High Grade Gliomas or Diffuse Intrinsic Pontine Gliomas	Phase I	Recruiting	Diffuse Intrinsic Pontine Glioma|Anaplastic Astrocytoma|High Grade Glioma	Drug: Lenalidomide|Radiation: Radiation Therapy	National Cancer Institute (NCI)	9/1/2016
Lenalidomide and Radiation Therapy in Treating Young Patients with Pontine Glioma or High-Grade Glioma	Phase I	Recruiting	Brain and Central Nervous System Tumors	Drug: lenalidomide|Other: laboratory biomarker analysis|Other: pharmacological study|Radiation: radiation therapy	NCI - Pediatric Oncology Branch|National Cancer Institute (NCI)	
PDGFR Inhibitor Crenolanib in Children/Young Adults With Diffuse Intrinsic Pontine Glioma or Recurrent High-Grade Glioma	Phase I	Recruiting	Diffuse Intrinsic Pontine Glioma|Progressive or Refractory High-Grade Glioma	Drug: Crenolanib|Drug: Crenolanib	St. Jude Children's Research Hospital|Arog Pharmaceuticals LLC	4/1/2015
Imiquimod/Brain Tumor Initiating Cell (BTIC) Vaccine in Brain Stem Glioma	Phase I	Not yet recruiting	Diffuse Intrinsic Pontine Glioma	Biological: Brain tumor initiating cells|Drug: Imiquimod	Masonic Cancer Center, University of Minnesota	6/1/2014
Diffuse Intrinsic Pontine Glioma (DIPG) Reirradiation (ReRT)	Phase I|Phase II	Recruiting	Brain Cancer	Radiation: Radiation Therapy	M.D. Anderson Cancer Center	
Convection-Enhanced Delivery of 124I-8H9 for Patients With Non-Progressive Diffuse Pontine Gliomas Previously Treated With External Beam Radiation Therapy	Phase I	Recruiting	Brain Cancer|Brain Stem Glioma	Radiation: Radioactive iodine-labeled monoclonal antibody 8H9	Memorial Sloan-Kettering Cancer Center|Weill Medical College of Cornell University|Johns Hopkins University	12/1/2014
A Phase II Study of Pegylated Interferon Alfa 2b (PEG-Intron(Trademark)) in Children with Diffuse Pontine Gliomas	Phase II	Completed	Diffuse Intrinsic Pontine Glioma	Procedure: adjuvant therapy|Biological: pegylated interferon alfa	National Cancer Institute (NCI)	1/1/2012
Combination Chemotherapy and Radiation Therapy with or Without Methotrexate in Treating Young Patients with Newly Diagnosed Gliomas	Phase III	Active, not recruiting	Brain and Central Nervous System Tumors	Drug: cisplatin|Drug: etoposide|Drug: ifosfamide|Drug: lomustine|Drug: methotrexate|Drug: prednisone|Drug: vincristine sulfate	Gesellschaft fur Padiatrische Onkologie und Hamatologie - Germany	
Chemotherapy and Radiation Therapy After Surgery in Treating Children with Newly Diagnosed Astrocytoma, Glioblastoma Multiforme, Gliosarcoma, or Diffuse Intrinsic Pontine Glioma	Phase II	Completed	Brain and Central Nervous System Tumors	Drug: temozolomide|Procedure: adjuvant therapy|Radiation: radiation therapy	Children's Oncology Group|National Cancer Institute (NCI)	

Veliparib, Radiation Therapy, and Temozolomide in Treating Younger Patients with Newly Diagnosed Diffuse Pontine Gliomas	Phase II|Phase II	Recruiting	Brain and Central Nervous System Tumors	Drug: temozolomide|Drug: veliparib|Genetic: gene expression analysis|Genetic: protein analysis|Other: laboratory biomarker analysis|Other: pharmacological study|Radiation: 3-dimensional conformal radiation therapy|Radiation: intensity-modulated radiation therapy	Pediatric Brain Tumor Consortium|National Cancer Institute (NCI)	
Cilengitide and Metronomic Temozolomide for Relapsed or Refractory High Grade Gliomas or Diffuse Intrinsic Pontine Gliomas in Children and Adolescents	Phase II	Recruiting	Gliomas	Drug: Cilengitide|Drug: Temozolomide	Martin-Luther-Universität Halle-Wittenberg|Merck KGaA	1/1/2015
Nimotuzumab in Children with Intrinsic Pontine Glioma		Active, not recruiting	Diffuse Instrinsic Ponitine Glioma	Drug: nimotuzumab	Oncoscience AG|Children`s Medical Hospital, University of Bonn, Germany|University of Wuerzburg|Dept. of Statistics, University of Dortmund, Germany|CRM Biometrics GmbH, Rheinbach, Germany|Heinrich-Heine University, Duesseldorf|Dr. Germany|Children`s Medical Hospital, Medical School Hannover, Hannover, Germany|Children`s Medical Hospital, University of Leipzig, Leipzig, Germany|Children`s Medical Hospital, University of Muenster, Muenster, Germany|Burdenko Neurosurgical Institute|Istituto Nazinonale Tumori, Div. of Paediatric Oncology,Milano, Italy	11/1/2008